Cell-free enzymatic biosystem for the conversion of glucose to malate

Ravneet Mandair

Doctor of Philosophy

Aston University

September, 2019

Aston University

Cell-free enzymatic biosystem for the conversion of glucose to malate

Ravneet Mandair

Doctor of Philosophy

2019

Thesis Summary

Platform chemicals are essential to industrial processes. Used as starting materials for the manufacture of diverse products, their cheap availability and efficient sourcing are an industrial requirement. Increasing concerns about the depletion of natural resources and growing environmental consciousness have led to a focus on the economics and ecological viability of biobased platform chemical production. Biobased strategies such as fermentation still have limitations that restrict their large scale industrial application. Current microbial biomanufacturing is hindered by the limitations caused by cells, as synthetic pathways and their optimizations are restricted by the physiological limits of the cellular production system. Cell-free metabolic engineering is pushing the boundaries of traditional bioengineering models by focusing on the use of *in vitro* combinations of catalytic enzymes prepared from purified proteins or crude lysates from cells, assembled in artificial cascades, for production of target commodities.

This thesis describes a cofactor balanced, cell-free, 5 enzyme biosystem for the sustainable production of malic acid from glucose, whereby 5 thermophilic proteins (glucose dehydrogenase, dihydroxy-acid dehydratase, 2-keto-3-deoxygluconate aldolase, glyceraldehyde dehydrogenase and malate dehydrogenase) were successfully expressed, purified and demonstrated to display enzyme activity. Enzyme immobilization has been used by many researchers to overcome instability problems and facilitate the repetitive use of enzymes. Recombinant glucose dehydrogenase from *S. solfataricus* was successfully purified and immobilized onto novel supports and demonstrated great potential for gluconic acid production from glucose, as well as bread waste hydrolysate in a sustainable production approach. Coupling of cofactor recycling enzymes (glucose dehydrogenase and malate dehydrogenase) was also explored and successfully demonstrated the simultaneous production of chemicals and cofactor recycling capabilities. The experimental work also identified potential bottlenecks affecting the feasibility of the cell-free biosystem and paves the way for optimized characterization of enzymes in the cascade, in the free-state, individually immobilized and co-immobilized.

Key words: Cell-free metabolic engineering, multienzyme cascades, sustainable chemical production, biocatalysis, enzyme immobilization

To my parents, for always telling me anything was possible

To my husband, for making everything possible

And to all the family and friends for pretending to understand my research

Acknowledgements

Contents

Abbreviations

2-ME	β-mercaptoethanol
AI	Auto-induction
AIDH	Glyceraldehyde dehydrogenase
BCA	Bicinchoninic acid
BSA	Bovine serum albumin
BWH	Bread waste hydrolysate
dd	Double distilled
DHAD	Dihydroxy-acid dehydratase
DTT	Dithiothreitol
E. coli	*Escherichia coli*
EDTA	Ethylenediaminetetraacetic acid
ES	Enzyme support solution
GDH	Glucose dehydrogenase
GdnHCl	Guanidine hydrochloride
IC	Ion chromatography
IPTG	Isopropyl β-D-1-thiogalactopyranoside
KDGA	2-keto-3-deoxygluconate aldolase
LB	Luria-Bertani
MDH	Malate dehydrogenase
Ni-NTA	Nickel nitrilotriacetic acid
OD	Optical density
PAGE	Polyacrylamide gel electrophoresis
PBS	Phosphate buffered saline
pH	Negative logarithm of the hydrogen ion concentration
SDS	Sodium dodecyl sulfate
TAE	Tris-acetate-EDTA
TEMED	N,N,N',N'-tetramethylethane-1,2-diamine
Tween 20	Polyoxyethylenesorbitan monolaurate

Units

°C	Celsius
g	Gram
g	Gravitational force
kDa	Kilo Dalton
L	Litre
µg	Microgram
mg	Milligram
µl	Microlitre
min	Minute
ml	Millilitre
mM	Millimole
M	Mole
nm	Nanometre
Rpm	Revolutions per minute
U	Units
V	Volts
µl	Microlitre

List of Figures

Chapter 8

List of Tables

1. Introduction

The objective for this research project was to design a cell-free biosystem consisting of purified enzymes to facilitate the conversion of glucose derived from waste products into malic acid. Immobilization of the purified enzymes was also explored to aid enzyme recycling.

1.1 Biobased production of platform chemicals

The term platform chemical is given to the chemical intermediates/building blocks/precursors derived from fossil resources, to make a variety of industrially-valuable chemicals and materials (Jang et al. 2012). A high percentage of today's platform chemicals and subsequent materials are derived from fossil fuels and their products, and historically the petrochemical industry has focused on 7 low cost, high volume commodity chemicals (methanol, ethylene, propene, butadiene, benzene, toluene and xylene), which are then used to manufacture nearly all other commodities (Dudley et al. 2015). Given that fossil fuels are a finite resource, their limited supply demands the development of renewable alternatives to petrochemically-derived products. There have been advances towards this, for example, the process of producing polylactide and polyethylene from lactic acid and ethylene has reached the stage of being industrially produced from biomass-derived lactic acid (Singhvi and Gokhale 2013). However, other commercial platform chemicals are still mass produced via petrochemical processes which utilize fossil fuels as the starting raw materials (Erickson et al. 2012). In recent years, increasing attention has shifted towards the sustainable production of chemicals given global concerns on the environment, limited resources and high oil prices (Dudley et al. 2015, Guterl and Sieber 2013).

One such platform chemical in high global demand is malic acid. Malic acid, along with other four carbon diacids such as succinic and fumaric acid, was reported as one of the top value-added chemicals from biomass in a 2004 US Department of Energy report (Bozell and Petersen 2010). The four carbon diacids can be converted into 1,4-butanediol (BDO) which can be further converted into high-value commodities (Figure 1.1). Oil prices, climate change concerns and advances in the field of metabolic engineering have renewed interest in bio-based production of chemicals including malic acid (Rollin et al. 2013). The petrochemical paradigm will not be replaced in a hurry, advances in engineering however, can develop access to novel chemicals and materials based on richer building blocks than currently used today (Bozell and Petersen 2010).
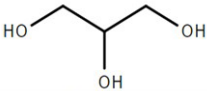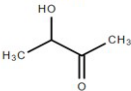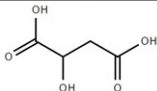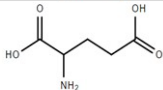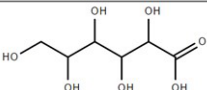
Name	Formula	Structure	Uses
Methanol	CH_3OH	$H_3C \longrightarrow OH$	Corrosion inhibitors, carpets, fabrics
Glycerol	$C_3H_8O_3$		Food packaging, fuels, gas purification
Acetoin	$C_4H_8O_2$		Molded plastics, paints, resins
Malic acid	$C_4H_6O_5$		Water chemicals, cleaners & detergents
Glutamic acid	$C_5H_9NO_4$		Cosmetics, aspirin, pharmaceuticals
Gluconic acid	$C_6H_{12}O_7$		Medical-dental products, suntan

Table 1.1. Examples of some platform chemicals, their formulas, structures and final products/uses in multiple industries such as, transportation, textiles, safe food supply, environmental, communication, housing, recreation and health and hygiene. All platform chemicals listed in the table have the potential to be produced from biomass feedstocks.

Biomass can be defined broadly as all matter on the earth's surface of biological origin and includes plant materials such as trees, grasses, agricultural crops, algal biomass and organic waste such as animal manure (Sengupta and Pike 2012). Biomass feedstocks replacing fossil feedstocks offer sustainable alternatives to the production of chemicals. Biomass degradation can be achieved in various ways such as enzymatic hydrolysis and chemical hydrolysis. Enzymatic hydrolytic processes offer an advantage in the sense that the hydrolysis of the biomass can be done simultaneously with the subsequent use of the hydrolysis products (Straathof 2014). Present strategies for obtaining chemicals from biomass feedstocks (Figure 1.1) focus greatly on the established fermentation techniques which involves the use of metabolic pathways of a living microbial cell (wild type or engineered) in a fermentation process. An alternative to using microbial cells for production of high value chemicals from biomass, is to use cell-free synthetic enzymatic pathways for which enzymes can be obtained from a single microorganism (Guterl et al. 2012).
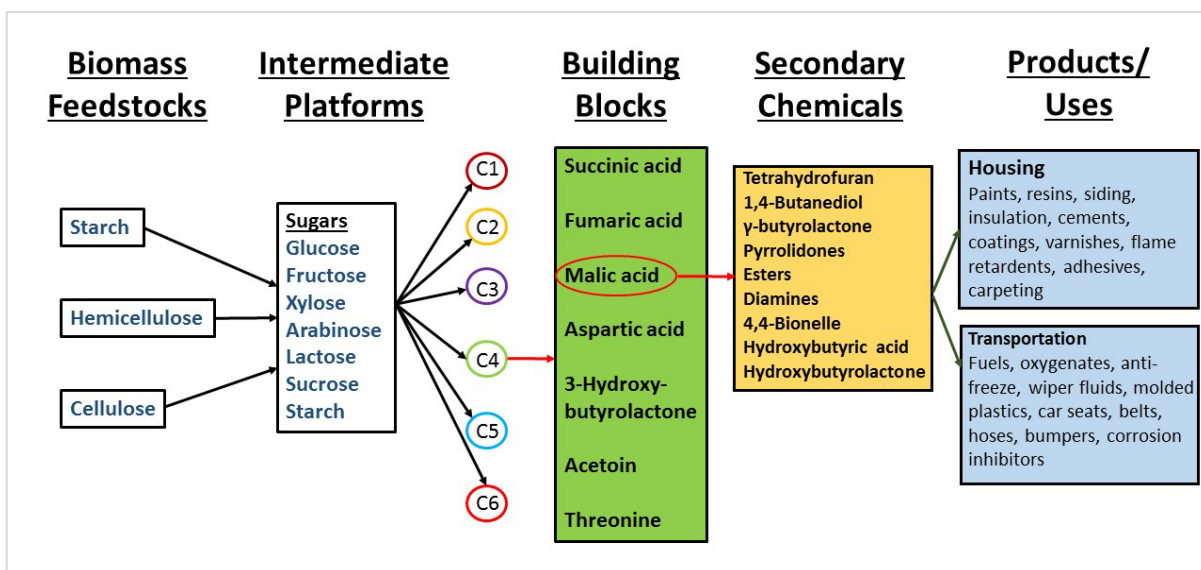
Figure 1.1. Figure based on the 2004 US Department of Energy report, model of a bio-based product flow-chart for biomass feedstocks, concentrating on the 4-carbon acid, malic acid.

1.2 Industrial production of malic acid

Malic acid, also known as 2-hydroxybutanedioic acid ($C_4H_6O_5$), is widely used in a range of industries. Malic acid along with succinic and fumaric acid are naturally occurring building blocks found as metabolic intermediates in most prokaryotic and eukaryotic microorganisms (Jang et al. 2012). Malic acid has commercially-diverse applications in the pharmaceutical, agricultural, food, synthetic resin and polymer industries (Deng et al. 2016, Zeikus et al. 1999). Malic acid is currently estimated to have a global market of $182.6 million, with increasing demand from the food and beverage industries for the use of malic acid as a flavour enhancer, forecasting industrial growth in the future. Commercial production of racemic malic acid is achieved by hydration of maleic anhydride and production was stated at 5000 tons/annum in the US (Miltenberger 2000). Maleic anhydride itself is produced petrochemically by vapour-phase oxidation of *n*-butane and has large scale applications in coatings and polymers. (S)-malic acid is also obtained in industry through the biocatalytic hydration of fumaric acid using fumarase for the production of pharmaceuticals (Takata and Tosa 1993). However, both of the production strategies utilise non-renewable sources and given the global demand of malic acid, it is only sensible that renewable alternatives should be sought after for large scale production of malic acid utilising renewable sources.

1.3 Biobased/biochemical production of malic acid

Malic acid alongside other C_4 acids, succinic and fumaric, are naturally occurring intermediates in the tricarboxylic acid (TCA) cycle and are naturally produced by many organisms (Figure 1.2).
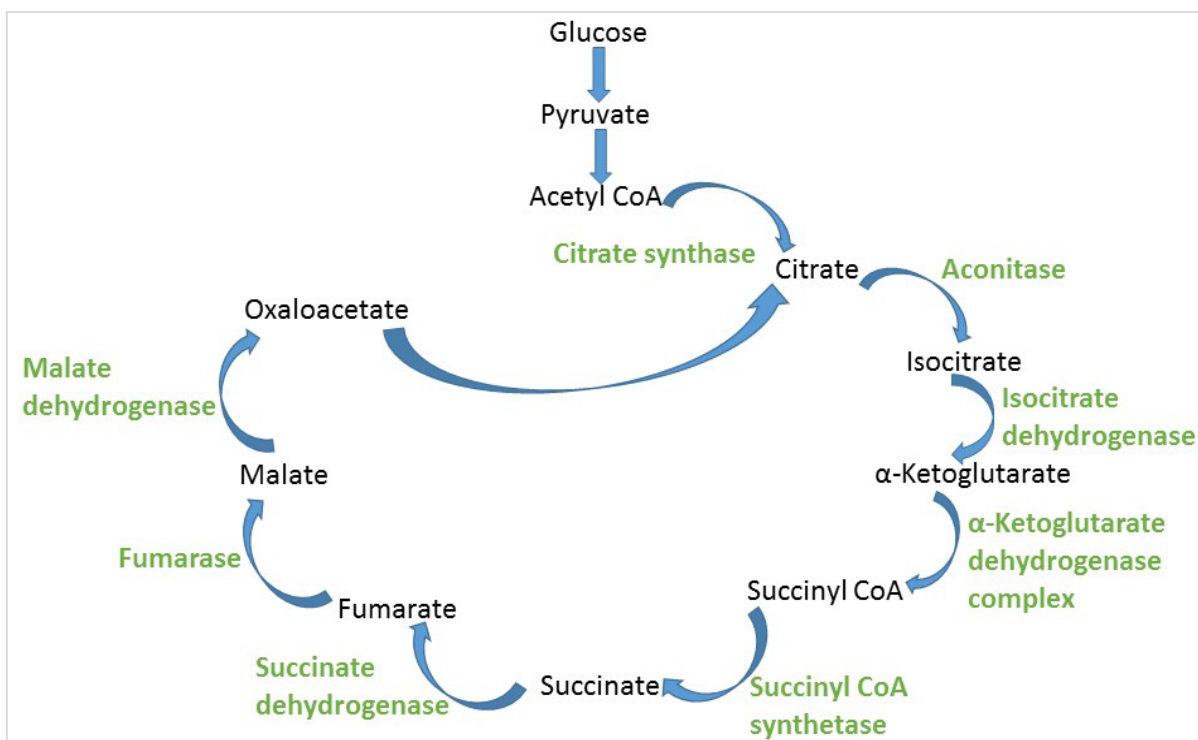
Figure 1.2. Schematic representation of the tricarboxylic acid (TCA) cycle with major intermediates and the enzymes catalysing these reactions. (Cofactors are not shown for simplicity).

When comparing the methods of production for malic acid, its bio-based production is superior to its chemical synthesis in terms of stereo-selectivity whereby the current chemical process produces a racemic mixture (Jang et al. 2012). The first patent for the production of l-malic acid via fermentation was filed in 1960 (Abe et al. 1962). An *Aspergillus flavus* strain was selected to be the best natural producer and optimization of the fermentation process resulted in final titres of 58.4g/litre after 9 days of fermentation. Later studies using the same strain reported that *de novo* enzyme synthesis during nitrogen starvation increased malate synthesis (Peleg et al. 1988). Carbon-13 nuclear magnetic resonance analysis of the products in the same study identified that the majority of the malic acid was produced via the reductive TCA cycle branch (pyruvate via oxaloacetate to malate) (Figure 1.2). Later optimizations with *A. flavus* have been reported to produce 113g/litre l-malic acid (Battat et al. 1991). Despite achieving high yields and titres, natural high capacity malic acid producers like the *A. flavus* have been disqualified from use in industrial production due to aflatoxin (carcinogen) production and/or special growth requirements, thereby well-characterized microorganisms such as yeast and *E. coli* are of more interest to researchers to produce malic acid (Jang et al. 2012). *Aspergillus oryzae* is a close relative or even an ecotype of the *A. flavus* and it was speculated that the former's high malic producing capability, which is generally regarded safe, can be paired with existing large scale fermentation (Payne et al. 2006). The yields achieved with *A. oryzae* are comparable to those of highly engineered *Escherichia coli* and exceed those of *Saccharomyces cerevisiae*. Further study explored the

possible use of *A. oryzae* on an industrial scale and predicted metabolic engineering targets to increase yields such as the over expression of pyruvate carboxylase (Knuf et al. 2013).

1.3.1 Using yeast for production of malic acid

Malic acid in fermented products derived from various fruit juices has been early knowledge and it had been generally supposed this was exclusively derived from preformed malic acid in the fruit. However, in 1924 it was established that l-malic acid is a product of fermentation when carrying out pure sugar solution fermentation by pure yeast cultures (Dakin 1924). Fermentative production of malic acid has since been successfully demonstrated in other organisms. One notable example is *S. cerevisiae* where a high yield of 12g/litre through the overexpression of cytosolic malate dehydrogenase was achieved (Pines et al. 1997). Another yeast strain to have demonstrated malic acid yield of up to 75g/litre is a natural isolate of *Zygosaccharomyces rouxii* under the optimum conditions of 30% glucose, initial pH 5.0 and 25°C incubation temperature. Acid precursors such as glutamic, malic and succinic aid the production of malic acid whereas this is not the case for another four carbon acid, succinic acid (Taing and Taing 2007).

There are four metabolic pathways for the production of malic acid in *S. cerevisiae* from glucose as represented in Figure 1.3 (Zelle et al. 2008):

1. Carboxylation of pyruvate to oxaloacetate, followed by the direct reduction of oxaloacetate to malate. Given that the pyruvate is end product of glycolysis, this nonoxidative pathway is ATP neutral and involves net fixation of CO_2.
2. Condensation of oxaloacetate and acetyl-coenzyme A to citric acid, followed by its oxidation to malate via the tricarboxylic acid cycle.
3. Formation of malate from 2 molecules of acetyl-CoA via the glyoxylate pathway.
4. Noncyclic pathway utilising glyoxylate cycle enzymes but oxaloacetate is replenished by pyruvate carboxylation.
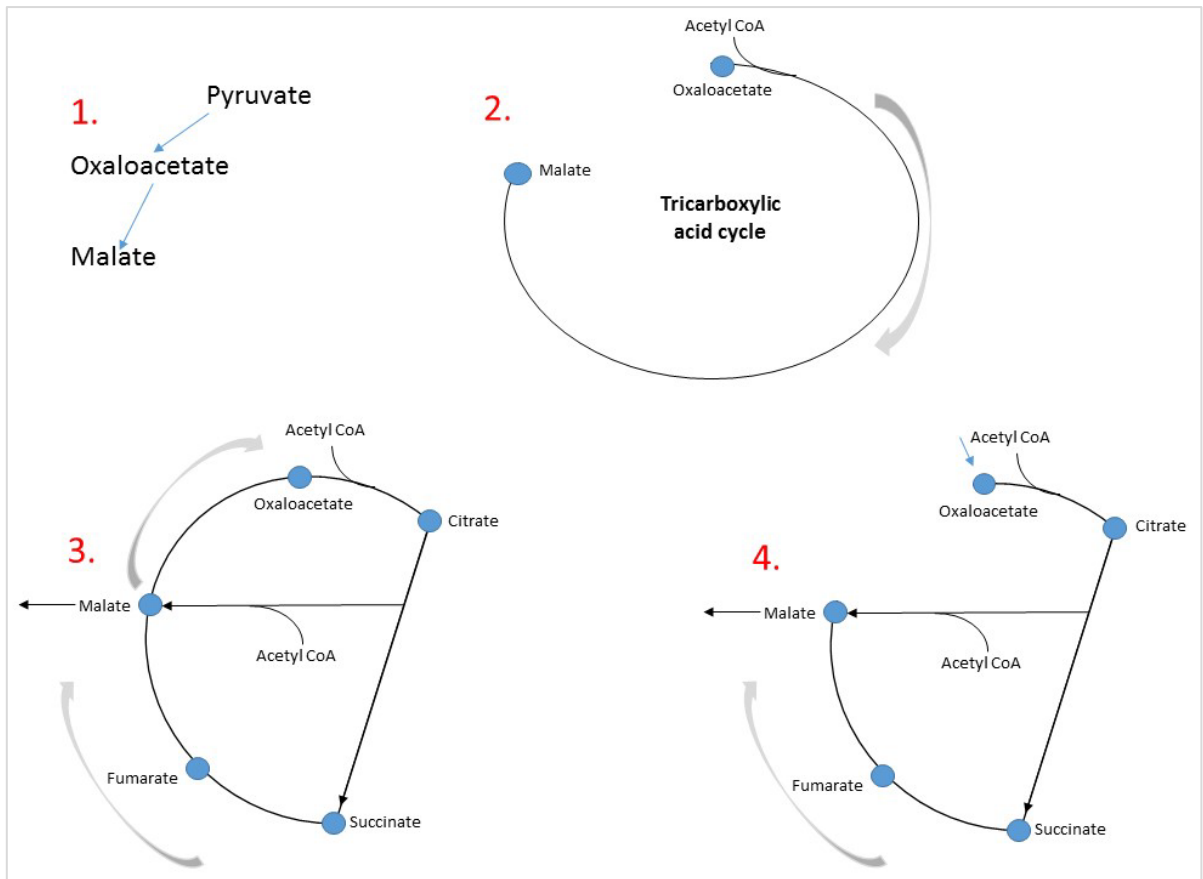
Figure 1.3. Four possible pathways for production of malate in S. cerevisiae as adapted from 'Malic acid production by Saccharomyces cerevisiae: Engineering of pyruvate carboxylation, oxaloacetate reduction, and malate export' (Zelle et al. 2008). All possibilities represent oxaloacetate and/or acetyl CoA as starting points. 1. Direct reduction of oxaloacetate to malate. 2. Condensation of oxaloacetate and acetyl-coenzyme A to citric acid, followed by its oxidation to malate via the tricarboxylic acid cycle. 3. Formation of malate from 2 molecules of acetyl-CoA via the cyclic glyoxylate pathway. 4. Noncyclic pathway utilizing glyoxylate cycle enzymes, but oxaloacetate is replenished by pyruvate carboxylation.

S. cerevisiae requires metabolic engineering for high production of organic acids such as malic due to the necessity to eliminate alcohol fermentation, which in this strain takes place even under full aerobic conditions given the presence of high sugar concentrations (Postma et al. 1989). The obstruction of metabolic redirection towards fermentation can be prevented by deletion of the 3 *S. cerevisiae* pyruvate decarboxylase genes (*PDC1, PDC5 and PDC6)*. Deletion of either *PDC1* or *PDC5* genes has little or no effect on the enzyme activity, however deletion of both *PDC1* and *PDC5* leads to undetectable enzyme activity in mutants. Product of *PDC6* on the other hand, does not seem to be required for wild-type enzyme activity in glucose medium (Hohmann 1991). Pyruvate decarboxylase-negative (Pdc−) strains seem to offer the perfect platform for metabolic engineering to direct reaction towards higher malate producing strains, however, C_2 compound auxotrophy and intolerance to high glucose concentrations hinder developments. Furthermore growth in synthetic medium in glucose limited chemostat cultures requires addition of ethanol or acetate and even in the presence of C_2 compound, these strains cannot grow (Flikweert et al. 1999). Application of evolutionary engineering in batch and

chemostat cultures identified a glucose tolerant, C_2-independent Pdc– *S. cerevisiae* strain. Under aerobic conditions, this strain demonstrated a high production of pyruvate, 135g/litre, a vital intermediate to malate production (van Maris et al. 2004). Keeping with all these factors, a favourable pathway for efficient malate production in yeast proceeds via carboxylation of pyruvate, followed by reduction of oxaloacetate to malate with a theoretical maximum yield of 2 mol malate/mol glucose. Introduction of 3 genetic modifications into an engineered glucose tolerant, C_2-independent Pdc– *S. cerevisiae* strain was used to explore the effect of these modifications. The modification was as follows:

1. Overexpression of native pyruvate carboxylase encoded by *PYC2*.
2. High level expression of an allele of malate dehydrogenase gene (*MDH3)* of which the encoded gene was retargeted to the cytosol via the deletion of the C-terminal peroxisomal targeting sequence.
3. Functional expression of the *Schizosaccharomyces pombe* malate transporter gene SpMAE1.

This research identified that the simultaneous introduction of all of the above modifications led to the highest malate yields and titres. In glucose growth batch cultures, malate production at titres of up to 59g/litre were achieved (Zelle et al. 2008).

1.3.2 Using bacteria for production of malic acid

E. coli is an excellent established biocatalytic platform for metabolic engineering. Variations of *E. coli* have been modified for the production of a four carbon acid, succinic acid (Jantama et al. 2008). A previously-engineered *E. coli* strain optimized for succinate production by increasing expression of pyruvate carboxykinase, includes malate as an intermediate in the process, requiring only a single reducing equivalent for synthesis from phosphoenolpyruvate. Mutation in fumarate reductase was sufficient to redirect reaction to malate. Using a two stage production system of aerobic cell growth and anaerobic malate production, the final strain (XZ658) was able to produce malate yields of 34g/litre, which at the time was equal or better than those of other known biocatalysts (Zhang et al. 2011).

E.coli serves as a key component in the biobased production of chemicals as synthetic metabolic engineering enables the construction of *in vitro* synthetic pathways through heat-treatment of the recombinant mesophiles having thermophilic enzymes. A key study constructed a synthetic pathway capable of direct conversion of glucose to malate (glucose + $2HCO_3^-$ +2H $\rightarrow$ 2 malate + $2H_2O$). The key enzyme in this pathway carrying out the reversible carboxylation of pyruvate is the malic enzyme derived from *Thermococcus kodakarensis*. This enzyme was coupled with a non-ATP-forming Embden-Meyerhof pathway to establish balance and regeneration of cofactors. *T. kodakarensis* malic enzyme

exhibits both malate forming (pyruvate carboxylation) and lactate forming (pyruvate reduction) activities, coupled with the concomitant oxidation of NAD(P)H to NAD(P)$^+$ and the concomitant reduction of NAD(P)$^+$ to NAD(P)H respectively. The coupling of the malic enzyme with thermodynamically favourable NAD(P)H regeneration enzymes theoretically shifts the equilibrium towards malate production (Figure 1.4). This CO_2 reduction mediated by the malic enzyme has been explored more in depth in recent years as it offers a promising approach to the greenhouse gas fixation and the production of useful commodities. The study was able to achieve a direct conversion of glucose to malate with a molar yield of 60% (Ye et al. 2013).
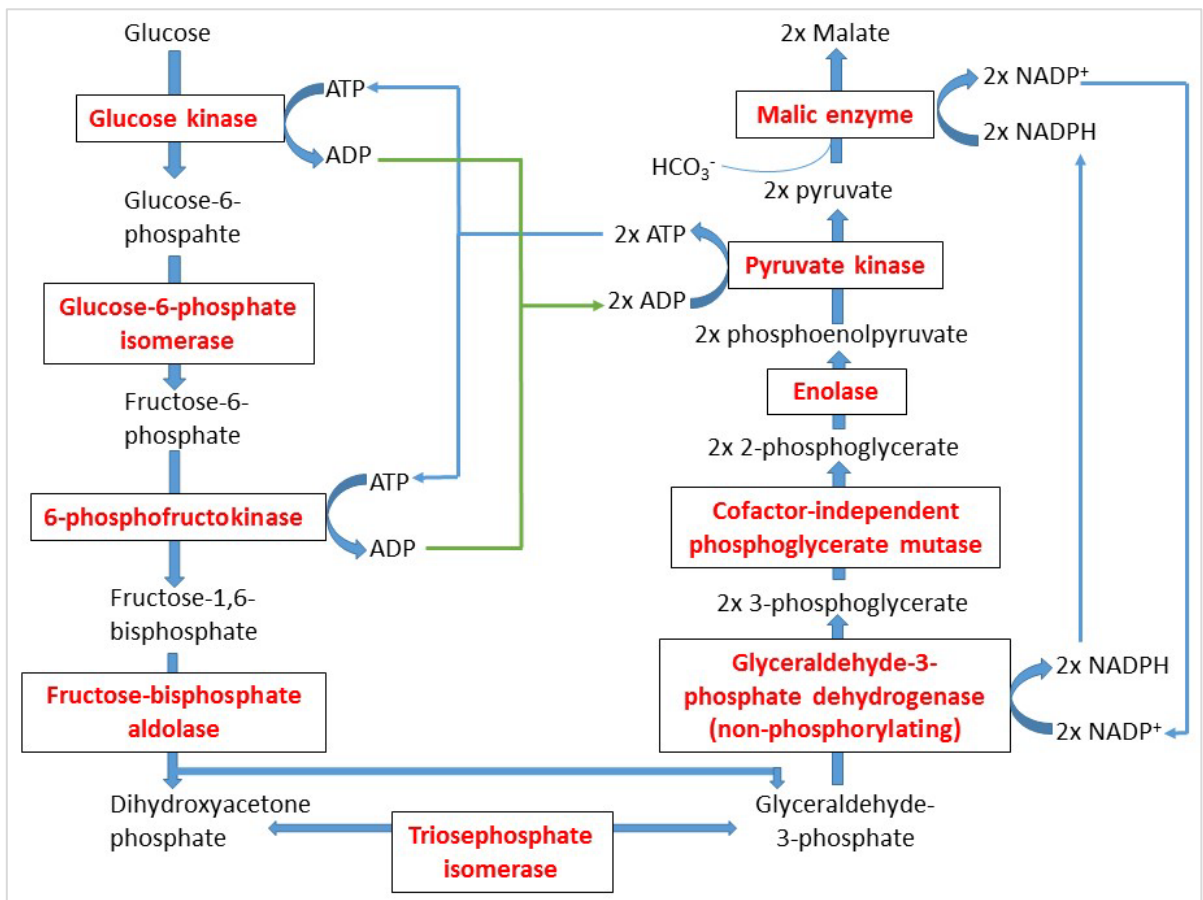
Figure 1.4. Schematic representation of artificial synthetic pathway designed for the direct conversion of glucose to malate, adapted from 'Direct conversion of glucose to malate by synthetic metabolic engineering' (Ye et al. 2013) All enzymes employed were sourced from thermotolerant sources: 7 glycolytic enzymes from *Thermus thermophilus*, cofactor-independent phosphoglycerate mutase from *Pyrococcus horikoshii*, non-phosphorylating glyceraldehyde-3-phosphate dehydrogenase and Malic enzyme from *Thermococcus kodakarensis*.

1.3.3 Other methods of malic acid production

Malic enzyme has been the focus of other studies in order to improve production of malic acid. As the general forward thermodynamically favourable reaction of malic enzymes is converting malate to pyruvate, reverse reaction of the enzyme is required. Malic enzyme of *Pseudomonas diminuta* IFO 13182 was used in a reverse reaction for HCO_3^- fixation into pyruvic acid to produce l-malic acid with cofactor regeneration (NADH). Glucose-6-phosphate dehydrogenase obtained from *Leuconostoc*

mesenteroides was used for the cofactor regeneration resulting in the production ratio of 38% after 24 hours of incubation at 30°C (Ohno et al. 2008). Similarly in an experiment carried out using malic enzyme of *Brevundimonas diminuta* IF013182 coupled with the electrochemical regeneration of NADH on an enzyme-mediator-immobilized electrode, resulted in the production of nearly 1.1mmol of malate from 12.5mmol of pyruvate and 2.5mmol of $NaHCO_3$ in 48 hours (Zheng et al. 2009).

1.4 Improving biobased strategies of malic acid production

Biobased strategies such as fermentation have limitations that restrict their large-scale industrial applications. Current microbial biomanufacturing is hindered by the limitations caused by cells, as synthetic pathways and their optimizations are restricted by the physiological limits of the cellular production system (Dudley et al. 2015). A key challenge is the requirement to control a cell's multiple metabolic pathways that lead to formation of unwanted intermediates (Guterl et al. 2012), thereby reducing conversion efficiencies. Moreover, construction of artificially-engineered pathways in living organisms leads to competition with the natural metabolic pathways of the cell for intermediates and cofactors which results in unsatisfactory yields of the actual product of interest. Furthermore, yields of target molecules are limited to non-toxic levels only (Matsuda et al. 2013). Ultimately, engineering synthetic pathways in cells leads to a competition between the cellular physiological and evolutionary objects and the process aims (Dudley et al. 2015, Kwok 2010).

There is a key idea that can be adapted to overcome the issues discussed above in biobased production of commodities including malic acid, called cell-free metabolic engineering (CFME). In a nutshell, the founding idea of CFME is the synthesis of complex biomolecular commodities without using intact cellular systems (Swartz 2012), but instead using purified enzyme systems or crude cell lysates (Dudley et al. 2015). CFME is orchestrated in a strategy which involves avoiding using living microorganisms and uses only enzymes involved in the synthetic pathways (Ninh et al. 2015). Although engineering on microbial hosts and single enzyme systems have been in use for some time now, developing cascades consisting of multiple enzymes in cell-free pathways is a recent development in comparison (Petroll et al. 2019) However, the practical applications of using enzymatic production systems has not been paid much attention owing to the economical unprofitability of processes involving enzyme purification which tends to be time and cost consuming. Hence, it is a critical issue hindering the possible industrialisation of these systems. Enzymatic production systems need to address the crucial factors of low cost stable biocatalytic module production with a high total turnover number (Ye et al. 2013).

	Cell systems		Cell-free systems	
	Advantages	**Disadvantages**	**Advantages**	**Disadvantages**
Pathway engineering	-Directed evolution	-Overproduction is typically opposed to microbe's goal -Cellular regulation difficult to predict/modify	-Chimeric pathways combined from multiple organisms -Allows for mixing with chemical catalysis which would be cytotoxic to cells	
Yields	-High yields achievable following optimization (Abe et al. 1962, Battat et al. 1991, Taing and Taing 2007)	-Low yields due to resources diverted to cellular metabolism and by-product formation -Occurrence of parallel reactions, product of metabolic activity may bear no structural resemblance compounds supplied	-No cellular pathways to compete for available resources -Can use higher enzyme concentrations than used in-vivo to increase yields	
Cell wall	-Allows for use of membrane proteins	-Barrier; product excretion can become a challenge	-Easy sampling and direct addition/ subtraction of substrate/product respectively	
Yield toxicity		-Viability of host compromised	-No viability constraints	
Stability		-Fermentation conditions can affect intracellular environment	-Controlled reactions by investigator -More resistant to conditions than living cells	
Cost	-Low; subject to high yields and low product extraction			-Catalyst cost and purification must be incorporated -Cofactor costs
Scaling up	-Fermentation heterogeneous at an industrial scale	-Contamination	-Linear scale-up	-System consistent at lab and larger scales
Maturity	-Well established methods with extensive practical knowledge		-Simpler systems	-Recently established

Table 1.2. Comparisons of cell and cell-free systems are shown with relevant advantages and disadvantages within various subfields as highlighted in 'Cell-free metabolic engineering: Biomanufacturing beyond the cell' (Dudley et al. 2015) and 'New biotechnology paradigm: cell-free biosystems for biomanufacturing' (Rollin et al. 2013).

1.5 Cell-free metabolic engineering

CFME is pushing the boundaries of traditional bioengineering models by focusing on the use of *in vitro* combinations of catalytic proteins prepared from purified enzymes or crude lysates of cells for production of target commodities. In recent years, developments in the engineering foundations of cell-free systems have been inspired and have led to the establishment of long enzymatic pathways, near theoretical conversion yields and new directions in protein purification, spatial organisation and enzymatic stability (Dudley et al. 2015). Various examples have also demonstrated that avoiding the cell barrier gives more control on the metabolism leading to efficient and broader production of metabolites (Rollin et al. 2013, Swartz 2018). One of the biggest potential applications of cell-free systems over microbial fermentation is the ability to catalyse biotransformations that cannot be done by microbes or chemical catalysts (Rollin et al. 2013)

Using enzymes commercially has traditionally been limited to single reactions or very short pathways (Straathof 2014). In the context of engineering, CFME has two approaches, purified enzymes or crude extracts. CFME research has largely focused on the use of individually purified enzymes that have been recombined to assemble the pathway of interest. These pathways can be precisely controlled as component variables, such as concentration and activity, are largely known. However, major challenge comes in the form of cofactor cost and regeneration (Rollin et al. 2013). Crude lysates or cell extracts on the other hand offer advantages in applications where lower costs and complex metabolic systems are required as they are cheaply generated and can contain a lot of proteins naturally present in cell metabolism (Swartz 2018). This can either be an advantage or disadvantage as the native metabolism if unwanted, can be difficult to eliminate or model. A further advantage offered by cell-free systems is that absence of substrate toxicity constraints (Takors 2012) and the potential handling of otherwise toxic/unstable intermediates (Schrittwieser et al. 2018). Other factors such as lower DNA synthesis prices, improved engineering and expression technologies have contributed to better access to enzymes utilized in cascade reactions (France et al. 2017).

1.5.1 Purified enzymes cell-free cascade systems

One of the early examples of cell-free systems was the production of ethanol from isolated yeast glycolytic enzymes (Welch and Scopes 1985) and since then a range of purified enzyme systems have been explored. Their development has brought to light a set of general rules in order to achieve high productivities and these guidelines closely mimic the vital properties of the *in vivo* state of growing cells, which is suggested to be the key to successful applications of CFME (Dudley et al. 2015)

1. Stable and robust enzymes.
2. Enzyme ratios and substrate/cofactor/buffer concentrations.

3. Providing a thermodynamic push towards product of interest (i.e. cofactor regeneration, product removal, substrate feeding).

Artificial metabolic pathways are becoming well explored approaches for biotransformation of industrial chemicals, however due to the separate preparation and purification required for this, the practical applications are limited. A study addressing this key challenge took genes encoding 9 thermophilic enzymes involved a non-ATP-forming chimeric glycolytic pathway and assembled them in an artificial operon and co-expression all of them in a single recombinant *E. coli* strain. The gene expression levels of the enzymes were controlled by their sequential order in the artificial operon. Interestingly, the study identified that the specific activities of the enzymes in the cell-free extract of the multiple-gene-expression *E. coli* were 5.0-1,370 times higher than those of an enzyme cocktail obtained from over expressed single-gene-expression strains. The purification strategy employed here consisted of the multiple-gene-expression cells being heat treated leading to indigenous protein denaturation. By coupling the heat-treated extract with other thermophilic enzymes such as H_2O forming NADH oxidase or lactate/malate dehydrogenase, one pot conversion of glucose to pyruvate or lactate respectively, was achieved (Ninh et al. 2015).

A key paper in the field of purified enzyme systems accomplished the conversion of glucose to ethanol and isobutanol using 6 and 9 enzymes respectively (Figure 1.5). The ubiquitous Embden-Meyerhof-Parnas pathway was shortened by using enzymes from hyperthermophilic archaea in a modified non-phosphorylative Entner-Doudoroff pathway. The crucial factor of cofactor balance was demonstrated in this paper as glucose was converted to pyruvate, generating 2 NADH in the process which were then recycled in the later step of conversion to isobutanol. This reaction produced a 57% molar yield of ethanol from glucose, which remains one of the best reported examples to date (Guterl et al. 2012). This study demonstrated the possibilities for constructing enzymes in artificial non-natural cascades, rather than 10 enzymes required by yeast cells to convert glucose to pyruvate, this minimized cascade used only 4. This minimized production is possible due to the intermediates not being required for the complicated cellular metabolic associated with whole cell approaches (Sperl and Sieber 2018). In another example, using the same first 4 enzymes in pathway design as the cascade by Guterl et al 5 thermophilic enzymes were utilized in a NADH balanced system to facilitate the conversion of glucose to lactate with a yield of ~90% (Xie et al. 2018).
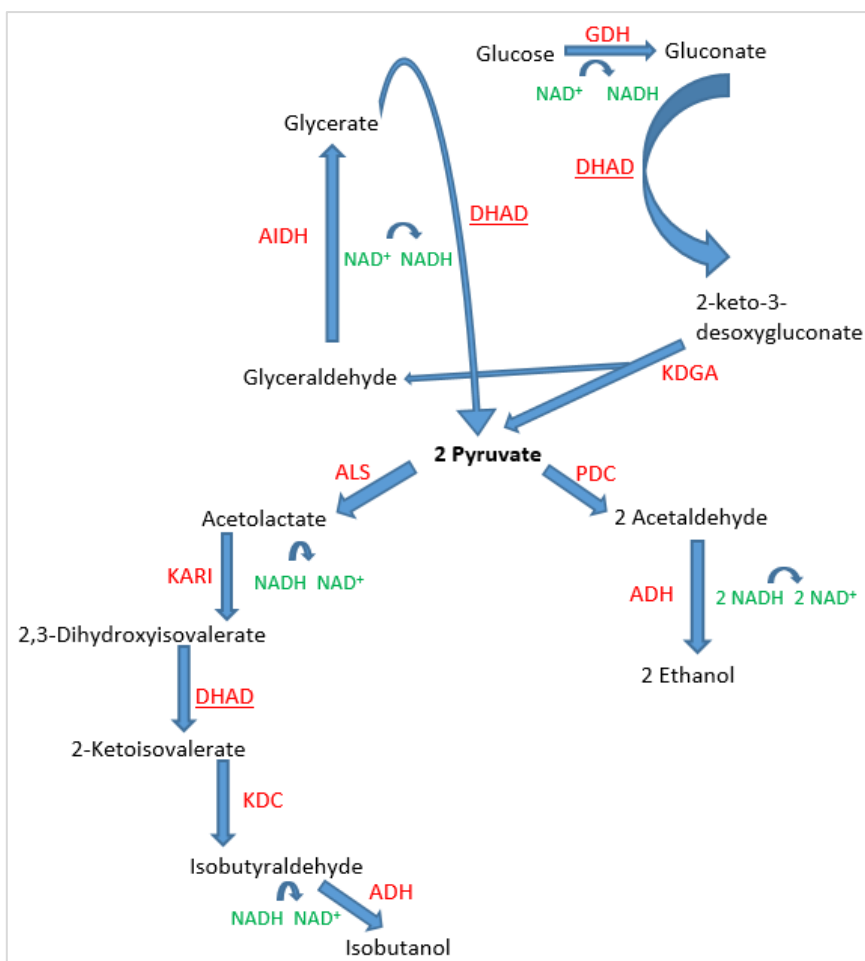
Figure 1.5. Schematic representation of cell free systems developed for the production of isobutanol and ethanol from glucose adapted from 'Cell-free metabolic engineering: production of chemicals by minimized reaction cascades' (Guterl et al. 2012). GDH, glucose dehydrogenase; DHAD, dihydroxy-acid dehydratase; KDGA, 2-keto-3-deoxygluconate aldolase; AIDH, glyceraldehyde dehydrogenase; PDC, pyruvate decarboxylase; ADH, alcohol dehydrogenase; ALS, Acetolactate synthase; KARI, ketolacid reductoisomerase; KDC, 2-ketoacid decarboxylase.

Artificial enzymatic cascades are fundamentally renewable alternatives to petrochemicals, but their appeal is further amplified as some systems have been designed to use by-products of other reactions as substrates or intermediates in further downstream processing. Glycerol is a by-product of bioethanol and biodiesel production, for example, during the industrial production of bioethanol, the fermentation of sugars by yeast is accompanied by significant production of glycerol (Rausch and Belyea 2006). At the time of publication, it was estimated that the world production of glycerol would reach 4200,000 tonnes by 2020 (Viana et al. 2014). However, the current industry glycerol applications require approximately a quarter of the total production, thus encouraging any developments of new processes that can facilitate the conversion of glycerol to high value goods.

Heterogeneous or homogeneous catalysis can be used with glycerol to obtain high value goods but biocatalysis is preferred as glycerol can be usually incompatible with chemical transformations due to its availability in dilute aqueous solutions. Despite this, conversion efficiencies are plagued by the ubiquitous issue of unwanted intermediates due to the multitude of cellular pathways. A cell-free

biosystem seems like the perfect answer but if production were to be approached in the natural metabolic pathways of glycerol metabolism, an excess of 8 enzymes are required to form pyruvate which is a central key intermediate. Gao et al addressed these exact issues and developed an artificial system facilitating the conversion of glycerol into pyruvic acid using only 3 enzymes, eliminating any need for additional cofactors. 9.3mM pyruvic acid was produced from 10mM glycerol and pyruvate was further converted to another useful four carbon commodity, acetoin, using two additional enzymes in a cell free environment as well. This cell-free system focuses on the production of pyruvate and since that is a key intermediate, this synthetic pathway has potential to be developed as a versatile bio-production system (Gao et al. 2015).

Hydrogen is a future energy carrier and a strong chemical commodity and currently can be produced via chemical/biocatalysis/combination of both (Zhang 2010). Hydrogen-producing microbes give a theoretical maximum yield of 4 hydrogen molecules per glucose, and to increase this yield, a non-natural synthetic pathway consisting of 13 enzymes was reported to demonstrate the feasibility of almost 12 hydrogen molecules per glucose from starch (Zhang et al. 2007). Further experimental work was able to expand the substrate range to include multiple glucan sources (Ye et al. 2009), leading to demonstration of sustainable approaches from using biomass feedstocks and stepping back from reliance on non-renewable feedstocks. Sustainable development of the corn starch industry was also addressed in a study where an enzymatic system with multiple enzymatic cascades was developed for formation of valuable platform chemicals from lactate separated from corn steep water. Pyruvate was produced as an important intermediate followed by conversion into acetaldehyde and acetoin which are further valuable platform chemicals (Li et al. 2017).

In recent years, the number of enzymatic cascades published for synthesis of commodities is growing steadily, however CFME has its own set of challenges, working with non-optimized catalysts can make defining operational windows difficult. Therefore, the enzymes to be employed must demonstrate excellent process stabilities as well as being available at low costs and large scale. Cofactor stability/regeneration also has to be taken into account in this context and enzyme recyclability and reusability are also of vital importance for economic analysis (Guterl and Sieber 2013). The following sections outline the challenges associated with designing efficient enzyme cascade systems and the solutions used to overcome them.

1.6 Applications of thermophiles in CFME

As previously highlighted, the stability and purification of enzymes to be utilized in enzymatic cascades have to be considered for achieving a feasible system. Display of stability at extreme temperatures by thermophiles can be accompanied by additional properties such as low water activity and high

hydrostatic pressure. The environments colonised by thermophiles include hot springs, fumaroles, submarine hydrothermal vents and oil reservoirs, and thermophiles are mainly archaea with some having been classified as eubacteria (Sellek and Chaudhuri 1999). Thermophilic enzyme production can be expressed in a native thermophilic host; however cultivation of any extremophile is not easy. It requires specialist equipment and faces slow growths and low yields, meaning heterologous gene expression using a common host such as *E. coli* is much preferred. The nutritional requirements for these thermophiles vary and therefore they are host to a wide variety of useful enzymes (Sellek and Chaudhuri 1999). The enzymatic cascade examples given in the previous section have already stated how some examples have utilized enzymes of thermophilic origin to design artificial reaction pathways. This is due to application of thermotolerant enzymes mitigating some of the major challenges facing CFME approaches. Despite the potential advantages of cell-free systems, there are four key challenges that require optimization if commercial application of these systems is to be tackled. These are: low-cost enzyme production, prolonged enzyme stability, enzyme/cofactor engineering and pathway optimization/modelling (Rollin et al. 2013). In response to tackling the first two challenges, heat treatment of recombinant mesophiles results in a one-step preparation of an enzyme cocktail avoiding costly purification strategies and the high operational stability of enzymes of thermophilic origin mitigate the challenges of protein synthesis and renewal (Ninh et al. 2015). For most approaches to tackling enzyme stability issues, using thermotolerant enzymes is usually a fair starting point, and if there is no thermotolerant enzyme available for the mesophilic enzyme equivalent, enzyme engineering can be next explored (Zhang 2015).

1.6.1 Exploiting unique metabolic enzymes found in thermophiles

Not only do thermophilic enzymes offer the advantages in low-cost enzyme production and long-term enzyme stability, unique metabolic pathways found in hyperthermophilic archaea contain unique metabolic enzymes with applications in enzymatic cascades. The Entner-Doudoroff pathway was first discovered in 1952 in *Pseudomonas saccharophila* and has been viewed as an alternative to the Embden-Meyerhof-Parnas glycolytic pathway (Conway 1992). Archaea have a complicated carbohydrate metabolism and utilize glucose via modifications of the classic Embden-Meyerhof-Parnas and the Entner-Doudoroff pathways. In the thermophilic aerobic archaeon *Sulfolobus solfataricus*, glucose degradation occurs via a branched Entner-Doudoroff pathways with a semi-phosphorylative and a non-phosphorylative branch (Siebers and Schonheit 2005, Ahmed et al. 2005). Due to the lack of a functional phosphofructokinase, the Embden-Meyerhof-Parnas is supposed to function for gluconeogenic purposes only (Kouril et al. 2013). The classical branch (phosphorylative) of the Entner-Doudoroff pathway seem to be only found in bacteria, however modifications such as the semi-

phosphorylative and a non-phosphorylative branches have been reported in all 3 domains of life: archaea, bacteria and eukarya (Conway 1992).

Glucose
NAD(P)H ← | Glucose dehydrogenase
Gluconate
| Gluconate dehydratase
2-keto-3-deoxygluconate
Pyruvate ← | 2-keto-3-deoxygluconate aldolase
Glyceraldehyde
Glyceraldehyde dehydrogenase | → NAD(P)H
Glycerate
Glycerate kinase | — ATP
2-phosphoglycerate
Enolase |
Phosphoenolpyruvate
Pyruvate kinase | → ATP
Pyruvate
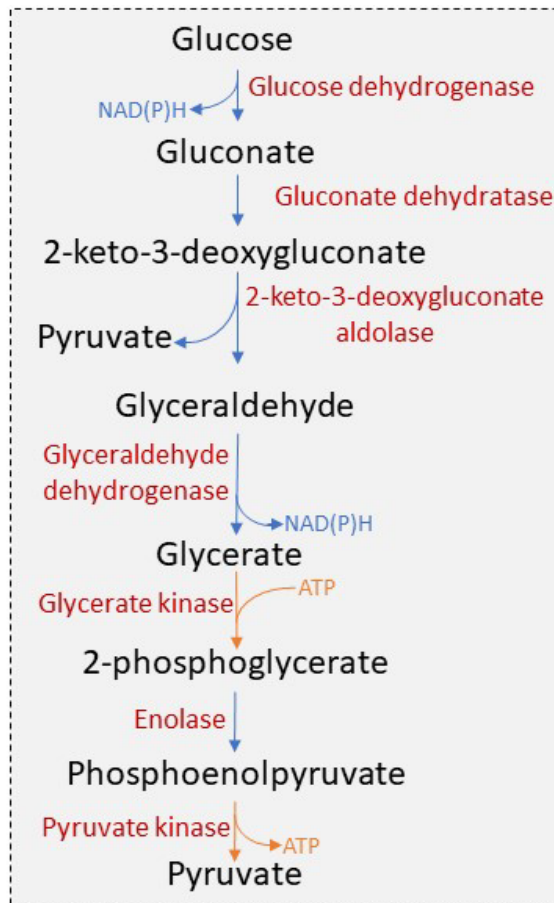
Figure 1.6. Overview of the non-phosphorylative Entner-Doudoroff pathway, with enzymes and characteristic phosphorylation level indicated (orange).

In both of the branches (semi-phosphorylative and non-phosphorylative), glucose is oxidized to gluconate by glucose dehydrogenase (Milburn et al. 2006), followed by dehydration of gluconate to 2-keto-3-deoxygluconate by dihydroxy-acid dehydratase (also referred to as gluconate dehydratase in literature) (Kim and Lee 2006). After these first two reactions the branches have the following reactions. In the semi-phosphorylative branch, 2-keto-3-deoxygluconate is phosphorylated by 2-keto-3-deoxygluconate kinase into 2-keto-3-deoxy-6-phosphogluconate. This is followed by the latter's cleavage by 2-keto-3-deoxygluconate aldolase into one molecule of glyceraldehyde-3-phosphate and pyruvate (Lamble et al. 2005). Glyceraldehyde-3-phosphate is degraded further by a $NADP^+$ dependent non-phosphorylating glyceraldehyde-3-phosphate dehydrogenase forming 3-phosphoglycerate and NAD(P)H and H^+ (Ettema et al. 2008). The resulting 3-phosphoglycerate can then be metabolized in the lower Embden-Meyerhof-Parnas pathway to yield the second pyruvate molecule. In the non-phosphorylative branch of the Entner-Doudoroff pathway, the 2-keto-3-deoxygluconate formed is not phosphorylated but undergoes cleavage via the same 2-keto-3-deoxygluconate aldolase into one

molecule of glyceraldehyde and pyruvate (Kouril et al. 2013). Glyceraldehyde is then oxidized into glycerate via aldehyde oxidoreductase followed by the conversion of glycerate into 2-phosphoglycerate via glycerate kinase (Kardinahl et al. 1999). Similarly to the semi-phosphorylative branch, the resulting 2-phosphoglycerate can then be metabolized in the lower Embden-Meyerhof-Parnas pathway to yield the second pyruvate molecule. The physiological significance and regulation of the semi-phosphorylative and non-phosphorylative branches are not clearly understood, however it has been suggested that the presence of 2 branches have a role in thermoadaptation of organisms growing at high temperatures (Ahmed et al. 2005), and the different pathways in vivo and their selection has been suggested to depend on the energy demands of the cell (Ahmed et al. 2005).

There are two key enzymes associated with the Entner-Doudoroff pathway, dihydroxy-acid dehydratase which catalyses the dehydration of gluconate to form 2-keto-3-deoxygluconate, and 2-keto-3-deoxygluconate aldolase which catalyses the cleavage of 2-keto-3-deoxygluconate to form pyruvate and glyceraldehyde. Given the unique metabolic pathways these enzymes are involved with the added benefit of unique reaction parameters (substrate promiscuities and specificities), enzymes of the thermophilic origin offer advantages in enzyme stability and ease of purification if incorporated into the pathway design of cell-free cascades, as well as non-natural pathway design construction via combinations of mesophilic and thermophilic proteins.

1.7 Cofactor balance

Many proof-of-concept pathways have been successfully demonstrated at the lab scale but it is still uncertain to what extent CFME systems can serve as commercial production systems. Another key barrier presents itself in the form of cofactor regeneration. Purified enzyme systems are required to supplement the reaction with the necessary cofactors. The nicotinamide nucleotides NAD^+ and $NADP^+$ are used by most redox enzymes and their balance is crucial in cell-free enzymatic pathways which lack metabolic regulation from living cells (Dudley et al. 2015). Co-factor balance needs to be crucially maintained as unbalance can lead to the disruption of the entire cascade. Cofactor costs and instability has led to developments in the design of cell-free systems that are not only cofactor balanced but attention is paid to ensure cofactor regeneration in the cascade, furthermore, to be economically viable, cofactor regeneration methods must be able to recycle the cofactor at least 100 to 10^6 times (Chenault et al. 1988). Cofactors cost countering solutions have been proposed in the form of biomimetic nicotinamide derivatives, whereby molecules such as 1-benzyl-1,4-dihydropyridine-3-carboxamide are structurally less complex than NAD(P)H and easier to synthesize but enzymatic methods for regeneration of reduced form and not adaptable to these cofactors (Nowak et al. 2017).

Furthermore, the general applications of these artificial cofactors require enzyme engineering to adapt enzymatic binding and conversion (Zhang et al. 2011).

Achieving the cofactor balance requirements has meant that the cofactor preference for certain enzymes has been engineered to alter preferences. A NADH-dependent pathway was constructed using engineered enzymes where the cofactor preference had been altered from NADPH to NADH for production of isobutanol. This aided in the development of economically competitive aerobic production conditions over the native anaerobic NADPH requiring conditions. Moreover, it was demonstrated that the engineered NADH-dependent pathway enables isobutanol production at 100% theoretical yield than the native NADPH-dependent pathway (Bastian et al. 2011), thus demonstrating how engineering cofactor preferences can be a competent solution to the critical issue of cell-free system commercialisation. Vice-versa, cofactor engineering has also been applied to shift preference from NADH to NADPH (Campbell et al. 2010) or has relaxed/boarded the cofactor specificity altogether.

Cofactor engineering has been split into three major approaches: rational design, swapping modules or directed evolution (Rollin et al. 2013). Module swapping refers to the technique of replacing an entire enzyme domain in order to alter cofactor specificity. This was performed successfully in a thermophilic bacterium where the specificity of isocitrate dehydrogenase was altered from $NADP^+$ to NAD^+. The mutant isocitrate dehydrogenase was found to be stable as the original wildtype enzyme (Yaoi et al. 1996). Directed evolution consists of using error-prone PCR to introduce mutations into a gene of interest and then screening the mutant library for transformants with the desired activity. This approach was employed with the thermotolerant NADPH dependent malic enzyme from *T. kodakarensis* to alter its preference from NADPH to NADH. It was serendipitously found that this cofactor preference also altered the reaction specificity of the enzyme. The native malic enzyme in this case catalyses the conversion of malate to pyruvate and the reverse reaction is thermodynamically unfavourable and yet is the one with productive appeal in the renewable production of malic acid. The shift in cofactor preference not only allows for the more thermally stable NAD^+/NADH to replace $NADP^+$/NADPH as the preferred cofactors, it also shifted the reaction towards malate production. The mutant enzyme with NADH as a cofactor gave 1.2 times higher concentration of malate than the wildtype enzyme with NADPH (Morimoto et al. 2014).

1.8 Spatial organisation

Cells have evolved to spatially organise pathways which are specialised in handling metabolic pathways with overlapping intermediates and to isolate them from any toxic intermediates, moreover enzymes have evolved to have the maximal activity in *in vivo* crowded macromolecular surroundings (Zhang

2015). Cell-free systems employing crude lysates tend to have enzymatic concentrations of around 1-10mg/ml (Jewett and Swartz 2004), this concentration is considerably lower for purified enzyme cell-free systems. In comparison to these figures, total cytoplasmic protein concentrations tend be approximately 200mg/ml (Jandt et al. 2013). Evolutionary design enables enzymes to have excellent activity, specificity and selectivity, all under physiological requirements, which do not always align with industrial requirements, and industrial application of enzymes may be prone to inhibition and have low stability (dos Santos et al. 2015). For these reasons, it is only reasonable that approaches to mimic optimal intracellular environments such as, compartmentalisation, scaffolding and immobilization, are explored (Rollin et al. 2013).

Immobilization of enzymes is a technique that is fast becoming a sought after solution to overcome some of the challenges faced by cell-free biosystems. Immobilization as a tool, is being used by researchers to improve enzyme features like activity selectivity, selectivity, specificity and inhibition resistance (dos Santos et al. 2015). It is a common industrial practice to increase enzyme life via immobilization but this is sometimes achieved at the expense of enzyme activity, inactivation of a percentage of immobilized enzymes, mass transfer limitations and slow reaction rates (Zhang et al. 2011). Despite the potential drawbacks, progress is being made to overcome limitations and many immobilization techniques have been proposed such as adsorption, covalent binding, entrapment, encapsulation, crosslinking and nanoparticle immobilization (Dudley et al. 2015).

1.9 Spatial organisation - a focus on immobilization strategies

Immobilization of enzymes is the attachment of the biocatalysts to a solid support that is insoluble in the reaction mixture (Jesionowski et al. 2014). It has been shown to substantially improve the stability of enzymes and provide a method of reusability of biocatalysts over catalytic cycles. Immobilization also changes the catalysts from a homogeneous form to a heterogenous form, allowing for the ease of separation of biocatalytic units from the reaction mix and reducing downstream purification strategies (Zdarta et al. 2018). For instance, cell-free production of isobutanol is an alternative to the cellular production, given the toxic effects of higher order alcohols on cells. Isobutanol production has been demonstrated successfully using 9 purified enzymes and isolating the enzymes directly responsible for the production of desired product is better than optimizing a complex full live cell system (Guterl et al. 2012). An immobilized cascade for production of isobutanol would also simplify alcohol/water separation as the solution would be free of proteins.

1.9.1 Immobilization support materials

Immobilization strategies can be applied in various techniques, and the difference between these techniques is that the different types of interactions formed and the type of support materials used. Therefore, deciding which immobilization technique and materials to employ requires knowing the reaction type and conditions as well the type of biocatalyst (Guzik et al. 2014). Support materials for immobilization are available in a variety and can be divided into 2 main groups, classic and new materials (Zdarta et al. 2018).

Classic materials are available in large varieties and can be classified as inorganic or organic materials (Zdarta et al. 2018). One of the most frequently used inorganic support material for immobilization is silica, it has wide practical applications and has high thermal and chemical resistance as well as offering high surface area and pore size for sorption applications (Jesionowski and Krysztafkiewicz 2002). Silica also provides benefits in the applications with multiple enzyme catalytic classes as it can be used in many forms (fumed silica, silica nanoparticles and silica gel) (Zucca and Sanjust 2014). Silica materials are also highly hydrophilic due to the presence of multiple hydroxyl groups on their surface, thereby improving enzyme immobilization (Zdarta et al. 2018). Mineral materials of mainly clay (bentonite, halloysite) are also used as supports for enzymatic biosystems. These materials have great economical appeal as they are sourced easily given their abundance in nature, are cheap and require no extensive treatment before application (Ghiaci et al. 2009). The inorganic materials classically used for immobilization purposes have some limitations such as limited biocompatibility, low affinity to biomolecules, and furthermore, cross linking agents may be needed to create covalent bonds between the enzyme and support. For this reason, some organic materials are also used for immobilization purposes and these can be either synthetic materials (polymers) or biopolymers (naturally sourced renewable materials) (Zdarta et al. 2018). The biggest advantage offered by organic materials is that they can form linkages between the enzyme and the support without the need for cross-linking agents which is a disadvantage posed by using inorganic materials for immobilization (Zdarta et al. 2018).

New materials are continually being reported to facilitate novel practical applications of immobilized enzymes and again, these materials can be inorganic or organic in their origin. One of the novel supports with wide potential applications are mesoporous supports (Zdarta et al. 2018). These are distinguished from other materials used for immobilization purposes as the properties of the support can be tailored to the enzyme via adjustment of synthesis conditions leading to matrices with desired pore structures (Matuszek et al. 2016). Overall, the new materials are highly tailorable with regards to synthesis to particular reaction/industry conditions (Zdarta et al. 2018).

1.9.2 Types of immobilization techniques

The main methods of immobilization of enzyme is divided into 4 categories (Mohamad et al. 2015):

1. Physical adsorption
2. Entrapment/Encapsulation
3. Cross-linking
4. Covalent bonding

1. Binding the enzyme to supports (typically synthetic resins, biopolymers or inorganic solids such as silicas) can be achieved via adsorption. Being the oldest and easiest immobilization technique, adsorption is the interaction between the enzyme and support through weak forces physical such as hydrogen bonds, hydrophobic, van der Waals, or ionic interactions (Jesionowski et al. 2014). These interactions can least withstand the rigorous conditions often imposed by industrial processes, whereby the physical binding would be too weak to retain enzyme on support leading to enzyme leaching (Sheldon and van Pelt 2013). This technique is reversible and enzymes can be detached from the support, a highly useful strategy when support is in need of reloading with fresh enzyme (Mohamad et al. 2015) as novel supports can be recycled with extended lifetimes.

2. Entrapment is the technique in which enzymes are irreversibly immobilized/entrapped inside polymer networks, this allows the substrates/products to pass but it retains enzyme inside. This entrapment is also not fully sufficient to completely prevent leakage so additional covalent linking is often required (Nisha et al. 2012, Sheldon and van Pelt 2013).

3. Cross-linking is also an irreversible immobilization technique whereby a carrier/support is not required (unlike the adsorption and entrapment techniques) to prevent enzyme loss into the reaction mix (Honda et al. 2005). Due to this, this method is also known as carrier-free immobilization. It is carried out by forming intermolecular cross-linkage between the enzymes using a cross-linking reagent such as glutaraldehyde (Sheldon 2007).

4. Covalent binding is another irreversible conventional method better at retaining the enzyme on support. The attachment between the enzyme and the support is achieved either through direct linking or through a spacer arm which can provide a great degree of mobility to the linked enzyme and these enzyme shave been reported to show higher activities in comparison to those attached directly (Nisha et al. 2012). However covalent interactions may irreversibly deactivate the enzyme leading to reaction process inefficiencies and added costs (Sheldon and van Pelt 2013).

1.9.3 Support properties for immobilization

Given the different types of immobilization protocols and materials available for immobilization, adequate selection of the protocol and support are crucial for an efficient system. The particle size in a support for immobilization plays a crucial role in handling of the supports, whereby too small particles will pose problems in handling of the particles in industrial applications (dos Santos et al. 2015). Larger particles can cause problems in efficient diffusion, in a given instance if the substrate diffusion rate is slower than the substrate consumption rate, the enzymes immobilized in the centre of the support material might not receive any substrate at all, reducing observed biocatalytic activity (Bortone et al. 2014). In general, the best support should have a high loading capacity as a larger amount of enzyme will be immobilized with a lower volume of support (dos Santos et al. 2015). The pore diameter is recommended to be 4-5 fold larger than the larger enzyme diameter to: (i) ensure the pore closing is avoided and new enzyme molecules can still enter after the initial enzymes have immobilized onto the support and (ii) the full surface of the support can be coated by the enzyme (Hudson et al. 2008).

1.10 Challenges and opportunities associated with immobilization

Despite the advances made in analysis of suitable support materials and immobilization techniques, one of the most common issues with immobilized enzymes is their display of diminished activities, this can be tackled via molecular engineering to improve activity and stability. Any engineering efforts require a detailed understanding between protein structure and function and this information is not always available. One possible way around this is using highly stable soluble proteins like folded green fluorescent protein and stabilised maltose binding domain, the coupling of these with enzymes of interest can increase solubility and possibly lessen protein-protein self-interactions (Magliery et al. 2011). This approach was applied to stabilise immobilized keto-acid decarboxylase and retain its activity. This was then further developed into a production scheme based on CFME to produce isobutanol. Two immobilized enzymes, keto-acid decarboxylase and alcohol dehydrogenase were immobilized on methacrylate resin with formate dehydrogenase in solution to aid cofactor recycling. This system produced isobutanol titres 8-20 times higher than the highest reported titres with *S. cerevisiae* on a mol/mol basis. Without *in situ* product removal, 55% conversion of ketoisovaleric acid to isobutanol was achieved and therefore increasing titre can be explored by continuous removal of the isobutanol (Grimaldi et al. 2016).

Immobilization strategies have also been focused on biocatalytically relevant cofactor recycling enzymes such as glucose dehydrogenase (GDH) and NADH oxidase (NOD). GDH belongs to the oxidoreductases family of enzymes which make up one quarter of all known enzymes and require

costly nicotinamide cofactors. Immobilization of the enzymes utilising expensive cofactors would therefore assist in the cost management as the cofactor could be reused and recycled in biosystems. Enzymes belonging to the oxidoreductases family have not been so well explored in immobilization, possibly owing to denaturation that comes with immobilization of multimeric enzymes leading to activity loss (Betancor et al. 2003). In a particular study, immobilization was explored in microspheres developed by ReSyn™ Biosciences (South Africa). Three variants of the aldehyde functional polymer microspheres were explored which varied only in their functional group densities. Immobilization of GDH resulted in the maintenance of approximately 40% of the activity, furthermore the immobilized GDH displayed improved activity in the acidic pH range (Twala, Sewell, & Jordaan, 2012).

1.11 Project aim and objectives

With biobased production of malic acid heavily dependent on microbial fermentation processes, alternatives are being sought to increase yields and cut costs. Cell free metabolic engineering provides a competitive answer given that the restrictions imposed by physiological limits of cellular production systems are overcome to an extent. Designing an artificial enzymatic cascade using enzymes exclusively from thermophiles mitigates the issue of time and cost consuming purification strategies, and cofactor balance can be achieved with the incorporation of additional biocatalytically relevant enzymes or they can be a part of the original cascade resulting in a reaction intermediate. Mimicking intracellular environments with the aid of enzyme immobilization can further enhance the appeal of cell-free system for the sustainable production of malic acid.

The objectives of this project were therefore to:

1. Design an enzymatic cascade to convert glucose to malic acid.
2. Produce and purify the recombinant enzymes of the cascade.
3. Characterize the activity of the produced enzymes.
4. Investigate the benefits of enzyme immobilization.

2. Materials and Methods

2.1 Reagents

All chemicals and consumables unless otherwise stated, were purchased in analytical grade from the following suppliers: Appleton Woods, Clontech, Bio-Rad, Cambio, Expedeon, Formedium, GE, GenScript, GeneFlow, Merck, Molekula, NEB, Qiagen, Sigma-Aldrich, StarLabs and Thermo Fisher Scientific.

2.2 Vector generation

Plasmids used in this study are listed in Table 2.1.

Enzyme	Abbreviation	Source	GenBank accession number
Glucose dehydrogenase	GDH	*Sulfolobus solfataricus*	CAA09918.1
Dihydroxy-acid dehydratase	DHAD	*Sulfolobus solfataricus*	AKA78631.1
2-Keto-3-deoxygluconate aldolase	KDGA	*Sulfolobus acidocaldarius*	AAY79644.1
Glyceraldehyde dehydrogenase	AIDH	*Thermoplasma acidophilum*	CAC11938.1
Malate dehydrogenase	MDH	*Thermococcus kodakarensis*	BAE47514.1

Table 2.1. List of enzymes utilized in the cascade.

All plasmids were synthesised and cloned into pET-30a via *Nde*I and *Bam*HI as the 5' and 3' restriction sites respectively. All protein sequences were designed with a N-terminal His$_{10}$ tag followed by a 6 glycine-serine linker. Among these, GDH, DHAD, KDGA and AIDH are wild-type sequences whereas MDH sequence has 3 mutations (R221G, K228R and I310V). These mutations were reported to alter the cofactor preference of MDH and also shift reaction specificity towards malate production (Morimoto et al. 2013). Gene synthesis was carried out by GenScript (New Jersey, United States) and plasmids were supplied as a concentrated miniprep of ~4µg of DNA.

2.2.1 *E.coli* competent cells

One Shot® TOP10 and One Shot® BL21(DE3) chemically competent *E. coli* cells were purchased from Sigma-Aldrich and stored at -80°C until use.

2.2.2 Bacterial media

For liquid Luria-Bertani (LB) broth, 20g/L LB was dissolved completely in water and autoclaved prior to use. For LB agar, 20g/L LB and 20g/L agar were dissolved in water, autoclaved and sufficiently cooled before pouring into sterile petri dishes. Antibiotic was added (kanamycin at 50µg/ml) to media at around 40°C.

2.2.2.1 Antibiotics

Stock solutions of 100mg/ml kanamycin were prepared by completely dissolving 1g of kanamycin powder into 10ml of double distilled (dd) water. The solution was then sterilized by filtering through a 0.2µm syringe filter and stored at -20°C. Kanamycin was used at a working concentration of 50µg/ml.

2.2.3 Transformation of *E.coli* for vector quantification

In order to amplify vector DNA (Table 2.1) for protein expression purposes, *E. coli* TOP10 competent cells were transformed and minipreps were performed to isolate each vector. 50µl aliquot of TOP10 cells was thawed on ice, and 2µl of vector DNA (~200ng/µl) was added before incubating on ice for 30 minutes. This was followed by heat shocking the tubes containing the competent bacterial cells and vector DNA for 30 seconds at 42°C. The tubes were immediately put back on ice for a further 2 minutes. 400µl of LB broth was added to the tube and incubated at 37°C, 220rpm for 1 hour. Following the incubation, 200µl of the sample was added to LB-agar kanamycin plates and incubated overnight at 37°C for no more than ~18 hours followed by storage at 4°C. When required, single bacterial colonies were picked from the plate, added to LB broth supplemented with kanamycin and incubated overnight at 37°C, 220rpm. Following overnight growth, the cultures were taken, centrifuged and vectors were isolated using a GeneJet Plasmid Miniprep kit (Thermo Scientific) according to the manufacturer's protocol. Vector DNA recovered was quantified using a NanoDrop, aliquoted and stored at -80°C until use.

2.2.3.1 Restriction digest

To verify the correct insert size, restriction digests were performed on the vector DNA obtained in Section 2.2.3. *Nde*I (NEB R0111S) and *Bam*HI-High fidelity (NEB R3136S) were used in 1µl quantities with 5µl of CutSmart buffer (NEB) and 2µl of vector DNA made up to a final volume of 25µl using ultra-pure water from a Type 1 Milli-Q Synthesis A10 water purification system. The digest was then incubated at 37°C for an hour and NdeI was then heat deactivated at 65°C for 20 minutes before adding ~3µl of 6x loading dye (Thermo Fisher Scientific R0611) before loading.

2.2.3.2 Agarose gel electrophoresis

1% agarose gels were prepared using 1g of agarose to every 100ml of 1x TAE (Tris-acetate-EDTA) buffer. Stock 50x TAE (Thermo Fisher Scientific B49) was used to make up 1x TAE buffer and gels were run at 100V to confirm correct insert sizes.

2.3 Protein expression

2.3.1 Bacterial media and stock solutions

LB broth (liquid/agar) was prepared as detailed in Section 2.2.2.

Kanamycin stock was prepared as detailed in Section 2.2.2.1.

Liquid Auto-induction (AI) media (Formedium AIMLB0210) was prepared by dissolving 34.85g/L AI media in water and autoclaving prior to use.

1M isopropyl β-D-1-thiogalactopyranoside (IPTG) was prepared by dissolving 2.38g of IPTG in a final volume of 10ml dd water, the solution was filtered sterilized with 0.2μm syringe filter and stored at -20°C. The working concentration of IPTG was 1mM.

2.3.2 Transformation of *E.coli* for protein expression

For protein expression purposes, *E. coli* BL21-DE3 competent cells were transformed. A 50μl aliquot of BL21-DE3 cells was thawed on ice, and 2μl of vector DNA (~200ng/μl) was added before incubating on ice for 30 minutes. This was followed by heat shocking the tubes containing the competent bacterial cells and vector DNA for 30 seconds at 42°C. The tubes were immediately put back on ice for a further 2 minutes. 400μl of LB broth was added to the tube and incubated at 37°C, 220rpm for 1 hour. Following the incubation, 200μl of the sample was added to LB-agar kanamycin plates and incubated overnight at 37°C for no more than ~18 hours followed by storage at 4°C.

2.3.2.1 Bacterial glycerol stocks

For long term storage of bacterial cultures, glycerol stocks were prepared for each protein. Following a transformation protocol (Section 2.3.2), single bacterial colonies were picked from the plate, added to LB broth supplemented with kanamycin and incubated overnight at 37°C, 220rpm. After overnight growth, 500μl culture was added to 500μl 50% glycerol, gently resuspended and stored at -80°C for long term storage. To recover bacteria from the plate, a sterile loop was used to scrape some of the frozen suspension on an LB agar kanamycin plate, ensuring the glycerol stock did not thaw. The streaked out plate was incubated overnight at 37°C for no more than ~18 hours followed by storage at 4°C.

2.3.3 Expression of recombinant proteins

Expression in LB broth-

For small scale expression of GDH, DHAD, KDGA, AIDH or MDH, single colonies from LB agar kanamycin plates were picked into 10ml LB broth supplemented with kanamycin and grown at 37°C, 220rpm in small baffled flasks until OD_{600} of >0.6. This was used as a pre-culture and 10ml was added to 1L LB broth (in 2L shake flasks) supplemented with kanamycin and grown at 37°C for 3-4 hours. OD_{600} was monitored until an absorbance 0.4-0.6 was achieved. This was followed by induction with 1mM IPTG and overnight incubation at room temperature, 220rpm (OD_{600} of ~7-10). Concentrated cell pellets were obtained by centrifugation and LB broth removed.

Expression in AI media-

For small scale expression of GDH, DHAD, KDGA, AIDH and MDH, single colonies from LB agar kanamycin plates were picked into 10ml AI media supplemented with kanamycin and grown at 37°C, 220rpm in small baffled flasks until OD_{600} of >0.6. This was used as a pre-culture and 10ml was added to 1L AI media (in 2L shake flasks) supplemented with kanamycin and grown overnight at room temperature, 220rpm (OD_{600} of ~8-12). Concentrated cell pellets were obtained by centrifugation and AI media removed.

2.4 Recombinant protein extraction

2.4.1 Stock solutions

1M HEPES buffer, pH 7.5 was prepared by dissolving 238.3g of HEPES powder in ~800ml of dd water, the pH adjusted to 7.5 with sodium hydroxide (NaOH). The final volume was made up to 1L with additional dd water and the solution was filtered sterilized with a 0.2μm bottle top filter unit (StarLabs) and stored at room temperature.

2M magnesium chloride ($MgCl_2$) was prepared by dissolving 95.2g of $MgCl_2$ into a final volume of 500ml dd water, the solution was filtered sterilized with 0.2μm bottle top filter unit and stored at room temperature.

50% glycerol was prepared by mixing 500ml dd water with 500ml 100% glycerol. The solution was sterilized either by filtration or autoclaved, and stored at room temperature.

DNase I Solution was purchased from Thermo Fisher Scientific (89836) and used as per the manufacturer's instructions.

EDTA-free protease inhibitor cocktail was purchased in tablet form from Sigma-Aldrich (4693132001) used as per the manufacturer's instructions.

2.4.2 Soluble protein extraction

2.4.2.1 Resuspension buffer

100mM HEPES pH 7.5, 200mM $MgCl_2$, 10% glycerol, DNase I solution and protease inhibitor tablets.

2.4.2.2 Cell lysis and extraction of crude lysates

Cell pellets obtained following expression of recombinant proteins (Section 2.3.3) were resuspended in resuspension buffer until completely homogenised. Cell lysates were prepared using a Bandelin sonuplus cell disruptor system on ice at 75% power for 20 minutes with 40 second sonication and 20 second pause pulses. Cell debris was removed by centrifugation at 80,000xg for 30 minutes at 4°C (Beckman Coulter Optima L-80 XP ultracentrifuge, 70.1 Ti rotor). The supernatant was heat treated (30 min at 70°C) and the centrifugation step repeated. The supernatant (referred to as crude enzyme/protein) achieved from this step was either used directly as an enzyme solution in assay conditions or purified further.

2.5 Protein purification

2.5.1 Purification buffers

Stock solutions are described in Section 2.4.1.

1M Tris-HCl buffer pH 7.5 was purchased from Thermo Fisher Scientific.

1M sodium chloride (NaCl) was prepared by dissolving 58.44g NaCl in 1L of dd water. The solution was filtered sterilized with 0.2μm bottle top filter unit and stored at room temperature.

1M imidazole solution purchased from Sigma-Aldrich (68268).

1M ethylenediaminetetraacetic acid (EDTA) pH 8 was prepared by adding 93g of EDTA to ~200ml of dd water, adding NaOH to aid full dissolving and dd water to make a final volume of 250ml. The solution was filtered sterilized with a 0.2μm bottle top filter unit and stored at room temperature.

Ni-NTA wash buffer- 100mM HEPES pH 7.5, 200mM $MgCl_2$, 10% glycerol.

Ni-NTA elution buffer- 100mM HEPES pH 7.5, 200mM $MgCl_2$, 10% glycerol with an imidazole gradient of 50-1000mM. Where applicable, 100mM working concentration of EDTA was added to the collection tubes of elution buffer to avoid leeching of nickel

Anion exchange wash buffer- 20mM Tris-HCl pH 7.5, 5% glycerol.

Anion exchange elution buffer- 20mM Tris-HCl pH 7.5, 5% glycerol with NaCl gradient of 50-1,000mM.

2.5.2 Sodium dodecyl sulfate–polyacrylamide gel electrophoresis (SDS-PAGE) and Western blot

2.5.2.1 Buffers and reagents

5x Laemmli sample buffer was prepared using 1.25ml 0.5M Tris-HCl pH 6.8, 2ml 50% glycerol, 2ml 10% SDS (sodium dodecyl sulfate), 0.5ml β-mercaptoethanol (2-ME), 10µl bromophenol blue and 2.25ml dd water.

SDS Tris buffer was prepared using 100ml 10x SDS Tris buffer (Geneflow) and 900ml dd water.

Western Tris buffer was prepared using 100ml 10x Tris buffer (Geneflow), 200ml methanol and 700ml dd water.

Phosphate buffered saline (PBS) was prepared with 10 PBS tablets dissolved in dd water to a final volume of 1L.

PBS Tween 20 (Wash buffer) was prepared with 1L PBS and 2ml Tween 2 (0.2%).

Blocking buffer was prepared by adding 2.5g of dried milk (5%) to 50ml of PBS.

10% separating gel was prepared using 1.9ml 30% polyacrylamide, 1.5ml 1.5M Tris-HCl pH 8.8, 60 µl 10% SDS, 2.15ml water, 20µl 20% ammonium persulfate and 4.5 µl TEMED (tetramethylethylenediamine).

12% separating gel was prepared using 2.3ml 30% polyacrylamide, 1.5ml 1.5M Tris-HCl pH 8.8, 60 µl 10% SDS, 1.8ml water, 20µl 20% ammonium persulfate and 4.5 µl TEMED.

4% stacking gel was prepared using 0.3ml 30% polyacrylamide, 0.6ml 0.5M Tris-HCl pH 6.8, 25µl 10% SDS, 1.5ml water, 10µl 20% ammonium persulfate and 2.5µl TEMED.

Antibodies used for western blot analysis:

- Primary- 6x-His Tag Monoclonal antibody (Clontech 631212)
- Secondary- Anti-mouse IgG HRP-linked antibody (NEB 7076S).

2.5.2.2 SDS-PAGE preparation

Glass plates were cleaned with 70% ethanol, allowed to dry and then inserted into clamps. The 10% separating gel was poured between the plates to approximately ¾ height. dd water was layered on top allowing the gel to set level. The water was poured off, the stacking gel was poured into the plates and a comb was then inserted before allowing the gel to set. The comb was removed when the gel

solidified. PageRuler plus prestained Protein ladder (Thermo Fisher Scientific 26619) was used for molecular weight reference. Samples to be loaded were prepared by mixing 20µl of sample with 5µl of 6x Laemmli sample buffer. Gels were then placed in a gel tank (Bio-Rad Protean 3 cell) and filled with SDS Tris buffer, loaded and run for 1.5 hours at 100V. The gel was then analysed by using a Coomassie protein stain for polyacrylamide gels (Expedeon ISB1L).

2.5.2.3 Western blot preparation

For western blot analysis, the SDS-PAGE was carried out as outlined in section 2.5.2.2, with the exception of adding the protein stain. Following SDS-PAGE, the stacking gel was removed from the separating gel and discarded. Fibre pads and filter papers (Whatman 3mm chromatography paper) were soaked in Western Tris buffer for 5 minutes. The PVDF (Polyvinylidene difluoride) (Bio-Rad 1620177) membrane was soaked in methanol for 5 minutes before assembly as follows:

• 1 Fibre pad

• 3 filter papers

• Gel

• PVDF membrane

• 3 filter pads

• 1 fibre pad

The cassette was placed into an electrical module after confirming the correct orientation. An ice block was placed into the tank and it was filled to just below the top of the cassette with the western running buffer. This was run for precisely an hour at 100V. Once the transfer was complete, the PVDF membrane was removed and placed into a plastic container. 50ml blocking buffer was added to it and left to block overnight covered in foil. The following day, 10µl primary antibody was added directly to the membrane in the blocking buffer at 1:5,000 dilution. This was then placed on rocker for 1 hour at 30rpm at room temperature. After an hour, 3 washes were carried out with PBS Tween on a rocker for 3-4 minutes per wash. 50ml fresh blocking buffer were then added to the membrane with 10µl secondary antibody at 1:5,000 dilution and rocked for an additional hour at 30rpm. 3 washes with PBS Tween were then repeated. An EZ-ECL chemiluminescence detection kit (Geneflow) was used to detect His-tagged protein bands according to the manufacturer's protocol. The membrane was visualised using a Sysgene box with auto capture feature.

2.5.3 Bicinchoninic acid (BCA) protein assay

Protein concentrations were determined using 1mg/ml bovine serum albumin (BSA) as standard in a 96-well plate. BSA standards were prepared at 0, 0.125, 0.25, 0.5, 0.75, 1, 1.5 and 2mg/ml. All standards were loaded in a final volume of 10μl in triplicate. Unknown samples were also added in a final volume of 10μl at range of different concentrations, to ensure a sample falling within the linear range of the standard curve. 200μl BCA reagent (50:1 ratio (v/v) between BCA solution and 4% (w/v) copper II sulfate solution) was added to each well of standards and unknowns. The 96-well plate was incubated at 37°C for no more than 30 minutes. Absorbance values were measured at 562nm in a Multiskan™ FC Microplate Photometer (Thermo Fisher Scientific). A standard curve was generated and the unknown sample concentrations were calculated in mg/ml.

2.5.4 Protein purification- Ni-NTA (nickel-nitrilotriacetic acid) affinity chromatography

The crude protein extracts obtained (Section 2.4.2.2) were resuspended with Ni-NTA resin (Qiagen) and incubated to bind (magnetic stirrer) either at 4°C or room temperature overnight. Following this, the resuspension was added to a polypropylene column (GE) and the flow through was collected. This was followed by 5 column volume washes of the resin. The His-tagged protein was then eluted from the resin using an imidazole gradient. Samples from each stage were collected to detect proteins by SDS-PAGE, following which the samples of interest were isolated. If required, the protein samples were concentrated further using an ultrafiltration unit, Vivaspin 20 centrifugal concentrators (molecular weight cut off 10kDa) by centrifugation at 3,900xg at 4°C. To ensure the PES (polyethersulfone) membranes of the concentrators did not get saturated and to prevent protein aggregation, the protein samples were not centrifuged for more than 10 minutes at a time and were resuspended by pipetting. The protein concentration was determined via bicinchoninic acid assay (BCA) and/or a NanoDrop. Confirmation of functional His-tagged protein was determined by western blot.

2.5.5 Protein purification- ÄKTA

Size exclusion chromatography was carried out on an ÄKTA pure protein purification system (GE). A Superdex 200 column with a 24ml bed column was used with a Unicorn version 7.0 software for analysis. The flow rate was set at 0.3ml/min and the fraction line and loop were washed with water followed by buffer (100mM HEPES pH 7.5, 200mM $MgCl_2$, 10% glycerol). Following washes, 500 μl sample to be analysed was injected ensuring no air bubbles were injected into the system. After the sample run had finished, the software-generated chromatogram was used to analyse sample compositions. Samples from each automated fraction were collected to detect proteins by SDS-PAGE, following which the samples of interest were isolated. If required, the protein samples were

concentrated further using concentrators as outlined in Section 2.5.4. The protein concentration was determined via bicinchoninic acid assay (BCA) and/or a NanoDrop.

2.5.6 Protein purification- Anion exchange

Anion exchange chromatography was employed as a secondary purification strategy whereby protein samples purified by Ni-NTA affinity chromatography were put through a secondary purification step in an attempt to improve overall purity. The protein sample to be analysed was buffer exchanged from 100mM HEPES pH 7.5, 200mM MgCl$_2$, 10% glycerol buffer to 20mM Tris-HCl pH 7.5, 5% glycerol buffer. The anion exchange column was washed with 5 column volumes of wash buffer (20mM Tris-HCl pH 7.5, 5% glycerol) then with the highest elution buffer (20mM Tris-HCl pH 7.5, 5% glycerol, 1M NaCl) for equilibration. The column was then equilibrated with 5 column volumes of wash buffer again. The protein sample was then applied to the column and circulated to ensure binding. The column was washed again with 5 column volumes of wash buffer or until the flow through appeared clear. Following this, elutions were performed with 5 column volumes of each NaCl gradient concentration. Samples from each stage were collected to detect proteins by SDS-PAGE, following which the samples of interest were isolated. If required, the protein samples were concentrated further using concentrators as outlined in Section 2.5.4. The protein concentration was determined via bicinchoninic acid assay (BCA) and/or a NanoDrop.

2.5.7 Protein purification- Inclusion bodies extraction, resolubilisation and purification

Due to poor recovery of soluble AIDH, cell pellets were treated for extraction, resolubilisation and purification of AIDH inclusion bodies.

2.5.7.1 Buffer and reagents

1M DL-Dithiothreitol (DTT) solution purchased from Sigma-Aldrich (43816).

8M buffered guanidine hydrochloride (GdnHCl) solution purchased from Sigma-Aldrich (G7294).

Triton X-100 purchased from Sigma-Aldrich (T8787).

Lysis buffer:

100mM HEPES pH 7.5

5mM EDTA

5mM DTT

10% glycerol

Protease inhibitors

DNase I

Wash buffer:

100mM HEPES pH 7.5

5mM EDTA

5mM DTT

2% Triton X-100

2M GdnHCl

10% glycerol

Extraction buffer:

100mM HEPES pH 7.5

5mM EDTA

6M GdnHCl

5mM DTT/2mM 2-ME

2.5.7.2 Inclusion bodies extraction, resolubilisation and purification protocol

Recombinant AIDH was expressed as outlined previously in Section 2.3.3. The resulting pellet was obtained by centrifugation and resuspended into 5ml of freshly prepared lysis buffer per gram wet weight of cell. The pellet was resuspended into the buffer with the aid of a homogenizer until completely homogenized. Cell lysates were prepared using a Bandelin sonuplus cell disruptor system on ice at 75% power for 20 minutes with 40 second sonication and 20 second pause pulses. Cell debris was removed by centrifugation at 80,000xg for 30 minutes at 4°C. The supernatant (this soluble fraction was purified using Ni-NTA affinity chromatography to recover any soluble AIDH) was poured off and the resulting pellet was resuspended in wash buffer (5ml per gram wet weight cells) to ensure the washing out of soluble proteins and cellular components (cell wall and outer membrane material). GdnHCl or urea both can be utilized in the wash step. If using GdnHCl, SDS is not used as it forms a precipitate and was replaced with Triton X-100. SDS use was compatible when using urea. The wash

buffer was prepared in two versions, one including all the components as listed in Section 2.5.7.1, and one without Triton X-100 and GdnHCl. After adding the pellet to wash buffer, resuspending and homogenizing, the suspension was centrifuged at 80,000xg for 30 minutes at 4°C and the supernatant discarded. This step was repeated twice, following which the pellet was resuspended in wash buffer minus Triton X-100 and GdnHCl, homogenized and centrifuged at 80,000xg for 30 minutes at 4°C. This final wash without Triton X-100 and GdnHCl aided the removal of excess Triton X-100. If required, the washed pellets were stored at this stage. The pellet was then resuspended in extraction buffer at 1ml buffer per gram wet weight of the original cell pellet. The cell suspension was purified one of two ways: (i) dialysis into HEPES 100mM pH 7.5, 200mM $MgCl_2$, 10% glycerol buffer with multiple cycles until GdnHCl, EDTA and DTT have been dialysed to a negligible amount or (ii) extracted unfolded protein refolded straight on the affinity column by binding with Ni-NTA resin and eluting protein with imidazole (in which case DTT was substituted with 2mM 2-ME in the extraction buffer).

2.6 Enzyme assays

Enzyme solutions (either crude or purified by techniques outlined in Section 2.5) were utilized for testing enzymatic activity. Standard assay conditions used for each enzyme are outlined in the sections below. Where the concentrations of enzyme or cofactor are subject to alteration depending on the experiment objectives, the actual assay conditions are mentioned in the respective results sections (Chapters 3-8).

2.6.1 GDH experimental conditions

2.6.1.1 GDH activity assay

The activity of GDH was assayed in 100 mM HEPES pH 7.4, 2.5% glycerol, 30mM $MgCl_2$, 100mM glucose, 5mM NAD^+. Unless otherwise stated, the activity assay for both immobilized and free-state GDH was conducted in a water bath at 55°C for 3 hours. At the end of the assay, samples were placed into pre-cooled racks and supernatants were filtered through 0.2 µm filters. The activity of GDH was detected by measuring the NADH concentrations of the supernatants with a plate reader at 340 nm. The enzyme concentration was measured using the BCA method.

2.6.1.2 Determination of kinetic constants

The kinetic constants for free-state and immobilized GDH were determined by measuring the reaction rates at regular time intervals and different substrate concentrations (0, 0.1, 0.5, 1, 2.5, 5, 10, 25, 50, 100mM). K_m and V_{max} values were calculated from Lineweaver-Burk plots.

2.6.1.3 Support materials

To immobilize GDH, three different commercial enzyme supports; methacrylate-based ECR8309F, styrene-based ECR1090M and methacrylate/divinylbenzene-based ECR1030M were purchased from Purolite, UK. Meso-macroporous SBA-15 (MM-SBA-15) was synthesised by Dr Jinesh Cherukkattu Manayil via a modified true liquid crystal templated (TLCT) SBA-15 synthesis (Parlett et al. 2013) which included a hard macropore template of polystyrene spheres. Polystyrene spheres were synthesised as reported elsewhere (Manayil et al. 2017). The structure-directing template (Pluronic P123l; 2 ml) was mixed with hydrochloric acid acidified water (~pH 2, 2.1ml) and sonicated at 40°C to produce a homogeneous gel. The sol-gel exhibited a hexagonal mesophase. 6g polystyrene were added to the sol-gel with stirring, resulting in the formation of a viscous solution. Tetramethoxysilane (4ml) was added and mixed with stirring to form a homogeneous liquid at 40°C. The evolved methanol was removed under a light vacuum (0.12 bar) at 40°C to form a viscous gel overnight. The gel was exposed to the atmosphere at room temperature for 24 hours to complete condensation before calcination at 500°C for 6 hours in air (ramp rate 2°C/min). The products were designated MM-SBA-15-300 and MM-SBA-15-200, 300 and 200 according to the size of the polystyrene beads used in the synthesis. Low angle XRD patterns were recorded on a Bruker D8 Advance diffractometer fitted with an X'celerator detector and Cu Kα (1.54 Å) source over the range 2θ = 0.3-10°. Nitrogen porosimetry was measured on a Quantachrome Nova 4000 porosimeter and analysed with NovaWin software. Samples were degassed at 120 °C overnight prior to analysis at -196 °C. Brunauer-Emmett-Teller (BET) surface areas were calculated in the relative pressure range of 0.01–0.2. The Barret-Joyner-Halenda (BJH) method was used to calculate pore diameters and pore volumes in the desorption isotherm for relative pressures >0.35. The polystyrene bead size and morphology of synthesised MM-SBA-15-200 and MM-SBA-15-300 were evidenced using Scanning Electron Microscope (SEM).

2.6.1.4 Immobilization of GDH

The immobilization of recombinant GDH onto different support materials was done by gently mixing the enzyme and the support material with enzyme support solution (ES- 100mM HEPES pH 7.4, 2.5% glycerol, 50 mM $MgCl_2$) at room temperature for 10 min. Unless otherwise stated, 0.03 mg GDH and 0.01 g support material were mixed with 1 ml ES. Following this, mixtures were stored at 4°C overnight. The amount of immobilized enzyme was detected by measuring the protein concentration before and after immobilization. Immobilization yield (%) was calculated using the equation below.

$$Immobilization\ yield\ (\%) = \frac{C_0 - C_s}{C_0} \times 100$$

Where C_0 and C_S denote the amount of enzyme before and after immobilization (mg), respectively (in collaboration with Dr Pinar Karagoz).

2.6.1.5 Thermal stability of free-state and immobilized GDH

The thermal stability of free-state and immobilized GDH was investigated at 55, 65 and 80°C after 1, 3, 18 and 24 hours. 0.03 mg free-state or immobilized GDH in 500 μl ES were incubated as required, instantly cooled down on ice for 2 min and stored at 4°C for 20 min. Cooled samples were gently mixed with assay mixture and the activities of free and immobilized GDH were evaluated as described in Section 2.6.1.1 (in collaboration with Dr Pinar Karagoz).

2.6.1.6 Reusability of immobilized GDH

To detect the reusability of GDH immobilized onto different supports, the immobilized enzyme was washed with ES after each use and stored at 4°C overnight and then re-suspended in fresh assay mixture to determine remaining activity. This procedure was repeated 10 times. The activity of the enzyme in the first cycle was defined as 100% and the remaining activities were calculated as follows:

$$Remaining\ activity\ (\%) = \frac{a_{x_{2...10}}}{a_1} \times 100$$

where a_1 and $a_{x2....10}$ denote the enzyme activity at the end of the first and subsequent cycles, respectively (in collaboration with Dr Pinar Karagoz).

2.6.1.7 Effect of immobilization on storage stability

The free-state and immobilized GDH were stored at 4°C to detect the effect of the support material and immobilization on their storage stability. The activity of the GDH was determined at 4-week time intervals (in collaboration with Dr Pinar Karagoz).

2.6.1.8 Determination of optimum temperature and pH

The activity profiles were studied at different temperatures (30-80°C) and pH ranges (5.0-10.5). The pH of the GDH assay buffer was adjusted using 3M HCl, 1M and 100mM NaOH (in collaboration with Dr Pinar Karagoz).

2.6.1.9 Preparation of Bread Waste Hydrolysate (BWH)

Sliced, soft white packaged bread (Warburton) was used as a feedstock. According to the manufacturer's nutritional information, one slice of bread (wet weight 28.8g) contained 13.1g carbohydrate (of which 0.8g were sugars), 2.6g protein and 0.6g fat. Slices were dried at 37°C overnight and broken into small pieces by hand. Pieces from 1 slice of bread were transferred into 250 ml

Erlenmeyer flasks, 100 ml water was added and the flask was placed in a shaking incubator at 60°C, 200 rpm for 1 hour. As previously described (Benabda et al. 2018), 5mg α-amylase from *Aspergillus oryzae* (Sigma-Aldrich 10065) and 7mg amyloglucosidase from *Rhizopus sp.* (Sigma-Aldrich A9228) were added to each flask and incubated at 60°C for 1.5 hours. Solid particles were separated by centrifugation for 20min, at 4100×g and 4°C. The supernatant was transferred into a flask and autoclaved at 121°C for 15 min. The glucose concentration of the hydrolysate and utilization of glucose by GDH was measured using glucose assay (Sigma-Aldrich GAGO20S) and gluconic acid assay (Sigma-Aldrich MAK279) kits. To investigate the activity and stability of free-state and immobilized GDH, BWH was used as the sole glucose source. The glucose concentration of the reaction mixture was set to 100mM using BWH liquor. Free and immobilized GDH were tested in 10ml reactions in 50ml sterile Falcon tubes placed in an orbital shaker at 200rpm and 55°C. Samples were taken during 3 hour reactions. Before measuring NADH, glucose and gluconic acid concentrations, samples were filtered through 0.2 μm filters and deproteinized using 10 kDa cut-off spin filters. As previously described, after 3 hours the supernatant was removed and the supports with immobilized enzymes were kept in ES overnight at 4°C and re-used in a new BWH-containing reaction mixture 10 times (Dr Pinar Karagoz).

2.6.1.10 SEM analysis

Scanning electron microscopy (SEM) images were taken with Dr Jinesh Cherukkattu Manayil using a JEOL JSM-7800F instrument equipped with EDX and operating at 10 kV. The samples were mounted using carbon tape on a sample holder. The images were also taken before and after enzyme immobilization to check the distribution of enzyme on the supports and to confirm their structural integrity.

2.6.2 DHAD experimental conditions

2.6.2.1 DHAD activity assay

As standard, the activity of DHAD was assayed in 100 mM HEPES pH 7.5, 2.5mM $MgCl_2$, 10mM gluconic acid or 10mM glyceric acid. Unless otherwise stated, the activity assay for DHAD was conducted in a shaking heat block at 55°C, 300rpm for 2 hours. At the end of the assay, samples were placed into pre-cooled racks and supernatants were filtered through 0.2 μm filters. The activity of DHAD was detected either by ion chromatography (IC), gluconic acid assay (MAK279-1KT) kits and/or pyruvic acid assay (MAK071-1KT) kits as DHAD displays substrate promiscuity. The kits were used as per manufacturer's instructions.

2.6.2.2 Activation of DHAD using β-mercaptoethanol

Activation of purified and crude DHAD was carried out as described elsewhere (Carsten et al. 2015). DHAD enzyme solution was incubated with 100mM HEPES pH 7.5 and 98mM 2-ME at 70°C for 45 minutes. Any precipitated proteins were removed via centrifugation at 18,000xg and the solution was buffer exchanged into 100mM HEPES pH 7.5 buffer.

2.6.2.3 Determination of kinetic constants

The kinetic constants for DHAD were determined by measuring the reaction rates at regular time intervals and different substrate concentrations (1, 2, 4, 6, 8, 10, 15, 20mM). K_m and V_{max} values were calculated from Lineweaver-Burk plots.

2.6.2.4 Effect of storage on DHAD activity

DHAD stock solution was tested for activity under the same assay conditions over a 50 day period.

2.6.3 KDGA experimental conditions

2.6.3.1 KDGA activity assay

As standard, the activity of KDGA was assayed in 100 mM HEPES pH 7.5, 20mM glyceraldehyde and 40mM pyruvate. Unless otherwise stated, the activity assay for KDGA was conducted in a shaking heat block at 55°C, 300rpm for 2 hours. At the end of the assay, samples were placed into pre-cooled racks and supernatants were filtered through 0.2 μm filters. The activity of KDGA was detected by IC.

2.6.3.2 Determination of kinetic constants

The kinetic constants for KDGA were determined by measuring the reaction rates at regular time intervals and different substrate concentrations (0.5, 1, 3, 5, 10, 20mM glyceraldehyde and 1, 2, 6, 10, 20, 40mM pyruvate in each condition respectively). K_m and V_{max} values were calculated from Lineweaver-Burk plots.

2.6.4 AIDH experimental conditions

2.6.4.1 AIDH activity assay

As standard, the activity of AIDH was assayed in 100 mM HEPES pH 7.5, 100mM glyceraldehyde and 5mM NAD^+. Unless otherwise stated, the activity assay for AIDH was conducted in 96 well plates in a FLUOstar Omega Microplate Reader (BMG LABTECH) at 55°C, for 2 hours.

2.6.5 MDH experimental conditions

2.6.5.1 MDH activity assay

As standard, the activity of MDH was assayed in 500mM HEPES pH 7.5, 5mM NH_4Cl, 0.5mM $MnCl_2$, 30mM pyruvate, 85mM $NaHCO_3$ and 1mM NADH. Unless otherwise stated, the activity assay for MDH was conducted in 96 well plates in a FLUOstar Omega Microplate Reader fitted with an atmospheric control unit at 55°C for 2 hours at 15% CO_2 and 5% O_2. The activity of GDH was detected by monitoring the timely NAD^+ concentrations of the supernatants with a plate reader at 340 nm.

2.6.5.2 Determination of kinetic constants

The kinetic constants for MDH were determined by measuring the reaction rates at regular time intervals and different substrate levels (0-75mM). K_m and V_{max} values were calculated from Lineweaver-Burk plots.

2.7 Standard curves

2.7.1 NADH standard curve

For the reaction using NAD^+/NADH as cofactor, the reaction progression can be followed by monitoring the reaction at 340nm. The concomitant formation/reduction in NADH levels were used to measure the concentration of product formed.
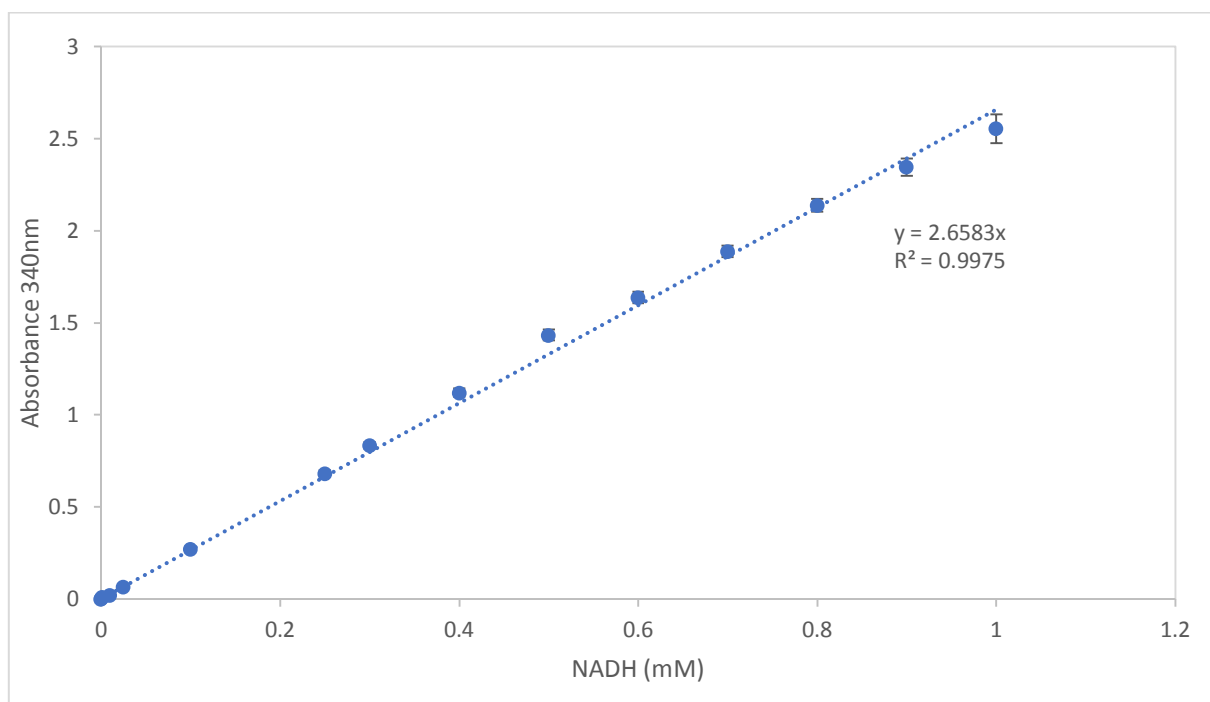
Figure 2.1. NADH absorbance standard curve. Concentrations of 0-1mM of NADH were assayed in triplicate and their absorbance was measured at 340nm at 55°C for 30 minutes. No significant change was observed in the absorbance values over the 30 minutes. Each data point represents an average of the absorbance value over 30 minutes.

2.7.2 IC standard curves

For enzymatic analysis via IC, known standard concentrations of enzymatic substrates/products were analysed via IC to produce standard curves. These standard curves were then used to calculate the unknown concentrations of chemicals of interest. All samples analysed via IC were performed in a Dionex™ Integrion™ HPIC™ System (Thermo Fisher Scientific). Unless otherwise stated all samples were diluted x10 and detected under reaction conditions of 5mM eluent at 30°C at 0.38ml/min flow rate.
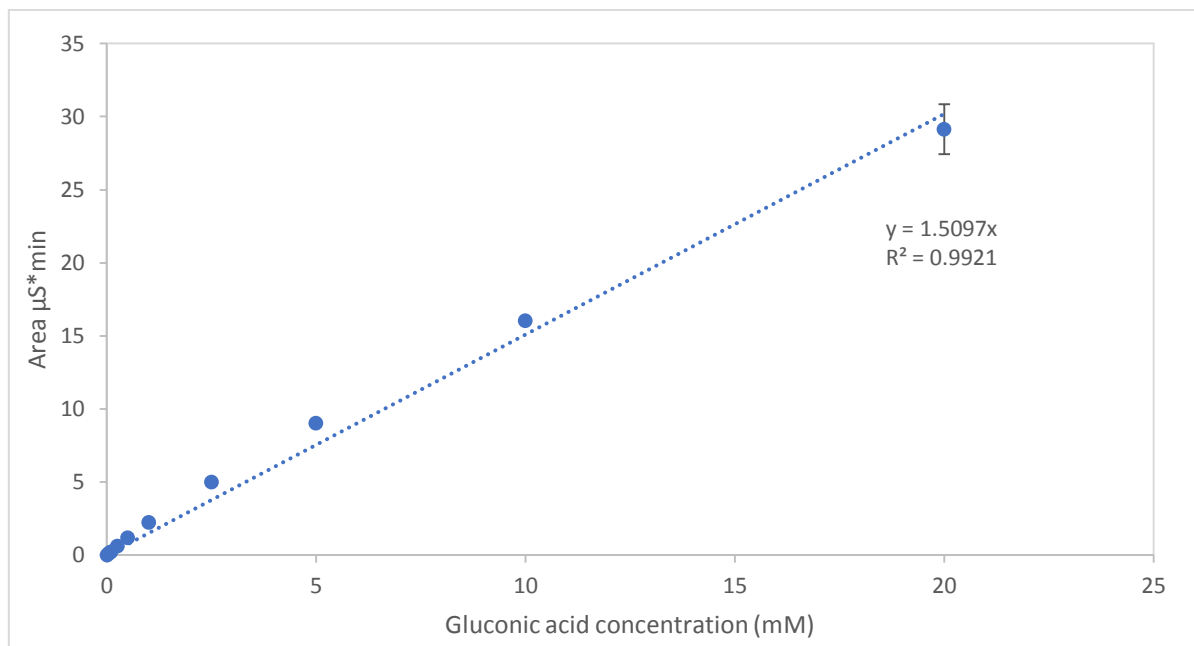
Figure 2.2. Gluconic acid standards as analysed via IC, each data point is an average of triplicate values.
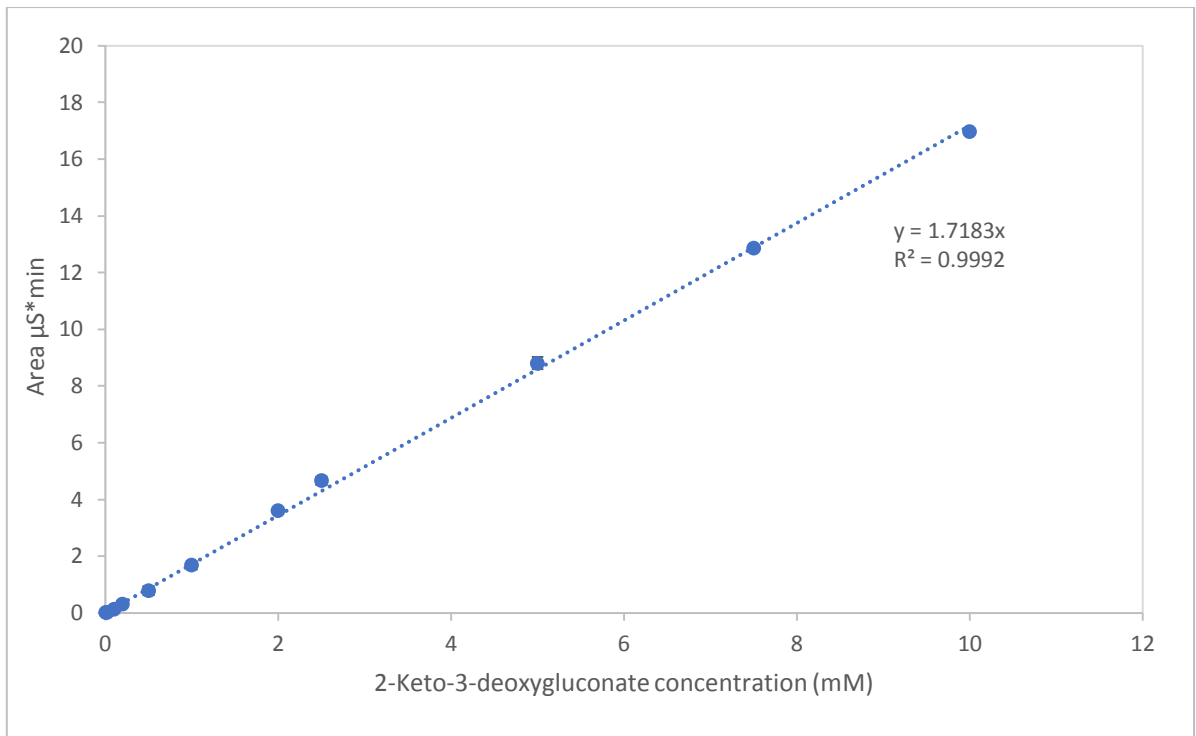
Figure 2.3. 2-keto-3-deoxygluconate standards as analysed via IC, each data point is an average of triplicate values.
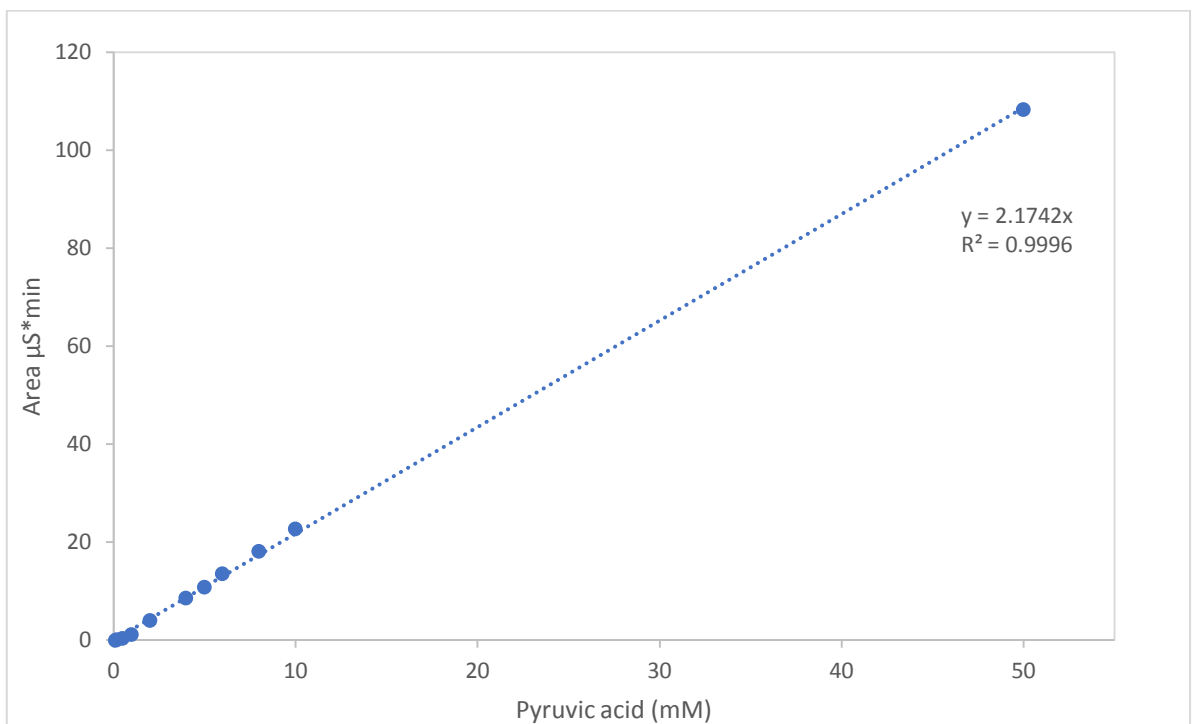
Figure 2.4. Pyruvic acid standards as analysed via IC, each data point is an average of triplicate values.
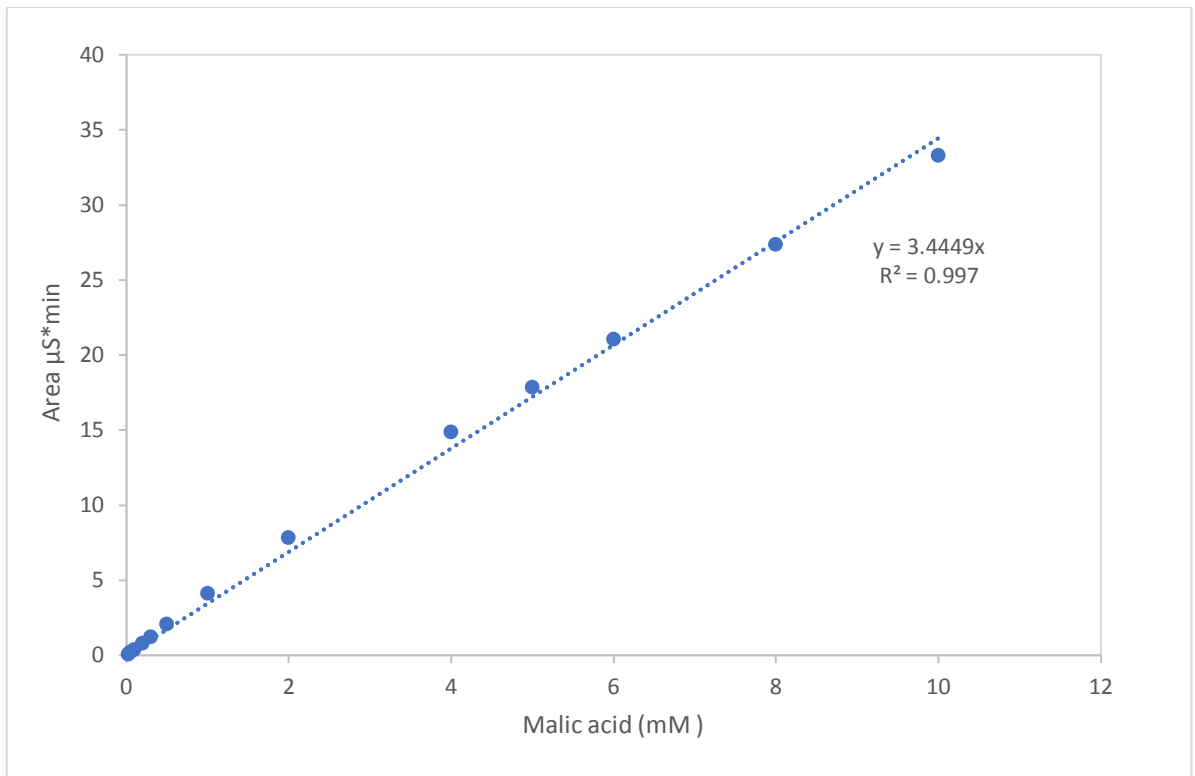
Figure 2.5. Malic acid standards as analysed via IC, each data point is an average of triplicate values.
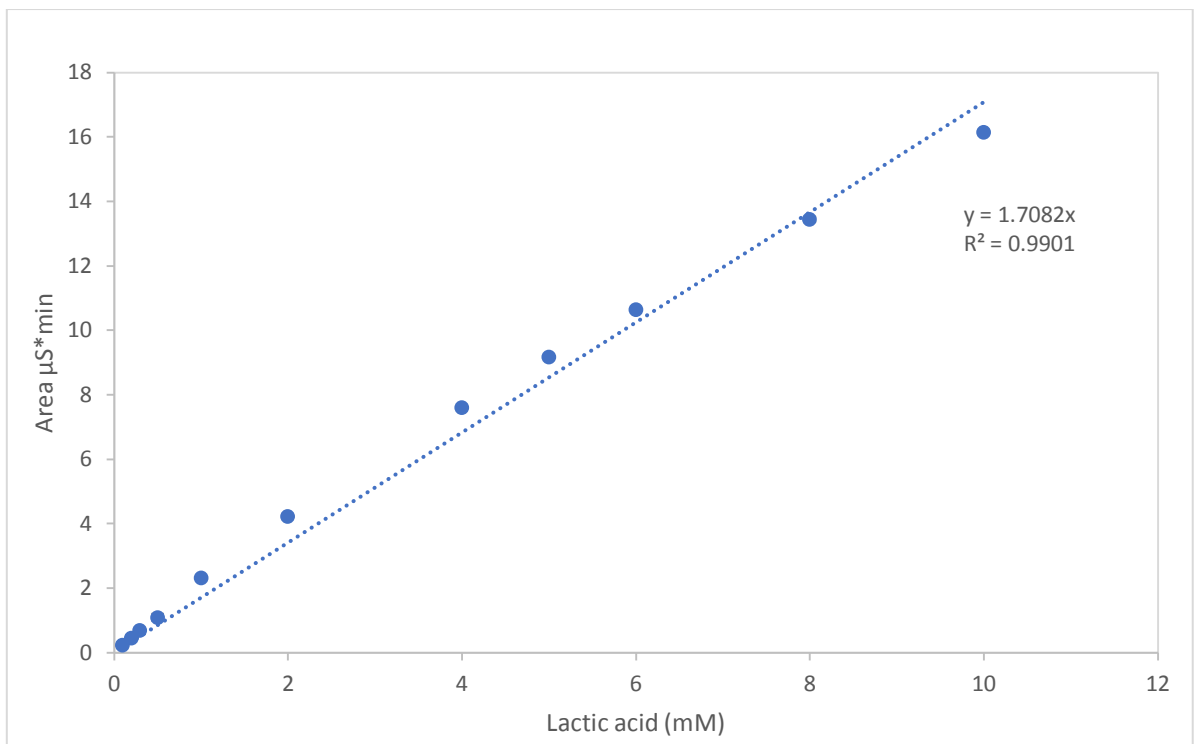
Figure 2.6. Lactic acid standards as analysed via IC, each data point is an average of triplicate values.

3. Cascade design to facilitate the conversion of glucose to malic acid

As per the main objective for the basis of this thesis, a synthetic cell-free enzymatic biosystem consisting of 5 enzymes was designed to facilitate the conversion of glucose to malic acid (Figure 3.1). The conversion of glucose to the key intermediate pyruvate was achieved via a modified non-phosphorylative branch of the Entner-Doudoroff pathway modelled on hyperthermophilic archaea (Ahmed et al. 2005). Pathway design takes into account the requirements of an efficient cell-free system as it is designed to minimise unwanted intermediates and is cofactor balanced. Cutting down time and cost consuming purification of enzymes has been mitigating by employing thermophilic enzymes which provide the option of one step heat denaturation preparation of enzyme solutions.
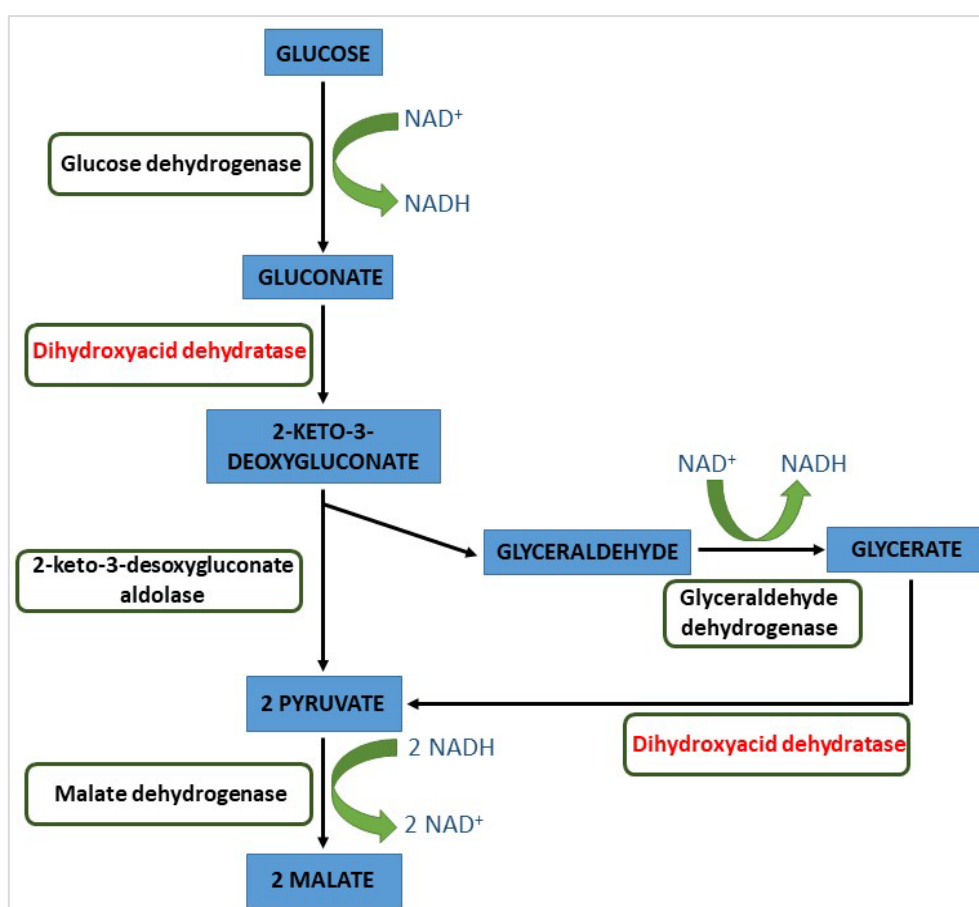
Figure 3.1. Schematic representation of artificial cell-free minimised enzymatic reaction cascade designed to produce malic acid (malate) from glucose. Dihydroxy-acid dehydratase being an enzyme with dual function, catalyses 2 reactions; gluconate to 2-keto-3-deoxygluconate, and is later responsible for the redirection of undesirable intermediate glyceraldehyde into pyruvate. Molecules of CO_2 and H_2O used or released in the individual reaction steps are not shown.

Previous research into cell-free production of malic acid has been successfully demonstrated as outlined in Chapter 1, Section 1.3.2 (Ye et al. 2013), however the number of enzymes employed in the synthetic cascade have been in excess of 10. This is economically unfavourable as increasing the number of enzymes in the cascade leads to a higher number of intermediates which can affect final

yields of the product of interest (Dudley et al. 2015) Use of enzymes from thermophilic sources not only offers ease of purification, their unique metabolic pathways also offer shorter routes to key metabolic intermediates such as pyruvate (Conway 1992). This was adapted successfully into the design and the number of enzymes employed in the cascade is 5, with added redirection of unwanted intermediates into key intermediates (Figure 3.1).

The enzymes used in the cascade design have all been employed from thermophilic organisms due to the thermostable advantages offered (Ninh et al. 2015, Zhang 2015) including one step heat denaturation purification. The Glucose dehydrogenase (GDH) and dihydroxy acid dehydratase (DHAD) gene sequences were obtained from *Sulfolobus solfataricus*, 2-keto-3-deoxygluconate aldolase (KDGA) from *Sulfolobus acidocaldarius*, glyceraldehyde dehydrogenase (AIDH) from *Thermoplasma acidophilum* and NADP (H)-dependent malic enzyme (MDH) was obtained from *Thermococcus kodakarensis* (gene sequences in appendix). To avoid phosphorylation and dephosphorylation steps in the pathway design, promiscuity of *S. solfataricus* DHAD has been exploited (Kim and Lee 2006), which is key to catalysing the transformation of both gluconate to 2-keto-3-deoxygluconate and glycerate to pyruvate, the latter transformation being the redirection of an unwanted intermediate into one that can be actively used in the cascade design. Employing AIDH aids with the reaction dynamic shift towards pyruvate formation as well as maintaining cofactor balance. Using NADH as the only electron carrier further minimizes reaction complexity (Guterl at al. 2012). Exploiting enzymes from the Entner-Doudoroff pathway has formed the basis of some cell-free biosystems as outlined in Chapter 1. The unique coupling of enzymes from the Entner-Doudoroff pathway and an engineered malate dehydrogenase with altered reaction specificity to produce malate from glucose was explored here in an artificial cascade, as well as investigating immobilization strategies. Thermodynamically, this reaction cascade is considered to be favourable as it is adapted from enzymes in the naturally occurring Entner-Doudoroff pathway as outlined in Figure 1.6. Taking into consideration the general rules for designing cell-free synthetic biosystems, the cascade design holds potential for developing a feasible system.

4. Using glucose dehydrogenase from *Sulfolobus solfataricus* to catalyse the first reaction step and produce gluconate from glucose

Glucose dehydrogenase (GDH) from the thermoacidophilic archaebacterium *Sulfolobus solfataricus* utilises a unique non-phosphorylative Entner-Doudoroff pathway to metabolise both glucose and galactose (Theodossis et al. 2005). Not only does it catalyse the oxidation of glucose to gluconate, it has been cited to show activity with a wide range of sugar substrates to further include xylose and L-arabinose (Milburn et al. 2006). These properties make GDH an attractive enzyme to catalyse the initial breakdown to sugars in multiple cascade systems. For the purpose of the cascade discussed in this thesis, GDH was used to catalyse the following reaction:

$$\text{Glucose} + \text{NAD}^+ \rightarrow \text{Gluconate} + \text{NADH}$$
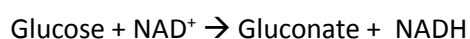
This chapter discusses the protein expression, purification and characterization of GDH. The key challenges faced in finding suitable methods of successful large-scale protein production are also explored. Immobilization has been used by many researchers to overcome instability problems and facilitate the repetitive use of enzymes, furthermore, it has the possibility to improve enzymatic efficiencies due to the increase of local enzyme concentration (Ahmed et al. 2017). Two novel, hierarchically-structured silica-based supports were developed for this purpose and the activity of free-state and immobilized GDH were compared under different pH and temperature conditions to assess their activity. This chapter also explores the stability, long-term storage and the re-use of immobilized GDH. To study the potential of an enzymatic approach to waste valorisation, the generation of gluconate from bread waste hydrolysate (BWH) using immobilized GDH was also analysed.

4.1 Transformation of GDH vector DNA into BL21-DE3 competent cells

Synthesised pET30a vectors containing GDH sequence arrived as a concentrated miniprep of ~4μg of DNA from GenScript (sequence in appendix). The original vector sample was archived and transformation of vector into DH5α competent cells was done followed by a miniprep to obtain 50μl of quantified vector DNA. GDH was transformed into BL21-DE3 cells as they have favourable characteristics for recombinant protein production such as protease deficiency, low acetate production under high glucose conditions and high permeability. Following successful transformation, single colonies were used to initiate protein expression. LB agar kanamycin plates with the successful transformation of vector DNA into BL21-DE3 were also used to prepare glycerol stocks for storage at -80°C for future applications.
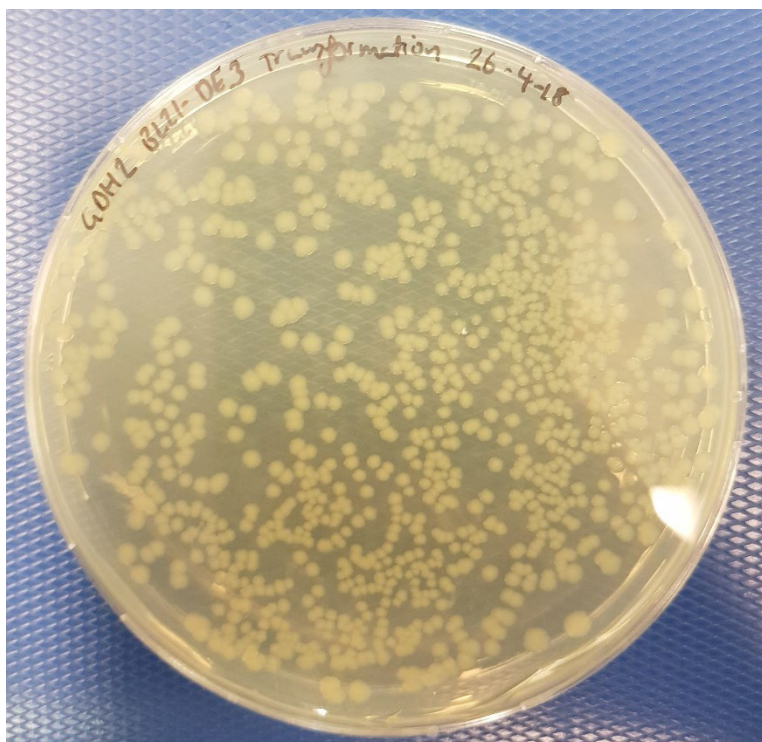
Figure 4.1. Quantified vector DNA obtained following miniprep was transformed into competent BL21-DE3 cells, successful transformation is shown by the presence of bacterial colonies on LB kanamycin plate.

4.2 Small scale GDH protein expression and purification in LB and AI media

Following the successful transformation of GDH vector DNA, protein expression and purification was initially carried out in a 1L final volume. Initial GDH expression was carried out in AI media with a final concentration of kanamycin at 50µg/ml at room temperature overnight. The cell pellet obtained from the cultures were resuspended, sonicated and heat treated as outlined in the methods sections. All resuspension, sonication, heat treatment and centrifugation steps were carried out in a 100mM HEPES pH 7.5, 50mM $MgCl_2$, 10% glycerol buffer unless otherwise stated. The suspension obtained following cell lysis, heat treatment at 70°C to denature host cellular components and centrifugation to remove cell debris, was used as GDH crude enzyme fraction. This crude GDH fraction was used to confirm enzyme activity before purification with Ni-NTA affinity chromatography.

4.3 Establishing enzymatic activity with crude GDH fraction

Before purifying the crude GDH fraction obtained in section 4.2, the crude fraction was assayed for activity by assaying GDH for catalysing the conversion of glucose to gluconate. The concentration of GDH in the crude fraction was not determined and 1ml of crude GDH was used in a 6ml reaction volume with the sole purpose of detecting any gluconate present. Any gluconate formed was detected via analysis with IC as outlined in the methods section. 50mM of glucose was used as substrate with 5mM of the cofactor, NAD^+. The reaction was set up in triplicate with 4 reaction controls as well, $control_1$ of 5mM gluconic acid as a positive control for the IC, $control_2$ without any glucose, $control_3$ without any

NAD$^+$ and control$_4$ without any crude GDH. All assay conditions and control conditions were incubated at 60°C for 1.5 hours before deproteinizing all samples that contained crude GDH followed by analysis via IC. A gluconic acid standard curve (Figure 2.1) was used to calculate the concentration of gluconate present in the assay conditions (Table 4.1).

	Crude GDH Assay	Control$_1$ 5mM gluconic acid	Control$_2$ No glucose	Control$_3$ No NAD$^+$	Control$_4$ No crude GDH
Gluconic acid (mM)	6.20	5.12	N/D	N/D	N/D

Table 4.1. IC analysis of gluconic acid production via crude GDH assayed with 50mM glucose and 5mM NAD$^+$ as substrate and cofactor respectively. Standard deviation for assay conditions= <0.134. N/D=None detected.

Positive enzymatic activity was successfully established via the crude GDH assay. 6.2mM of gluconate was detected via IC in the assay conditions, with the overestimation attributed to error associated with the standard curve. The positive control for the IC analysis also matched to what was expected, 5mM of known gluconic acid was loaded onto the IC as calculated using the peak area and gluconic acid standard curve and was calculated to be 5.12mM which is a slight over estimation by 0.12mM, but still within range. As expected, no peaks corresponding to gluconic acid were seen in controls $_{2, 3}$ and $_4$ as these conditions were missing either the substrate (glucose), cofactor (NAD$^+$), or crude GDH respectively. The retention time for all peaks corresponding to gluconic acid were all observed to be similar. Following on from positive confirmation of enzymatic activity in crude GDH, the crude fraction was then purified via Ni-NTA chromatography in the following section.

4.4 Ni-NTA affinity chromatography of crude GDH

The crude fraction of GDH (50ml in 100mM HEPES pH 7.5, 50mM MgCl$_2$, 10% glycerol buffer) obtained from small scale expression of GDH as outlined in section 4.2, was bound to 5ml of Ni-NTA overnight at room temperature. Following this, the suspension was transferred to polypropylene column and the flow through was collected and the Ni-NTA resin washed with 100mM HEPES pH 7.5, 50mM MgCl$_2$, 10% glycerol buffer. A gradient consisting of 50mM-1M imidazole in 100mM HEPES pH 7.5, 50mM MgCl$_2$, 10% glycerol buffer was then used to elute off bound protein. All samples collected from Ni-NTA affinity chromatography were analysed via SDS-PAGE (Figure 4.2). GDH binding to Ni-NTA via the His$_{10}$ tag was successful as evident from comparing samples in Lane 2 and 3 of Figure 4.2. Crude GHD sample in Lane 2 presents a thick band at around 43kDa which is the size of the GDH monomer. As seen in Lane 3 of Figure 4.2, after binding the crude fraction with Ni-NTA and collecting the flow through, the intensity of the band at size 43kDa was considerably less indicating the GDH in the crude fraction had successfully bound to the Ni-NTA resin. 400-600mM imidazole was indicated to the optimal concentration to elute off GDH.
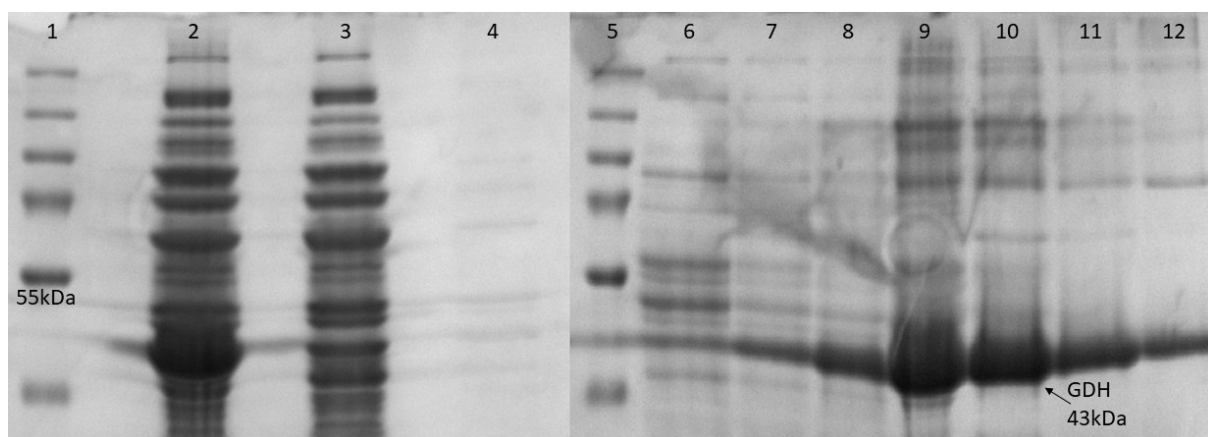
Figure 4.2. SDS-PAGE analysis of Ni-NTA purification attempt of GDH. Samples in all lanes, except Lane 2, are from elutions obtained from the column following Ni-NTA affinity chromatography. Lane 2 contains sample of crude GDH prior to binding with Ni-NTA resin. Lane 3 contains the flow through collected from column and Lane 4 contains the HEPES buffer washes (100mM HEPES pH 7.5, 10% glycerol, 50mM $MgCl_2$). Lanes 6, 7, 8, 9, 10, 11 and 12 contain HEPES buffer imidazole elutions with 50, 100, 200, 400, 600, 800 and 1000mM imidazole respectively.

Fractions from Lanes 9, 10 and 11 of Figure 4.2 containing the highest amount of GDH eluted were pooled (30ml final volume). 100mM final concentration of EDTA was also added to the sample to aid dialysis. Previous attempts of purification of an unrelated glucose dehydrogenase had highlighted the idea of using EDTA to stop protein aggregation during dialysis. Previous attempts of purifying another GDH had run into multiple instances of protein aggregation during the dialysis stage. A solution to this was explored via the addition of 100mM final concentration of EDTA to the dialysis tubing. The elution of bound protein with imidazole also leads to leached nickel ions from the column and into the collection tubing. During Ni-NTA affinity chromatography, both imidazole and the His_{10} tag chelate the nickel, and the removal of just imidazole during dialysis can result in the sample being insoluble. The addition of EDTA assists successful dialysis as it is assumed to chelate the nickel ions and thereby prevents protein-protein self-interactions and a successful dialysis cycle. The 30ml of GDH solution was successfully put through 3 cycles of dialysis until the imidazole and EDTA were dialysed out and their respective concentrations in the solution were negligible. The GDH sample was then concentrated down in volume and its protein concentration was determined via BCA to be 4.42mg/ml.

4.5 Size-exclusion chromatography and protein identification of GDH to determine presence of oligomers

The small scale expression of GDH gave a single band on the SDS-PAGE matching the expected size of the GDH monomer (Figure 4.2, Lane 9), however there are other non-specific bands. To confirm the ratio of protein of interest versus non-specific proteins in the eluted fractions, GDH from section 4.4 was diluted down to 1mg/ml and loaded onto the ÄKTA system and, as size-exclusion chromatography separates molecules in solution based on their molecular weight, the peaks on a chromatogram are

indicative of the different size proteins in the sample. The chromatogram obtained from the size-exclusion of GDH (Figure 4.3) automatically identified 2 peaks and aliquoted them into a collection plate as different fractions.
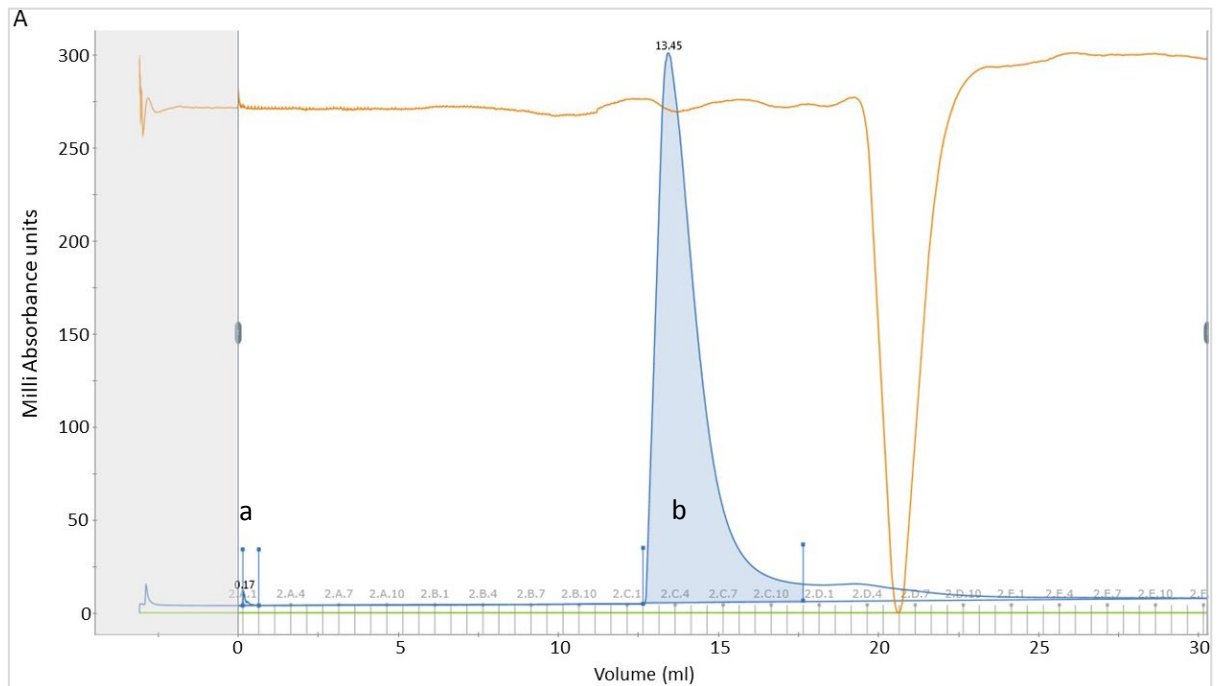
Peak	Retention (ml)	Area (ml*mAU)	Area %	Fractions	Volume (ml)
a	0.17	0.77	0.17	A1	0.5
b	13.45	447.9	99.83	C2-C11	5

Figure 4.3. Size exclusion chromatography of GDH. Figure 4.3A displays the chromatogram obtained from the software. The blue trace represents the UV absorbance at 280nm and the 3 peaks are indicative of the quantity of protein detected. The brown trace reflects the conductivity monitor which measures conductivity of buffer and samples for online monitoring of the true gradient. The green trace is applied if there is another buffer being used, since this sample was run in one buffer only, the trace has a value of 0. Figure 4.3B lists the retention time of each peak as well as the final volume collected of all fractions.

The samples corresponding to those in peak B were determined to be GDH via SDS-PAGE. As this peak made up more than 99% of the total sample loaded, the sample was taken to be 100% GDH.

4.6 Testing enzymatic activity of purified GDH via NADH absorbance assay at 340nm

Following the purification of crude GDH via Ni-NTA affinity chromatography, a 4.42mg/ml enzyme stock was obtained. This purified stock was tested for functional activity to catalyse the conversion of glucose to gluconate. As this reaction uses a cofactor in the form of NAD^+, the primary catalysed reaction can be indirectly followed by the formation of NADH. NADH shows absorption at 340nm while NAD^+ does not, hence any increase in absorbance as measured at 340nm can be correlated to the formation of gluconate as NADH forms a secondary by-product from this reaction as the reaction ratios are 1:1, 1mM of NADH formed should theoretically equate to 1mM of gluconate.

The activity of purified GDH was tested at 6 different enzyme concentrations, 0.003, 0.015, 0.03, 0.06, 0.15 and 0.3mg/ml. All conditions were done in triplicates with 3 reaction controls, control$_1$ without any GDH, control$_2$ without any cofactor, NAD$^+$, and control$_3$ without any substrate, glucose. The assay conditions were 100mM HEPES pH 7.5, 50mM MgCl$_2$, 10% glycerol, 50mM glucose and 5mM NAD$^+$ as outlined in the methods. The assay conditions were consistent through all conditions and the only different variable was the protein concentration of GDH added. The assay and control conditions reagents were loaded into 96 well plates, followed by the addition of the relevant concentration of GDH to each corresponding condition before immediately starting absorbance readings at 340nm for 120 minutes at 60°C. Reaction control 1 was used the background absorbance value and this was deducted from the absorbance values of all the assay condition (Figure 4.4).
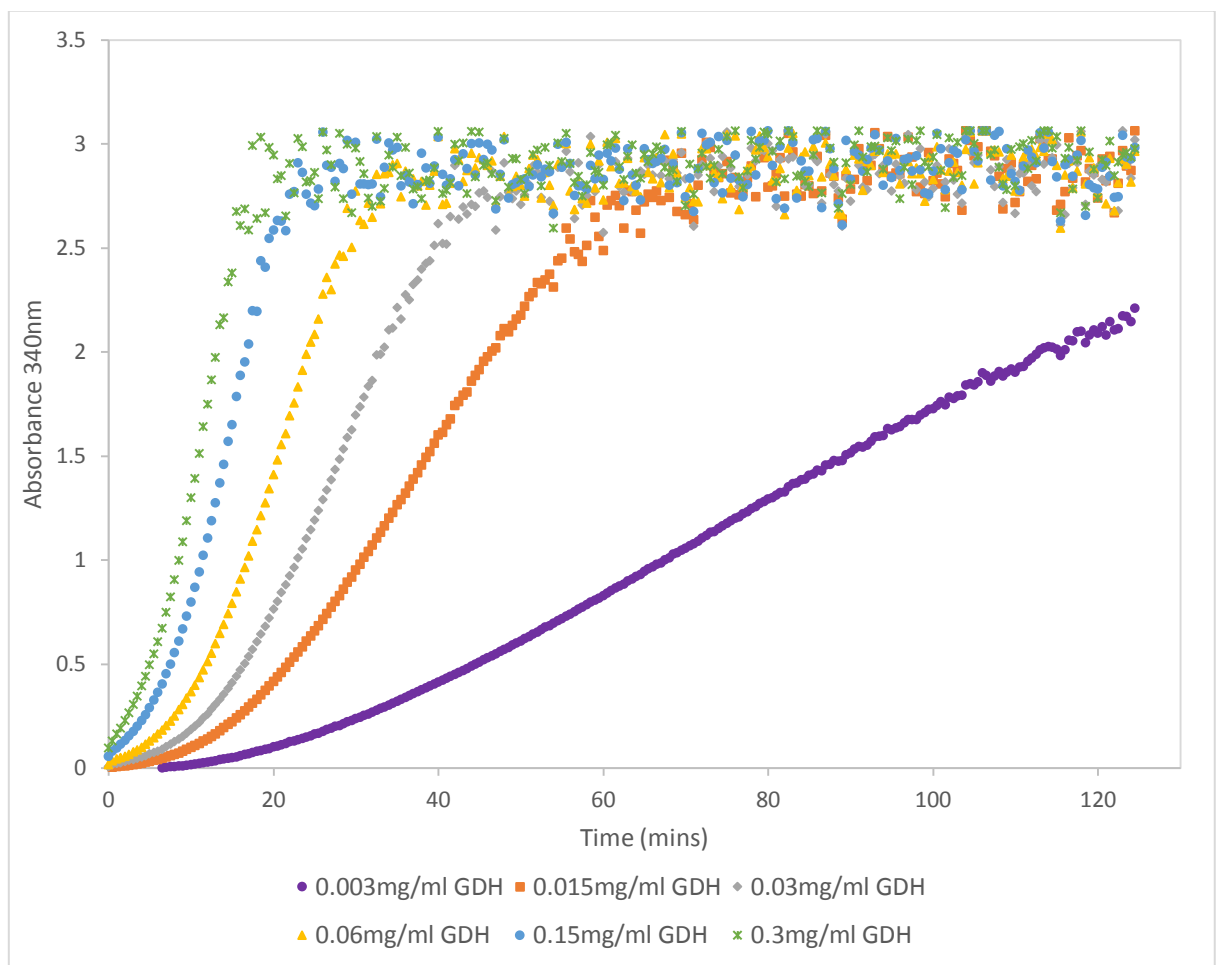
Figure 4.4. NADH absorbance curves at 340nm from 6 different GDH assay conditions with 6 enzyme concentrations at 0.003, 0.015, 0.03, 0.06, 0.15 and 0.3mg/ml GDH. Standard deviations for all GDH assay conditions: 0.003mg/ml= <0.088, 0.015 mg/ml= <0.22, 0.03 mg/ml= <0.21, 0.06 mg/ml= <0.19, 0.15 mg/ml= <0.196 and 0.3 mg/ml= <0.22.

NADH standard curve (Figure 2.1) was used to calculate the final concentration of NADH formed in all reaction conditions, however this posed an issue. As seen in Figure 4.4, all conditions upon reaching an absorbance of around 3 at 340nm, display very sporadic absorbance readings. This is due to the

absorbance values getting out of absorbance range for the plate reader. Only the 0.003mg/ml GDH condition had an end absorbance 340nm that that fell within the range of the standard curve after the reaction time of 120 minutes, thereby only this condition was calculated as NADH mM formed (Table 4.2).

	GDH mg/ml					
	0.003	**0.015**	**0.03**	**0.06**	**0.15**	**0.3**
Absorbance 340nm after 120 minutes	2.21	*3.06*	*3.02*	*2.97*	*2.98*	*2.98*
NADH (mM)	0.83	*1.15*	*1.14*	*1.12*	*1.12*	*1.12*

Table 4.2. End point NADH absorbance readings of GDH assays at 6 enzyme concentrations, 0.003, 0.015, 0.03, 0.06, 0.15 and 0.3mg/ml GDH, after 120 minutes. NADH standard curve (y= 2.6583x, R^2= 0.9975) was used to calculate the NADH mM formed. Only the 0.003mg/ml had an end point reading which fell within the range of the NADH standard curve, remaining 5 assay conditions (grey, italics) had end values outside the range of the curve, thereby the NADH concentration calculated are not reliable.

Following the failure to accurately calculate the concentration of NADH formed in 5 assay conditions, all assay conditions were analysed via IC and concentration of gluconate measured via the peak formed and gluconic acid standard curve (Figure 2.2).

4.7 Analysis of gluconate formation in GDH assays carried out in section 4.6 via IC

Samples from the assays in section 4.6 were deproteinized after the assay was completed at 120 minutes. Following these, the samples were analysed via IC for gluconate formation as outlined in the methods section. As mentioned at the end of the previous section, the gluconic acid standard curve was used to calculate the concentration of gluconate formed in all assay conditions (Table 4.3). Control 1, without any GDH, was also loaded for comparative purposes and no peak was seen at the retention time of gluconic acid in the control sample.

	GDH mg/ml					
	0.003	**0.015**	**0.03**	**0.06**	**0.15**	**0.3**
Gluconic acid (mM)	2.92	3.24	4.59	5.08	5.50	5.56

Table 4.3. IC analysis of samples from GDH assays at 6 enzyme concentrations, 0.003, 0.015, 0.03, 0.06, 0.15 and 0.3mg/ml GDH, after 120 minutes, deproteinized and analysed for gluconate formation. All calculated gluconic acid mM concentrations are from gluconic acid standard curve (y = 1.2304x, R^2= 0.9967).

Following the analysis of these samples via IC, the 0.003mg/ml GDH sample analysed via NADH assay as outlined in Table 4.2 was directly comparable to the 0.003mg/ml GDH sample analysed via IC as in Table 4.3. As mentioned previously, the conversion of glucose to gluconate as catalysed by GDH, uses of a cofactor in the form of NAD$^+$. The primary catalysed reaction can be indirectly followed by the formation of NADH. NADH shows absorption at 340nm while NAD$^+$ does not, hence any increase in

absorbance as measured at 340nm can be correlated to the formation of gluconate as NADH forms a secondary by-product from this reaction. As the reaction ratios are 1:1, 1mM of NADH formed should theoretically equate to 1mM of gluconate. Therefore, the NADH mM concentration calculated in Table 4.2 should be similar in value to the gluconic acid concentration calculated from analysis via IC. These values, however showed a big difference between the amount of gluconate as calculated via NADH absorbance assay (0.83mM) and that calculated via IC (2.92mM), so there was a considerable discrepancy with data for which the expectations for both methods of analysis are to obtain similar values. This discrepancy could have been caused due to the experimental design of the NADH absorbance assay (Figure 4.4). End point readings were not reliable in this experiment and in spite of the end value of the 0.003mg/ml condition was within the range of the NADH standard curve, it was near the highest end where the values begin to fall out of the linear range, by this analogy the end point value of even the 0.003mg/ml GDH assay condition cannot be taken in full confidence. The discrepancy was explored further by repeating GDH with selected enzyme concentrations and time points.

4.8 GDH activity analysis via NADH absorbance assay at 340nm and IC to determine efficiency of methods of analysis

Following the inconsistency between in the gluconic acid concentrations calculated via NADH absorbance assay at 340nm and IC analysis, a new set of experiments were performed to determine if both methods of analysis are able to provide similar concentrations of gluconic acid at the end points. The same experiment as outlined in section 4.6 was set up again with the following changes as these conditions offer intermediate initial rates of reactions as seen in Figure 4.4. The activity of purified GDH was tested at only 2 enzyme concentrations, 0.03 and 0.06mg/ml. All conditions were done in triplicates with a reaction control without any GDH. The assay conditions were 100mM HEPES pH 7.5, 50mM $MgCl_2$, 10% glycerol, 50mM glucose and 5mM NAD^+ as outlined in the methods. The assay and control conditions were loaded into 96 well plates, followed by the addition of the relevant concentration of GDH to each condition before immediately starting absorbance readings at 340nm for either 10 or 20 minutes at 60°C. 2 time points were tested as the absorbance curve in Figure 4.4 indicates the absorbance values around these time points for the 2 GDH concentrations tested, fall in the middle of the NADH standard curve, thereby omitting reliability issues with any data obtained. Reaction control 1 was used the background absorbance value and this was deducted from the absorbance values of all the assay conditions. Following the completion of the 2 reaction conditions at 10 and 20 minutes, the end point value was converted to the amount of NADH formed via the NADH standard curve, thereby the amount of gluconate formed in the assay (Table 4.4).

	0.03mg/ml GDH		0.06mg/ml GDH	
Reaction time (min)	10	20	10	20
Absorbance 340nm after 120 minutes	1.06	2.07	1.83	2.74
NADH (mM)	0.80	1.56	1.38	2.06

Table 4.4. End point NADH absorbance readings of GDH assays at 2 enzyme concentrations, 0.03 and 0.06mg/ml GDH, after 10 and 20 minutes. NADH standard curve (y= 2.6583x, R^2= 0.9975) was used to calculate the NADH mM formed.

Samples from the GDH assays performed above were deproteinized after the assays was completed at 10 and 20 minutes. Following this, the samples were analysed via IC for gluconate formation as outlined in the methods section. A gluconic acid standard curve was used to calculate the concentration of gluconate formed in all assay conditions (Table 4.5). Control 1, without any GDH, was also loaded for comparative purposes and no peak was seen at the retention time of gluconic acid in the control sample.

	0.03mg/ml GDH		0.06mg/ml GDH	
Reaction time (min)	10	20	10	20
Gluconic acid (mM)	0.96	1.61	1.50	2.46

Table 4.5. IC analysis of samples from GDH assays at 2 enzyme concentrations, 0.03 and 0.06mg/ml GDH, after 10 and 20 minutes, deproteinized and analysed for gluconate formation. All calculated gluconic acid mM concentrations are from gluconic acid standard curve (y = 1.2304x, R^2= 0.9967).

After analysing samples from the 2 GDH enzyme and time conditions with 2 different methods of quantification, the data obtained displayed similar values as expected. The 0.03mg/ml GDH assay at 10 minutes was calculated to have formed 0.8mM gluconate via NADH absorbance assay whereby analysis via IC calculated gluconate concentration to be 0.96mM. At 20 minutes the values calculated were different by 0.05mM only as the 0.03mg/ml GDH assay at 20 minutes was calculated to have formed 1.56mM gluconate via NADH absorbance assay whereby analysis via IC calculated gluconate concentration to be 1.61mM. For the 0.06mg/ml GDH assay at 10 minutes, 1.38Mm gluconate was calculated via the NADH absorbance assay and 1.50mM via IC, and at 20 minutes, 2.06mM gluconate calculated via NADH absorbance assay and 2.46mM via IC. The trend in values was much closer here in comparison to the experiment ran initially (section 4.6 and 4.7).

The following work was done in collaboration with Dr Pinar Karagoz and Dr Jinesh Cherukkattu Manayil.

4.9 Immobilization of purified GDH

Immobilization has been used by many researchers to overcome instability problems and facilitate the repetitive use of enzymes (dos Santos et al. 2015). Furthermore, it has the possibility to improve enzymatic efficiencies due to the increase of local enzyme concentration (Ahmed et al. 2017). The successful development of an immobilized enzyme process depends on the properties of the enzyme, the specific immobilization process and the properties of the support, including its morphology, composition, particle size, pore structure, specific surface area, surface functional groups and rigidity (Hartmann and Kostrov 2013) . Due to their robust surface chemistry and tuneable morphology, porous silica supports have been extensively studied for enzyme immobilization. Following the positive confirmation of activity displayed by the purified GDH as outlined in the previous section, large scale enzyme preparation was carried out and purified as mentioned in section 4.4. This batch of purified GDH was immobilized onto support materials (2 novel and 3 commercially available) and the activity of free-state and immobilized GDH were compared under various conditions to and their activity was assessed.

4.9.1 Support materials and immobilization of GDH

To immobilize GDH, three different commercial enzyme supports; methacrylate-based ECR8309F, styrene-based ECR1090M and methacrylate/divinylbenzene-based ECR1030M were purchased from Purolite, UK. Novel supports designated as MM-SBA-15-300 and MM-SBA-15-200 were produced as outlined in the methods section by Dr Jinesh Cherukkattu Manayil. The characteristics of all support materials used in this study are shown in Table 4.6.

Support Material	Type of support	Surface functional group	Immobilization type	Particle size (µm)	Surface area (m²/g)	Pore diameter (nm)	Immobilization efficiency (%)
ECR8309F	Amino C2 Methacrylate	NH$_2$ (short spacer)	Covalent or ionic	150-300	70-220	60-120	59±10
ECR1090M	Macroporous styrene	None	Adsorption/hydrophobic interaction	300-700	750-850	90-110	76±16
ECR1030M	DVB/Methacrylate	None	Adsorption/hydrophobic interaction	300-700	80-120	20-30	73±11
MM-SBA-15-300	Hierarchical porous silica	None	Adsorption/entrapment	100-300*	350-380	290-300 (4.4**)	98±2
MM-SBA-15-200	Hierarchical porous silica	None	Adsorption/entrapment	100-300*	270-300	240-250 (39**)	98±2

Table 4.6. Specification of support materials and their immobilization efficiencies. *Particle size determined by SEM analysis **Mesopores determined from N$_2$ porosimetry by BJH analysis.

Purified GDH was immobilized onto the different support materials listed in Table 4.6 without the use of cross-linking agents. Due to the presence of hydroxyl groups that facilitate enzyme binding, silica-based materials are efficient and attractive supports for enzyme immobilization. The hierarchical structure of macro-meso-porous structured silica-based materials used in this study is shown schematically in Figure 4.5.
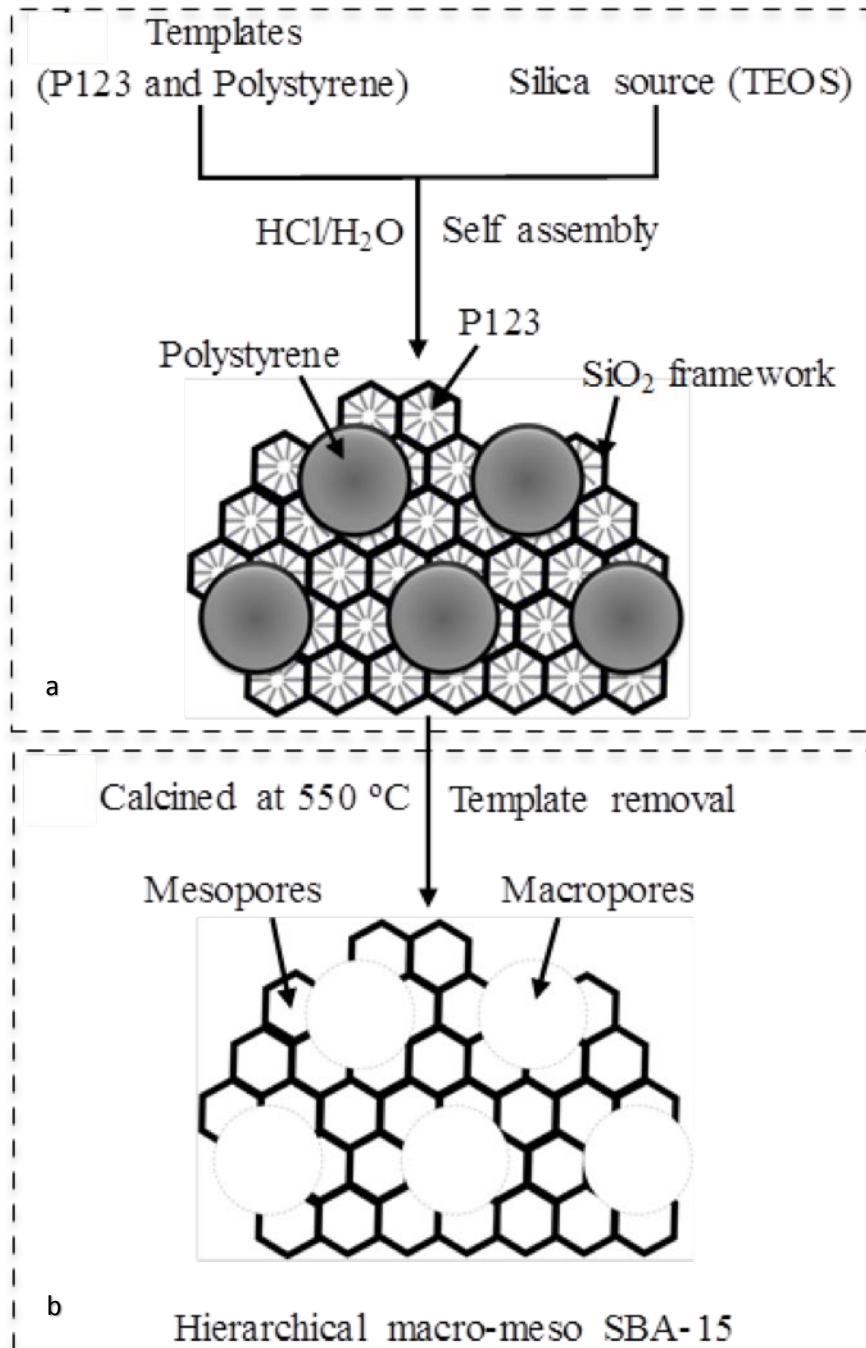
Figure 4.5. Schematic representation of the synthesis of the SiO$_2$ framework containing polystyrene templates (a) and removal of the template (b) to construct the macro-meso structured hierarchical porous material SBA-15.

With the introduction of macroporosity into mesoporous SBA-15 using polystyrene beads, a well-defined interconnected macro-meso network of SBA-15 is formed. The SEM analysis confirmed the formation of macro-meso SBA-15 (Figure 4.6a and b).

a

b

c

d
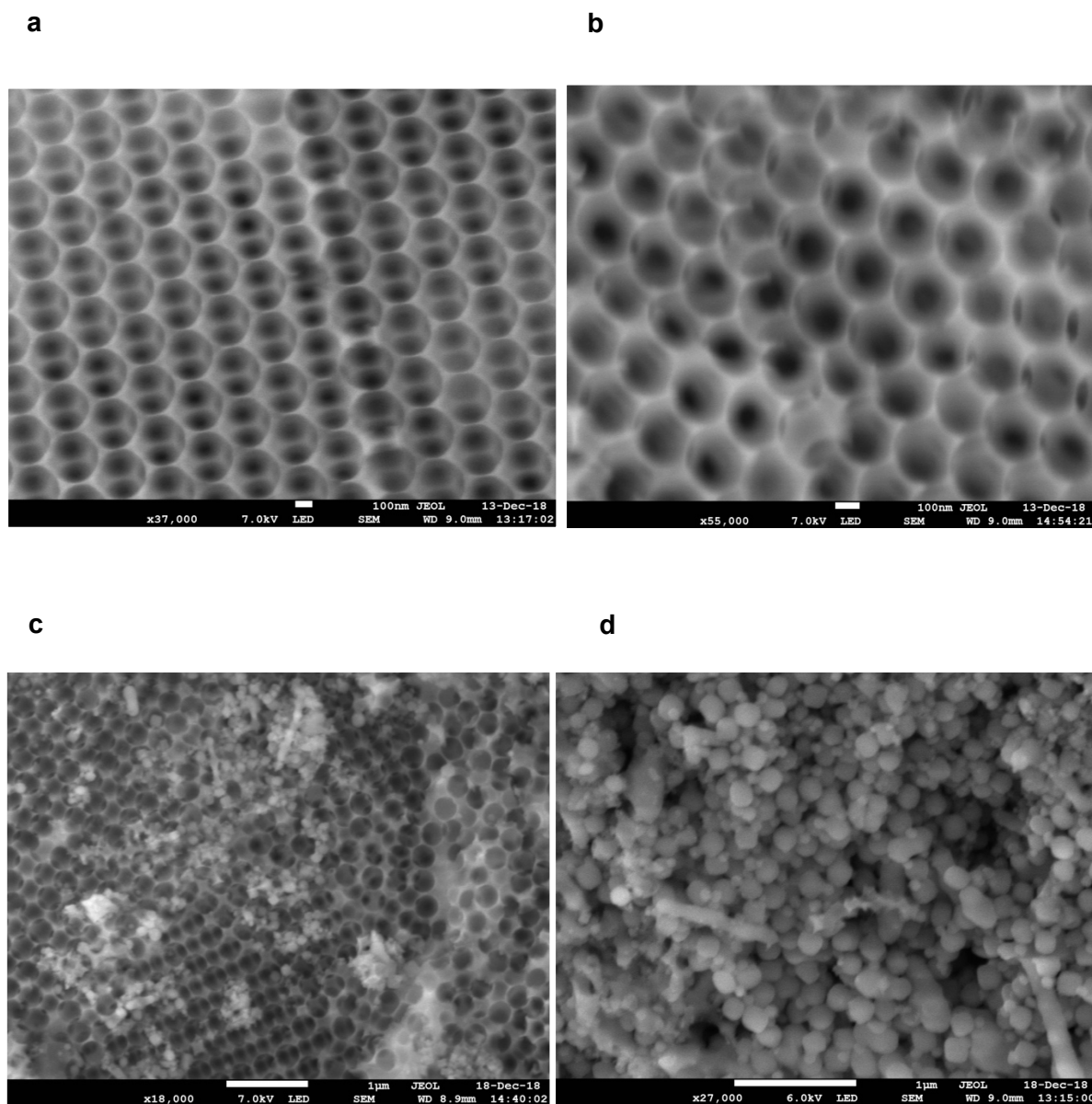
Figure 4.6. SEM of hierarchical structured (a) MM-SBA-15-300, (b) MM-SBA-15-200, (c) GDH immobilized onto MM-SBA-15-300 and (d) MM-SBA-15-200.

The macropore diameter was consistent with the size of the polystyrene bead used in the synthesis. Mesoporous generation was further confirmed by N_2 porosimetry and both MMSBA-15 samples possessed surface areas of ~300 $\pm$ 50 m^2/g. The values were comparable with the commercial macroporous polymer support, ECR8309F, which has a slightly lower surface area of 70-220 m^2/g. The other commercial supports have significantly higher (~700 $\pm$ 50 m^2/g, ECR1090M) or lower (~100 $\pm$ 20 m^2/g) surface areas (Table 4.6). The pore diameters of macro-meso-porous structured MM-SBA-15-300 and MM-SBA-15-200 were 2 to 10 times higher than commercial supports (ECR8309F, ECR1090M,

ECR1030M). In addition, the large surface areas of MM-SBA-15-300 and MM-SBA15-200 are comparable with those of commercial supports. Under the same immobilization conditions, 3mg GDH was immobilized onto 1 g support. Table 4.6 shows that the immobilization efficiency of macro-meso-porous structured silica-based MM-SBA-15-300 and MM-SBA-15-200 were significantly higher than that of all three-commercial support materials. 98% of the GDH was successfully immobilized onto MM-SBA-15 supports. SEM of immobilized GDH onto these hierarchical silica supports is shown in Figure 4.6. The macropore provides a dimension for effective entrapment of enzyme molecules. As a result of its smaller pore diameter, higher amounts of immobilized enzyme were visible on the surface of MM-SBA-15-200 than MM-SBA-15-300 (Figure 4.6d and c respectively).

4.10 Exploring thermal stability of free-state and immobilized GDH

To understand the stability of GDH under non-physiological conditions, free-state and immobilized GDH were assayed to investigate thermal stability at 55, 65 and 80°C after 1, 3, 18 and 24 hours. 0.03mg free-state or immobilized GDH in 500µl enzyme support solution (100mM HEPES pH 7.4, 2.5% glycerol, 50 mM $MgCl_2$) was incubated as required, instantly cooled down on ice for 2 minutes and stored at 4°C for 20 minutes as outlined in the methods section. Cooled samples were gently mixed with assay mixture consisting of 100 mM HEPES pH 7.4, 2.5% glycerol, 30 mM $MgCl_2$, 100 mM glucose, 5 mM NAD^+. Unless otherwise stated, the activity assay for both immobilized and free-state GDH was conducted in a water bath at 55°C for 3 hours. At the end of the assay, samples were placed into pre-cooled racks and supernatants were filtered through 0.2 µm filters. The activity of GDH was detected by measuring the NADH concentrations of the supernatants via a plate reader at 340 nm.

The free-state and immobilized GDH were thermostable at 55 and 65°C, since no significant activity loss was detected (data not shown). However, the samples heated at 80°C for 18 hours lost all activity. Figure 4.7 shows that the thermal stability of GDH immobilized onto ECR8309F, an amino methacrylate support, was significantly higher than the stability of free-state GDH over 60 minutes. However, the thermal stability of GDH immobilized onto ECR1090M and ECR1030M was not significantly increased. The thermal stability of GDH immobilized onto macro-meso-structured MM-SBA-15 supports was significantly lower than GDH immobilized onto commercial supports.
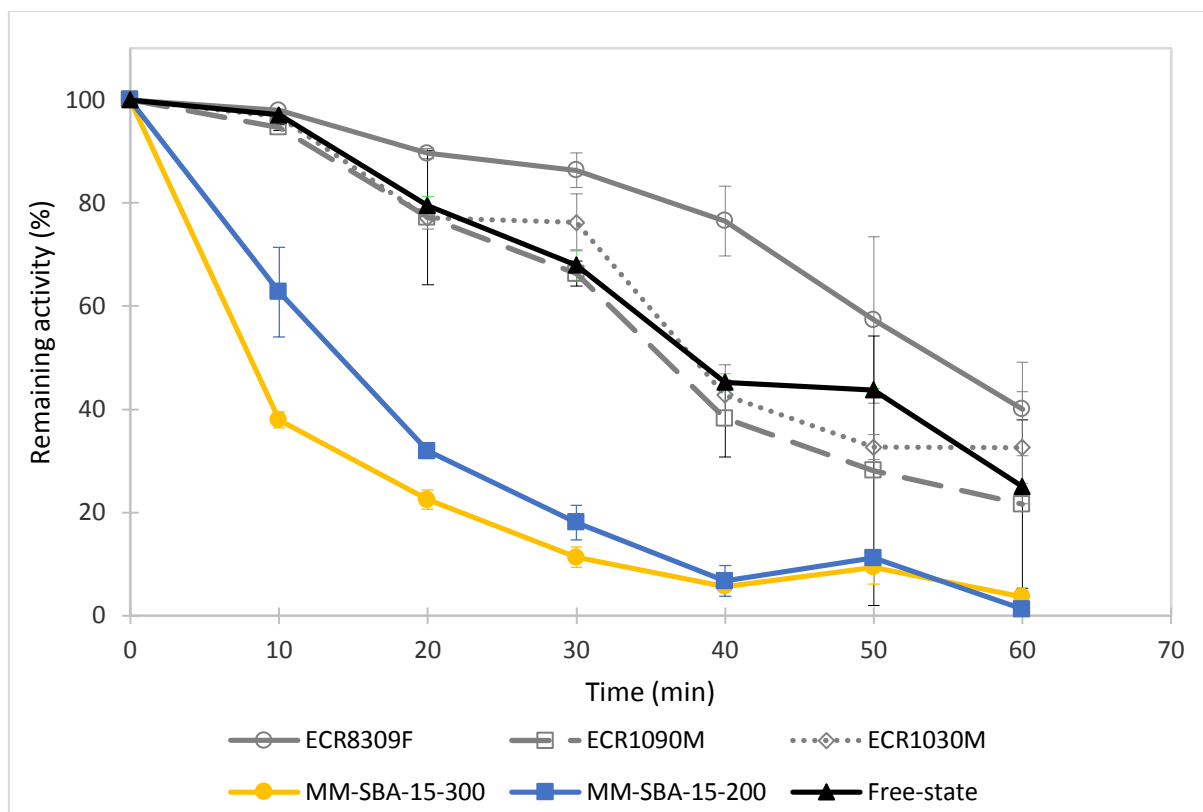
Figure 4.7. Thermal stability of free-state and immobilized GDH on commercial (ECR8309F, ECR1090M, ECR1030M) and hierarchical (MM-SBA-15-300 and MM-SBA-15-200) support materials at 80°C.

4.11 Reusability of immobilized GDH

As free-state enzymes are difficult to recover and re-use (Li et al. 2018), immobilization of enzymes allows cost-effective re-use in a repeated batch or continuously-running processes (Yu et al.2017). In this section, the re-usability of GDH was studied over 10 cycles as outlined in the methods section. During the first 5 cycles, the activity of GDH immobilized on macro-meso-structured MM-SBA15-300 and MM-SBA15-200 was significantly more stable than when it was immobilized on commercial supports (Figure 4.8). At the end of the 5th cycle, GDH immobilized on MM-SBA-15-300 and MM-SBA-15-200 retained 55% and 49% of its initial activity, respectively. The activity of GDH immobilized on ECR1090M, ECR1030M and ECR8309M were 35, 22, and 17% of initial activity, respectively. The reduction of enzymatic activity after each cycle is likely caused by the leakage of unbound enzyme and/or accumulated reaction product on the surface of the material, thereby limiting the diffusion of the substrate and the product.
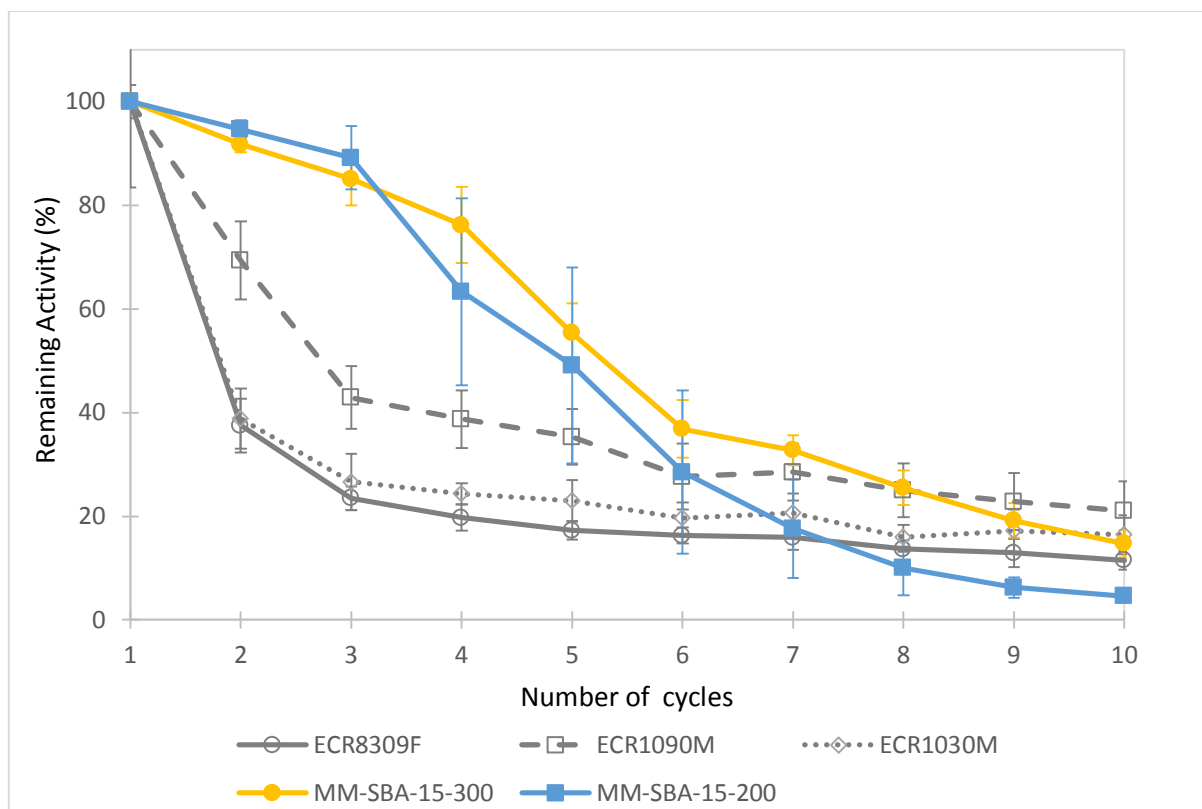
Figure 4.8. Re-usability of immobilized enzyme on commercial and hierarchical supports and their loss of activity after each re-use.

4.12 Storage stability of immobilized GDH

To determine storage stability, free-state and immobilized GDH were stored at 4°C in enzyme support solution (100mM HEPES pH 7.4, 2.5% glycerol, 50 mM $MgCl_2$) for 12 weeks and the enzymatic activity was measured at various time points. Figure 4.9 shows that the catalytic properties of free-state GDH were well preserved in enzyme support solution at 4°C, with 90% activity being retained at the end of the 12-week storage period. However, the activity of GDH immobilized on commercial supports was significantly reduced with increasing storage time. This might be due to pore blockage or hindered accessibility to the enzyme active site, and the amount of enzyme leaking from the supports increased with time. After 8 weeks, 24.7-36.1% of the initial protein loading had leaked from the supports and at the end of the 12-week storage period, the amount of leaked protein increased to 30-43% (Table 4.7). At the end of the 12-week storage period, the remaining activity of GDH immobilized onto MM-SBA-15 supports was 60% higher than that of GDH immobilized onto commercial support materials. In addition, during the 12-week storage period, the remaining activity of GDH immobilized onto silica supports showed similar characteristics to the free-state enzyme.
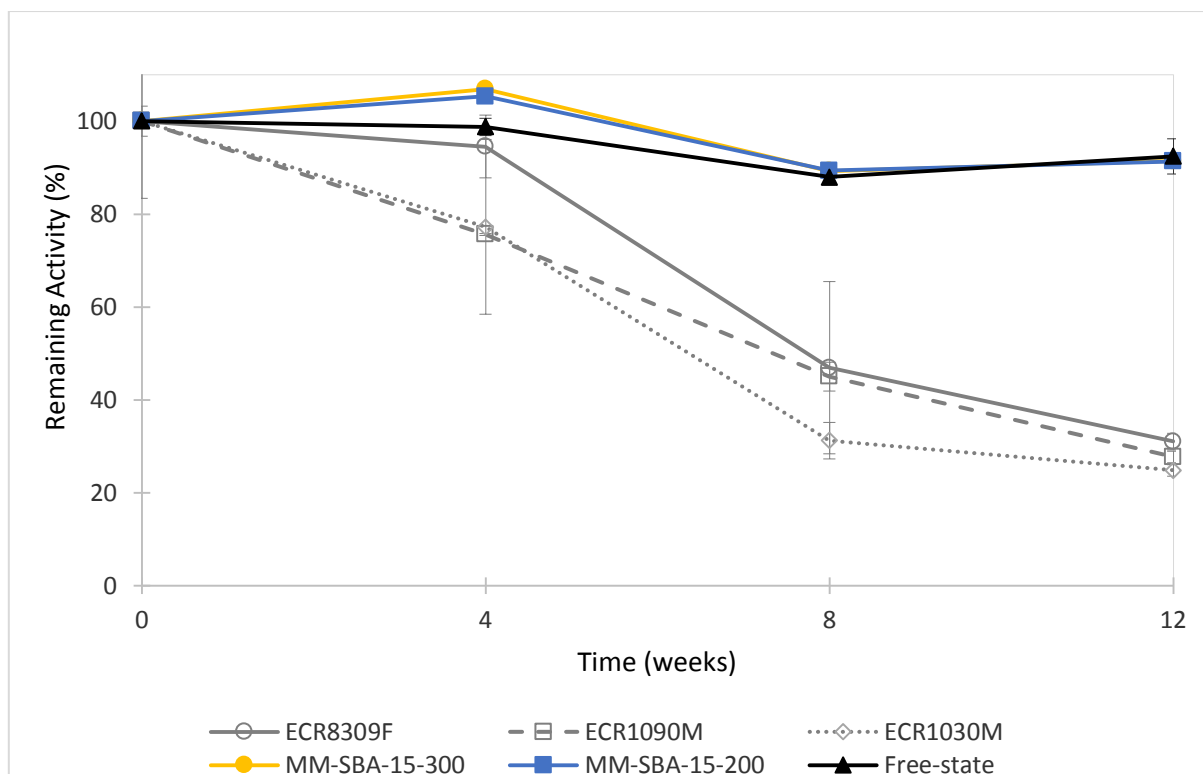
Figure 4.9. Effect of the immobilization and the nature of the support material on the activity of free-state or immobilized GDH stored at 4°C for 12 weeks.

Support Material	ECR8309F	ECR100M	ECR1030M	MM-SBA-15-300	MM-SBA-15-200
Protein leakage (%) after 8-week storage	24±7	31±1	36±3	35±1	36±1
Protein leakage (%) after 12-week storage	30±2	30±1	34±1	40±1	43±3

Table 4.7. Effect of the storage period and the support material on GDH leakage.

4.13 Establishing kinetic parameters of free state and immobilized GDH

The Michaelis-Menten model was used to calculate the apparent V_{max} and K_m values of free-state GDH and GDH immobilized onto MM-SBA-15 supports (Table 4.8). The apparent V_{max} and K_m values of free state GDH were 5.91 U/mg and 0.87 mM, respectively. After immobilization, the V_{max} values of the GDH immobilized onto MM-SBA-15-300 and MM-SBA-15-200 reduced to 0.83 and 1.14 U/mg, respectively. Overall, when GDH was immobilized onto hierarchical supports, there was a 5–7-fold decrease in V_{max}. Compared with free-state GDH, the K_m values of GDH immobilized onto MM-SBA-15-300 and MM-SBA-15-200 increased from 0.87 to 1.88 and 1.22 mM, respectively. Compared to the free-state enzyme and the enzyme immobilized onto MM-SBA-15-200, higher K_m values were observed for GDH immobilized onto MM-SBA-15-300.

Kinetic parameters	Free-state	MM-SBA-15-300	MM-SBA-15-200
V_{max} (U/mg)	5.91	0.83	1.13
K_m (mM)	0.87	1.88	1.22
k_{cat} (1/s)	3.94	0.55	0.76

Table 4.8. Kinetic parameters for free-state and immobilized GDH.

4.14 Establishing optimum conditions for GDH immobilized on macro-meso structured SBA supports

The activity of GDH immobilized onto MM-SBA-15-300 and MM-SBA-15-200 were investigated at different temperature and pH conditions. The effect of temperature on the activity of free-state and immobilized GDH was investigated from 30-80°C at pH 7.4. Free and immobilized enzyme showed optimum activity at 50°C (Figure 4.10a). At temperatures higher than 50°C, immobilized GDH showed better relative activity than the free-state enzyme. As shown in Figure 4.10a, GDH immobilized on MM-SBA-15-300 and MM-SBA-15-200 showed similar characteristics at all temperatures. Figure 4.10b shows the effect of pH on the activity of free and immobilized GDH. The optimum pH for immobilized and free state GDH was pH 7.8. Even at high pH conditions, the activity of GDH was retained, with higher activity remaining for immobilized GDH. At pH 9.6, the residual activity of free-state GDH was 78.8%, while the activity of GDH immobilized onto MM-SBA-15-300 and MM-SBA-15-200 was 93.7% and 95.0, respectively. When the pH was adjusted to 10.5, immobilized GDH retained half its activity, while the free-state GDH retained only 18.7% of its activity.
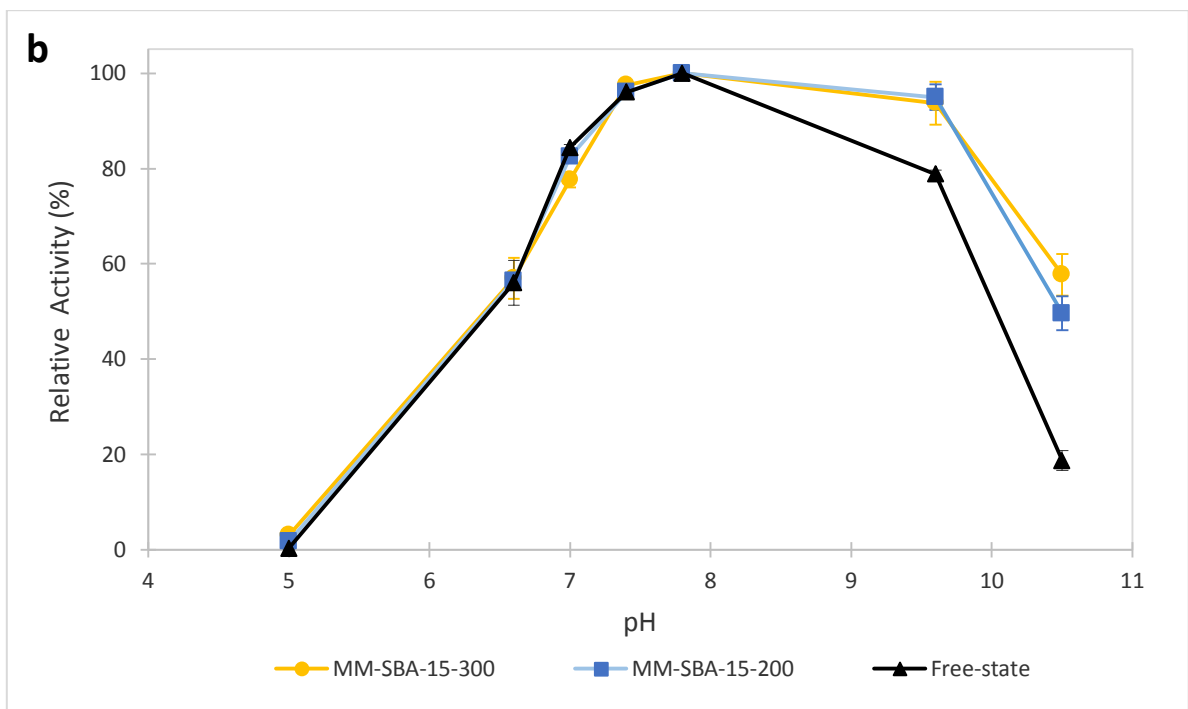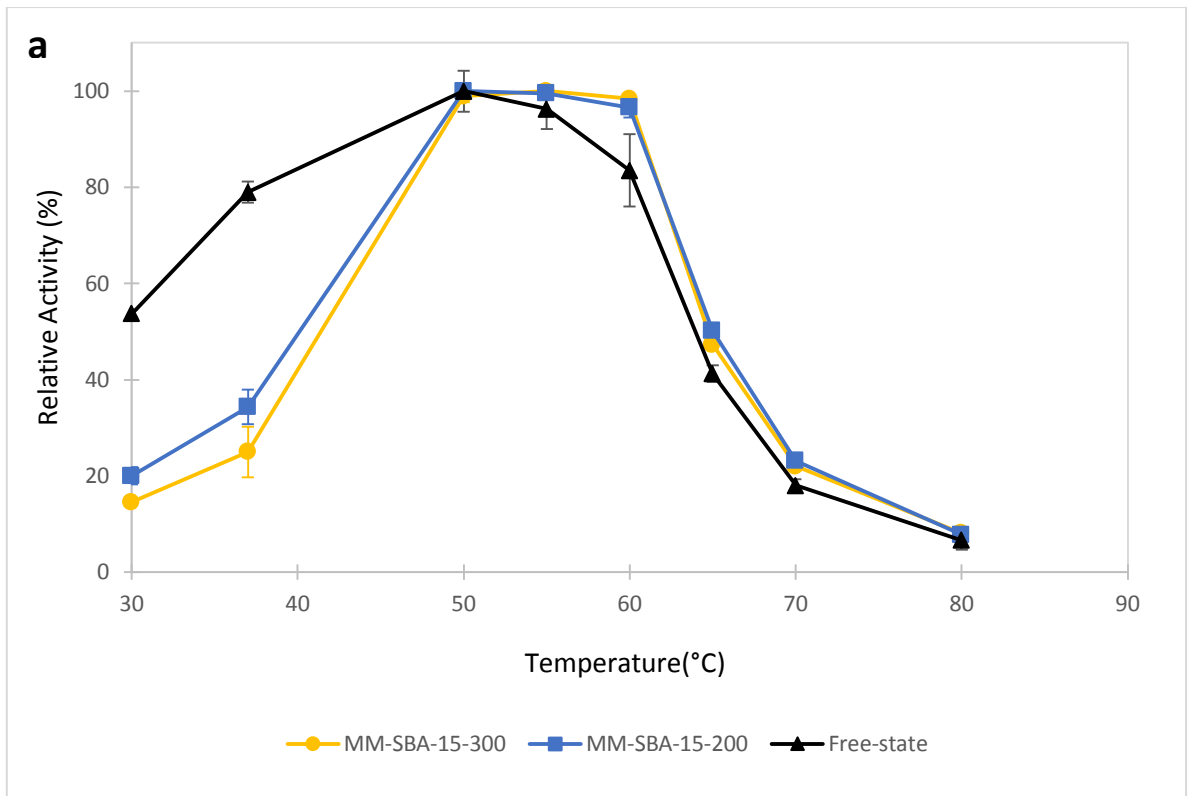
Figure 4.10. Effect of (a) temperature and (b) pH on the activity of GDH when it is in a free-state or immobilized on MM-SBA-15-300 or MM-SBA-15-200.

The effect of enzyme/support ratio on GDH immobilization onto macro-meso structured silica supports was investigated by increasing the amount of protein during the immobilization process. Table 4.9 shows the immobilization efficiency and relative activity of the immobilized GDH at different enzyme loadings. As shown in Table 4.9, almost 100% of the GDH was successfully immobilized when the GDH/support ratio was between 1/1 and 5/1. After this point, immobilization efficiency slightly decreased to 98% and 82% for MM-SBA-15-300 and MM-SBA-15-200, respectively. However, the relative activity of the immobilized GDH increased until the GDH/support ratio reached 5/1. When the MM-SBA-15-300 was used as a support, suitable GDH/support ratios were between 3/1 and 25/1, which achieved high relative activity and high immobilization efficiency. Similarly, for MM-SBA-15-200, suitable GDH/support ratios were between 3/1 and 10/1.

GDH/support ratio (mg/g)		1/1	2/1	3/1	5/1	10/1	25/1
Immobilization efficiency (%)	MM-SBA-15-300	100±0	100±0	99±1	96±4	98±1	98±1
	MM-SBA-15-200	100±0	100±0	99±1	100±0	98±1	82±2
Relative activity (%)	MM-SBA-15-300	89±7	91±3	93±1	95±1	98±1	99±1
	MM-SBA-15-200	64±4	86±5	98±2	99±1	99±1	99±1

Table 4.9. Effect of enzyme/support ratio on enzyme immobilization efficiency and activity.

4.15 Conversion of Bread waste hydrolysate (BWH)

To investigate the stability and activity of free-state and immobilized GDH on waste-based sugars, BWH was used. BWH was prepared as described previously and the glucose concentration of BWH was 63.1±3.3 g/L. This sugar-rich liquor was used as the sole glucose source in the reaction mixture. The final glucose concentration was adjusted to 100 mM using BWH. Figure 4.11 shows the remaining activity after each use of immobilized GDH. After 7 cycles, the remaining activities of immobilized GDH were 64 and 55% on MM-SBA-15-300 and MM-SBA-15-200, respectively. After this point, further use of immobilized enzymes reduced the activity to more than 50% of its initial activity. After 10 cycles, the remaining activities of GDH immobilized onto MM-SBA-15-300 and MM-SBA-15-200 were reduced to 34 and 33%, respectively.
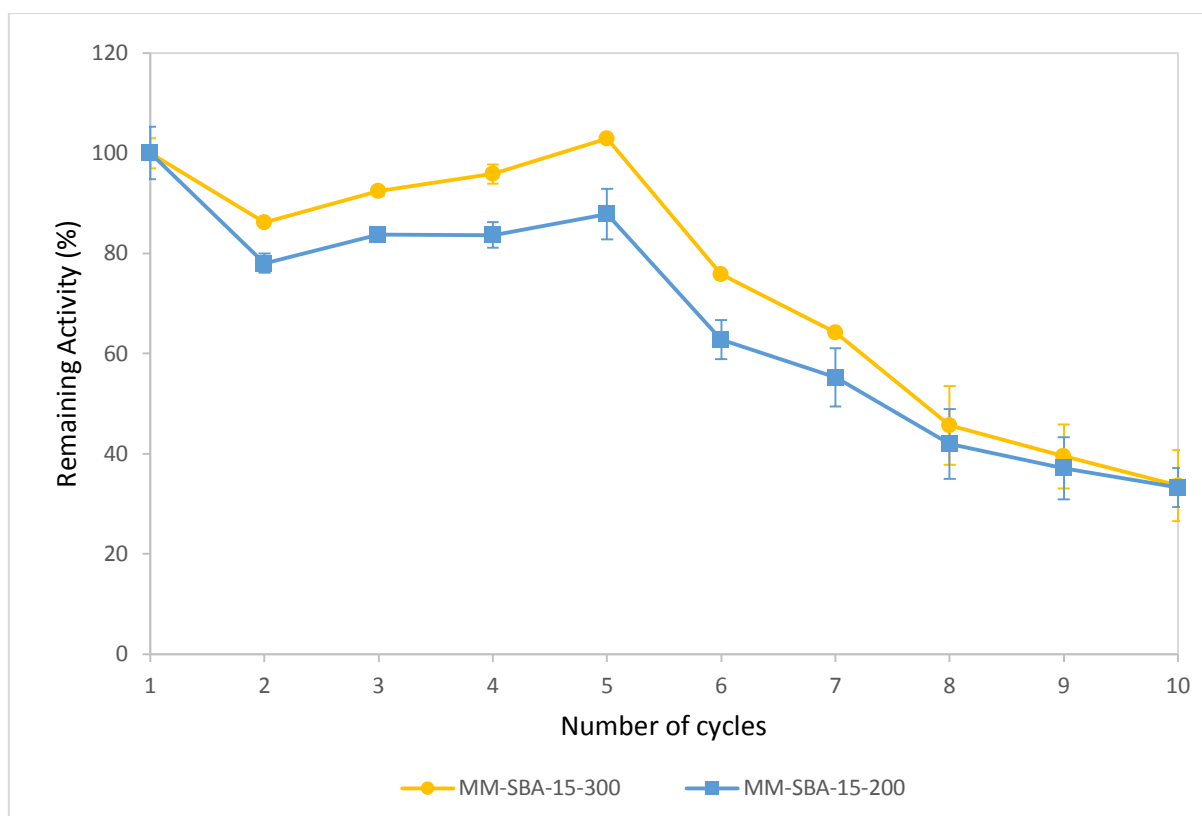
Figure 4.11. Re-usability of GDH immobilized on MM-SBA-15-300 or MM-SBA-15-200 in BWH and the loss of activity after each re-use cycle.

As can be seen from Table 4.10, 45% of the glucose in BWH was converted by free-state GDH. A 2-fold decrease in the conversion yield was observed when immobilized GDH was used. GA production efficiencies by free-state GDH and GDH immobilized onto MM-SBA-15-300 and MM-SBA-15-200 were calculated as 47, 32 and 35 gGA/gGDH, respectively. In every cycle, the GA production efficiency of the GDH immobilized onto MM-SBA-15-200 was higher than MM-SBA-15-300 and after the 10th cycle, the GA production efficiency of GDH immobilized on MM-SBA-15-200 was double that of MM-SBA-15-300.

Parameter	Free-state GDH	GDH-MM-SBA-15-300 1st cycle	GDH-MM-SBA-15-200 1st cycle	GDH-MM-SBA-15-300 5th cycle	GDH-MM-SBA-15-200 5th cycle	GDH-MM-SBA-15-300 10th cycle	GDH-MM-SBA-15-200 10th cycle
Conversion of glucose in BWH (%)	45±8	23±2	25±2	21±4	23±3	25±2	22±2
Gluconic acid (GA) production from BWH (gGA/gGDH)	47±1	32±1	35±1	31±1	38±2	12±1	25±3

Table 4.10. Bio-catalytic productivity of immobilized and free-state GDH on bread waste hydrolysate (BWH).

This chapter has discussed the production of recombinant GDH from *S. solfataricus* and its successful purification and immobilization onto different supports, commercial and novel. GDH immobilized onto a novel, hierarchically-structured macroporous-mesoporous silica support showed great potential for gluconic acid production from glucose as well as BWH. Hierarchically porous MM-SBA-15 showed better immobilization efficiency than commercial supports. Moreover, GDH immobilized onto these materials showed excellent reusability. The use of GDH immobilized onto hierarchically-structured supports has the potential to be incorporated into next generation bio-refineries and waste valorization studies.

5. Dihydroxy-acid dehydratase as a key enzyme in the conversion of multiple intermediates in artificial cascades

Dihydroxy-acid dehydratase (DHAD) is a key enzyme in the Entner-Doudoroff pathway, which itself is an alternative series of reactions to catalyse glucose into pyruvate. DHAD plays its role following the initial conversion of glucose to gluconate via glucose dehydrogenase (GDH), by facilitating the conversion of gluconate to 2-keto-3-deoxygluconate. The substrate promiscuity displayed by DHAD makes it an attractive enzyme to utilise in artificial enzyme cascades. For the purpose of this project, DHAD promiscuity has been exploited at a further step in the cascade to catalyse the reaction of glycerate into pyruvate.
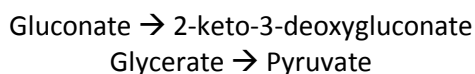
Gluconate → 2-keto-3-deoxygluconate
Glycerate → Pyruvate

This chapter discusses the protein expression, purification and characterization of DHAD. The key challenges faced in finding suitable methods of optimizing and detecting enzyme activity are also reviewed.

5.1 Transformation of DHAD vector DNA into BL21-DE3 competent cells

Synthesised pET30a vectors containing DHAD sequence arrived as a concentrated miniprep of ~4µg of DNA from GenScript (sequence in appendix). The original vector samples were archived and transformation of each vector into DH5α competent cells was done followed by a miniprep to obtain 50µl of quantified vector DNA. DHAD was transformed into *E. coli* BL21-DE3 cells and single colonies were used to initiate protein expression. LB agar kanamycin plates with the successful transformation of vector DNA into BL21-DE3 were also used to prepare glycerol stocks for storage at -80°C for future applications.

Figure 5.1. Quantified vector DNA obtained following miniprep was transformed into competent *E. coli* BL21-DE3 cells, successful transformation is shown in this figure by the presence of bacterial colonies on LB kanamycin plate.

5.2 Small scale DHAD protein expression and purification in LB and AI media

Following the successful transformation of DHAD vector DNA, protein expression and purification was initially carried out in a 2L final volume of LB broth. Initial DHAD expression was carried out in LB broth with a final concentration of kanamycin at 50µg/ml. The final OD_{600} was an average of 3.94 across both 1L flasks. The cell pellets obtained from the cultures by centrifugation were resuspended, sonicated and heat treated as outlined in the methods sections. The crude protein fraction obtained from the prior steps was purified using 5 ml of Ni-NTA resin as outlined in the methods chapter. All resuspension, sonication, heat treatment and purification steps were carried out in a 100mM HEPES pH 7.5, 200mM $MgCl_2$, 10% glycerol buffer unless otherwise stated.
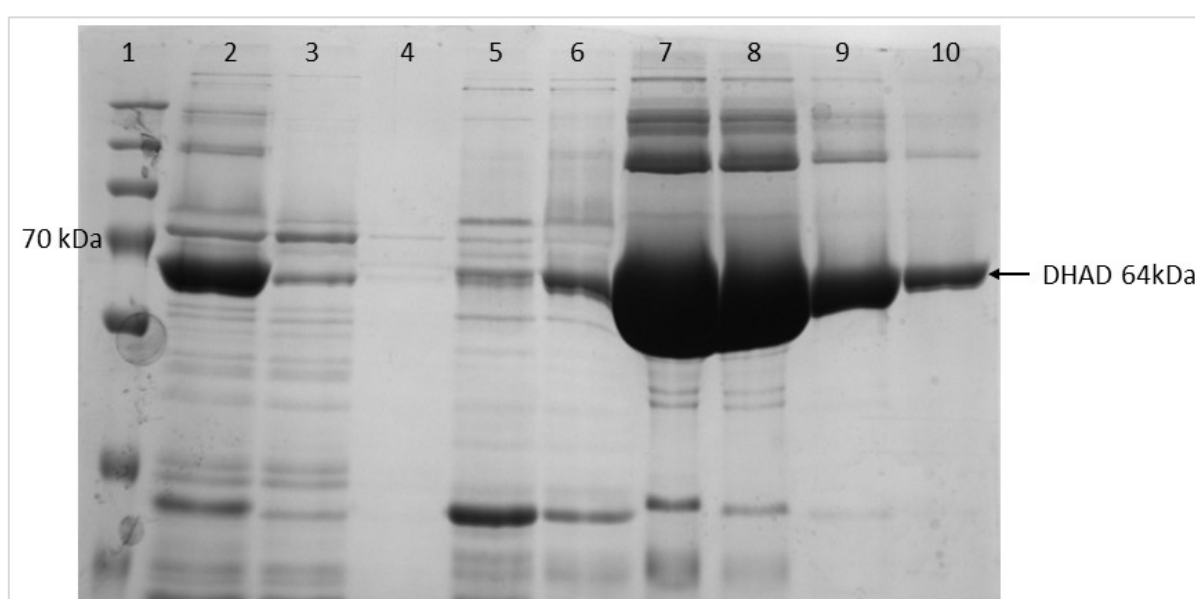
Figure 5.2. SDS-PAGE analysis of DHAD expressed in *E. coli* BL21-DE3 and LB broth. Lane 2 contains crude protein prior to binding with Ni-NTA. Lanes 2 and 3 contain the flow through from the column and HEPES buffer washes (100mM HEPES pH 7.5, 200mM $MgCl_2$, 10% glycerol) respectively. Lane 5 contains HEPES buffer with 50mM imidazole. Lanes 6-10 contain HEPES buffer with 600mM imidazole elutions.

Fractions 7 and 8 from the above purification were pooled and the total 4ml fraction was buffer exchanged into the HEPES buffer (100mM HEPES pH 7.5, 200mM $MgCl_2$, 10% glycerol) using a protein concentrator, and the imidazole was removed by washing the protein with excess buffer. A final protein concentration of 0.5mg/ml was obtained in a 1.5ml volume and no issues of protein aggregation were encountered in this attempt.

Following successful expression and purification of DHAD in LB broth, AI media was also tested as it allows for a higher cell density growth followed by automatic induction of protein expression from lac promoters. 2L of AI media was used to grow cultures of DHAD overnight and the final OD_{600} was an average of 8.96 across both flasks. As with the cultures grown in LB broth, the subsequent steps carried out after expression were the same.
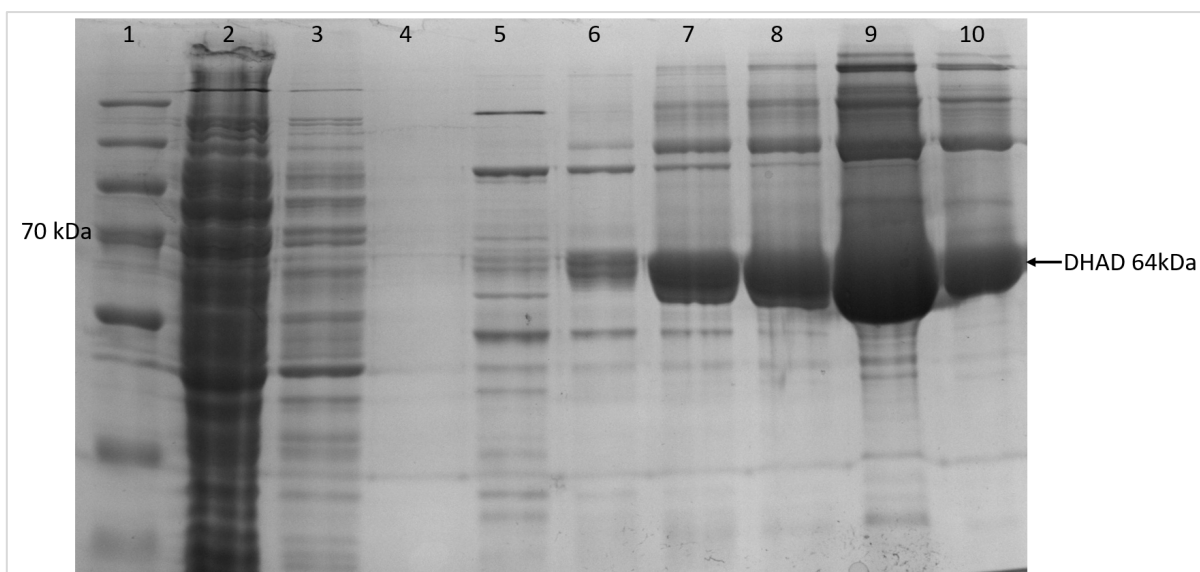
Figure 5.3. SDS-PAGE analysis of DHAD expressed in *E. coli* BL21 (DE3) and AI media. Lane 2 contains the flow through from the column, lane 3 and 4 contain HEPES buffer washes (100mM HEPES pH 7.5, 200mM MgCl$_2$, 10% glycerol), lanes 5, 6, 7, 8 contain HEPES buffer and imidazole elutions at the concentrations of 20, 40, 60 and 80mM respectively. Lane 9 is HEPES buffer and imidazole elution at 600mM and lane 10 is 1M imidazole elution.

Given the final OD$_{600}$ of the cultures obtained from AI media was over twice as high as those from LB broth, a higher protein yield was anticipated. With the previous attempt, an imidazole gradient was not tested and the protein was all eluted off with a single 600mM elution, collected in five 2ml fractions (Figure 5.2). As seen in Figure 5.2, there were a lot of other protein bands which are not desired as they diminish the purity of the final protein sample. For this reason, the DHAD protein produced from the AI media cultures were eluted off using a protein gradient in an attempt to get rid of non-desired proteins before eluting off the product of interest (Figure 5.3). Lanes 5-8 contain HEPES buffer and imidazole washes at 20, 40, 60 and 80mM imidazole respectively. The 600mM imidazole elution followed these, however, as it can be seen from Figures 5.2 and 5.3, the additional imidazole washes were not entirely effective at eluting off non-desired proteins. Presumably due to the higher protein yield obtained, DHAD was eluted off in the lower concentration imidazole washes as well (Figure 5.3, lanes 7 and 8). Two fractions containing the highest amount of protein as determined by the SDS-PAGE were taken forward for further processing (Figure 5.3, lanes 9 and 10), and they were desalted using PD-10 columns. At this stage, both of the desalted fractions were noticed to display signs of protein aggregation. This could be attributed to the high levels of protein overexpression which upon desalting and thereby removal of any leached nickel and imidazole would increase protein-protein self-interactions and increase chances of protein aggregation. The two fractions were filtered through a sterile 0.2μm filter straight after the desalting step to remove the protein aggregates and prevent any further aggregation from taking place. Although protein yield was sacrificed in doing so, further protein aggregation downstream was not observed in these samples. Figure 5.4 shows the samples before and after the filtration step.
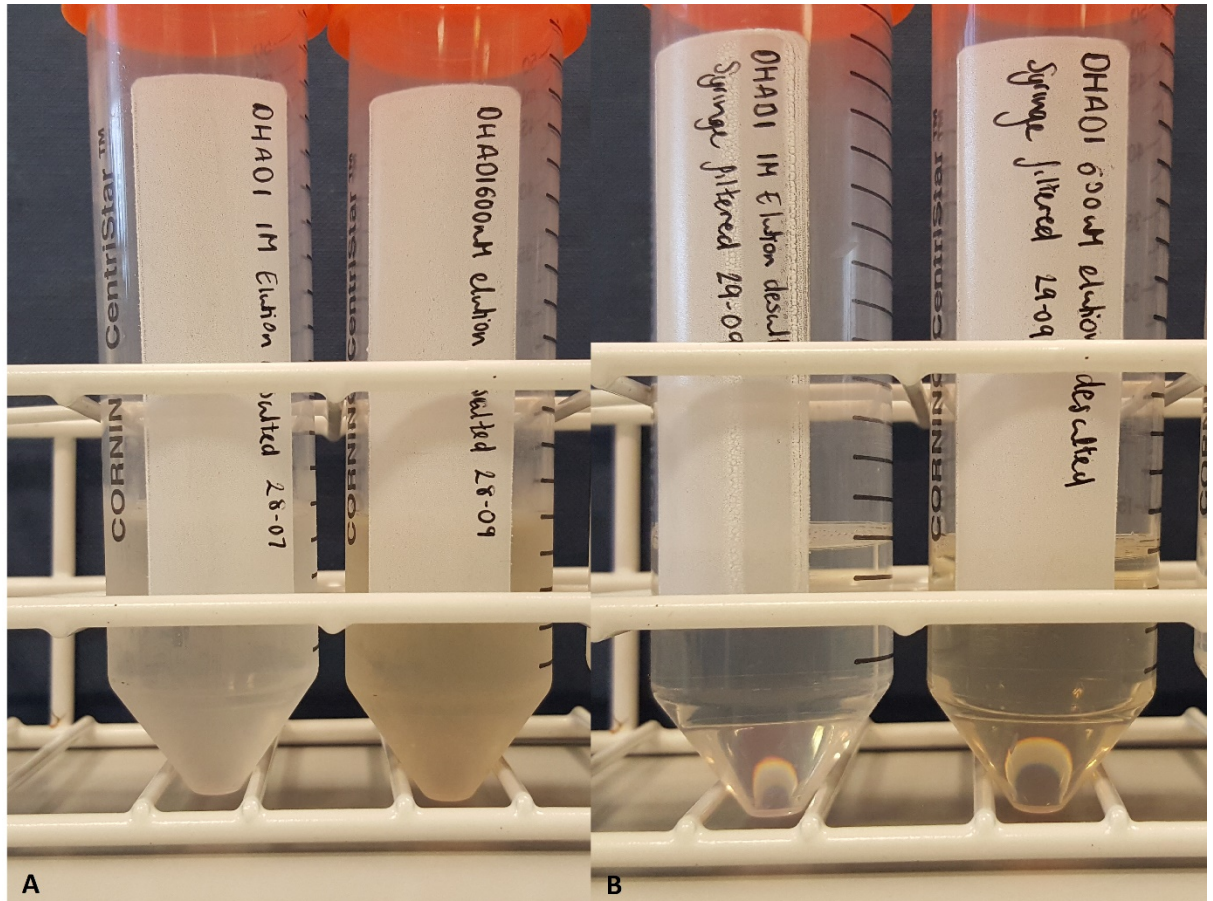
Figure 5.4. DHAD desalted fractions following purification with Ni-NTA. Fractions prior to filtration displaying signs of protein aggregates (A), fractions following filtration and aggregates removal (B).

Following concentration of both fractions, their individual protein concentrations were determined with a BCA, DHAD 600mM imidazole fraction was concentrated down to 8.79mg/ml and DHAD 1M imidazole fraction was concentrated down to 1.34mg/ml.

5.3 Anion exchange of DHAD as a secondary purification step to improve purity

From the initial expression of DHAD as discussed in section 5.2, it was evident that the first cycle of purification is not specific enough to give a protein sample of high purity. Therefore, anion exchange of DHAD was performed as an attempt at a secondary purification step. The DHAD fraction obtained from the Ni-NTA purification at a concentration of 1.34mg/ml (as discussed in section 5.2) was used as the sample for anion exchange. 5ml of this sample was buffer exchanged into 20mM Tris HCl pH 7.5, 5% glycerol buffer which was applied to the column before eluting fractions off with a NaCl gradient ranging from 50mM to 1M. All the final elutions were loaded onto a SDS-PAGE to analyse the effectiveness of the secondary purification step (Figure 5.5). The 50-200mM NaCl elutions were effective at eluting off the protein at the highest purity with only very faint bands for non-specific proteins as seen in the SDS-PAGE. However, 300 and 400mM NaCl elutions produced a similar SDS-PAGE band profile as previously seen in gels from LB broth and AI media purifications. There is an

intense band around the 70kDa, indicative of the DHAD monomer which is 64kDa. Bands were consistently seen around the 130kDa and 250kDa mark which would be consistent with the presence of oligomers (Figure 5.5).
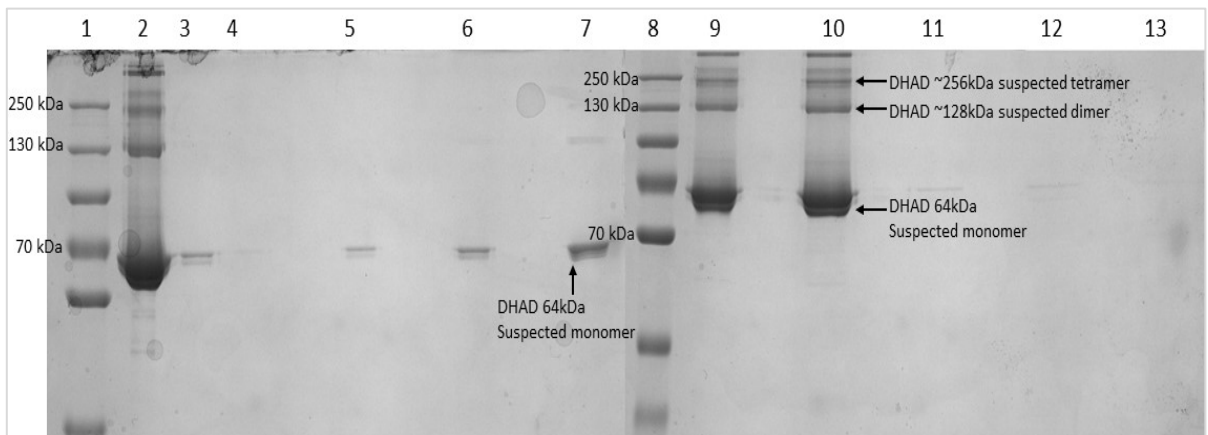
Figure 5.5. Anion exchange of DHAD as a secondary purification step. Lane 2 contains the DHAD sample after buffer exchange into 20mM Tris-HCl, pH 7.5, 5% glycerol buffer; followed by flow through from the column in lane 3, and 5x column wash in lane 4. Lane 5, 6 and 7 contain 20mM Tris-HCl, pH 7.5, 5% glycerol buffer with 50, 100 and 200mM NaCl elutions respectively. Lanes 9, 10, 11, 12 and 13 contain 300, 400, 500, 750mM and 1M NaCl elution, respectively.

Fractions from lanes 5, 6 and 7 were pooled and hereby referred to as sample 1 and fractions from lane 9 and 10 and were pooled hereby referred to as sample 2, both of these fractions were concentrated down a final volume of 1ml and buffer exchanged back into the HEPES buffer as mentioned in 5.2. BCA determined the final concentrations of sample 1 to be 0.1mg/ml and sample 2 to be 1.2mg/ml. As multiple purification steps were applied to DHAD, protein yield was compromised with each added step. For characterization studies to follow, a highly concentrated yield of DHAD in a larger volume was required and therefore, the protocol had to be adjusted in an attempt to achieve these requirements.

5.4 Size-exclusion chromatography and protein identification of DHAD to determine presence of oligomers

As mentioned in section 5.3, bands were consistently seen around the 130kDa and 250kDa mark on the SDS-PAGE which would be consistent with the presence of oligomers. To determine this, a fresh batch of DHAD was purified using Ni-NTA as previously described in section 5.2. The final concentration of this batch as determined by BCA was 5.2mg/ml. As size-exclusion chromatography separates molecules in solution based on their molecular weight, the peaks on a chromatogram are indicative of the different size proteins in the sample. The chromatogram obtained from the size-exclusion of DHAD (Figure 5.6) automatically identified 3 peaks and aliquoted them into a collection plate as different fractions. Multiple samples from each identified peak, a, b and c, were loaded onto a SDS-PAGE in order to visualise their composition. The SDS-PAGE obtained from the samples (Figure 5.7) shows the

composition is exactly the same in all samples loaded, confirming the presence of oligomers. Despite being identified as different peaks, the only difference between them is the quantity of protein present. A concentrated protein sample has been previously observed to elute off in multiple peaks in size-exclusion chromatography and it would seem that this is the case here. In Figure 5.7, samples in lanes 2 and 3 are from peak a, samples in lane 4 and 5 are from peak b and lastly, samples in lane 5 and 6 are from peak c (Figure 5.6A). It is evident from the gel in Figure 5.7 that the same bands are constantly seen in all the samples, differing only in their intensities, which correlates with the different concentrations of protein present in the different fractions. Following the SDS-PAGE, as a further confirmation of oligomers, the DHAD bands indicated in Figure 5.7 were excised from the gel and were analysed with mass spectrometry to confirm protein identification.
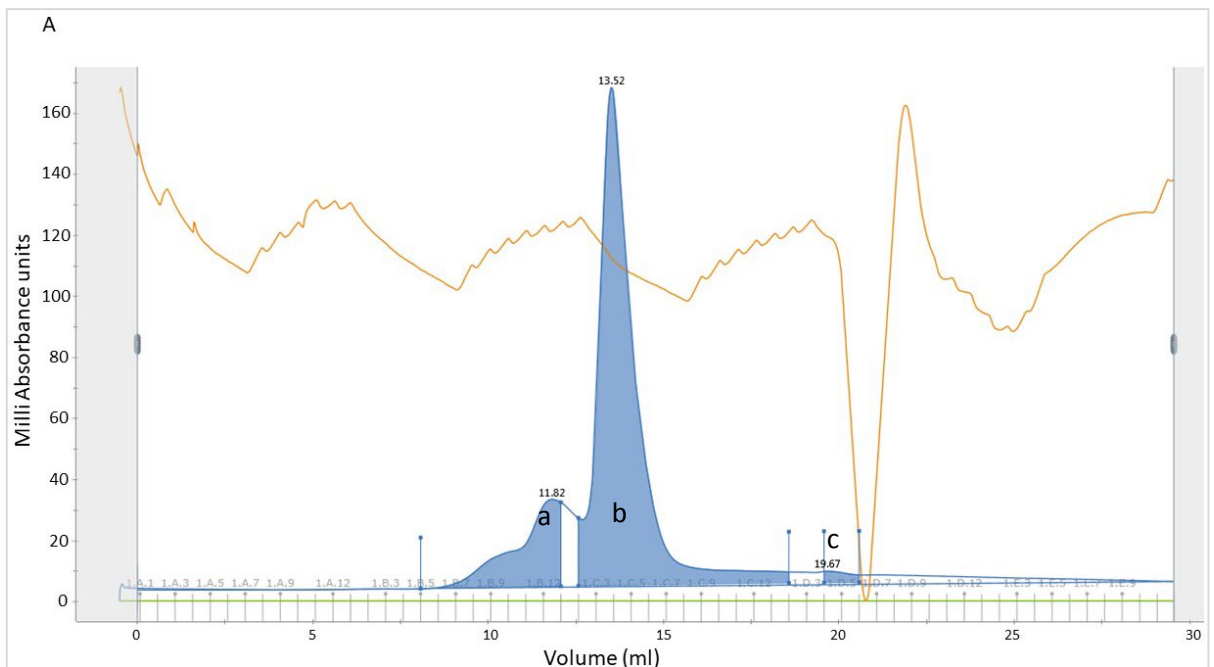
Peak	Retention (ml)	Area (ml*mAU)	Area %	Fractions	Volume (ml)
a	11.82	40.89	17.18	B5-B12	7.80
b	13.52	193.9	81.49	C2-D1	7.79
c	19.67	3.16	1.33	D4-D5	7.68

Figure 5.6. Size exclusion chromatography of DHAD. Figure 5.6A displays the chromatogram obtained from the software. The blue trace represents the UV absorbance at 280nm and the 3 peaks are indicative of the quantity of protein detected. The brown trace reflects the conductivity monitor which measures conductivity of buffer and samples for online monitoring of the true gradient. The green trace is applied if there is another buffer being used, since this sample was run in one buffer only, the trace has a value of 0. Figure 5.6B lists the retention time of each peak as well as the final volume collected of all fractions.
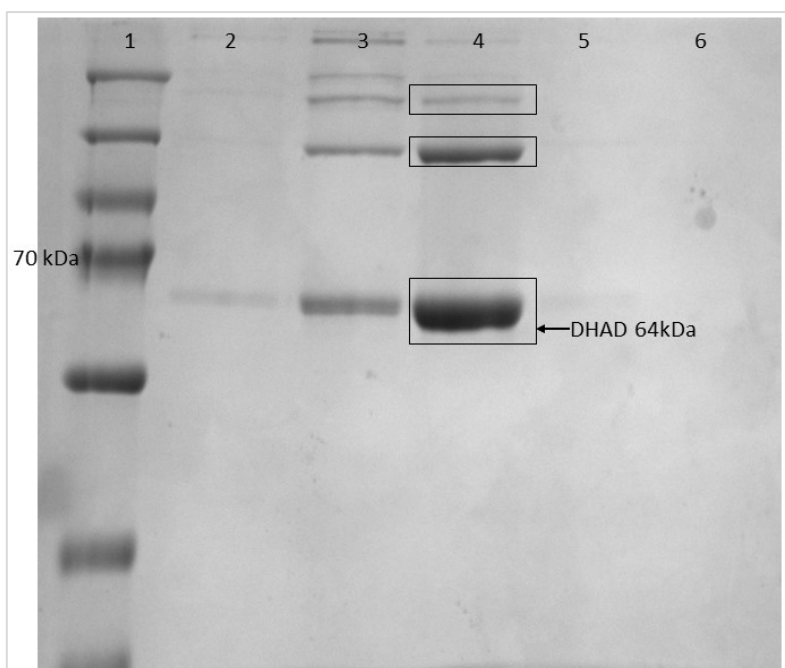
Figure 5.7. SDS-PAGE analysis of DHAD following size exclusion chromatography. Lane 2 and 3 contain samples from peak a, taken from fractions B8 and B12 respectively. Lane 4 and 5 contain samples from peak b, taken from fractions C5 and C10 respectively. Lane 6 contains sample from peak c, taken from fraction D4. The bands indicated in the figure were excised for mass spectrometry analysis.

Mass spectrometry analysis of the bands shown in Figure 5.7 positively identified all 3 bands as being DHAD. Using ImageJ scientific image analysis, the confirmed DHAD bands were calculated as a percentage of the total protein concentration. Using this method allowed for the actual concentration of DHAD to be determined in a sample with other non-specific proteins purified during Ni-NTA purification in future experiments.

5.5 DHAD initial activity analysis via IC (ion chromatography)

Following the size exclusion analysis of DHAD in section 5.4 and positive identification of oligomers with mass spectrometry, a purified enzyme stock of 1mg/ml was used to test enzyme activity in a 1ml final reaction volume with a final concentration of 0.1mg DHAD and 10mM gluconic acid. Gluconic acid serves as one of the substrates for DHAD whereby it is converted to 2-keto-3-deoxygluconate. The assay was set up with a reaction time of 20 hours on a shaking heat block at 60°C, 300rpm. The assay samples were analysed via IC. A known range of concentrations for both gluconic acid and 2-keto-3-deoxygluconate were run on the IC and standard curves were generated (Figure 2.2 and 2.3). These standard curves were then used to calculate the amount of substrate consumed and product formed from the enzyme reaction. Following the 20-hour incubation for the assay, the samples were deproteinized and diluted x100 before loading onto the IC for analysis (Table 5.1).

	Retention time (min)	Concentration after dilution (mM)	Actual concentration (mM)
Gluconic acid	3.39	0.04	4.27
		0.04	3.79
2-Keto 3-desoxygluconate	4.03	0.04	4.06
		0.04	4.22

Table 5.1. IC analysis of assay samples. Assay controls determined gluconic acid concentration via IC standard curve to be 10.15mM. Assay run in duplicate, values obtained from both samples are shown.

The IC analysis of the DHAD initial reaction determined that the purified protein produced is active and is successful at converting the substrate into the desired product. Reaction parameters could now be optimized, and in order to test multiple reaction conditions, a larger batch of DHAD expression protein purification was attempted.

5.6 Large scale expression of DHAD in AI media followed by purification via Ni-NTA

Following successful confirmation of activity displayed by DHAD, large scale expression and purification of DHAD was attempted. Several attempts were made whereby the expression, sonication, heat treatment and subsequent binding and purification using Ni-NTA were successful. However, removing the imidazole from the eluted fractions proved to be challenging. Since these attempts at purification were large scale and the final fractions requiring imidazole removal were too large in volume to efficiently buffer exchange using spin columns, dialysis was the most efficient solution for buffer exchange of these samples. During dialysis however, a persistent problem was faced with sample precipitating out of solution on numerous attempts. Attempts were made by changing the ratio of volumes however the problem still persisted. A solution was provided in the addition of EDTA to the imidazole eluted fractions to be dialysed. This was tested by preparing a large scale DHAD expression (4L), the resulting cell pellet being resuspended in 100ml 100mM HEPES pH 7.5, 200mM $MgCl_2$, 10% glycerol buffer. Following sonication, heat treatment and centrifugation to obtain crude DHAD protein fraction, the soluble protein fraction was bound to 10ml of Ni-NTA overnight. The Ni-NTA bound soluble fraction was split into 2 polypropylene columns hence all elutions were obtained in duplicates. Ni-NTA purification was carried out as outlined in the methods chapter (Figure 5.8).
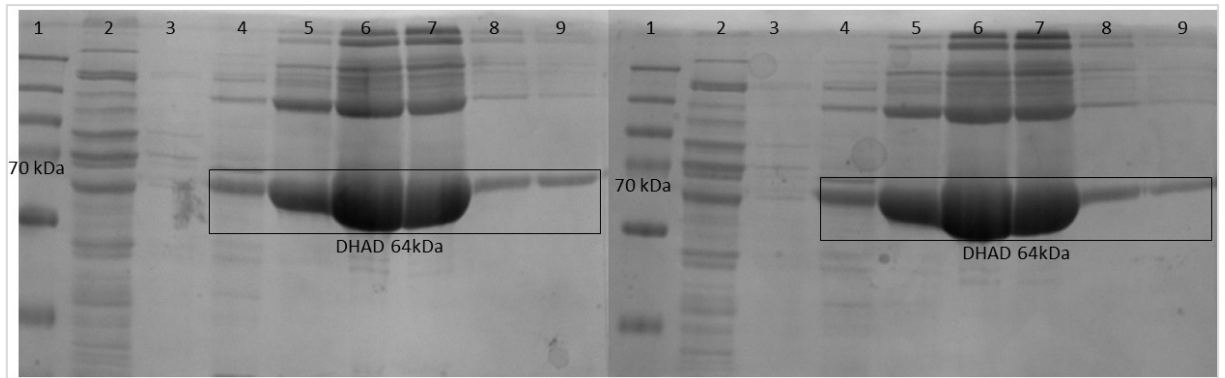
Figure 5.8. SDS-PAGE analysis of DHAD following Ni-NTA purification done in duplicate. Lane 2 contains flow through, lane 3 contains HEPES buffer wash and lanes 4-9 contain HEPES buffer and imidazole elutions at concentration of 50, 100, 200 400 600 and 1000mM respectively.

The HEPES buffer imidazole elutions were collected in 10ml fractions, fractions from lanes 6 and 7 from the purification replicates were pooled (20ml total). One 20ml fraction was dialysed without any added EDTA against 1L of 100ml 100mM HEPES pH 7.5, 200mM MgCl$_2$, 10% glycerol buffer. The second fraction had EDTA added at a final concentration of 100mM and was dialysed against 1L of 100ml 100mM HEPES pH 7.5, 200mM MgCl$_2$, 10% glycerol buffer as well, both dialysis carried out overnight at 4°C. Overnight dialysis was found to have been effective only in the fraction which had EDTA added to it (Figure 5.9), the fraction without EDTA as seen in Figure 5.9 has precipitated out in the dialysis tubing.
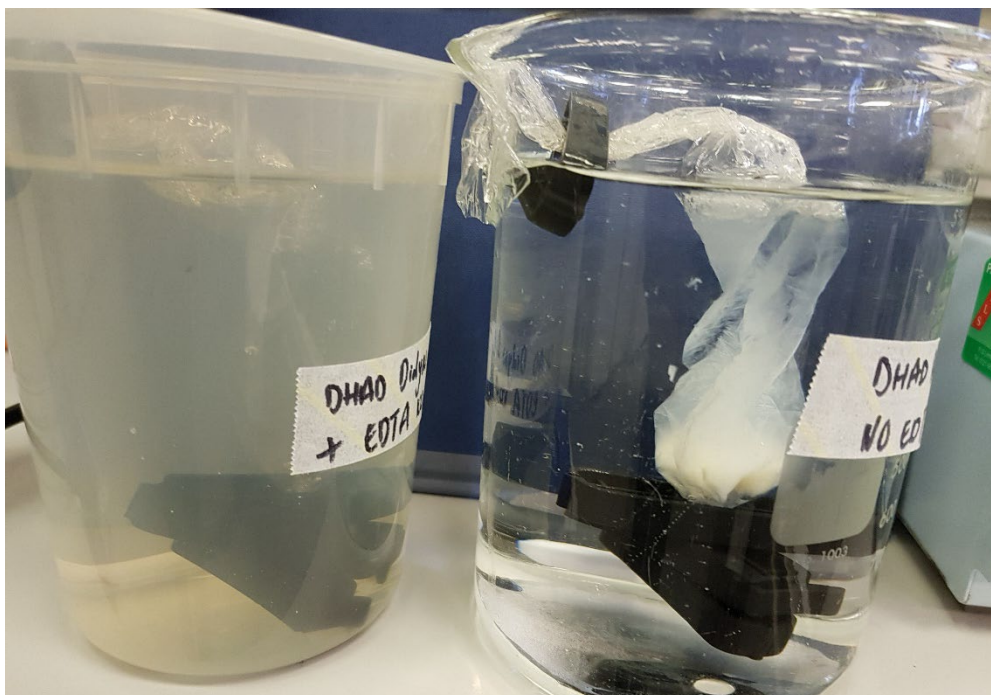
Figure 5.9. Dialysis of imidazole elution from Ni-NTA purified fractions of DHAD. Dialysis is only effective in the replicate with the addition of 100mM EDTA. The fraction without EDTA can be observed to have precipitated out leaving behind a white solid in the dialysis tubing.

Establishing the effectiveness of EDTA at reducing protein precipitation during the first cycle of dialysis, 2 more cycles of dialysis were carried out without any additional EDTA. The latter 2 cycles were calculated to have diluted the imidazole and EDTA concentrations to a negligible concentration so the final DHAD fraction was stored in a 100mM HEPES pH 7.5, 200mM $MgCl_2$, 10% glycerol buffer for further downstream analysis. This fraction was concentrated and its protein concentration was determined to be 3.31mg/ml via BCA.

5.7 IC analysis of DHAD activity with a range of enzyme concentrations

Solving the problem of DHAD precipitating out during large scale preparation with the aid of EDTA in section 5.6, further DHAD stocks were obtained in a sufficient amount to perform further enzyme characterization experiments. 6-reaction conditions were set up in 1ml volumes. 5mg/ml DHAD stock was added in final volumes of 2.5, 5, 10, 20, 50 and 100µl to each condition with 50mM gluconic acid. End point conversion efficiencies were tested after incubation at 55°C for 2 hours, followed by deproteinizing samples and loading onto the IC for analysis alongside the control condition. Due to technical issues with low range of values in the standard curve for 2-keto-3-deoxygluconate at the time of the experiment, the analysis from these assay conditions was only analysed by the consumption of gluconic acid.

A new standard curve for gluconic acid was also generated to accommodate a higher range of concentrations, the standards were diluted by a factor of 10. Using the equation generated from the standard curve, the concentration of each standard was calculated back to check the error factor (Table 5.2). The highest overestimation in calculated concentration was of 0.47mM and lowest underestimation was of 0.26mM.

Gluconic acid concentration (Mm)	Dilution factor	Retention time (min)	Area (mS*min)	Area average (mS*min)	Concentration calculated via curve (mM)
2.5	10	3.59	3.68	3.66	2.97
	10	3.59	3.62		
5	10	3.62	6.57	6.47	5.26
	10	3.61	6.38		
7.5	10	3.63	9.20	9.25	7.51
	10	3.63	9.29		
10	10	3.66	11.81	11.99	9.74
	10	3.69	12.16		

Table 5.2. Analysis of known gluconic acid concentrations via IC. The known concentrations are recalculated using the standard curve to determine possible error factor.

To fit within the range of the standard curve, all assay samples were diluted by a factor 100 before loading onto the IC (final dilution factor of 10 on account of standard curve being at a dilution factor

of 10 previously) The control samples without any DHAD were also analysed via IC and using the standard curve for gluconic acid and factoring in the dilution factor, the gluconic acid concentration calculated was an average of 68.55mM (standard deviation = 0.068). This was an overestimation by 18.55mM as originally 50mM of gluconic acid had been added to all assay conditions. Regardless, the gluconic acid consumption was calculated by subtracting the gluconic acid remaining in each assay condition from 68.55mM (3). Despite the overestimation issue, the original objective for this experiment was considered achieved as the general data trend as seen in Table 5.3 showed the assay conditions with higher DHAD concentrations also consumed increasing gluconic acid over the reaction period.

	DHAD 5mg/ml stock volume added (µl)					
	5	*10*	*50*	*100*	*200*	*500*
Gluconic acid remaining (mM)	5.67	5.43	5.3	5.29	5.27	4.75
***10 for dilution factor**	56.73	54.32	52.99	52.88	52.70	47.53
Gluconic acid consumption (mM)	11.82	14.23	15.55	15.67	15.85	21.02

Table 5.3. DHAD activity analysis via IC. Control with no DHAD and 50mM gluconic acid was also analysed via IC (data not shown in table). Standard deviation for all conditions= <0.49

The enzymatic activity analysis of DHAD carried out as described until this point were all with fresh purified batches of DHAD. These experiments led to positive confirmation of enzyme activity and following this, DHAD enzyme kinetics were explored. Batches of DHAD were therefore produced and snap frozen for long term storage at -80°C to be thawed out and used as required. Unless stated otherwise, the following experiments were carried out with DHAD stocks thawed out from storage at -80°C.

5.8 DHAD activity analysis using gluconate assay kit

5.8.1 Optimizing assay and control dilution factors for compatibility with kit

The next set of experiments to follow were pilot experiments to optimize the reaction conditions for enzyme kinetics. Unlike the experimental setup in section 5.7, the objective for the set of experiments discussed in this section was to establish DHAD activity at lower enzyme concentration and various time points. 3 final enzyme concentrations were tested, 0.1µg/ml, 1µg/ml and 10µg/ml, each at time intervals of 15, 30, 60 and 120 minutes with 20mM gluconic acid as substrate. All reaction conditions were carried out with controls included, with incubation at 55°C and 220rpm. Following the end of the desired incubation period, all samples were deproteinized straight away before analysis with gluconic

acid assay kit. Gluconic acid assay kits were used as they offer an advantage in sensitivity. With lower enzyme concentrations being employed in shorter assay times, the IC analysis is not sensitive for accurate detection. As this was an initial test, the detection kit was only used to assay the depletion of gluconic acid in the 10µg/ml 120 minutes assay condition, on the basis that this condition would display the highest levels of gluconic acid depletion. Sensitivity levels for the detection kit was <2µM gluconate, therefore all samples to be analysed had to be diluted by a suitable dilution factor to be within the detection range of the kit. For this initial test, a range of dilutions were tested to determine which one fits best within the range, for both the assay samples and controls. Gluconate standard was provided in the kit and a range of standards were run alongside each assay (Figure 5.10) on the same 96 well plate.
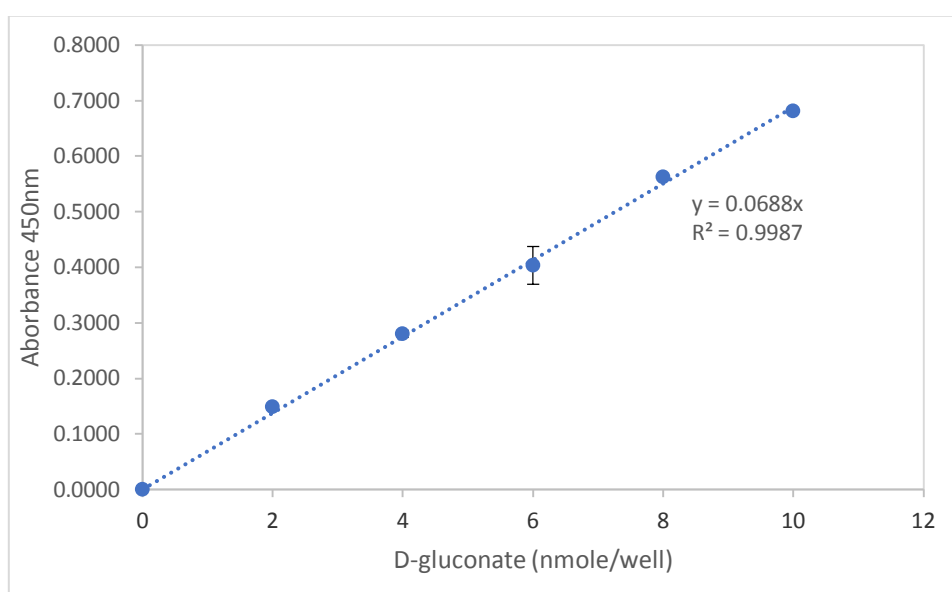
Figure 5.10. D-gluconate standards. Standard deviation for all conditions= <0.03.

Initially, the deproteinized 10µg/ml 120 minutes assay condition samples and controls were diluted by a factor of 2000 and 1000 on the same 96 well plate as the gluconate standards (Figure 5.10), however the final absorbance readings for these were far too low to fit within the range of the standard curve (Table 5.4). A further 2 dilution factors, 500 and 250, were then tested, without running a gluconate standard curve alongside, to estimate if either of these dilution factor was a better fit for the range (Table 5.4).

	DHAD 1µg/ml 120 min assay				Control 20mM gluconic acid (no DHAD)			
Dilution factor	2000	1000	500	250	2000	1000	500	250
Absorbance 450nm	0.04	0.09	0.13	0.26	0.02	0.17	0.26	0.43

Table 5.4. Testing a range of dilutions for assay and control conditions via gluconate detection kit to determine the best dilution factor for fit within range of gluconate standards. Standard deviation for all conditions= <0.029.

From Table 5.4, it was evident that dilution of factor of 250 was sufficient for analysis of both assay and control condition as it is a suitable fit within the range of the gluconate standard curve obtained with the prior set of dilution factor tests. Since the latter two dilution factors of 500 and 250 were assayed without their own gluconate standards, the final absorbance readings from the DHAD 10μg/ml 120 minutes assay condition were not analysed any further to calculate gluconate consumption as it would not be reliable data. Although this experiment was intended as a pilot study to optimize enzyme kinetic experiments for DHAD, the requirement for optimization of assay variables was presented. Therefore, the objective altered into identifying the optimum assay conditions which was ultimately successfully achieved. Any further assays performed with the gluconic acid kit utilise a dilution factor of either 200 or 250 for all samples and controls which gives values that fit well into the range of the standard curve.

5.8.2 Retesting DHAD 0.01mg/ml, all timed conditions with gluconate assay kit and optimized dilution factor

The deproteinized samples from the DHAD 10μg/ml 15, 30, 60 and 120 minute conditions (5.8.1) were all stored at 4°C. Following the establishment of the optimum dilution factor to be used with the gluconic acid assay kit, all the samples from this condition were analysed with the kit. The objective of this experiment was to determine if the assay times need to be adjusted for enzyme activity. All samples and controls were diluted by a factor of 200 and alongside a fresh set of gluconate standards (R^2=0.9), were all analysed as per manufacturer's instructions for the gluconic acid assay kit. The final absorbance readings obtained for the 4 timed conditions and control are shown in Table 5.5, from which it can be concluded that there is no significant difference between the assay and control readings (Control absorbance 450nm=0.406, DHAD 10μg/ml assay 120 min absorbance 450nm=0.405).

	DHAD 0.01mg/ml activity assay				Control no DHAD
	15 min	30 min	60 min	120 min	120 min
Absorbance 450nm	0.41	0.40	0.39	0.41	0.41

Table 5.5. Testing all time points of DHAD 0.01mg/ml via gluconate detection kit to monitor gluconic acid depletion over time. Control condition with substrate only sampled at final time point of 120 minutes. Standard deviation for all conditions= <0.024

As these set of experiments were performed with DHAD stocks thawed from storage at -80°C, possible batch degradation of DHAD was considered as a plausible explanation for the apparent lack of activity displayed by the enzyme.

5.9 Exploiting substrate promiscuity of DHAD to confirm activity via pyruvic acid assay kit

Following on from inconclusive data about activity displayed by DHAD towards gluconate, its substrate promiscuity was exploited. Although experimental data from section 5.8 hinted at potential storage induced enzyme degradation, this was tested to confirm or deny possible degradation. DHAD also facilitates the conversion of glyceric acid to pyruvic acid, and using the pyruvic acid assay kit, accumulation of pyruvate can be monitored. Multiple batches of DHAD were tested to ensure the results obtained in section 5.8.2 were not due to a single batch anomaly. 3 batches of DHAD were tested, DHAD batch 1, which was snap frozen and stored at -80°C, DHAD batch 1a stored at 4°C and DHAD batch 2 snap frozen and stored at -80°C. 2 concentrations of DHAD were tested, 0.01mg/ml and 0.1mg/ml with 20mM glyceric acid as substrate at a reaction time of 1 hour. All other reaction parameters were the same as stated in section 5.8.1. Pyruvic acid assay kit contains pyruvate standards which were run alongside assay samples and control containing no DHAD.
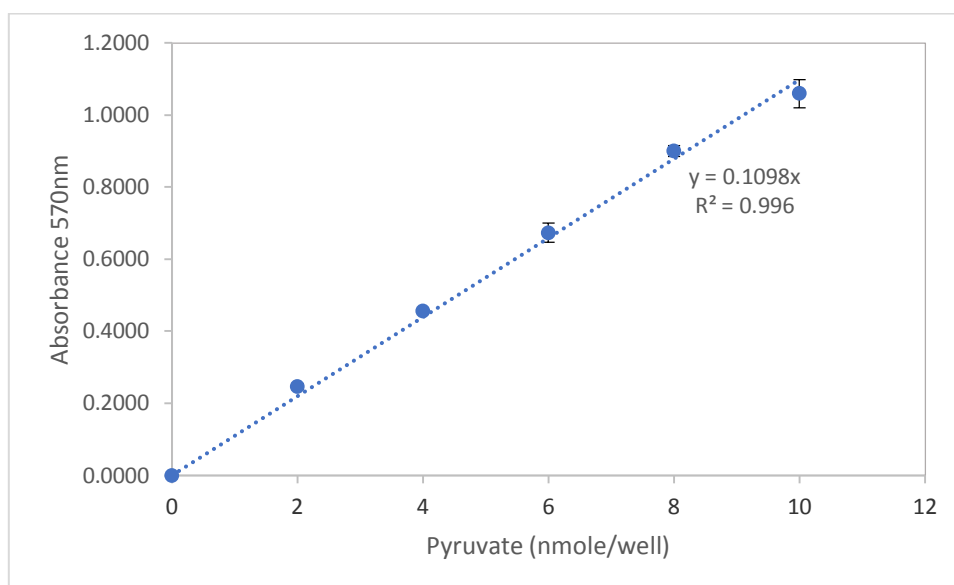
Figure 5.11. Pyruvate standards. Standard deviation for all conditions= <0.039.

	DHAD batch 1		DHAD batch 1a		DHAD batch 2		Control no DHAD
DHAD mg/ml	0.01	0.1	0.01	0.1	0.01	0.1	N/A
Absorbance 570nm	0.06	0.59	0.01	0.13	0.01	0.09	0.00
Pyruvate ng/µl	0.93	9.55	0.21	2.04	0.13	1.46	0.05

Table 5.6. Analysis of pyruvate production using pyruvic acid assay kit from 2 different batches of DHAD and storage conditions. Standard deviation for all conditions= <0.02.

Batch 1 of DHAD gave the highest absorbance reading when tested with the pyruvic acid assay kit from all the batches tested, calculated amount of pyruvate in this reaction was 9.55ng/µl. As expected, the control sample showed the lowest absorbance reading indicating no pyruvate present in sample. The experiments conducted for analysis with gluconate assay kit (section 5.8) were done using 0.01mg/ml

DHAD as the highest enzyme concentration. For the purpose of detecting product with certainty, the activity assays conducted in this section for analysis with pyruvic acid assay kit were performed with an additional enzyme concentration of 0.1mg/ml. The 10-fold increase in enzyme activity was sufficient to detect pyruvate.

5.10 Increased DHAD concentration activity analysis using gluconate assay kit

As established from section 5.9, increased enzyme concentration of DHAD in the reaction following the conversion of glyceric acid to pyruvate, pyruvate was detected with the pyruvic acid assay kit. Following this, increased DHAD concentration was then also used to retest activity using gluconic acid as substrate and gluconate assay kit to monitor the consumption of gluconic acid. 0.05mg/ml and 0.1mg/ml DHAD were tested with 20mM gluconic acid as substrate, all other reaction parameters were the same as stated in section 5.8.1. Dilution factor of 200 was applied to all assay and control conditions as determined previously in section 5.8.1, and gluconate standards were run alongside assay and control samples (R^2= 0.99).

	DHAD 0.05mg/ml	DHAD 0.1mg/ml	Control no DHAD
Absorbance at 450nm	0.40	0.37	0.42

Table 5.7. Testing activity of DHAD 0.05mg/ml and 0.1mg/ml via gluconate detection kit to monitor gluconic acid depletion. Standard deviation for all conditions= <0.007.

The absorbance values obtained for the 0.1mg/ml DHAD and the control (20mM gluconic acid, no DHAD) samples were used to calculate the amount of gluconic acid present in each the assay and control condition. The control condition was calculated to have 44.41ng/μl of gluconate still present, whereas the 0.1mg/ml DHAD condition was calculated to have 39.15ng/μl of gluconate present. There was still considerable amount of gluconic acid present in the assay condition, leading to the conclusion that gluconic acid levels in the assay have not been depleted and the enzyme is displaying very low levels of activity, possibly due to -80°C storage induced degradation.

5.11 Testing activation of DHAD using 2-Mercaptoethanol (2-ME) to improve activity

Establishing optimum enzyme activity of DHAD was difficult due to stored batches of purified DHAD displaying poor levels of activity even when higher enzyme concentrations were used in assays. Literature has been cited to use 2-ME to improve enzyme activity as it was established to be 'activating' the enzyme (Carsten et al. 2015). An aliquot of DHAD batch 1 (previously used as stated in section 5.9) was used for this experiment and the experimental condition contained 1.6mg/ml DHAD in a 100mM HEPES pH 7.5 buffer supplemented with 98mM 2-ME. This solution was then 'activated' as per methodology. The resulting enzyme solution was buffer exchanged into 100mM HEPES pH 7.5 buffer to remove 2-ME. This activated DHAD was assayed under the same conditions using gluconate assay

kit as stated in section 5.10 using DHAD stock sample as a control, in an attempt to determine the effect of the 'activation' protocol on the activity of DHAD.

	Activated DHAD		Non-activated DHAD		Control
	0.05mg/ml	0.1mg/ml	0.05mg/ml	0.1mg/ml	No DHAD
Absorbance 450nm	0.45	0.44	0.56	0.46	0.67

Table 5.8. Testing activity of 2-ME activated and non-activated DHAD 0.05mg/ml and 0.1mg/ml via gluconate detection kit to monitor gluconic acid depletion. Standard deviation for all conditions= <0.19.

The control samples for this experiment gave a mean absorbance value of 0.67. For all previous experiments done where the same control was run, the absorbance values have been 0.43, 0.41 and 0.42 (section 5.8.1, 5.8.2 and 5.10 respectively). This absorbance value from this experiment falls outside of the normal range expected from this sample as it has been consistent in the past experiments, moreover the value of 0.67 falls outside the range of the gluconate standards (R^2= 0.98). The absorbance values obtained from the experimental conditions of activated and non-activated DHAD are inconclusive as well. In The condition 0.1mg/ml for both conditions gave similar absorbance values, indicating that the activation protocol has not had a significant effect on improving the activity of the enzyme.

5.12 Activating crude DHAD to establish improved enzyme activity instead of purified DHAD

Following unsuccessful experiments to establish higher levels of activity from the purified DHAD, an approach was devised to use crude DHAD in an attempt to establish activity instead. From this point onwards, unless otherwise stated, fresh DHAD was used for enzymatic activity purposes. As per methodology in chapter 2, DHAD was expressed and a final wet weight pellet of 19.43g was obtained. Following the heat treatment purification of DHAD, the crude was dialysed into a final buffer of 100mM HEPES pH 7. This solution displayed slight aggregation during the dialysis cycle, hence was centrifuged to separate out the aggregates, followed by filtration with a 0.2µm syringe filter. The crude fraction was analysed via SDS-PAGE and analysed by ImageJ to estimate actual DHAD concentration in the total crude sample. The total crude sample was estimated to be consisting of 92% DHAD. The crude fraction was concentrated and the DHAD protein concentration was determined to be 31.87mg/ml. Using 2-ME to activate DHAD in order to increase activity was then reattempted with crude DHAD in an attempt to establish if an improved result could be achieved compared to section 5.11. Crude DHAD was activated with 2-ME as described elsewhere (Carsten et al. 2015), following centrifugation to get rid of any precipitates formed. After buffer exchanging the resulting solution into 100mM HEPES pH 7 to remove the 2-ME, the protein solution was concentrated down to a final volume of 1ml. As some of the protein had precipitated during the activation procedure, a BCA was performed to determine the new protein concentration, which was determined to be 2.82mg/ml. A fraction of the crude DHAD was

also diluted down to 2.82mg/ml, this was done in order to run a control of unactivated DHAD alongside the activated version to observe any distinguishable differences in activity attributed to activation.

5.12.1 Analysis of activated crude DHAD activity using gluconic acid assay kit

For both the activated and unactivated DHAD assay conditions, 2 enzyme concentrations were tested, 0.1mg/ml and 1mg/ml using 20mM gluconic acid as substrate for 60 minutes at 55°C. Upon completion of 60 minutes, all samples were deproteinized before analysis with gluconic acid assay kit. A control condition without any DHAD was run alongside and as per standard and a gluconic acid standard curve was run alongside all samples (R^2= 0.99).

	Activated DHAD mg/ml		DHAD mg/ml		Control
	0.1	1	0.1	1	No DHAD
Absorbance 450nm	0.37	0.24	0.34	0.25	0.39
Gluconic acid mM	21.39	14.12	19.68	14.83	22.63

Table 5.9. Testing activity of 2-ME activated and non-activated crude DHAD 0.1mg/ml and 1mg/ml via gluconate detection kit to monitor gluconic acid depletion. Standard deviation for all conditions = <0.037.

The control conditions without any DHAD containing only 20mM gluconic acid substrate has been slightly overestimated by the kit to contain 22.63mM gluconic acid, there is certain error factor involved when using the detection kit as it is very sensitive, so this was expected. The 1mg/ml DHAD conditions for both the activated and unactivated crude DHAD have shown significant depletion of gluconic acid as they both have approximately 14mM gluconic acid remaining. However, since the objected of this experiment was to establish whether activation improved the activity of DHAD, that has not been achieved. From the data it can be deducted that both activated and unactivated crude DHAD have consumed the same amount of gluconic acid within the time frame of 60 minutes, therefore activation is not adding any value to the preparation of DHAD and so any further activation protocols were not performed from here onwards. Only a very small volume of the deproteinized samples from this activity assay were needed to do the dilutions in order to run the gluconic acid assay kit. The remaining deproteinized samples from the assay conditions and controls were in excess of 300µl and therefore were also run on the IC to compare both methods of analysis.

5.12.2 Analysis of activated crude DHAD activity using IC

The remaining deproteinized samples from the crude DHAD activity assay comparing activated and unactivated DHAD were also analysed via IC to establish which method is more effective and if values obtained from both correlate. The gluconic acid assay kits are only measuring the depletion of the substrate (gluconic acid) and not the formation of product (2-keto-3-deoxygluconate), whereas analysis IC shows both of the data. All gluconic acid and 2-keto-3-deoxygluconate concentrations were calculated using standard curves (Figure 2.2 and 2.3).

	Activated DHAD		Unactivated DHAD		Control
	0.1mg/ml	1mg/ml	0.1mg/ml	1mg/ml	No DHAD
Gluconic acid mM	19.84	12.99	17.12	11.86	19.59
2-keto-3-deoxygluconate mM	N/D	6.77	N/D	6.545	N/D

Table 5.10. IC activity analysis of 2-ME activated and non-activated crude DHAD 0.1mg/ml and 1mg/ml to monitor gluconic acid depletion and 2-keto-3-deoxygluconate formation. Standard deviation for all conditions = <0.85. (N/D=none detected).

Comparing the results from the gluconic acid assay kit for this assay (section 5.12.1) and the IC analysis, the data is not consistent. From Table 5.9, it has been calculated using the kit that the final concentration of gluconic acid remaining in both the activated and unactivated 1mg/ml DHAD assay conditions is 14.12 and 14.83mM respectively. Given that the gluconic acid assay kit estimated the control condition's concentration to be 22.63mM, 8.51 and 7.81mM of gluconic acid has been consumed in the activated and unactivated 1mg/ml DHAD conditions respectively (Table 5.9), and theoretically been converted to 2-keto-3-deoxygluonate. From the IC analysis data in Table 5.10, measuring the exact peaks corresponding to 2-keto-3-deoxygluconate, it has been calculated that 6.77mM and 6.55mM of 2-keto-3-deoxygluconate has been produced from the activated and unactivated 1mg/ml DHAD conditions respectively. The control shows the gluconic acid to have been calculated to be 19.59mM (Table 5.10) and considering the original substrate added to all conditions was 20mM, the IC analysis has given an estimate much closer to the actual concentration added in comparison to the gluconic acid assay kit, which had estimated the concentration to be 22.63mM (Table 5.9). The IC however, is not sensitive enough to detect the 2-keto-3-deoxygluconate at low concentrations therefore the gluconic acid assay kit is a better option for the analysis of lower enzyme concentrations assay conditions.

5.13 Testing crude DHAD activity under different substrate and enzyme concentrations

Following the experimental data which established that activation of both purified and crude DHAD using 2-ME is not significantly improving the enzyme activity (section 5.11 and 5.12), crude DHAD with no activation was used for all further assay condition optimizations. 2 substrate concentrations were tested, 2 and 20mM gluconic acid, each with 1, 2.5 or 5mg/ml DHAD enzyme solution. Each condition was tested at 3 different time points of 15, 30 and 60 minutes and upon completion of the respective time points, all samples were deproteinized and analysed for gluconic acid depletion using gluconic acid assay kit.

5.13.1 2mM gluconic acid assays with range of enzyme concentrations and time points analysed with gluconic acid assay kit

Gluconic acids standards were run alongside all 2mM assay and control conditions.

	15 minutes			30 minutes			60 minutes		
	1mg/ml DHAD	2.5mg/ml DHAD	5mg/ml DHAD	1mg/ml DHAD	2.5mg/ml DHAD	5mg/ml DHAD	1mg/ml DHAD	2.5mg/ml DHAD	5mg/ml DHAD
Absorbance 450nm	0.05	0.04	0.02	0.00	0.00	0.00	0.00	0.00	0.00
Gluconic acid mM	1.31	0.98	0.41	0.00	0.00	0.00	0.00	0.00	0.00

Table 5.11. Testing activity of crude DHAD with 2mM gluconic acid with 3 different enzyme concentration at 3 different time points. Standard deviation for all conditions= <0.02

In the 2mM gluconic acid assays, after 15 minutes, higher DHAD conditions consumed more gluconic acid as there was 1.31, 0.98 and 0.41mM gluconic acid remaining in the 1, 2.5 and 5mg/ml DHAD assays respectively. At 30 and 60 minutes, no gluconic acid was detected in any of the assay conditions indicating 100% conversion of gluconic acid to 2-keto-3-deoxygluconate. However, the controls for this experiment were not as expected. 2mM gluconic acid without DHAD was run as a control with each time point, no change is expected in the concentration of gluconic acid. Using the kit however gave the final concentration of the controls to be 4.8, 4 and 1.45mM from the 15, 30 and 60 minute conditions respectively. 4.8 and 4mM are a gross overestimate from the original 2mM added into the controls whereas 1.45mM is an underestimation. There is an substantial error factor when using the gluconic acid assay kit as there is a large dilution factor involved and pipetting errors with such small volumes are to be expected. Following analysis of 2mM all assay conditions on one 96 well plate, the same analysis was repeated for the second assay conditions consisting of 20mM gluconic acid.

5.13.2 20mM gluconic acid assays with range of enzyme concentrations and time points analysed with gluconic acid assay kit

	15 minutes			30 minutes			60 minutes		
	1mg/ml DHAD	2.5mg/ml DHAD	5mg/ml DHAD	1mg/ml DHAD	2.5mg/ml DHAD	5mg/ml DHAD	1mg/ml DHAD	2.5mg/ml DHAD	5mg/ml DHAD
Absorbance 450nm	0.35	0.35	0.30	0.34	0.27	0.22	0.32	0.22	0.1
Gluconic acid mM	19.39	19.4	16.72	18.6	14.77	11.97	17.6	12.03	5.40

Table 5.12. Testing activity of crude DHAD with 20mM gluconic acid with 3 different enzyme concentration at 3 different time points. Standard deviation for all conditions= <0.025.

Similarly to the 2mM gluconic acid assay conditions stated in Table 5.11, after 60 minutes, higher DHAD conditions consumed more gluconic acid as there is 17.6, 12.03 and 5.4mM gluconic acid remaining in the 1, 2.5 and 5mg/ml DHAD assays respectively. Even after 60 minutes, the highest DHAD concentration of 5mg/ml has converted just under 15mM of the total 20mM of gluconic acid. Similarly to the 2mM gluconic acid assays, the controls for this experiment were not as expected. 20mM gluconic acid without DHAD was run as a control with each time point and therefore no change was

expected in the concentration of gluconic acid. Using the kit however, gave the final concentration of the controls to be 26.87, 22.33 and 21.29mM from the 15, 30 and 60 minute control conditions respectively. All of the control conditions were overestimated in concentration in comparison to the original 20mM gluconic acid added into the controls.

Another set of negative controls were run with the DHAD enzyme solutions at the 3 given concentrations without any substrate to check that the enzyme solution itself is not contributing towards any absorbance readings. The maximum false positive reading obtained from these controls was of 0.68mM gluconic acid. This detection kit uses a coupled enzyme reaction to generate a colorimetric signal propionate to the amount of D-gluconate present, other assay components could be contributing this false positive and therefore the background absorbance values are not reliable. For this reason, use of gluconic acid assay kits was ceased from here onwards. The IC allows for the direct selection of 2-keto-3-deoxygluconate peaks formed, therefore all further assays were analysed by the direct quantification of the product formed. Only a small volume of deproteinized samples from all assay conditions (as outlined in 5.13) were required for the gluconic acid assay kit and therefore, all samples from assays carried out in this section were also analysed via IC.

5.13.3 2mM gluconic acid assays with range of enzyme concentrations and time points analysed via IC

All deproteinized samples from the 2mM gluconic acid assays (5.13) were analysed via IC and the final 2-keto-3-deoxygluconate concentrations were calculated using a standard curve (Figure 2.3).

	2-keto-3-deoxygluconate produced (mM)		
Time (min)	DHAD 1mg/ml	DHAD 2.5mg/ml	DHAD 5mg/ml
0	0	0	0
15	0.62	1	1.48
30	1.92	2.7	1.98
60	2.66	2.49	2.42

Table 5.13. IC activity analysis of 2mM gluconic acid assays with a range of enzyme concentrations at different time points. Standard deviation for all conditions= <0.44.
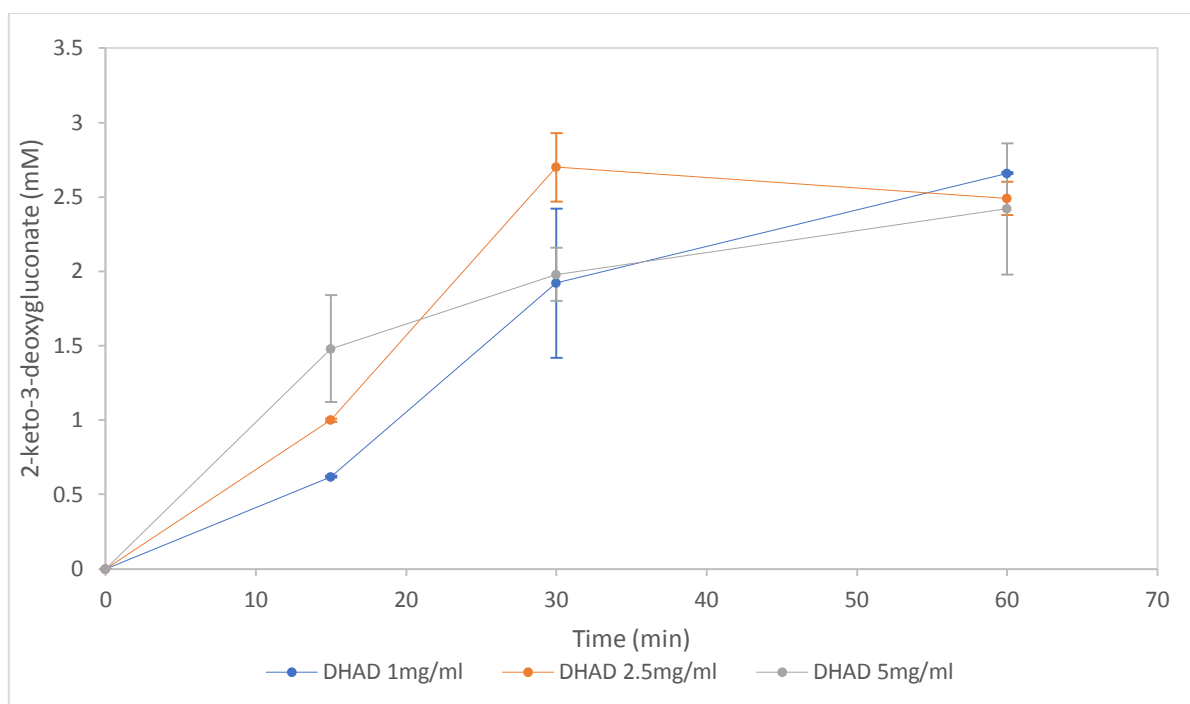
Figure 5.12. Graphical representation of the IC activity analysis of 2mM gluconic acid assays with a range of enzyme concentrations at different time points. Standard deviation for all conditions= <0.44.

A negative control of 2mM was analysed via the IC and using the corresponding standard curve (Figure 2.2), its concentration was calculated to be 2.54mM, so there was an over estimation by 0.54mM. Based on this value, 2.54mM of 2-keto-3-deoxygluconate would be expected as the final product if 100% conversion of substrate to product had occurred. From Table 5.13 and Figure 5.12, it can be seen that the final concentrations of 2-keto-3-deoxygluconate obtained after 60 minutes are in the range of 2.42-2.66mM 2-keto-3-deoxygluconate. Given the error factor involved in subjective IC peak selection, this is taken to be 100% conversion as there were no peaks seen indicative of any residual gluconic acid in the sample.

5.13.4 20mM gluconic acid assays with range of enzyme concentrations and time points analysed via IC

Following the analysis of 2mM gluconic acid assays, all deproteinized samples from the 20mM gluconic acid assays (section 5.13) were analysed via IC as well and the final 2-keto-3-deoxygluconate concentrations were calculated using the standard curve (Figure 2.3).

	2-keto-3-deoxygluconate produced mM		
Time (min)	DHAD 1mg/ml	DHAD 2.5mg/ml	DHAD 5mg/ml
0	0	0	0
15	0.52	1.27	2.96
30	1.27	3.26	6.24
60	2.48	5.97	11.08

Table 5.14. IC activity analysis of 20mM gluconic acid assays with a range of enzyme concentrations at different time points. Standard deviation for all conditions= <2.47.
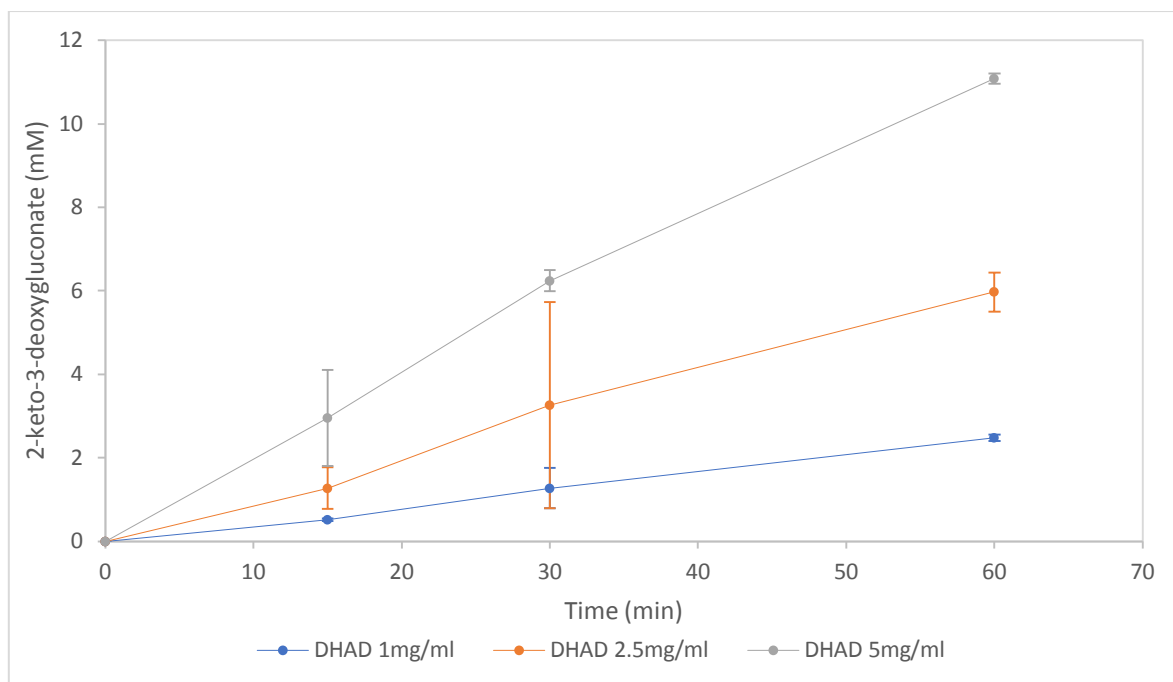
Figure 5.13. Graphical representation of the IC activity analysis of 20mM gluconic acid assays with a range of enzyme concentrations at different time points. Standard deviation for all conditions= <2.47.

A negative control of 20mM gluconic acid was analysed via the IC and using the corresponding standard curve (Figure 2.2) its concentration was calculated to be 17.18mM, so this was an under estimation by 2.82mM. Based on this value, 17.18mM of 2-keto-3-deoxygluconate would be expected as the final product if 100% conversion of substrate to product had occurred. From Table 5.14 and Figure 5.13, it can be seen that the final concentrations of 2-keto-3-deoxygluconate obtained after 60 minutes are in the range of 2.48-11.08 mM 2-keto-3-deoxygluconate from the 3 different enzyme concentrations. 100% conversion was not achieved for any of the conditions after 60 minutes.

5.14 Establishing DHAD enzyme kinetics

Following the experimental data obtained in 5.13, 1mg/ml final DHAD concentration was tested with a range of gluconic acid concentrations (1-40mM gluconic acid) for enzyme kinetics calculations. All conditions were run alongside negative controls to check if the concentration of known standards is calculated to be the similar from the standard curves (Table 5.15). The 40mM gluconic acid condition was abandoned as the retention time for both gluconic acid and 2-keto-3-deoxygluconate are in the same time range and smaller concentrations of 3-keto-3-deoxygluconate are overshadowed by the large gluconic acid peaks, making it hard to distinguish between them.

Gluconic acid (mM)	Calculated gluconic acid concentration from standard curve (mM)
1	1.28
2	2.38
4	4.24
6	6.13
8	7.70
10	9.97
15	12.27
20	17.14

Table 5.15. IC analysis of negative assay controls with known concentrations of gluconic acid without addition of DHAD. Standard deviation for all conditions = <0.84

Table 5.16 shows production of 2-keto-3-deoxygluconate using 1mg/ml DHAD in assays with gluconic acid as substrate at various time points. Given the error factor in the concentration calculations as evident from Table 5.15, some conditions are overestimating the amount of 2-keto-3-deoxygluconate present as the final value is over the concentration of substrate added to the reaction. This is due to the error factor in using the IC to calculate final concentrations. Due to the nature of peak selection, this is a factor which cannot be mitigated easily.

Time (min)	2-keto-3-deoxygluconate production mM							
	1mM GA	2mM GA	4mM GA	6mM GA	8mM GA	10mM GA	15mM GA	20mM GA
2	0.05	0.08	0.12	0.17	0.20	0.24	0.34	N/D
4	0.13	0.17	0.23	0.34	0.39	0.29	0.45	0.79
6	0.22	0.28	0.47	0.54	0.50	0.51	0.65	0.77
10	0.41	0.68	0.76	1.00	1.07	1.06	0.91	0.84
15	0.62	0.99	1.37	1.32	1.49	1.89	1.22	1.16
30	1.14	1.79	2.42	2.62	2.48	3.53	2.58	1.67
60	1.32	2.29	3.79	4.22	4.65	4.54	3.99	3.57
120	1.32	2.64	4.59	5.73	5.84	6.29	5.75	4.30
300	1.29	2.50	5.26	6.94	7.16	8.60	7.23	5.54
1440	1.72	2.39	4.87	7.15	9.10	12.12	15.19	13.94

Table 5.16. IC activity analysis of production of 2-keto-3-doxygluconate under 1mg/ml DHAD assays with gluconic acid (GA) as substrate, tested in the range of 1-20mM at various time points. 20mM gluconic acid 2 min condition data point missing as 2-keto-3-deoxygluconate peak difficult to isolate. Standard deviation of all conditions= <1.57.

For ease of data representation, graphical representation from Table 5.15 has been split between 2 graphs, Figure 5.14A shows 1-6mM gluconic acid assay conditions, while Figure 5.14B shows 8-20mM gluconic acid assay conditions.
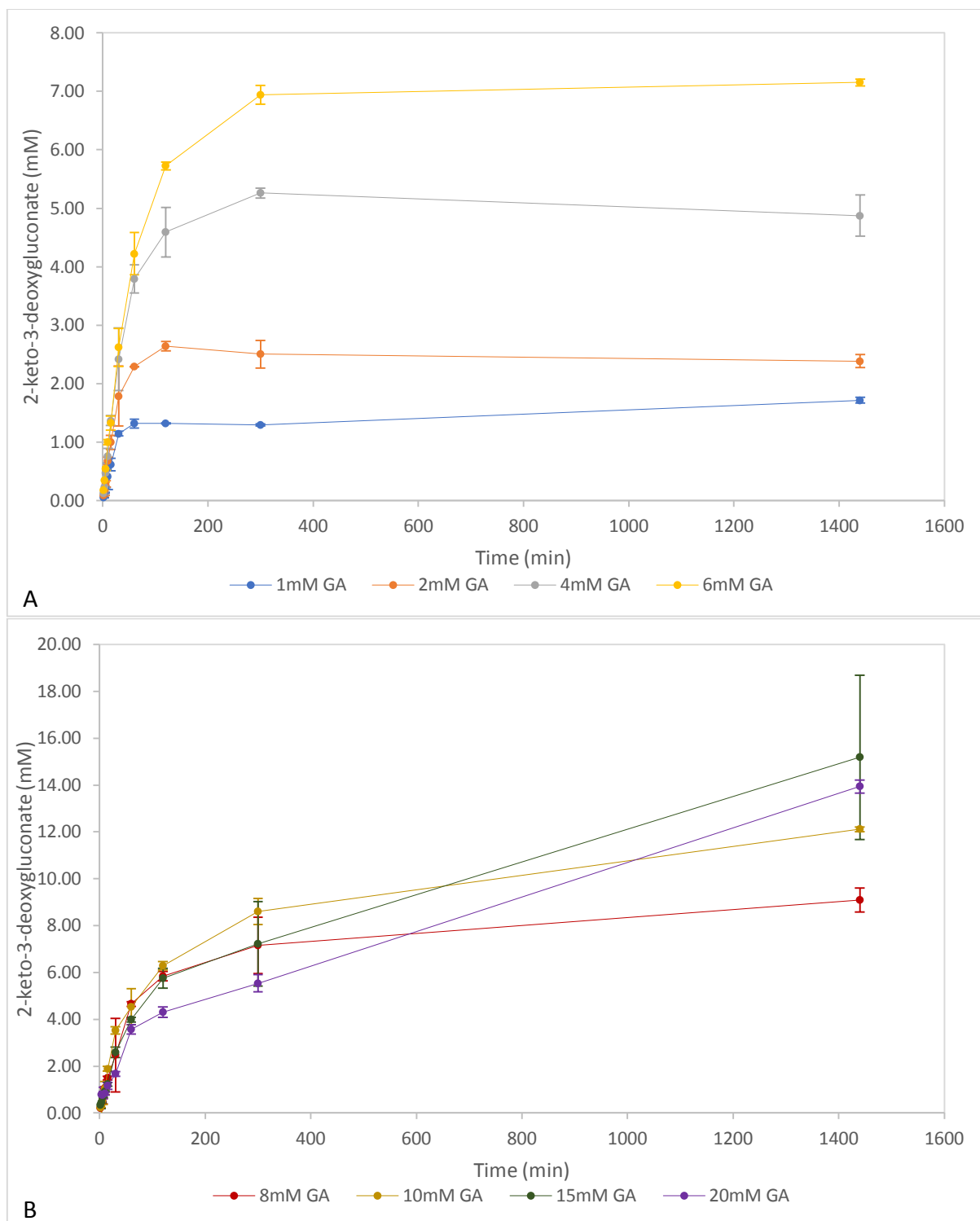
Figure 5.14. Graphical representation of 2-keto-3-deoxygluconate production using 1mg/ml DHAD with various concentrations of gluconic acid. Figure 5.14A represents product formation when using 1-6mM gluconic acid and Figure 5.14B represents the same with 8-20mM gluconic acid. Standard deviation of all conditions = <1.57.

Figure 5.15A shows the initial activity of DHAD at different substrate concentrations and Figure 5.15B shows the Lineweaver-Burk plot for the kinetics calculation. The Michealis-Menten model was used to calculate the apparent V_{max} and K_m values of DHAD which was calculated to be 0.117U/mg and 1.736mM respectively.
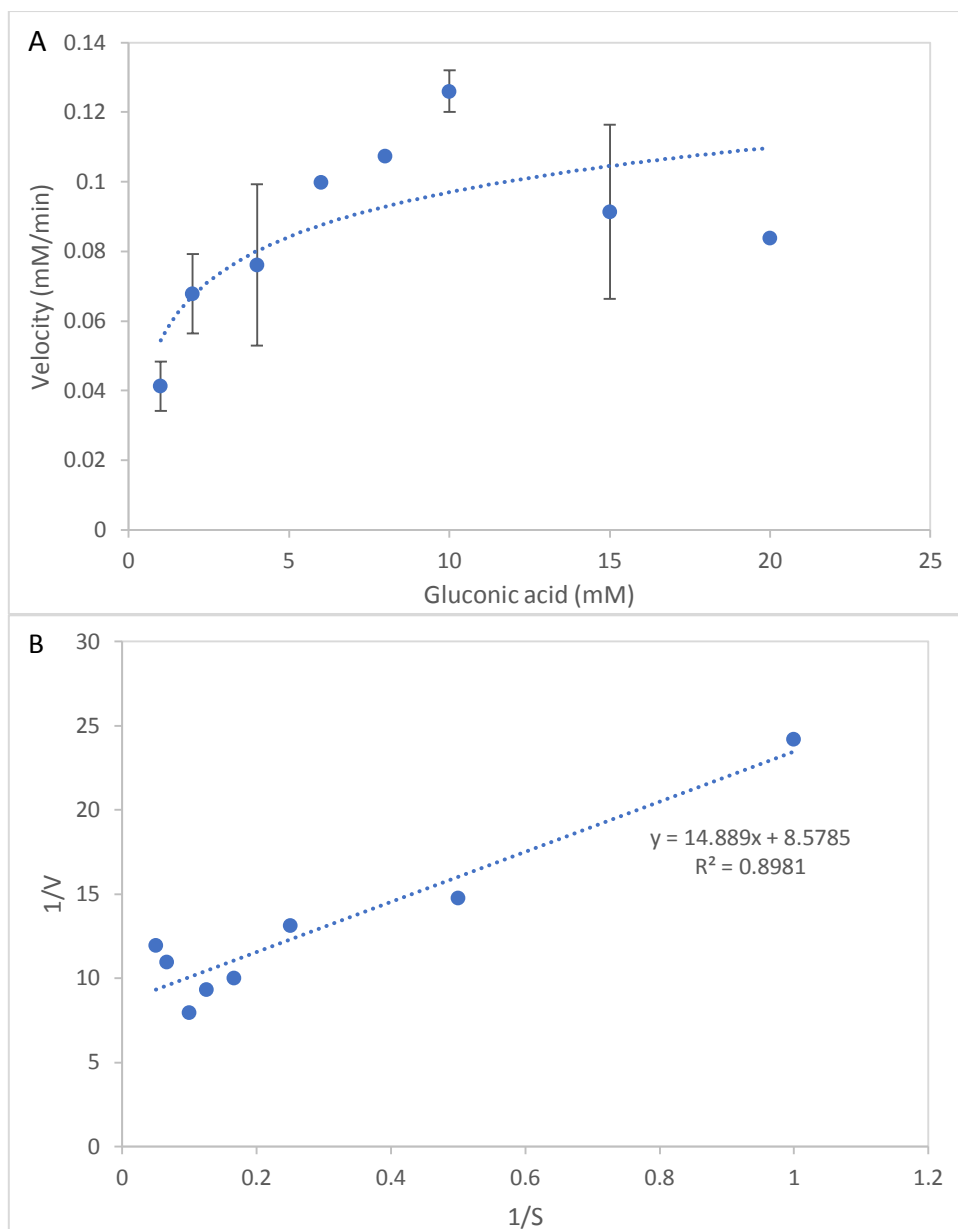
Figure 5.15. Initial activity of DHAD at various gluconic acid concentrations (A), Lineweaver-Burk plot for the kinetic analysis (B).

5.15 Effect of storage on DHAD enzymatic activity

Literature has been cited to advise the use of freshly prepared DHAD whenever possible as activity loss has been widely reported when enzymatic solution is stored at 4°C and -80°C. This was also demonstrated by the experiments carried out with thawed DHAD stocks, which displayed poor activities (section 5.8-5.11). Activity loss of DHAD was therefore tested over the course of 50 days, with freshly prepared DHAD stock being tested on day 0 before being stored at 4°C with subsequent activity analysis on day 28 and day 50 (Figure 5.16). 6mM gluconic acid was used as substrate and activity was tested at 2, 4, 6, 10, 15 and 30 minute time intervals. All reaction conditions were the same outlined in the protocol and 5.14. From the loss of activity over the initial 30 minutes of testing, it is evident

that the stock faces degradation while at storage and storage condition at 4°C is not a suitable solution to the problem.
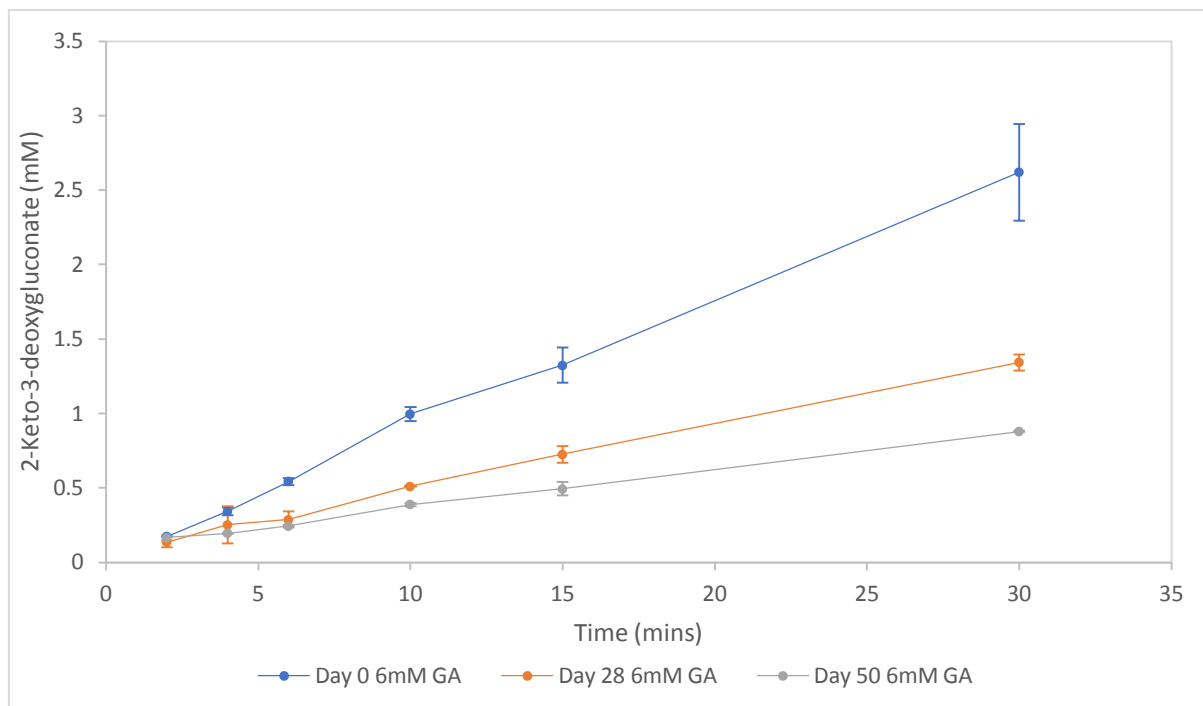
Figure 5.16. IC activity analysis of 1mg/ml DHAD stored at 4°C over the course of 50 days using 6mM of gluconic acid as substrate (GA). Standard deviation of all conditions= <0.32.

This chapter has outlined the successful expression, purification and quantification techniques employed for the production of DHAD. Activity of DHAD has successfully been established and its main reaction of interest in the overall cascade has been optimized and characterized. However, there are still outstanding issues of optimizing storage conditions and improving enzyme activity without compromising enzyme purity that require to be tackled to possibly obtaining an improved outcome.

6. 2-keto-3-deoxy-gluconate aldolase catalyses the aldol cleavage of 2-keto-3-deoxy-gluconate to form pyruvate and glyceraldehyde

The hyperthermophilic archaeon *Sulfolobus solfataricus* metabolizes glucose via a novel non-phosphorylated Enter-Doudoroff pathway, whereby the initial reaction is the NAD^+-dependent dehydrogenation of glucose to gluconate (Chapter 4), which is then dehydrated to form 2-keto-3-deoxygluconate (Chapter 5), 2-keto-3-deoxygluconate then undergoes a reversible aldol cleavage catalysed by 2-keto-3-deoxygluconate aldolase (KDGA) to give pyruvate and glyceraldehyde.

2-Keto-3-deoxygluconate → Pyruvate + Glyceraldehyde
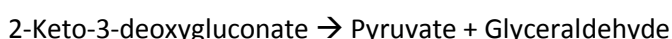
KDGA from a thermostable archaeon with its inherent thermostability and ability to utilize non-phosphorylated substrates can offer multiple advantages over other enzyme systems. This chapter discusses the protein expression, purification and characterization of KDGA.

6.1 Transformation of KDGA vector DNA into BL21-DE3 competent cells

Synthesised pET30a vectors containing KDGA sequence arrived as a concentrated miniprep of ~4μg of DNA from GenScript (sequence in appendix). The original vector sample was archived and transformation of vector into DH5α competent cells was done followed by a miniprep to obtain 50μl of quantified vector DNA. KDGA vector DNA was transformed into BL21-DE3 cells as they have favourable characteristics for recombinant protein production such as protease deficiency, low acetate production under high glucose conditions and high permeability. Following successful transformation, single colonies were used to initiate protein expression. LB agar kanamycin plates with the successful transformation of vector DNA into BL21-DE3 were also used to prepare glycerol stocks for storage at -80°C for future applications.
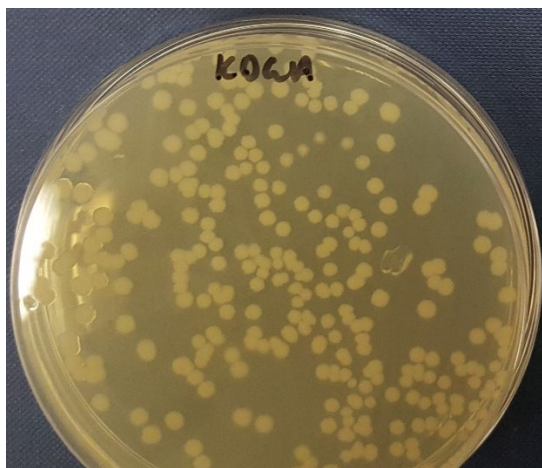
Figure 6.1. Quantified vector DNA obtained following miniprep was transformed into competent BL21-DE3 cells, successful transformation is shown by the presence of bacterial colonies on LB kanamycin plate.

6.2 Small scale KDGA protein expression and purification in AI media

Following the successful transformation of KDGA vector DNA, protein expression and purification was initially carried out in a 2L final volume. Initial KDGA expression was carried out in AI media with a final concentration of kanamycin at 50µg/ml at room temperature overnight for which the final OD_{600} was 9.61. The cell pellet obtained from the cultures was resuspended, sonicated and heat treated as outlined in the methods sections. All resuspension, sonication, heat treatment and centrifugation steps were carried out in a 100mM HEPES pH 7.5, 200mM $MgCl_2$, 10% glycerol buffer unless otherwise stated. The suspension obtained following cell lysis, heat treatment to denature host cellular components and centrifugation to remove cell debris, was used as the KDGA crude enzyme fraction for purification via Ni-NTA affinity chromatography.

6.3 Ni-NTA affinity chromatography of crude KDGA

The crude fraction of KDGA (50ml in 100mM HEPES pH 7.5, 200mM $MgCl_2$, 10% glycerol buffer) obtained from small scale expression of KDGA as outlined in section 6.2, was bound to 5ml of Ni-NTA resin overnight at room temperature. Following this, the suspension was transferred to a polypropylene column, the flow through was collected and the Ni-NTA resin washed with 100mM HEPES pH 7.5, 200mM $MgCl_2$, 10% glycerol buffer. Three concentrations of imidazole in 100mM HEPES pH 7.5, 200mM $MgCl_2$, 10% glycerol buffer were then used to elute off bound protein. All samples collected from Ni-NTA affinity chromatography were analysed via SDS-PAGE (Figure 6.2). KDGA binding to Ni-NTA via the His_{10} tag was successful as evident from comparing samples in lanes 2 and 3 of Figure 6.2. The crude KDGA sample in lane 2 presents a thick band at around 34kDa which is the size of the KDGA monomer. As seen in lane 3 of Figure 6.2, after binding the crude fraction with Ni-NTA and collecting the flow through, the intensity of the band at 34kDa is very faint, indicating the KDGA in the crude fraction has successfully bound to the Ni-NTA. 500mM imidazole was sufficient to elute off KDGA (Figure 6.2, lanes 6 and 7). The original elution of KDGA as shown in lane 6 of Figure 6.2 precipitated out soon after the elution was collected and the sample loaded into lane 6 was following the centrifugation to remove aggregated protein. The removal of protein aggregates did not prevent further aggregation, and several aggregation/centrifugation cycles were done after which it was not taken forward for processing under risk of causing other elutions to aggregate if pooled.
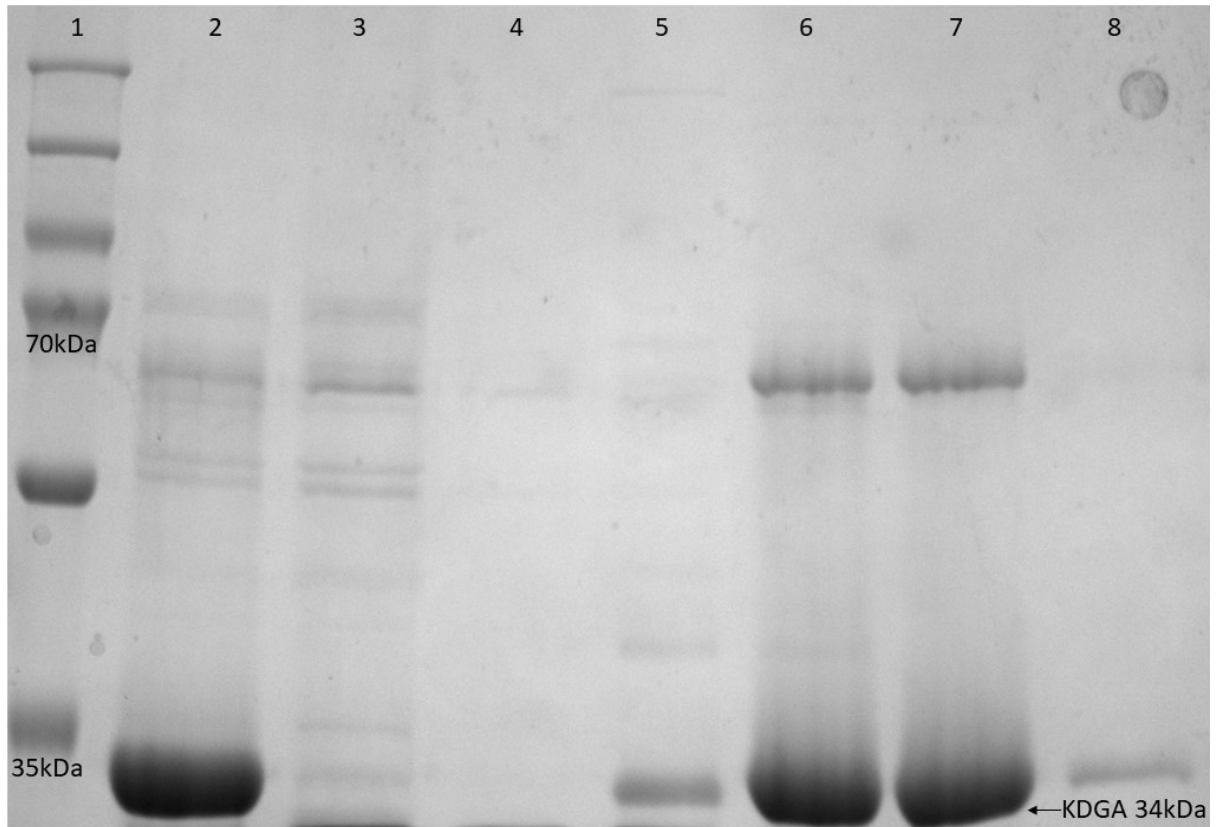
Figure 6.2. SDS-PAGE analysis of Ni-NTA purification attempt of KDGA. Samples in all lanes, except lane 2, are from elutions obtained from the column following Ni-NTA affinity chromatography. Lane 2 contains sample of crude KDGA prior to binding with Ni-NTA. Lane 3 contains the flow through collected from column and lane 4 contains the HEPES buffer washes (100mM HEPES pH 7.5, 10% glycerol, 200mM $MgCl_2$). Lanes 5, 6, 7 and 8 contain HEPES buffer imidazole elutions with 100, 500, 500 and 1000mM imidazole respectively.

Fraction from lane 7 containing the highest amount of KDGA eluted was taken forward (10ml final volume) and 100mM final concentration of EDTA was also added to the sample to aid dialysis. Previous attempts of purification of GDH and DHAD in Chapters 4 and 5 respectively have highlighted the idea of using EDTA to stop protein aggregation during dialysis. The elution of bound protein with imidazole also leads to leached nickel ions from the column and into the collection tubing. During Ni-NTA affinity chromatography, both imidazole the His_{10} tag chelate the nickel, and the removal of just imidazole during dialysis can result in the sample being insoluble. The addition of EDTA assists successful dialysis as it is assumed to chelate the nickel ions and thereby prevents protein-protein self-interactions and results in a successful dialysis cycle. The 10ml of KDGA solution was successfully put through 2 cycles of dialysis until the imidazole and EDTA were dialysed out and their respective concentrations in the solution were negligible (<0.01mM). The concentration of $MgCl_2$ was reduced to 100 and 50mM in the first and second cycle of dialysis respectively, and the final storage buffer for KDGA was 100mM HEPES pH 7.5, 10% glycerol, 50mM $MgCl_2$.

2 cycles of dialysis were performed:

1- 10ml elution dialysed in 1L of 100mM HEPES pH 7.5, 10% glycerol, 100mM $MgCl_2$ buffer at a dilution factor of 100.

2- 30ml elution dialysed in 1L of 100mM HEPES pH 7.5, 10% glycerol, 50mM $MgCl_2$ buffer at a dilution factor of 100.

The GDH sample was then concentrated down in volume and its protein concentration was determined via BCA to be 1.2mg/ml. Large scale preparations of KDGA were purified in further attempts similarly as outlined above, and following the determination of protein concentration, the 1ml aliquots were snap frozen and stored at -80°C until required.

6.4 Size-exclusion chromatography and protein identification of KDGA to determine presence of oligomers

The small scale expression of KDGA gave a single band on the SDS-PAGE matching the expected size of the KDGA monomer (Figure 6.2, lane 6 and 7), however there is one other main band seen around the 70kDa position which was suspected to be a KDGA dimer. To confirm the presence of oligomers, KDGA purified from section 6.3 was loaded onto the ÄKTA system and as size-exclusion chromatography separates molecules in solution based on their molecular weight, the peaks on a chromatogram are indicative of the different size proteins in the sample. The chromatogram obtained from the size-exclusion of KDGA (Figure 6.3) automatically identified 2 peaks and aliquoted them into a collection plate as different fractions.
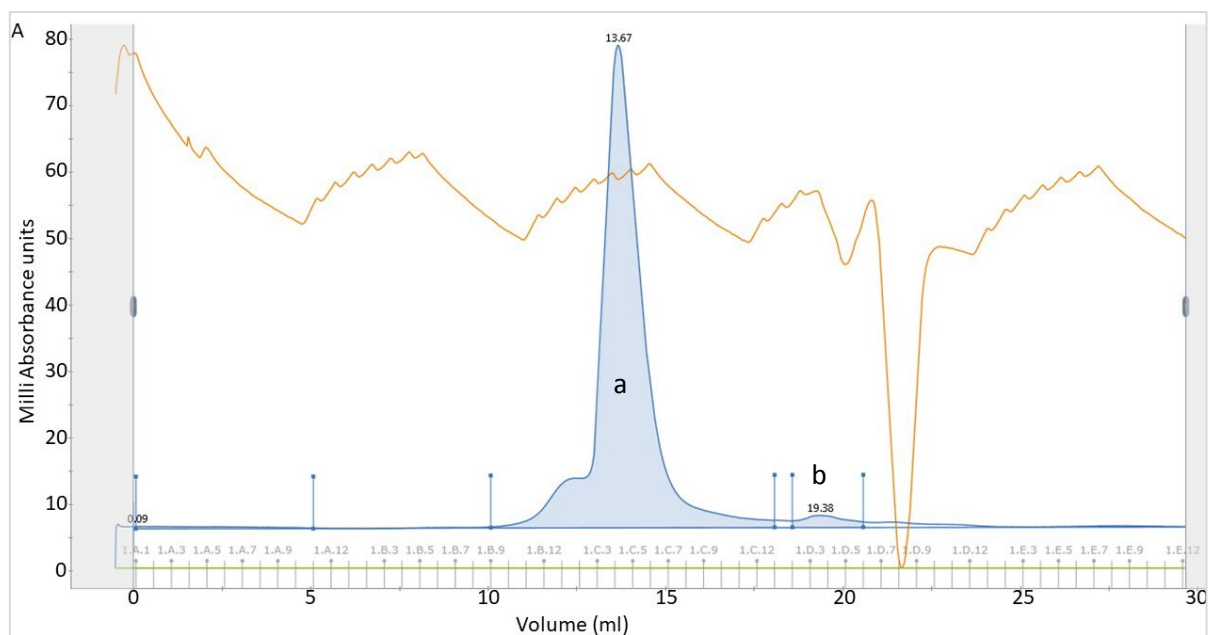
Peak	Retention (ml)	Area (ml*mAU)	Area %	Fractions	Volume (ml)
a	13.67	98.21	96.18	B9-C12	8
b	19.38	2.61	2.55	D2-D5	2

Figure 6.3. Size exclusion chromatography of KDGA. Figure 6.3A displays the chromatogram obtained from the software. The blue trace represents the UV absorbance at 280nm and the 2 peaks are indicative of the quantity of protein detected. The brown trace reflects the conductivity monitor which measures conductivity of buffer and samples for online monitoring of the true gradient. The green trace is applied if there is another buffer being used, since this sample was run in one buffer only, the trace has a value of 0. Figure 6.3B lists the retention time of each peak as well as the final volume collected of all fractions.

The chromatogram also identified a peak at retention volume of 0.094ml which comprised a total of 1.27% of the total area, since this retention volume falls within the range of the void volume, this peak and its analysis was disregarded. 2 samples from peak a and one sample from peak b were loaded onto a SDS-PAGE gel in order to visualise their composition. The SDS-PAGE obtained from the samples (Figure 6.4) shows the composition is exactly the same in all samples loaded, confirming the presence of oligomers. No visible bands can be seen in lane 4 which contained the sample taken from peak b, however as can be seen on the chromatogram in Figure 6.3A, the peak is very small in comparison to peak a, hence very little protein would be expected to be in this elution. In Figure 6.4, the sample in lane 2 and 3 is from peak a and sample in lane 4 is from peak b (Figure 6.3A). It is evident from the gel in Figure 6.4 that the same bands are constantly seen in all the samples, differing only in their intensities, which correlates with the different concentrations of protein present in the different fractions. Following the SDS-PAGE, as a further confirmation of oligomers, the KDGA bands indicated in Figure 6.4 were excised from the gel and were analysed with mass spectrometry to confirm protein identification.
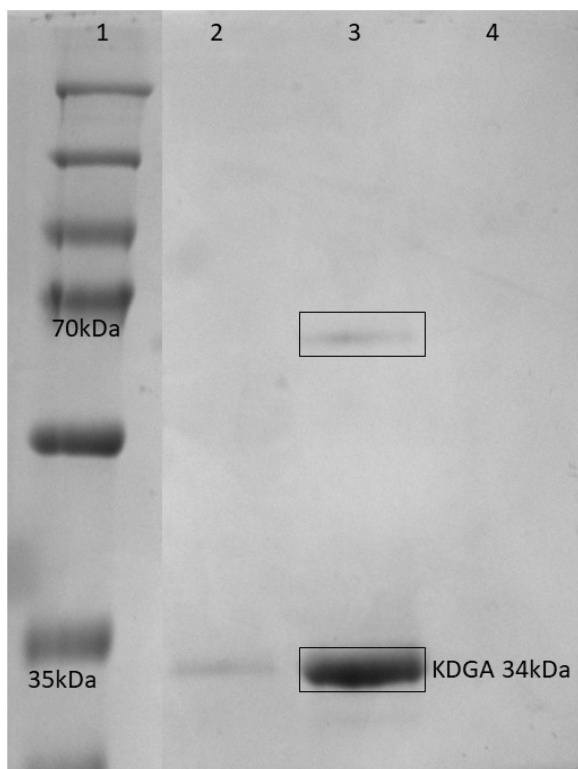
Figure 6.4. SDS-PAGE analysis of KDGA following size exclusion chromatography. Lane 2 and 3 contains samples from peak A, taken from fractions B12 and C5 respectively. Lane 4 contains sample from peak B, taken from fraction D3. The bands indicated in the figure were excised for mass spectrometry analysis.

Mass spectrometry analysis of the bands shown in Figure 6.4 positively identified both as being KDGA. As peak A comprised 96.18% of the total area and this would have been higher if not for the false peak identified at the retention volume of 0.094ml, the composition of the Ni-NTA purified KDGA in this instance and the protein concentration determined by the corresponding BCA was taken as the final KDGA concentration. For any further attempts at purification, ImageJ scientific image analysis was used and the confirmed KDGA bands (via mass spectrometry) were calculated as a percentage of the total protein concentration. Using this method allowed for the actual concentration of KDGA to be determined in a sample with other non-specific proteins purified during Ni-NTA purification in future experiments.

6.5 Producing 2-keto-3-deoxygluconate for use as substrate with KDGA

2-Keto-3-deoxygluconate is the product of the following reaction catalysed by DHAD as discussed in the previous chapter:

Gluconate → 2-keto-3-deoxygluconate
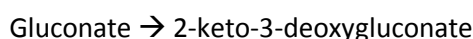
The commercial availability of 2-keto-3-deoxygluconate is in very small quantities and as a lithium salt, therefore purchasing this substrate for testing functional activity of KDGA was not an economically favoured option. Furthermore, additional reaction controls would be required to address the presence

of lithium ions in the reaction mixture and reaction parameters would not be the same in the eventual testing of the cascade. For these reasons, 2-keto-3-deoxygluconate was attempted to be produced on a large scale using DHAD. From the previous chapter, the kinetic parameters of DHAD were established and 15mM gluconic acid gave 15mM 2-keto-3-deoxygluconate as analysed via IC (Table 5.16) with very little residual gluconic acid remaining. The same reaction with 15mM of gluconic acid was set up to obtain 15mM of 2-keto-3-deoxygluconate which was then intended to use to test the functional activity of KDGA. 1mg/ml DHAD was used to catalyse the conversion of 15mM gluconic acid in 2x 50ml reaction volume and incubated for 1440 minutes at 55°C. Following the end of the reaction incubation period, the samples were deproteinized and the conversion efficiency of gluconate to 2-keto-3-deoxygluconate was analysed via IC.

	Gluconic acid mM	2-Keto-3-deoxygluconate mM
Reaction mix 1	8.07	8.97
Reaction mix 2	8.33	8.38

Table 6.1. IC composition analysis of 2x 50ml DHAD reaction mix to produce 2-keto-3-deoxygluconate. 15mM gluconic acid was used as substrate for this reaction of which 8.07 and 8.33mM remained in the reaction mixture after incubation for 1440 minutes at 55°C.

The DHAD stock used in the reaction mix had been stored at 4°C and was not a fresh stock, the issues with DHAD storage and decreasing enzyme activity over time were previously discussed in detail in Chapter 5. Only 50% conversion of total gluconic acid was achieved and this was presumed due to the DHAD batch used and the loss of activity within the batch. A 100ml final volume solution was obtained which contained ~8mM of gluconic acid and ~8mM of 2-keto-3-doxygluconate. Despite it not being ideal, the mixture of 50/50 gluconic acid/2-keto-3-deoxygluconate was used as the substrate to test functional KDGA activity.

6.6 Testing KDGA activity using 2-keto-3-deoxygluconate present with gluconic acid in solution

Since a 100ml deproteinized solution of 50/50 gluconic acid/2-keto-3-deoxygluconate was already obtained from the previous section, this was tested as substrate for any activity with KDGA despite the presence of gluconic acid in the solution. 3 concentrations of KDGA were tested, 0.0001, 0.001 and 0.1mg/ml KDGA at 4 different time points of 15, 30, 60 and 120 minutes. All reaction and control conditions were set up in triplicate 1ml volumes and incubated at 55°C, 300rpm shaking, before deproteinizing and analysis via IC. The final substrate concentration of 2-keto-3-deoxygluconate assayed in all conditions was 5mM due to low concentrations of the experimentally produced 2-keto-3-deoxygluconate stock in section 6.5. Initially only the 0.1mg/ml KDGA assay at 120 minutes and its subsequent control was analysed via IC (Figure 6.5). This reaction condition would theoretically display the highest conversion rate of the 2-keto-3-deoxygluconate to pyruvate and glyceraldehyde.
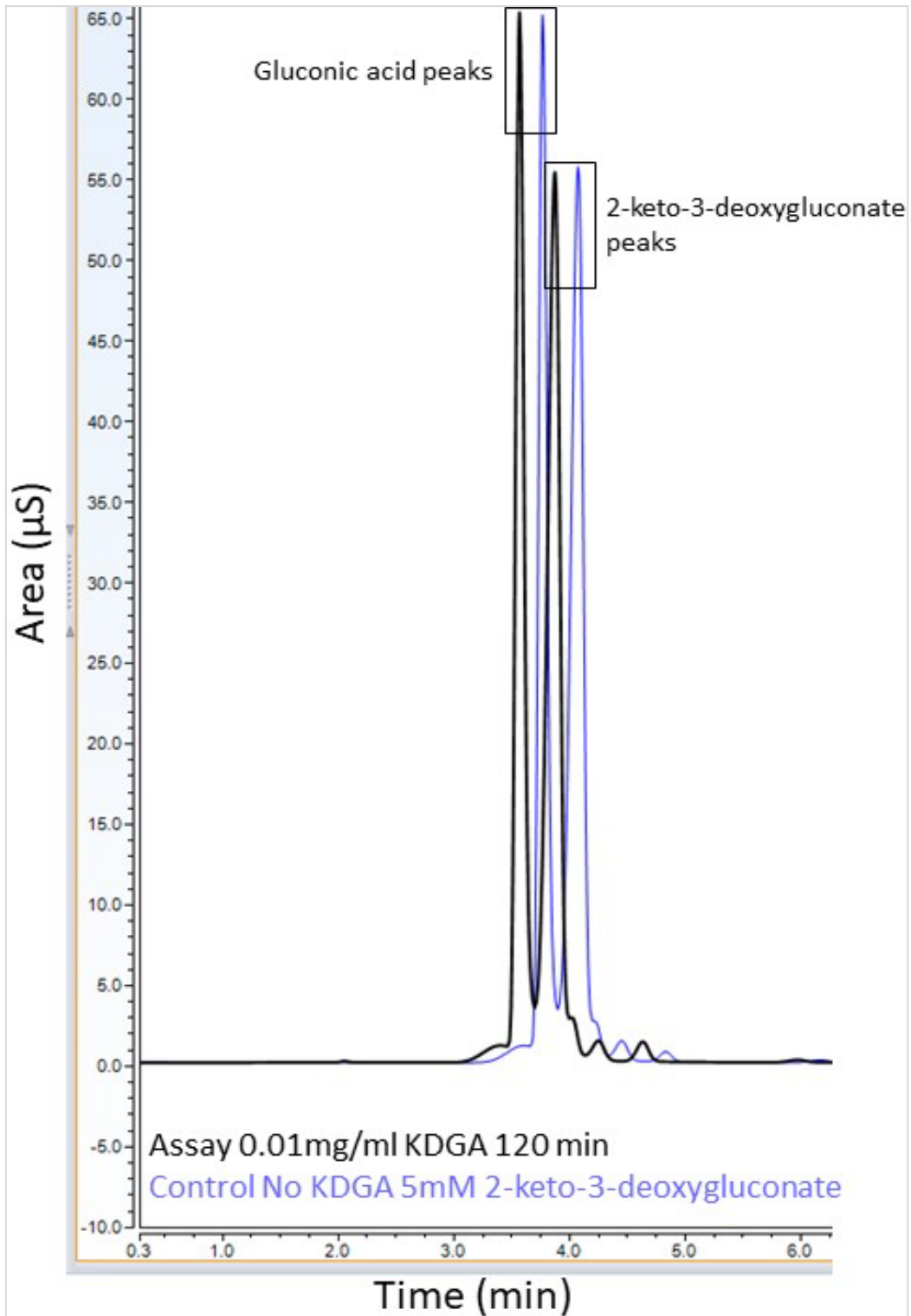
Figure 6.5. IC analysis of 0.01mg/ml KDGA 120min assay condition and its subsequent control with no KDGA. For overlaying purposes, the trace of the control condition is shifted to the right to allow for direct side by side visual, otherwise the retention times are similar for gluconic acid and 2-keto-3-deoxygluconate peaks in both assay and control conditions.

As seen in Figure 6.5, the 2-keto-3-deoxygluconate peaks are of a similar area for both the control and assay conditions meaning that 2-keto-3-doxygluconate in the assay conditions has not been converted to desired products of pyruvate and glyceraldehyde as its concentration largely remaining unchanged.

6.7 Testing reverse catalysed reaction of KDHA to form 2-keto-3-deoxygluconate from pyruvate and glyceraldehyde

The IC analysis of the KDGA forward reaction revealed no peaks for the desired products of pyruvate and glyceraldehyde as outlined in section 6.6. As the aldol cleavage of 2-keto-3-deoxygluconate is a reversible reaction, the reaction parameters were also explored in reverse:

Pyruvate + Glyceraldehyde → 2-Keto-3-deoxygluconate
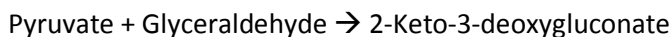
Due to ease of commercial availability of pyruvate and glyceraldehyde, the reverse reaction parameters were easier to manipulate with variations in concentrations without any restrictions. 20mM glyceraldehyde and 50mM pyruvate were used as substrates to test the conversion to 2-keto-3-deoxygluconate by 0.25mg/ml KDGA. Two controls were also run alongside the assay condition (Control 1- 20mM glyceraldehyde and 50mM pyruvate, no KDGA and Control 2- no substrates, 0.25mg/ml KDGA), all in triplicate. The reaction and controls were incubated for 15 minutes at 55°C, 300rpm shaking before being deproteinized and analysed via IC. The column used for the IC could not be used to detect glyceraldehyde, therefore a reduction in the concentration of pyruvate and the presence of a peak with the retention time of 2-keto-3-deoxygluconate was used as a positive confirmation of the functional activity of KDGA (Table 6.2).

	Concentration detected by IC (mM)	
	Pyruvate	**2-keto-3-deoxygluconate**
Control 1	47.23	N/D
Control 2	N/D	N/D
Assay	46.87	1.77

Table 6.2. IC analysis of the assay and control conditions of reverse activity analysis of KDGA to form 2-keto-3-deoxygluconate from pyruvate and glyceraldehyde. (N/D= none detected).

The pyruvate and 2-keto-3-deoxygluconate peaks were calculated as their respective concentrations from the pyruvic acid and 2-keto-3-deoxygluconate standard curves (Figure 2.3 and 2.4) as outlined in the Methods chapter. 50mM of pyruvic acid was added into the assay condition and the same was added to reaction Control 2. As shown in Table 6.2, the control condition has been calculated to contain 47.23mM pyruvic acid, this is a slight underestimation from the 50mM added to both assay and control conditions. However, this discrepancy was expected as 50mM pyruvic acid was the final value in the standard curve, and around these higher concentrations of pyruvic acid, the IC chromatogram peaks begin to plateau and widen, indicating the concentration of the solution loaded exceeded the analytical limitations of the device. For these reasons, the underestimation of the 50mM pyruvic acid to 47.23mM was expected. The presence of the 2-keto-3-doxygluconate peak was taken to be a true indication of the functionality of the enzyme in the reverse direction, as indicated in Figure 6.6.
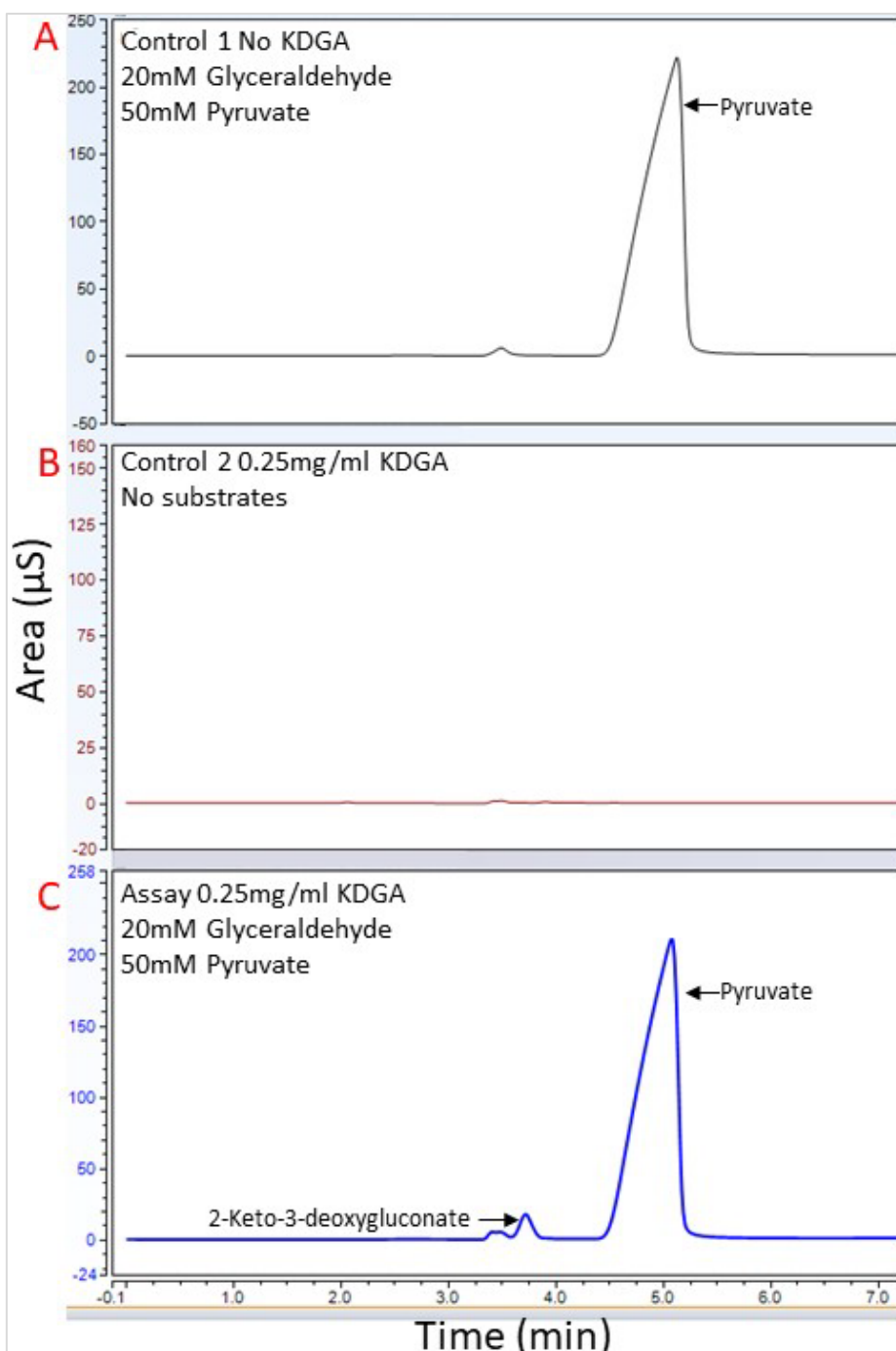
Figure 6.6. IC chromatogram peaks of reverse catalysed reaction of KDGA to form 2-keto-3-deoxygluconate from pyruvate and glyceraldehyde. Panel A contains reaction control 1 with substrates but no KDGA. Panel B is reaction control 2 with KDGA but no substrates. Panel C is the assay with 0.25mg/ml KDGA and 20mM glyceraldehyde and 50mM pyruvate. 2-Keto-3-deoxygluconate peak was observed in the assay condition confirming functional activity of KDGA.

A peak with the expected retention time of 2-keto-3-doxygluconate was identified in the analysis of the assay chromatogram (Figure 6.6, Panel C) whereas no such peak was observed in either one of the controls (Figure 6.6, Panels A and B). This experiment confirmed a functional KDGA stock and also provided a feasible alternative to testing the forward reaction due to the lack of commercial substrate, 2-keto-3-deoxygluconate.

6.8 Preliminary pilot studies to establish best assay conditions for KDGA kinetic studies

Before establishing KDGA kinetics parameters, pilot experiments were performed where a range of enzyme concentrations were tested with 2 substrate concentrations over certain time points. Three different KDGA concentrations were tested, 0.5, 1, 2.5mg/ml, firstly with low substrate concentrations of 1mM glyceraldehyde and 2mM pyruvate and then with high substrate concentration of 10mM glyceraldehyde and 20mM pyruvate. Each assay condition (with relevant controls) as described above was tested at 3 time points of 15, 30 and 60 minutes for formation of 2-keto-3-deoxygluconate. Analysis was carried out via IC after deproteinizing assay samples.

6.8.1 1mM glyceraldehyde and 2mM pyruvate assay with 0.5, 1 and 2.5mg/ml KDGA at 3 time points

Table 6.3 lists the 2-keto-3-deoxygluconate concentrations calculated using 2-keto-3-deoxygluconate standard curve (Figure 2.3).

Time (min)	2-Keto-3-deoxygluconate (mM)		
	0.5 mg/ml KDGA	1mg/ml KDGA	2.5mg/ml KDGA
0	0	0	0
15	0.07	0.15	0.47
30	0.17	0.28	0.63
60	0.22	0.31	0.63

Table 6.3. IC analysis of KDGA activity assay (0.25, 1 and 2.5mg/ml) with 1mM glyceraldehyde and 2mM pyruvate as substrates at 15, 30 and 60 minutes, for the formation of 2-keto-3-doxygluconate. Standard deviation of all conditions= <0.065.
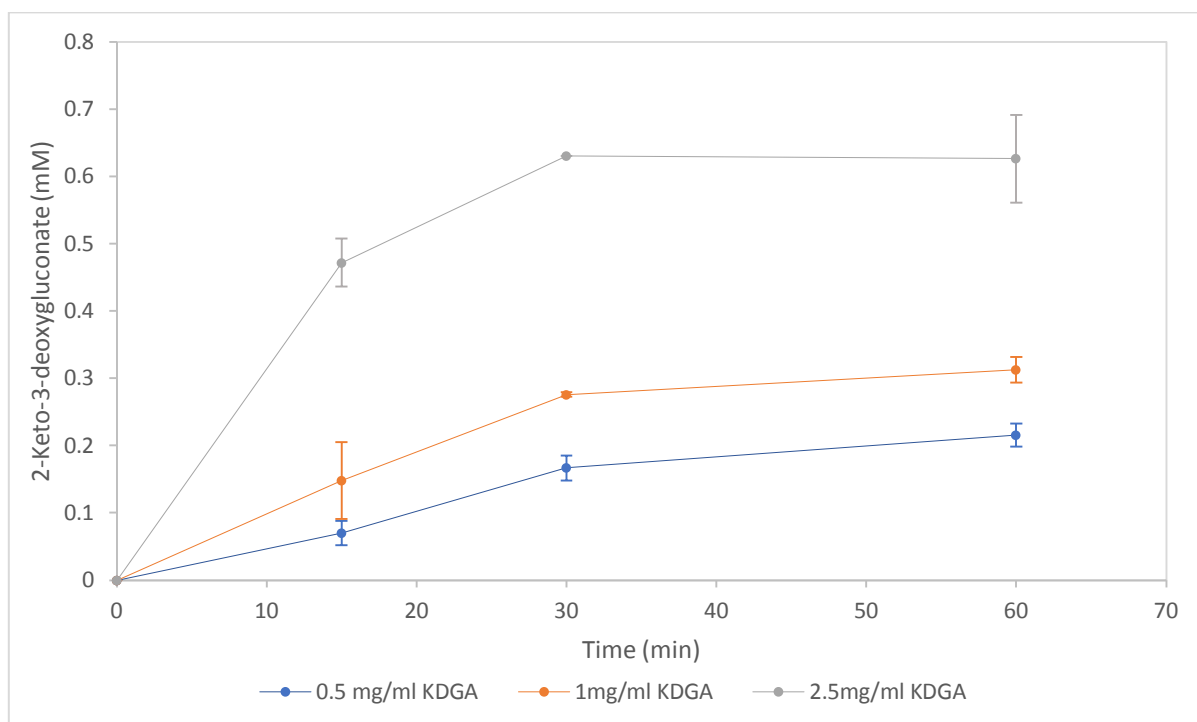
Figure 6.7. Graphical representation of IC analysis of KDGA activity assay (0.25, 1 and 2.5mg/ml) with 1mM glyceraldehyde and 2mM pyruvate as substrates at 15, 30 and 60 minutes, for the formation of 2-keto-3-doxygluconate.

The highest concentration of 2-keto-3-deoxygluconate detected from all the assay conditions in the low substrate concentration was at 30 minutes with 2.5mg/ml KDGA, whereby 0.63mM of 2-keto-3-deoxygluconate was detected.

6.8.2 10mM glyceraldehyde and 20mM pyruvate assay with 0.5, 1 and 2.5mg/ml KDGA at 3 time points

Table 6.4 lists the 2-keto-3-deoxygluconate concentrations as calculated using 2-keto-3-deoxygluconate standard curve (Figure 2.3).

Time (min)	2-Keto-3-deoxygluconate (mM)		
	0.5 mg/ml KDGA	1mg/ml KDGA	2.5mg/ml KDGA
0	0	0	0
15	1.4	2.82	5.47
30	3.51	5.88	8.5
60	5.22	7.52	8

Table 6.4. IC analysis of KDGA activity assay (0.25, 1 and 2.5mg/ml) with 10mM glyceraldehyde and 20mM pyruvate as substrates at 15, 30 and 60 minutes, for the formation of 2-keto-3-doxygluconate. Standard deviation of all conditions= <1.76.
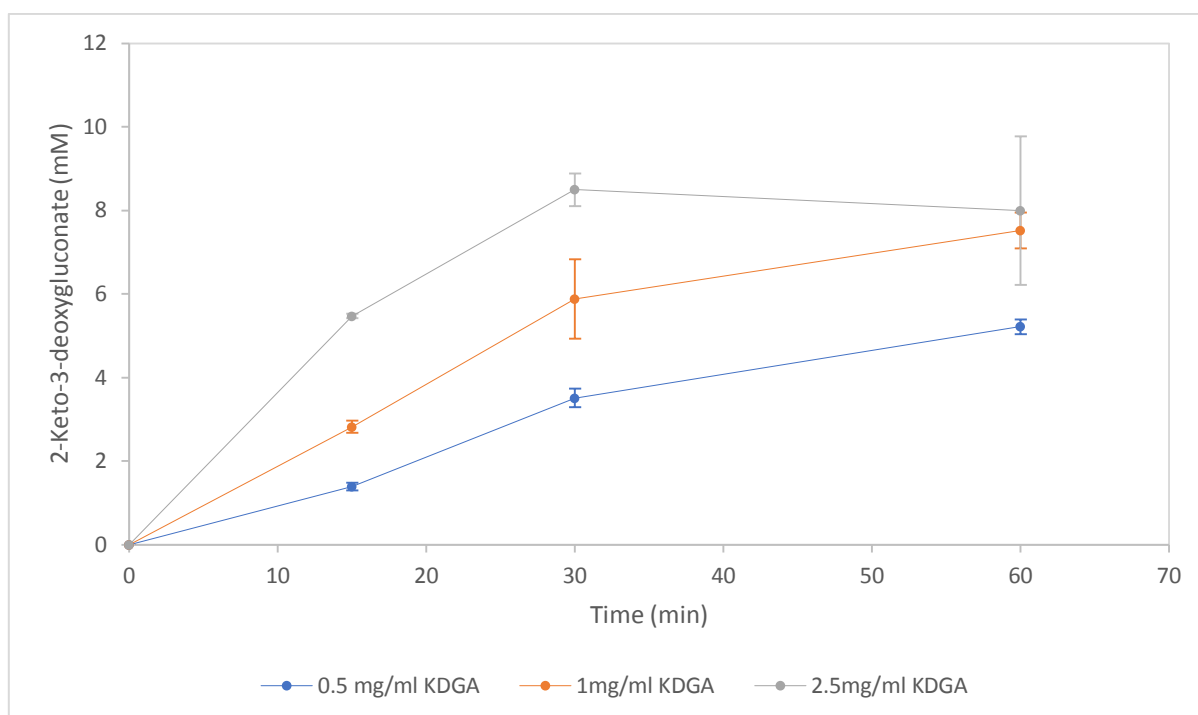
Figure 6.8. Graphical representation of IC analysis of KDGA activity assay (0.25, 1 and 2.5mg/ml) with 10mM glyceraldehyde and 20mM pyruvate as substrates at 15, 30 and 60 minutes, for the formation of 2-keto-3-deoxygluconate.

The assay conditions with the high substrate concentrations (10mM glyceraldehyde and 20mM pyruvate) produced 8.495 and 7.995mM of 2-keto-3-deoxygluconate at 60 minutes by both 1mg/ml and 2.5mg/ml KDGA. Therefore, all further kinetic studies were established to be done with KDGA concentration of 1mg/ml. The 1mg/ml DHAD assay analysis carried out with 10mM glyceraldehyde and

20mM pyruvate at 15, 30 and 60 minutes is shown in Figure 6.9 as the 2-keto-3-deoxygluconate peak can be seen as the incubation time increases, and the pyruvic acid peak can be seen decreasing as it is converted into 2-keto-3-deoxygluconate (Figure 6.9).
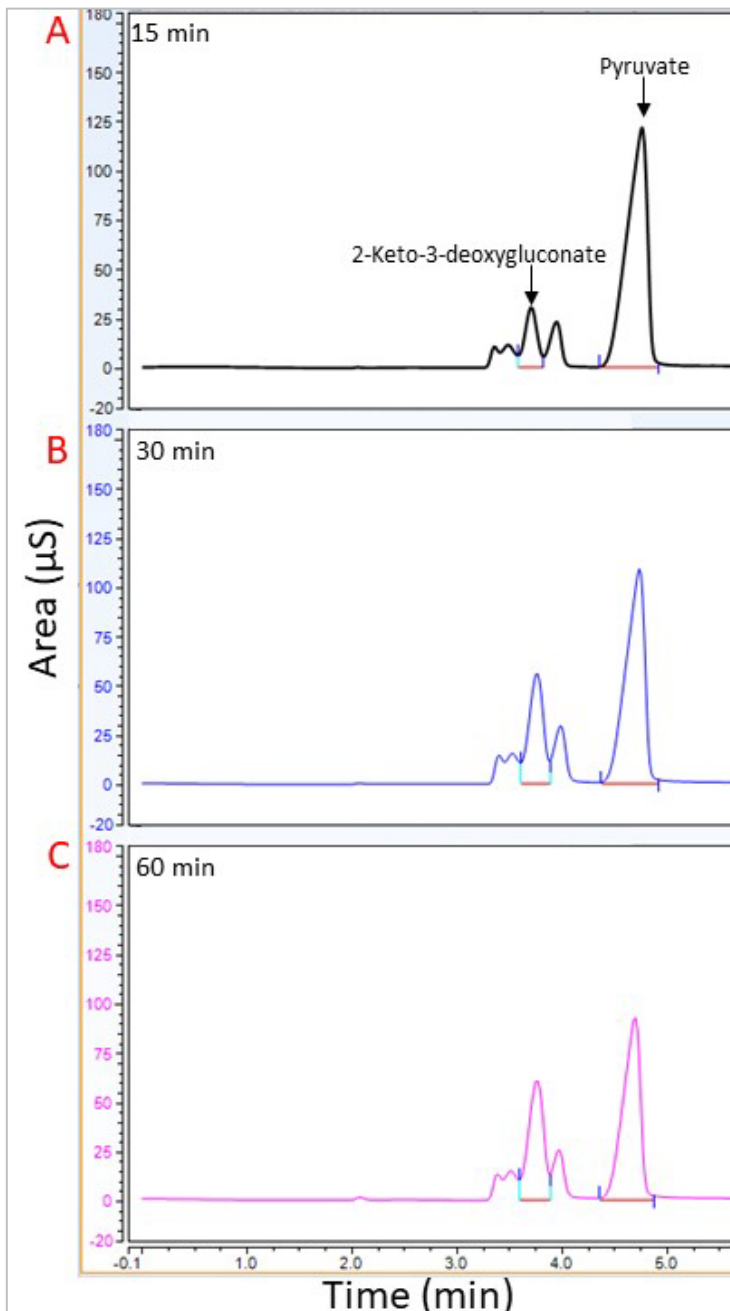
Figure 6.9. IC analysis of 1mg/ml KDGA assay with 10mM glyceraldehyde and 20mM pyruvate as substrates. Panel A is reaction components at 15 minutes, panel B is reaction components at 30 minutes and panel C is reaction components at 60 minutes. All samples were deproteinized once their appropriate incubation times were completed before loaded onto the IC for analysis. Glyceraldehyde could not be detected on the particular column used with the IC. The area of the pyruvate peak is seen to be decreasing over the 60 minutes while the 2-keto-3-deoxygluconate peak is seen to be increasing in area over the same time period.

6.9 Exploring the effect of glyceraldehyde and pyruvate concentration ratios on the production of 2-keto-3-deoxygluconate

Previously performed studies (Wolterink-van Loo et al. 2007) have used 20mM glyceraldehyde and 50mM pyruvate for any activity measurements of KDGA. The rationale for using this ratio was explored as the theoretical yield is 1:1. To test this, three ratios of glyceraldehyde and pyruvate were tested under experimental conditions:

1. 10mM glyceraldehyde + 20mM pyruvate (as previously used for KDGA activity analysis in sections 6.7 and 6.8.2 and Buchanan et al. 1999, Wolterink-van Loo et al. 2007)
2. 20mM glyceraldehyde + 20mM pyruvate (1:1 ratio)
3. 20mM glyceraldehyde + 10mM pyruvate (reverse ratios of those condition in 1)

Each condition was run with its own control without any KDGA, all assay and control conditions were incubated at 55°C at 300rpm shaking for one hour before deproteinizing and analysis via IC. 2-Keto-3-deoxygluconate was not detected in any of the control conditions. The pyruvate concentrations in the control and assay conditions were calculated using a pyruvic acid standard curve (Figure 2.4), as was the 2-keto-3-deoxygluconate concentration formed in the assay conditions from its respective standard curve (Figure 2.3).

	Pyruvate (mM)	2-Keto-3-deoxygluconate (mM)
Assay 10mM glyceraldehyde + 20mM pyruvate	11.54	8.34
Control 10mM glyceraldehyde + 20mM pyruvate	19.35	N/D
Assay 20mM glyceraldehyde + 20mM pyruvate	6.88	13.1
Control 20mM glyceraldehyde + 20mM pyruvate	19.2	N/D
Assay 20mM glyceraldehyde + 10mM pyruvate	2.56	7.9
Control 20mM glyceraldehyde + 10mM pyruvate	9.52	N/D

Table 6.5. IC 0.25mg/ml KDGA activity analysis with 3 ratios of glyceraldehyde and pyruvate in the formation of 2-keto-3-deoxygluconate after 60 minutes. Standard deviation for all assay and control conditions= <0.6. N/D= none detected.

No 2-keto-3-deoxygluconate peaks were detected in any of the controls as expected since there is no KDGA added to catalyse the conversion of glyceraldehyde and pyruvate to 2-keto-3-deoxygluconate. As for the ratios used, the 10mM glyceraldehyde + 20mM pyruvate substrate ratios produced 8.34mM 2-keto-3-deoxygluconate. The reverse of this condition with opposite substrate ratios, 20mM glyceraldehyde and 10mM pyruvate gave slightly lower 2-keto-2-deoxygluconate concentration of 7.9mM. As for the condition where the concentration of glyceraldehyde used was doubled to 20mM from 10mM, the concentration of 2-keto-3-deoxygluconate formed would also expected to be doubled. As this was not the case, performing further experiments with an increased concentration of

glyceraldehyde would lead to unnecessary addition of substrate without it contributing significantly to the yield increase overall, therefore the rationale for using 10mM glyceraldehyde and 20mM pyruvate as cited in literature was justified.

6.10 Establishing KDGA enzyme kinetics

Following the experimental data obtained in sections 6.82 and 6.9, 1mg/ml final KDGA concentration was tested with a range of glyceraldehyde and pyruvate concentrations in which the ratio of glyceraldehyde to pyruvate was always kept 1:2 respectively, and the enzyme kinetics experiments were performed. All conditions were ran alongside negative controls to check if the concentration of known substrate concentrations added to assays (only pyruvate as glyceraldehyde could not be detected on the IC column) were calculated to be similar concentrations from the standard curve (Table 6.6).

Pyruvic acid (mM)	Calculated pyruvic acid concentration from standard curve (mM)
1	0.88
2	1.28
6	4.91
10	9.31
20	18.88
40	38.31

Table 6.6. IC analysis of negative assay controls with known concentrations of pyruvic acid without addition of KDGA. Standard deviation for all conditions = <2.68

As outlined in Table 6.6, the concentrations of added pyruvic acid to the assay conditions are slightly underestimated when they are recalculated using the pyruvic acid standard curve. This is due to the error factor in using the IC to calculate final concentrations. Due to the nature of peak selection, this is a factor which cannot be mitigated easily. Enzyme kinetics experiments were run and the final concentration of 2-keto-3-deoxygluconate obtained from all conditions is outlined in Table 6.7 below and a graphical representation is shown in Figure 6.10.

	2-keto-3-deoxygluconate production (mM)					
Time (min)	0.5mM GL 1mM PA	1mM GL 2mM PA	3mM GL 6mM PA	5mM GL 10mM PA	10mM GL 20mM PA	20mM GL 40mM PA
2	N/A	N/A	0.25	0.53	0.81	1.81
4	N/A	N/A	0.36	0.66	1.30	3.33
6	N/A	N/A	0.48	0.91	1.97	3.93
10	N/A	0.18	0.66	0.99	3.65	5.78
15	N/A	0.28	0.79	1.71	4.68	9.29
30	N/A	0.28	1.24	3.37	7.31	17.70

Table 6.7. IC activity analysis of production of 2-keto-3-doxygluconate with 1mg/ml KDGA assays with glyceraldehyde (GL) and pyruvate (PA) as substrates, tested in the range of 0.5-20mM glyceraldehyde and 1-40mM pyruvate at various time points. 0.5mM GL 1mM PA and some 1mM GL 2mM PA data points missing as 2-keto-3-deoxygluconate peak was very difficult to isolate due to surrounding buffer component peaks (N/A). Standard deviation of all conditions= <0.94.

The missing data points (N/A) in Table 6.7 are due to surrounding buffer component peaks with very similar retention times to that of 2-keto-3-deoxygluconate. They were also seen in each condition control and since the initial concentrations of 2-keto-3-deoxygluconate are very small peaks, especially when the overall substrate concentrations used in the assay conditions are low, it was very hard to objectively isolate the peak associated with 2-keto-3-deoxygluconate.
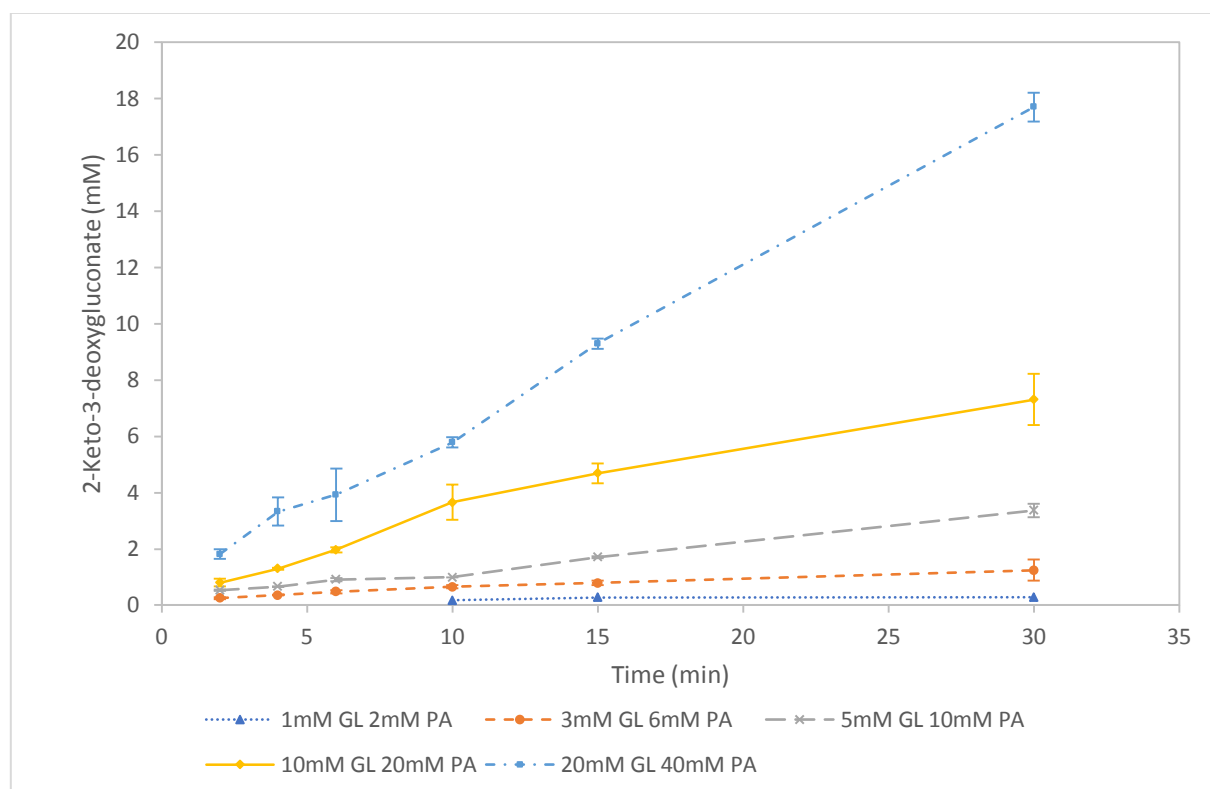
Figure 6.10. Graphical representation of 2-keto-3-doxygluconate productions with 1mg/ml KDGA using various concentrations of glyceraldehyde (GL) and pyruvate (PA) as substrates over a time course of 30 minutes. Standard deviation of all conditions= <0.94.

Figure 6.11A shows the initial activity of KDGA at different substrate concentrations and Figure 6.11B shows the Lineweaver-Burk plot for the kinetics calculation. The Michealis-Menten model was used to

calculate the apparent V_{max} and K_m values of KDGA which was calculated to be 0.287U/mg and 32.426mM respectively. There are two substrates present in the assay condition (glyceraldehyde and pyruvate) and as pyruvate was the only one which could be detected via IC, this was used to calculate the enzyme kinetics.

A

$y = 113.13x - 3.4889$
$R^2 = 0.9918$

B
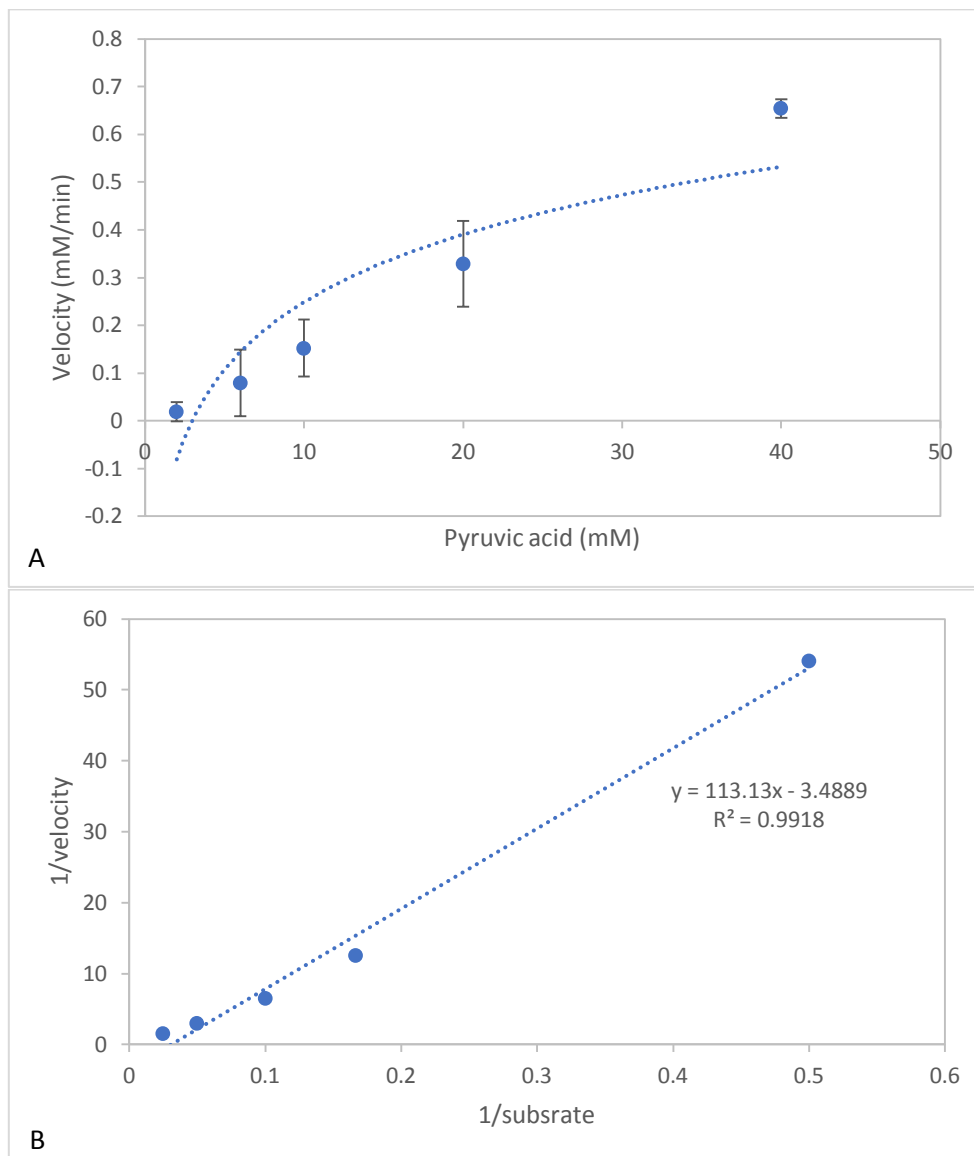
Figure 6.11. Initial activity of KDGA at various gluconic acid concentrations (A), Lineweaver-Burk plot for the kinetic analysis (B).

This chapter has outlined the successful expression, purification and quantification techniques employed for the production of KDGA. Activity of KDGA in the reverse direction has successfully been established and its forward reaction of interest in the overall cascade has been optimized and characterized.

7. Using glyceraldehyde dehydrogenase to shift reaction equilibrium towards production of desired intermediate-pyruvate

As outlined in Chapter 6, the prior step in the cascade catalysed by 2-keto-3-deoxygluconate aldolase catalyses the cleavage of 2-keto-3-deoxygluconate into pyruvate and glyceraldehyde, with only the former product of pyruvate being an intermediate of interest in relation to the cascade design discussed in this thesis. Glyceraldehyde is as an unwanted by-product which reduces the theoretical yield efficiency of the final product, malic acid. A solution to this was explored with the addition of glyceraldehyde dehydrogenase (AIDH) to the cascade design. AIDH catalyses the conversion of glyceraldehyde to glycerate and as outlined previously in Chapter 5, substrate promiscuity of DHAD can be exploited as it can also catalyse the conversion of glycerate to pyruvate. This thereby reduces the unwanted intermediates formed and pushes the reaction forward in the desired direction. AIDH from *Thermoplasma acidophilum* has been cited to display high substrate specificity towards glyceraldehyde (Guterl et al. 2012) and therefore is a suitable option for application in this cascade. Previous attempts at expression and purification of AIDH from *Thermoplasma acidophilum* have highlighted issues with purification from inclusion bodies (Steffler and Sieber 2013). This chapter discusses the protein expression, issues with purification from the soluble and insoluble fraction and attempts at methods of optimization of AIDH purification and characterization are also explored.

7.1 Transformation of AIDH vector DNA into BL21-DE3 competent cells

Synthesised pET30a vectors containing AIDH sequence arrived as a concentrated miniprep of ~4µg of DNA from GenScript (sequence in appendix). Original vector sample was archived and transformation of vector into DH5α competent cells was done followed by a miniprep to obtain 50µl of quantified vector DNA. AIDH was transformed into BL21-DE3 cells as they have favourable characteristics for recombinant protein production such as protease deficiency, low acetate production under high glucose conditions and high permeability. Following successful transformation, single colonies were used to initiate protein expression. LB agar kanamycin plates with the successful transformation of vector DNA into BL21-DE3 were also used to prepare glycerol stocks for storage at -80°C for future applications.
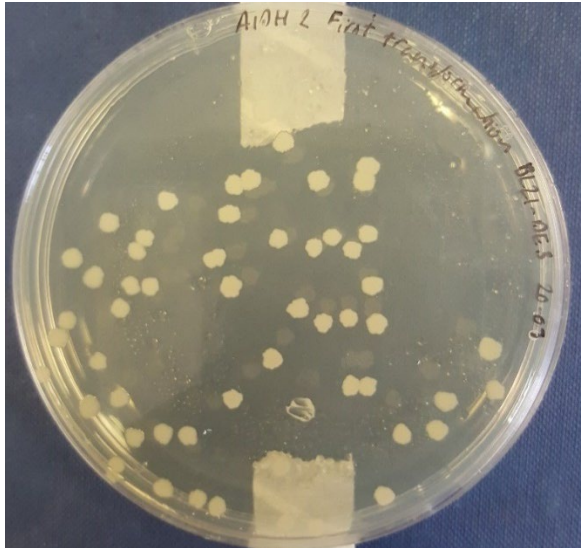
Figure 7.1. Quantified vector DNA obtained following miniprep was transformed into competent BL21-DE3 cells, successful transformation is shown by the presence of bacterial colonies on LB kanamycin plate.

7.2 AIDH protein expression in AI media

Following successful transformation of AIDH vector DNA, protein expression for crude protein fraction preparation was initially carried out in a 4L final culture volume of AI media with a final concentration of kanamycin at 50μg/ml. An average OD_{600} of 9.055 was read across the 4 flasks.

7.2.1 AIDH soluble fraction preparation and purification with Ni-NTA

The cell pellets obtained from the cultures in 7.2 were resuspended, sonicated and heat treated as outlined in the methods sections. Following centrifugation of AIDH cultures and isolation of the cell pellet, the medium was not discarded as standard but an aliquot was stored to be analysed via SDS-PAGE. This was done in order to confirm whether or not the protein was being secreted into the AI medium itself (Figure 7.2, lane 2). Regarding the cell pellet obtained, all resuspension, sonication, heat treatment and purification steps were carried out in a 100mM HEPES pH 7.5, 10% glycerol buffer unless otherwise stated. As this cell pellet was processed with the main goal of downstream processing of AIDH inclusion bodies, no $MgCl_2$ was added to the buffer used for resuspension, sonication and heat treatment of the cell pellet as presence of salt promotes refolding (Singh et al. 2015) and the inclusion bodies protocol was to be done under denaturing conditions to unfold and correctly refold the protein. Following resuspension, sonication and heat treatment of cell pellet, 100ml of soluble crude protein fraction obtained from this stage was bound to and purified using 5 ml of Ni-NTA as outlined in the methods section. This step was carried out to determine if any soluble AIDH is present in the crude fraction and if it can be purified using Ni-NTA or whether the majority of the AIDH protein is present in the inclusion bodies. Following the Ni-NTA purification protocol as outlined in the methods section, one key change was made during this purification protocol. 200mM of $MgCl_2$ was added to the HEPES buffer mix (100mM HEPES pH 7.5, 10% glycerol, 200mM $MgCl_2$) used for washes and the imidazole

elutions. The reintroduction of the MgCl$_2$ into the buffer assists protein stability in the soluble fraction. Following buffer washes and imidazole elutions, all elutions obtained were analysed via SDS-PAGE (Figure 7.2).
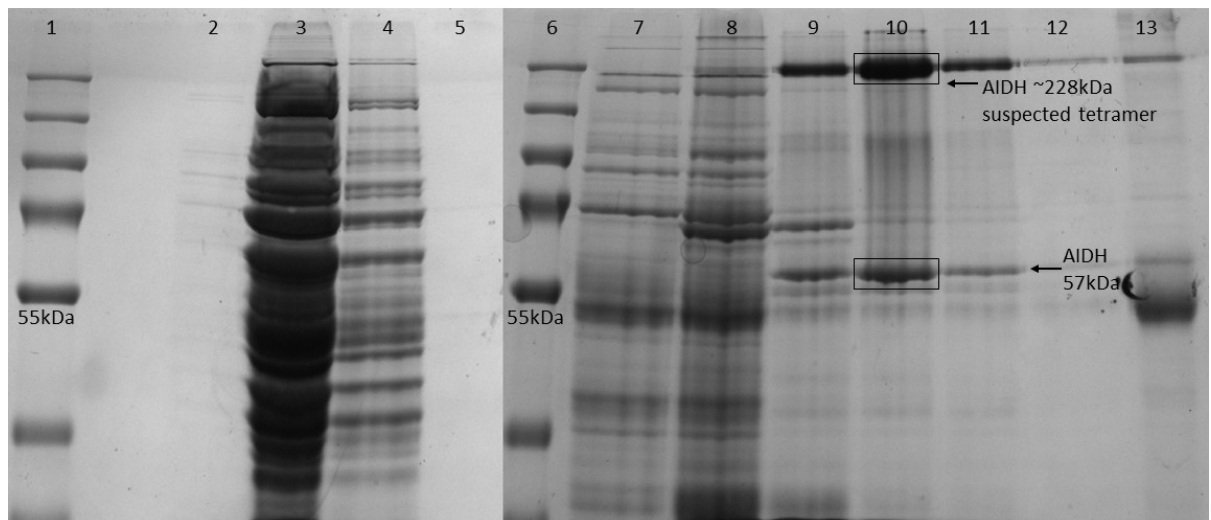
Figure 7.2. SDS-PAGE analysis of soluble AIDH fraction obtained following expression in *E. coli* BL21-DE3 and AI media. Samples in all lanes are from elutions obtained from the column following Ni-NTA affinity chromatography. Lane 2 contains AI medium after centrifugation to isolate the cell pellet to check for any secreted proteins. Lane 3 is the flow through from the column and lanes 4 and 5 contain HEPES buffer washes (100mM HEPES pH 7.5, 10% glycerol, 200mM MgCl$_2$). Lane 7, 8, 9, 10, 11, 12 and 13 contain HEPES buffer imidazole elutions with 50, 100, 200, 400, 600, 800 and 1000mM imidazole respectively.

AIDH monomer is 57 kDa and as seen in Figure 7.2, lanes 9, 10 and 11 feature strong bands at the position correlating to this size. There was a strong band seen around the 230 kDa size as seen in lanes 9, 10 and 11. This was suspected to be a tetramer of AIDH and along with the AIDH monomer, both of these bands were excised from the gel and analysed via mass spectrometry to confirm protein ID. Mass spectrometry analysis identified both of these bands to be AIDH from *Thermoplasma acidophilum* (data in appendix). The full fraction of the elution sample loaded in lane 10 was buffer exchanged using a protein concentrator spin column until negligible amounts of imidazole remained. Following this, an attempt was made to concentrate the protein down to a smaller volume during which the protein aggregated and recovery of soluble protein was very poor.

7.2.2 AIDH insoluble fraction preparation and purification with Ni-NTA

Cell pellet obtained from the expression of AIDH in AI media was processed as outlined at the beginning of section 7.2.1 and the soluble crude fraction was purified using Ni-NTA as shown in Figure 7.2. The cell pellet obtained following the sonication, heat treatment and centrifugation during the soluble fraction preparation was processed downstream for AIDH inclusion bodies. As mentioned in section 7.2.1, the resuspension and all subsequent steps carried out with the initial AIDH pellet obtained following expression and growth in AI media were carried out in 100mM HEPES pH 7.5, 10% glycerol

buffer without any MgCl₂, therefore it contained no traces of salt to promote refolding and was suitable to be processed under denaturing conditions. The cell pellet was resuspended in 50ml of denaturation buffer consisting of 6M guanidine hydrochloride (GdnHCl), 2mM DTT and 20mM HEPES pH 7.5 (as outlined in the materials section) and incubated to denature the protein and unfold it completely. The expectation after incubation of the cell pellet with denaturation buffer was to have the AIDH completely unfolded in solution which was followed by centrifugation to get rid of cellular debris. The 50ml of denaturation buffer containing unfolded AIDH was split into two 25ml fractions.

7.2.2.1 Refolding of denatured AIDH in GdnHCl with Ni-NTA

Two different methods to refold the unfolded AIDH were attempted with each 25ml fraction. The first method was to bind one 25ml fraction with 2.5ml Ni-NTA before purification using imidazole as outlined in the methods and done previously with the soluble fraction in section 7.2.1. The idea behind this attempt was that the unfolded AIDH in the GdnHCl, DTT and HEPES buffer solution binds to Ni-NTA with the aid of the His₁₀ tag. This was followed by affinity chromatography which gradually removes the GdnHCl and DTT in the flow through from the column, and the excess HEPES buffer mix (100mM HEPES pH 7.5, 10% glycerol, 200mM MgCl₂) washes remove traces of GdnHCl and DTT from the Ni-NTA resin until their concentrations are negligible. Removing AIDH from GdnHCl solution promotes refolding and the introduction of MgCl₂ and glycerol in the buffer further encourages protein refolding and stability (Singh et al. 2015). This was followed by imidazole elutions to elute any bound protein from the Ni-NTA. 3 different imidazole concentrations were used to elute any bound protein (Figure 7.3).
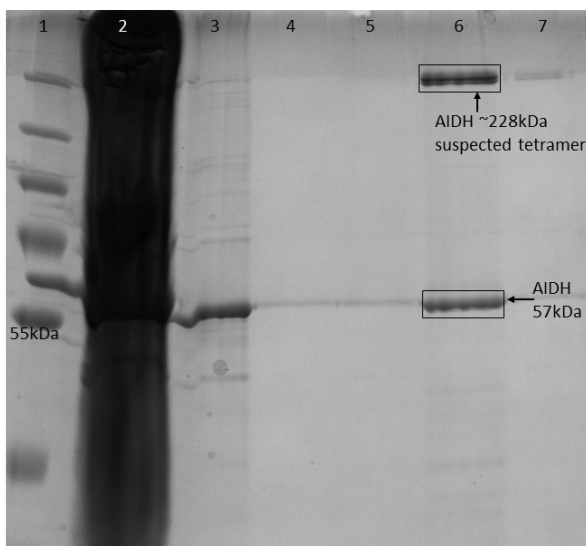
Figure 7.3. SDS-PAGE analysis of Ni-NTA purification attempt of AIDH inclusion bodies following extraction with GdnHCl. Samples in all lanes are from elutions obtained from the column following Ni-NTA affinity chromatography. Lane 2 contains flow through of denaturation buffer. Lanes 3 and 4 contain samples from HEPES buffer washes (100mM HEPES pH 7.5, 10% glycerol, 200mM MgCl₂). Lanes 5, 6 and 7 contain HEPES buffer imidazole elutions with 100, 500 and 1000mM imidazole respectively.

From Figure 7.3, it is evident that binding the unfolded protein under denaturing conditions with Ni-NTA and then eluting any bound protein off with imidazole was an effective strategy. The HEPES buffer washes were effective at removing GdnHCl and DTT as the flow through contains a very high amount of GdnHCl and upon addition to the SDS-PAGE, it precipitated resulting in the smear seen in lane 2. A negligible amount of GdnHCl in the following washes resulted in the elution of bound AIDH as seen in lane 6. As mentioned previously, AIDH monomer is 57 kDa and as seen in Figure 7.3 lane 6 features a single band at the position correlating to this size. There was a strong band around 230 kDa as seen in lane 6 and faintly in lane 7 as well. This was suspected to be a tetramer of AIDH and along with the AIDH monomer, both of these bands were excised from the gel and analysed via mass spectrometry to confirm protein ID. Mass spectrometry analysis identified both of these bands to be AIDH from *Thermoplasma acidophilum* (data in appendix). Going forward, refolding of AIDH while carrying out affinity chromatography seems an effective strategy and the protocol was to be optimized before attempting it again. The full fraction of the elution sample loaded in lane 6 was buffer exchanged using a protein concentrator spin column until negligible amounts of imidazole remained. Following this, an attempt was made to concentrate the protein down to a smaller volume during which a 1.27mg/ml concentrated sample of AIDH was obtained as determined via BCA. This sample was stored before analysis for enzymatic activity at a later stage.

7.2.2.2 Refolding of denatured AIDH in GdnHCl via dialysis

As mentioned in section 7.2.2, the unfolded AIDH in denaturation buffer was split into two 25ml fractions, the first of which was processed as outlined in section 7.2.2.1 with a successful attempt at refolding unfolded AIDH using Ni-NTA chromatography. The second 25ml fraction was attempted to be refolded using a dialysis technique. The idea behind this attempt was similar to that of the approach in section 7.2.2.1 in the sense that gradual removal of GdnHCl from the solution promotes refolding of the protein in solution which could then be bound with Ni-NTA to remove any unwanted proteins. The 25ml fraction was dialysed against 500ml of 100mM HEPES pH 7.5, 10% glycerol, 200mM $MgCl_2$ buffer overnight. This was not effective as aggregates were seen inside the dialysis tubing (Figure 7.4A). The sample from the dialysis tubing was centrifuged to separate the aggregates from the supernatant (Figure 7.4B), which was analysed via SDS-PAGE (Figure 7.5) to observe the composition of the sample.
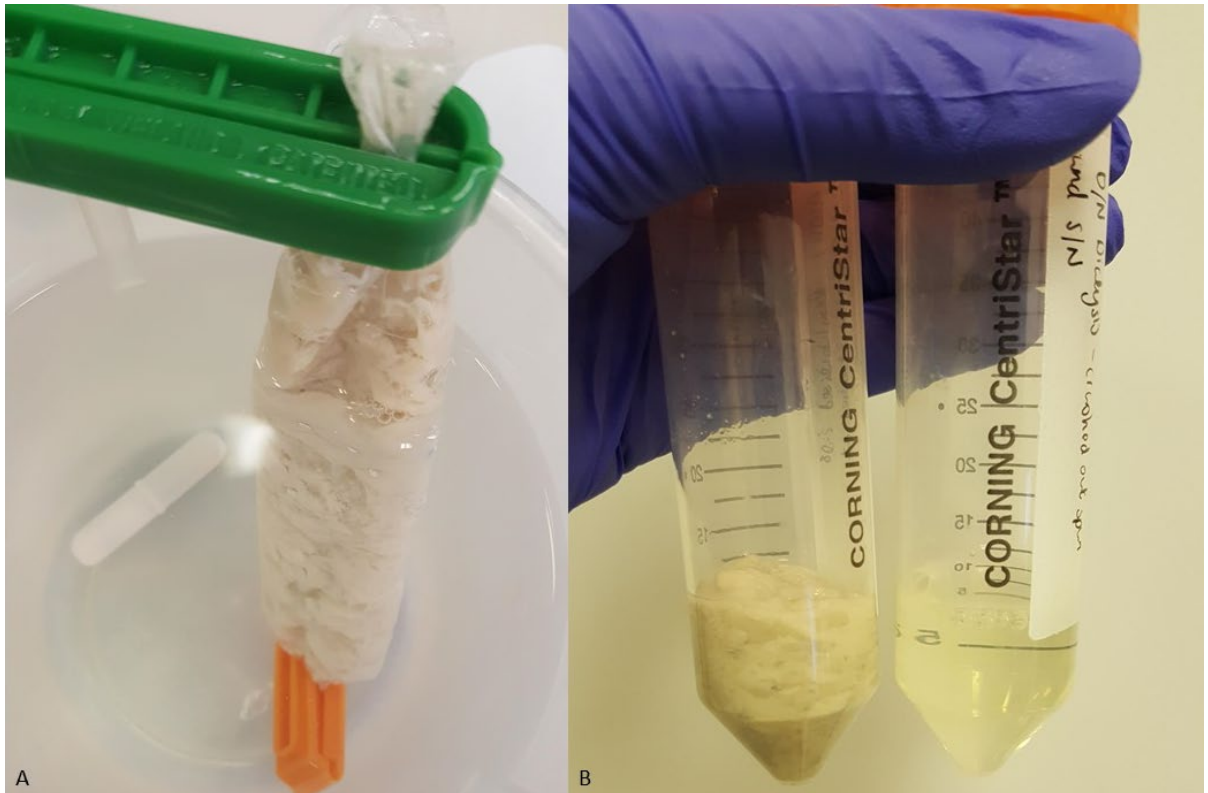
Figure 7.4. Dialysis of 25ml unfolded AIDH in denaturation buffer consisting of 6M GdnHCl, 2mM DTT and 20mM HEPES pH 7.5 against 500ml of 100mM HEPES pH 7.5, 10% glycerol, 200mM $MgCl_2$. Aggregates are visible inside the dialysis tubing (Figure 7.4A). Aggregates from the dialysis tubing were centrifuged at 30,000rpm to separate the aggregates from the supernatant (Figure 7.4B).
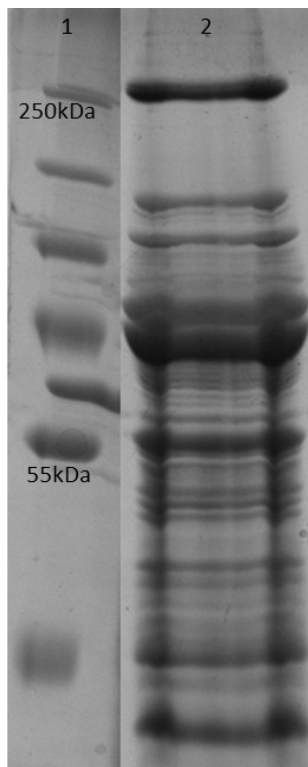
Figure 7.5. SDS-PAGE analysis of supernatant obtained from the centrifugation of aggregates formed in the dialysis tubing following the unsuccessful attempt at dialysing the 25ml unfolded AIDH in denaturation buffer consisting of 6M GdnHCl, 2mM DTT and 20mM HEPES pH 7.5 against 500ml of 100mM HEPES pH 7.5, 10% glycerol, 200mM $MgCl_2$.

From the SDS-PAGE analysis of the supernatant it can be seen that in comparison to the method of refolding denatured AIDH with Ni-NTA (Figure 7.3), refolding denatured AIDH via dialysis produces a lot of non-specific proteins (Figure 7.5) as there was no Ni-NTA to select for the binding of His_{10} tagged AIDH. Following a successful dialysis series to remove GdnHCl and DTT to negligible levels, the presumed refolded AIDH still requires Ni-NTA affinity chromatography to remove non-specific proteins, for this reason refolding the denatured AIDH via binding with Ni-NTA in the unfolded state followed by eluting protein with imidazole presents itself to be a more efficient method. There was also a prominent band seen around the ~250kDa marker which has previously also been seen during the soluble AIDH fraction Ni-NTA purification (Figure 7.2) as outlined in section 7.2.1 and also during the Ni-NTA purification attempt of AIDH inclusion bodies following extraction with GdnHCl (Figure 7.3) as outlined in section 7.2.2.1. Both of these bands were suspected AIDH tetramers and have been positively identified as AIDH from *Thermoplasma acidophilum* via mass spectrometry analysis. The band seen in Figure 7.5 at around the 250kDa mark could be SDS-induced aggregates or, also be correlating to folded subdomains which can presumably associate with complimentary binding surfaces in an intermolecular manner to form oligomers and eventually aggregates (Palmer and Wingfield 2004).

7.2.2.3 Comparing methods of refolding denatured AIDH with Ni-NTA or via dialysis

From sections 7.2.2.1 and 7.2.2.2 it is evident that binding denatured AIDH in a 6M GdnHCl, 2mM DTT and 20mM HEPES pH 7.5 buffer with Ni-NTA followed by affinity chromatography and elution of bound AIDH with imidazole is an efficient method in comparison to dialysis of denatured AIDH in a 6M GdnHCl, 2mM DTT and 20mM HEPES pH 7.5 buffer. As seen in Figure 7.5 lane 2, there are still various unwanted bands correlating to other proteins in the sample, hence a secondary step would be required to obtain a higher purity AIDH sample regardless. Binding denatured AIDH with Ni-NTA and omitting the dialysis eliminates a step and improves efficiency. Moreover, the success of the dialysis step depends on establishing optimum dialysis conditions in terms of dialysis buffer volume ratios, temperature, buffer components and speed of dialysis etc. The failure of the dialysis refolding attempt of AIDH as outlined in section 7.2.2.2 can therefore be attributed to a multitude of factors. The protocol developed for use in the preparation and extraction of the AIDH inclusion bodies as outlined in 7.2.2 was simplified at the time of attempt. Inclusion bodies are typically of a whiteish colour in their appearance whereas the cell pellet obtained following the sonication, heat treatment and centrifugation during the soluble fraction preparation as outlined in section 7.2.1 and was processed downstream for AIDH inclusion bodies was of a brownish appearance. This is indicative of the presence of other cellular components and presumably the AIDH inclusion bodies had not been extracted efficiently. The denaturation buffer consisting of GdnHCl, DTT and HEPES consisted of basic

denaturation buffer components and it was therefore decided to optimize the extraction of inclusion bodies further before reattempting refolding of denatured AIDH in GdnHCl with Ni-NTA. The experimental data gathered from section 7.2 and all its subsequent subsections successfully demonstrated positive protein ID of AIDH and also provided directions in which to optimize the extraction and purification of soluble AIDH from AIDH inclusion bodies.

7.3 Testing enzymatic functionality of soluble AIDH obtained from refolding of denatured AIDH with Ni-NTA

A 1.27mg/ml soluble AIDH stock was obtained following the successful refolding of denatured AIDH in GdnHCl with Ni-NTA as outlined in 7.2.2.1. The other attempts of purifying AIDH from the crude soluble fraction as outlined in 7.2.1 resulted in protein precipitation during an attempt to concentrate the Ni-NTA purified protein and gave very poor recovery of AIDH. Refolding of denatured AIDH in GdnHCl via dialysis also lead to protein aggregation in the dialysis tubing, hence the only soluble AIDH stock came from the successful refolding of denatured AIDH in GdnHCl being bound to Ni-NTA followed by elution of bound AIDH with the aid of imidazole. AIDH was assayed for activity and since it uses NAD^+ as a cofactor, the reaction can easily be followed at 340nm by the concomitant reduction of NAD to NADH.

$$Glyceraldehyde + NAD^+ \rightarrow Glycerate + NADH$$

0.32 mg/ml of AIDH was assayed in triplicates of 200µl volume with 100mM of glyceraldehyde in excess and 5mM of NAD^+. A control without any AIDH was analysed in triplicate alongside the assay as well and this was also used as a blank for assay conditions (Figure 7.6).
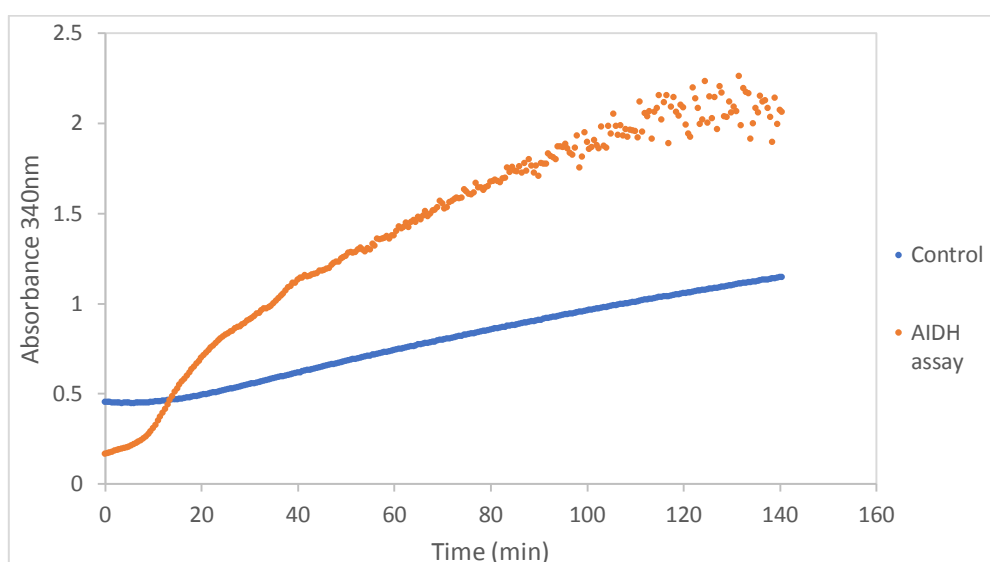
Figure 7.6. 0.32mg/ml AIDH enzymatic activity analysis via absorbance at 340nm. All conditions were done in triplicates, standard deviation for control= <0.04, standard deviation for assay= <0.197.

From the initial AIDH activity analysis as seen in Figure 7.6, the control for this experiment did not show a linear absorbance without any major fluctuations. The control condition had no AIDH to catalyse the

conversion of glyceraldehyde to glycerate and thereby theoretically no NADH should be present in the assay to contribute to the increase in absorbance values at 340nm. However, as seen in Figure 7.6 there is a gradual increase in the absorbance values of the control. This made the overall experimental design unreliable as the assay condition absorbance readings cannot be confidently attributed to the activity of AIDH. This anomaly in the increasing absorbance readings of the control were explored in the following section to determine its cause.

7.4 Exploring AIDH assay components to explore the cause of increasing absorbance values in control conditions

To determine which assay component/s is/are having an absorbance increasing effect on the AIDH control condition, different combinations of assay components were compared for their absorbance values at 340nm in different combinations. The secondary product of the reaction, NADH was also tested with assay conditions to determine if the reaction progression might be contributing to the unusual absorbance 340nm readings seen in the control conditions in Figure 7.6. Overall 7 different assay conditions were tested, firstly the 3 different concentrations of glyceraldehyde (10, 50 and 100mM) with 100mM HEPES pH 7.5. Glyceraldehyde and NAD^+ were also tested together at 50mM glyceraldehyde + 2.5mM NAD^+ and 100mM glyceraldehyde and 5mM NAD^+ both in 100mM HEPES pH 7.5. Glyceraldehyde and NADH were also tested with 100mM HEPES pH 7.5 at 50mM glyceraldehyde + 2.5mM NADH and 100mM glyceraldehyde and 5mM NADH. Absorbance readings of all conditions over the course of ~180 minutes are shown in Figure 7.7. Glyceraldehyde on its own at various concentrations (10, 50 and 100mM) shows very little fluctuation in readings over the course of the assay period. However, glyceraldehyde + NAD^+ display an increase in absorbance values and as previous mentioned, glyceraldehyde on its own demonstrated no major changes in absorbance values, therefore, even though 2 different concentrations of glyceraldehyde were tested with 2 concentrations of NAD^+, the difference in the increase of absorbance values for the condition was attributed to the higher NAD^+ concentration. The conditions of glyceraldehyde at 50 and 100mM tested with 2.5 and 5mM of NADH respectively gave absorbance readings as expected. NADH at concentrations above 2mM gives absorbance values that fall outside the readable range of the spectrophotometer and therefore gives erratic absorbance values similar to those seen in Figure 7.7 at around 3.5 absorbance 340nm. However, given their consistent values over the course of the assay period, it is likely that the progression of the reaction and production of NADH as the secondary product did not contribute to the increased absorbance values observed in the control as seen in Figure 7.6.
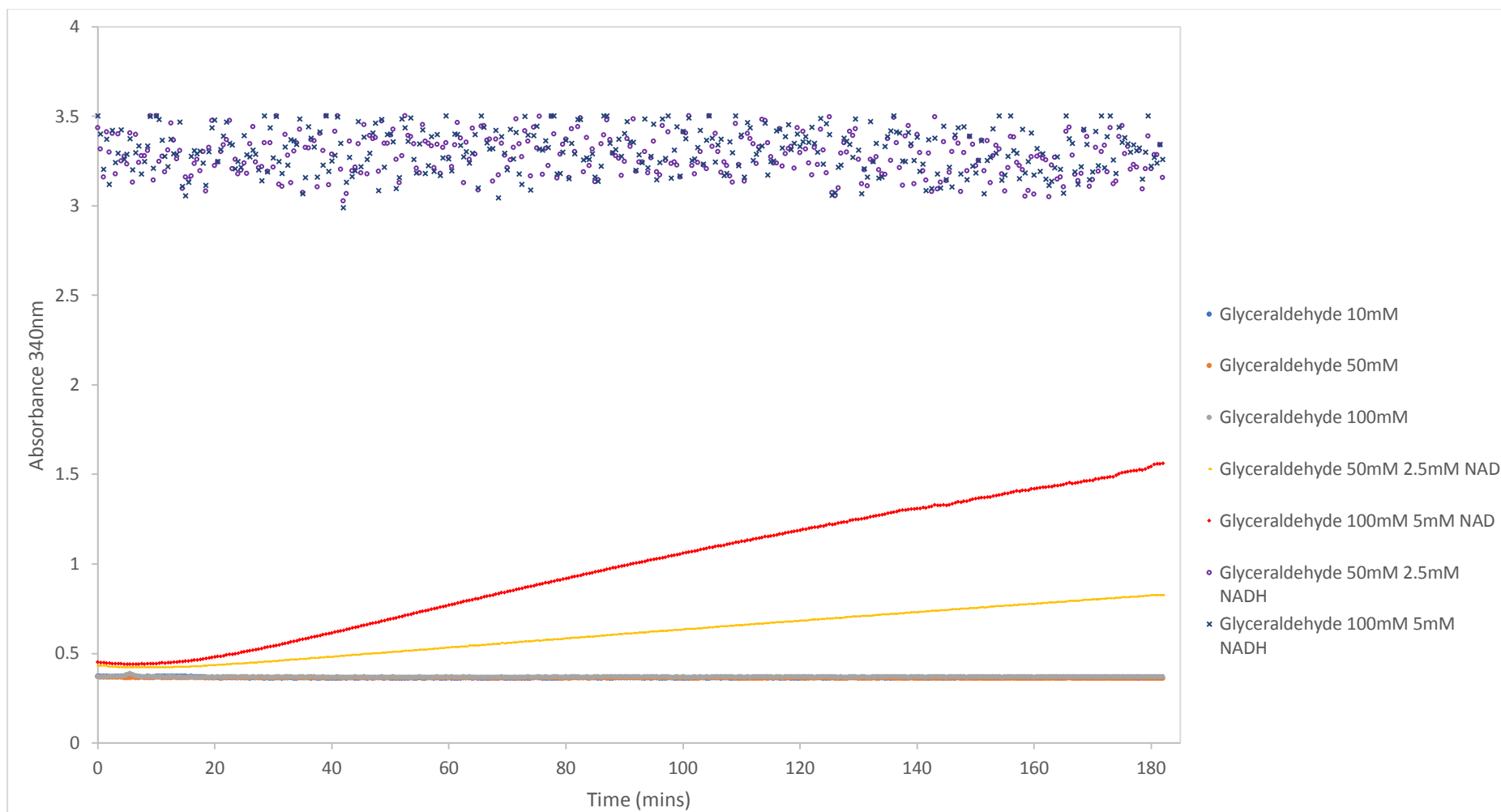
Figure 7.7. Testing effect of AIDH assay components to determine if any components are contributing to the increased absorbance 340nm as previously seen in the control condition. All conditions ran in triplicates and standard deviations are as follows: Glyceraldehyde 10, 50 and 100mM <0.022, glyceraldehyde 50mM + 2.5mM NAD$^+$<0.035, glyceraldehyde 100mM + 5mM NAD$^+$<0.049, glyceraldehyde 50mM + 2.5mM NADH <0.3 and glyceraldehyde 100mM + 5mM NADH <0.25.

From the data obtained in Figure 7.7, it was concluded that the increase in absorbance values of the AIDH assay control are due to the interaction of glyceraldehyde and NAD^+. Some aldehydes can break down to carboxylic acids in water/air, and this breakdown could possibly be providing the electrons required to form NADH from NAD^+ over time, leading to an increase in the control absorbance even in the absence of AIDH to catalyse the formation of NADH as a secondary reaction product.

7.5 Optimizing the extraction and purification protocol of soluble AIDH from AIDH inclusion bodies

Following the successful attempt of refolding denatured AIDH in section 7.2.2, the method of extraction and purification was optimized to improve yield of soluble protein recovered as required for experimental purposes. In the earlier attempt (section 7.2.2), it was assumed that inclusion bodies were not extracted efficiently, therefore a higher yield of soluble AIDH was not achieved as the protocol developed for use in the preparation and extraction of the AIDH inclusion bodies was simplified at the time of attempt. Inclusion bodies are typically of a whiteish colour in their appearance whereas the cell pellet obtained following the sonication, heat treatment and centrifugation during the soluble fraction preparation (section 7.2.1) and was processed downstream for AIDH inclusion bodies, was of a brownish appearance. This is indicative of the presence of other cellular components and presumably the AIDH inclusion bodies had not been extracted efficiently. This was the main aim for this optimization, to extract AIDH inclusion bodies efficiently and purify soluble AIDH to recover higher yield of soluble protein for experimental purposes. A modified protocol for the extraction and purification of AIDH inclusion bodies was developed as outlined in the methods (section 2.5.7) and experimental strategy is described here.

Following expression of AIDH and isolation of the cell pellet as outlined in section 7.2, no attempt was made to purify AIDH from the soluble fraction as previously done in section 7.2.1. Following expression, the cell pellet was processed directly for inclusion bodies extraction and purification as the attempt to analyse the soluble fraction as previously done in section 7.2.1 resulted in low yields of AIDH, which precipitated during concentration, meaning it was not efficient to extract the small amount of soluble AIDH expressed. The cell pellet was resuspended in lysis buffer for sonication with the lysis buffer being added as 5ml per gram wet weight of cells and prepared fresh prior to use each time. The lysis buffer composition was as follows:

> 100mM HEPES pH 7.5
> 5mM EDTA
> 5mM DTT
> 10% Glycerol
> Protease inhibitors (1 tablet per 50ml)
> DNase I (5µl per 50mls)

No MgCl$_2$ was added to the lysis buffer as it promotes protein refolding (Palmer and Wingfield 2004) and the buffer conditions were to be kept in favour of denaturing to allow for maximum recovery of protein to be refolded at a later stage.

Following addition of lysis buffer to pellet, it was homogenized until fully resuspended and then sonicated as outlined in the methods. The lysed cell suspension was centrifuged and the supernatant was removed from the cell pellet. The cell pellet was then resuspended in wash buffer with the intention of washing out soluble proteins and cellular components such as cell wall and outer membrane material. Adding detergent such as Triton X-100 or SDS aids the extraction of lipid and membrane-associated proteins (Palmer and Wingfield 2004) therefore they form an integral component of the wash buffer. GdnHCl or urea are known to be used as part of the wash steps in protocols, however GdnHCl is not compatible with SDS as forms a precipitate, therefore if the processed protein samples are to be analysed via SDS-PAGE downstream, it is recommended to use Triton X-100 instead of SDS as the detergent (Palmer and Wingfield 2004). If urea is being employed as the denaturant in the washes and extraction of inclusion bodies then SDS is compatible as the detergent. For the purpose of this protocol, GdnHCl was used as the denaturant and Triton X-100 was used as the detergent. The wash buffer was added as 5ml of wash buffer per gram wet weight cells (pellet obtained following the centrifugation of the lysed cell suspension and removal of supernatant), and as with the lysis buffer, also being prepared just prior to use. The wash buffer composition was as follows:

- 100mM HEPES pH 7.5
- 5mM EDTA
- 5mM DTT
- 10% Glycerol
- 2% Triton X-100
- 2M GdnHCl

Two versions of the wash buffer were prepared; one as outlined above and another without the addition of GdnHCl and Triton X-100. Following addition of cell pellet to wash buffer, it was homogenized until fully resuspended and then centrifuged with the supernatant discarded and pellet retained for the next wash step. This was then repeated 2 more time or until the supernatant is no longer cloudy or coloured. A colourless and clear supernatant is indicative of removal of most cellular components, lipids and membrane associate components. When the supernatant is no longer cloudy or coloured, the cell pellet is resuspended in the final wash buffer made up without the addition of GdnHCl and Triton X-100, which is then centrifuged with the supernatant discarded and cell pellet retained for the next step. This final wash without GdnHCl and Triton X-100 aids the removal of Triton

X-100 from the cell pellet as Triton X-100 can stick to dialysis membranes. If required, the washed cell pellets can also be stored at this stage before further downstream processing.

The final stage of this protocol involved the suspension of the cell pellet obtained following the wash stage into extraction buffer. This extraction buffer was added as 1ml of extraction buffer per gram wet weight of the original cells. The extraction buffer composition was as follows:

- 100mM HEPES pH 7.5
- 5mM EDTA
- 6M GdnHCl
- 5mM DTT

If this buffer is cloudy it can be filtered and be stored in the fridge for 1 month without DTT (Palmer and Wingfield 2004). Following the resuspension of the cell pellet into the extraction buffer, the cell suspension was incubated and stirred for a minimum of 2 hours before processing further. This incubation period allowed for the AIDH in the inclusion bodies to homogenize in the denatured state. Following the incubation period, the cell suspension could be refolded either by binding with Ni-NTA in the denatured state and then eluting refolded protein via affinity chromatography and use of imidazole (as previously attempted in section 7.2.2.1). The cell suspension could also be transferred into dialysis tubing and dialysed into the required buffer (as previously attempted in section 7.2.2.2) with the dialysis cycles being repeated until GdnHCl, EDTA and DTT have been dialysed to a negligible amount. If the cell suspension was to be refolded on the affinity column, DTT was omitted from the extraction buffer and substituted with 2mM β-mercaptoethanol as DTT is a strong reducing agent and will reduce the nickel ions in the Ni-NTA resin (Palmer and Wingfield 2004). In addition, strong chelating agent such as EDTA are not recommended as they will strip the nickel ions from the column, significantly reducing the binding efficiency of the His tagged protein.

7.6 Attempt 1 of utilising modified protocol for extraction and purification protocol of soluble AIDH from AIDH inclusion bodies

Having designed a modified protocol for the extraction and purification of AIDH inclusion bodies as outlined in section 7.5, it was experimentally tested with a freshly expressed batch of AIDH. 2L of AI media were used to grow AIDH cultures where a final OD_{600} of 5.76 and 5.83 was achieved. 17.7g of combined cell pellet was obtained following centrifugation which was resuspended in 90ml of lysis buffer made up as detailed in section 7.5. After homogenization, the cell suspension was sonicated as outlined in the method section. The lysed cell suspension was centrifuged and the supernatant was removed from the cell pellet. 3.3g of cell pellet was obtained following the lysis, sonication and centrifugation steps. This cell pellet was then resuspended in 16.5ml of wash buffer until completely homogenized before being centrifuged and supernatant removed and pellet retained. This wash step

was repeated a total of 3 times and with an additional fourth wash without any GdnHCl and Triton X-100 for the reasons previously discussed in section 7.5. Wash 4 was observed to have a colourless and clear supernatant which is indicative of removal of most cellular components, lipids and membrane associated components (Figure 7.8).
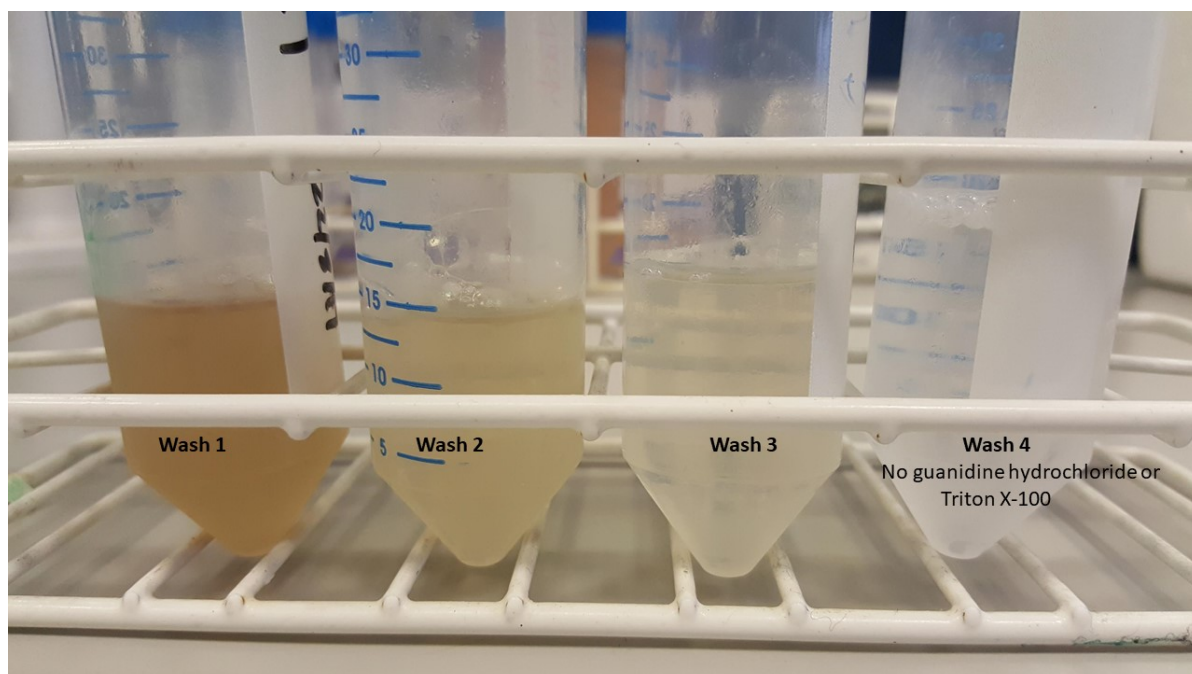
Figure 7.8. Supernatants removed following the homogenization and centrifugation of cell pellets with wash buffer. Washes 1-3 consists of HEPES, EDTA, DTT, glycerol, Triton X-100 and GdnHCl whereas wash 4 is without GdnHCl and Triton X-100.

In this attempt, wash 3 was not completely clear and still retained a colour to it (Figure 7.8), for any further replicates, it was noted that an improvement might be to repeat the wash step containing the GdnHCl and Triton X-100 until the supernatant is clear and colourless before doing a final wash without the addition of GdnHCl and Triton X-100 to ensure all other components have been removed. The pellet obtained after the wash steps was observed to be much lighter in appearance in comparison to that cell pellet processed for the extraction of inclusion bodies in 7.2.2, however it was not completely white in appearance and still had a tinge of colour to it. For any further attempts, it was noted that it might be necessary to continue the washes with wash buffer containing GdnHCl and Triton X-100 until pellet is white in appearance. Following the wash steps, the cell pellet obtained was stored at -80°C before final step of extraction of inclusion bodies. Extraction buffer was added as 1ml per gram wet weight of the original cells. The original cell pellet was 17.7g. This was rounded up to 20g and 20ml of extraction buffer was prepared and the pellet was resuspended until completely homogenized with the extraction buffer. The suspension was incubated for 2.5 hours at room temperature. Dialysis was attempted to remove the extraction buffer components and dialyse the suspension into 100mM HEPES pH 7.5, 200mM $MgCl_2$, 10% glycerol buffer. The previous dialysis attempt (section 7.2.2.2) was

unsuccessful and this was attributed to the higher presence of contaminating proteins, as the protocol did not employ extra wash steps. For the attempt discussed in this section, the modified protocol included wash steps to remove soluble proteins and other cellular components, thereby theoretically, failure of dialysis due to contaminating proteins was lowered. It is also a quicker alternative to refolding on the column. 20ml of extraction buffer suspension was dialysed against 200ml of 100mM HEPES pH 7.5, 200mM $MgCl_2$, 10% glycerol buffer at dilution factor of 10. This was not successful and the protein aggregates could be seen inside the dialysis tubing (Figure 7.9).

Figure 7.9. Dialysis of 20ml AIDH inclusion bodies extracted with HEPES, EDTA, GdnHCl and DTT dialysed against 200ml of 100mM HEPES pH 7.5, 200mM $MgCl_2$, 10% glycerol buffer at dilution factor of 10. Dialysis attempt was not successful and protein aggregates can be seen in the dialysis tubing.

Following the unsuccessful attempt at dialysis as seen in Figure 7.9, this attempt at extraction of soluble AIDH from AIDH inclusion bodies was not successful due to failure at the final stage of dialysis. This attempt was therefore abandoned here and purification of soluble AIDH via binding AIDH in its denatured state in the extraction buffer was decided to be explored next.

7.7 Attempt 2 at extraction and purification of soluble AIDH from AIDH inclusion bodies using Ni-NTA

Following the unsuccessful dialysis attempt at refolding the denatured AIDH extracted from inclusion bodies in section 7.6, refolding the denatured AIDH via binding with Ni-NTA and eluting with imidazole

was then explored. Previously stored glycerol stocks were used to streak out a LB agar kanamycin plate from which colonies were used to grow 4 precultures. These precultures were used to grow four 1L cultures of AIDH in AI media supplemented with 50µg/ml kanamycin of which the average OD_{600} was 7.85. 30.6g of cell pellet was obtained following centrifugation which was resuspended in 150ml of lysis buffer made up as detailed in 7.5. After homogenization, the cell suspension was sonicated as outlined in the methods. The lysed cell suspension was centrifuged and the supernatant was removed from the cell pellet. 21.7g of cell pellet was obtained following the lysis, sonication and centrifugation steps. This cell pellet was then resuspended in 110ml of wash buffer until completely homogenized before being centrifuged and supernatant removed and pellet retained. This wash step was repeated a total of 3 times and with an additional fourth wash without any GdnHCl and Triton X-100 for the reasons previously discussed in section 7.5. Washes 3 and 4 was observed to have colourless and clear supernatant which is indicative of removal of most cellular components, lipids and membrane associate components (Figure 7.10).
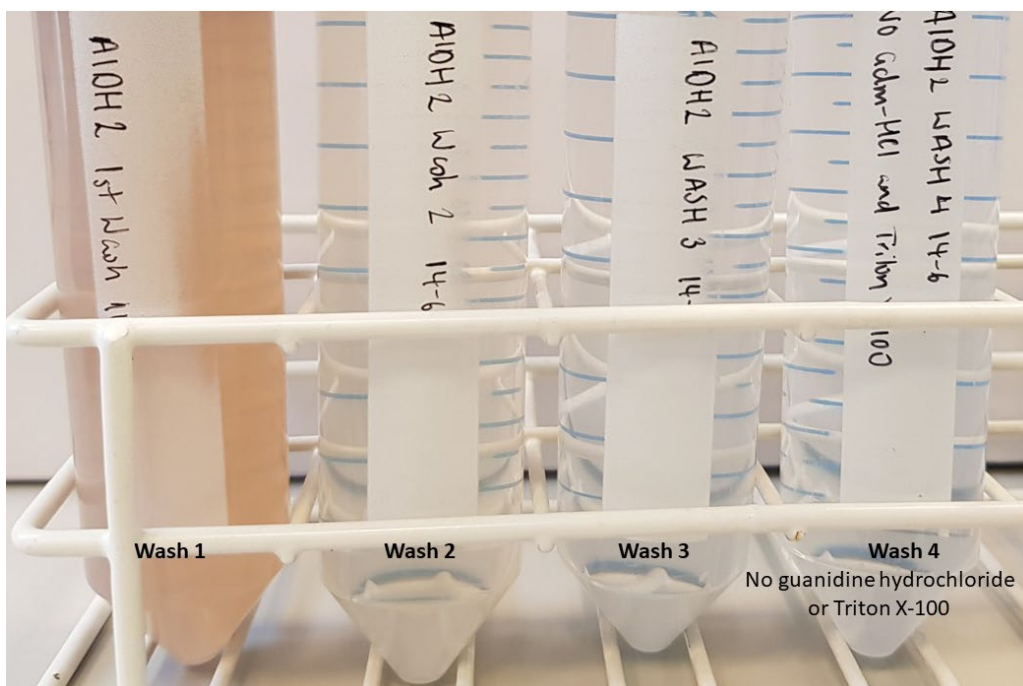
Figure 7.10. Supernatants removed following the homogenization and centrifugation of cell pellets with wash buffer. Washes 1-3 consists of HEPES, EDTA, DTT, glycerol, Triton X-100 and GdnHCl whereas wash 4 is without GdnHCl and Triton X-100.

The cell pellet following homogenization and centrifugation was observed to be getting lighter following each wash, this is what the expectation would be of an efficiently extracted inclusion bodies pellet as they are known to be typically white in appearance. All 4 washes from Figure 7.10 were analysed via SDS-PAGE (Figure 7.11).
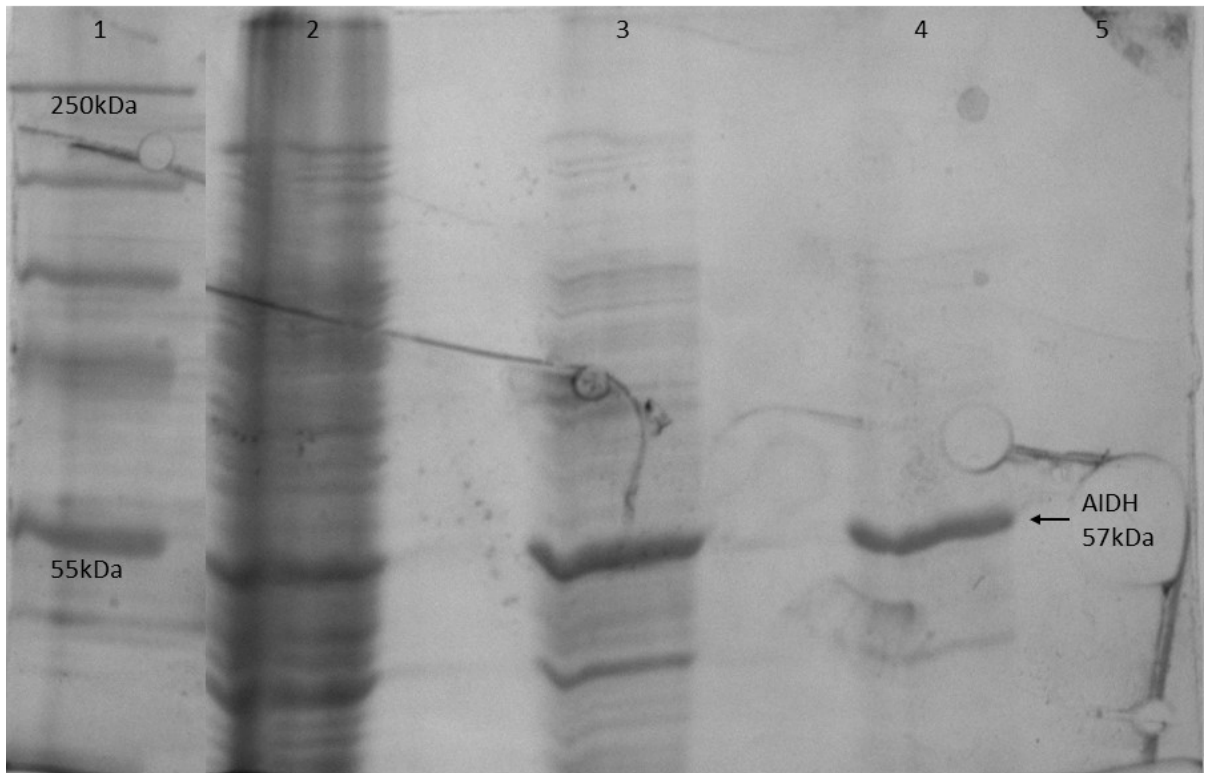
Figure 7.11. SDS-PAGE analysis of supernatants removed following the homogenization and centrifugation of cell pellets with wash buffer. Lane 2, 3 and 4 consists of wash buffer with HEPES, EDTA, DTT, glycerol, Triton X-100 and GdnHCl whereas lane 5 consists of wash buffer HEPES, EDTA, DTT and glycerol only.

Lanes 2, 3 and 4 consist of wash buffer containing HEPES, EDTA, DTT, glycerol, Triton X-100 and GdnHCl where the latter is added at a concentration of 2M. The presence of GdnHCl explains the band corresponding to AIDH seen at the 57kDa position. The experimental strategy behind these washes was to remove other soluble proteins, however with these washes, the protein of interest in the inclusion bodies may also be partially extracted and being removed in the washes, as demonstrated by the presence of the AIDH bands present on the SDS-PAGE (Figure 7.11). Lane 5 in Figure 7.11 is the last wash buffer without any GdnHCl, thereby explaining why there is no band on the SDS-PAGE as there is no GdnHCl in the wash to extract any AIDH. A 5.7g AIDH inclusion bodies pellet was extracted following the washes which displayed the typical whiteish appearance associated with inclusion bodies (Figure 7.12).

Figure 7.12. AIDH inclusion bodies pellet extracted following 4x homogenization and centrifugation with wash buffer consisting of HEPES, EDTA, DTT, glycerol, Triton X-100 and GdnHCl where wash 4 is without GdnHCl and Triton X-100.

Following the successful isolation of AIDH exclusion bodies, the pellet was stored at -80°C for prior to the next stage in the protocol, which is homogenizing the exclusion bodies pellet in extraction buffer and incubating to allow AIDH to be in the denatured state. As outlined in section 7.6, previously dialysis was attempted to remove the extraction buffer components following incubation and dialyse the suspension into 100mM HEPES pH 7.5, 200mM $MgCl_2$, 10% glycerol buffer. This was not successful and the protein aggregates could be seen inside the dialysis tubing (Figure 7.9). For this reasoning in this attempt, following the homogenization of AIDH inclusion bodies in extraction buffer, the decision was made to bind the AIDH in its denatured state to Ni-NTA and elute off bound protein with imidazole via affinity chromatography during as discussed in section 7.5. As also previously outlined in section 7.5, changes were made to the composition of the extraction buffer because if the cell suspension is to be refolded straight on the affinity column, it is recommended that DTT is omitted from the extraction buffer and substituted with 2mM β-mercaptoethanol as DTT is a strong reducing agent and will reduce the nickel ions in the Ni-NTA resin. In addition, strong chelating agent such as EDTA is also not recommended as it will strip the nickel ions from the column, significantly reducing the binding efficiency of the His tagged protein. The EDTA was an oversight on this attempt, whereby the DTT was replaced with β-mercaptoethanol but the EDTA was added in error which therefore led to the stripping of nickel from the column in the eventual attempt to purify the AIDH. The composition of the extraction buffer in this attempt was as follows:

- 100mM HEPES pH 7.5
- 5mM EDTA
- 6M GdnHCl
- 2mM β-mercaptoethanol

146

The inclusion bodies pellet isolated from the washes (Figure 7.12) was resuspended into 30ml of extraction buffer as it to be added as 1ml per gram wet weight of the original cells (original cell pellet weight 30.6g). The 30ml of homogenized extraction buffer was incubated with 5ml of Ni-NTA overnight at room temperature to allow for the binding of AIDH in its denatured state to the Ni-NTA. Upon addition of the cell suspension to polypropylene columns to collect flow through, the solution was viscous which is when the error of the addition of EDTA to the extraction buffer was realised. Regardless, Ni-NTA affinity chromatography was proceeded with followed by 3x 50ml washes with 100mM HEPES pH 7.5, 50mM $MgCl_2$, 10% glycerol buffer to remove any residual GdnHCl, EDTA and β-mercaptoethanol. During the buffer washes, white residues were noticed inside the polypropylene column and in the collection tubes which was presumed to be protein aggregates. The aggregation levels were reduced as the number of buffer washes increased, presumably due to the majority of aggregates being removed in the first washes. A high yield of AIDH was not expected due to chelation of Nickel resulting in insufficient binding, leading to very little protein recovery. Recovery of any soluble AIDH bound to Ni-NTA was attempted to be eluted from the column using 2x 500mM imidazole 100mM HEPES pH 7.5, 50mM $MgCl_2$, 10% glycerol elutions (Figure 7.13).
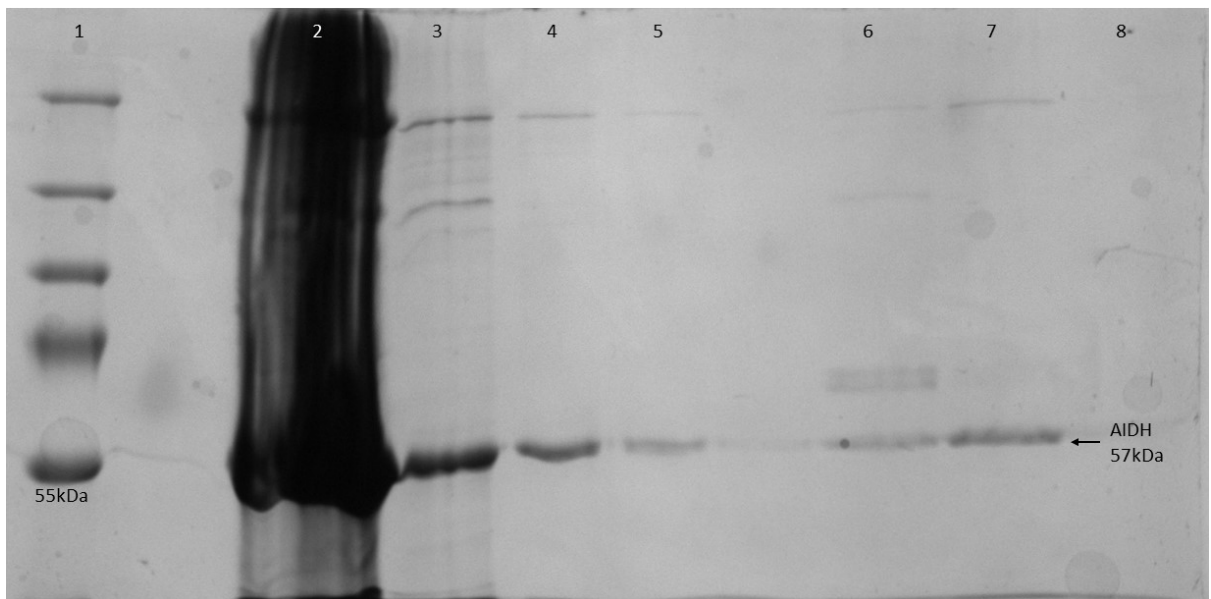
Figure 7.13. SDS-PAGE analysis of Ni-NTA purification attempt of AIDH inclusion bodies following extraction with GdnHCl. Samples in all lanes are from elutions obtained from the column following Ni-NTA affinity chromatography. Lane 2 contains flow through of extraction buffer. Lanes 3, 4 and 5 contain samples from HEPES buffer washes (100mM HEPES pH 7.5, 10% glycerol, 50mM $MgCl_2$). Lanes 6 and 7 contain HEPES buffer imidazole elutions with 500mM imidazole and lane 8 contains HEPES buffer imidazole elution with 1M imidazole.

From the analysis of the SDS-PAGE gel, it was theorised that AIDH inclusion bodies purification had failed in this attempt due to insufficient binding with Ni-NTA, caused by the chelation of nickel by EDTA erroneously present in the extraction buffer. Since inclusion bodies contain very little host protein, the concentration of the protein of interest, in this case AIDH, is presumably very high. The extraction

147

buffer provides denaturation conditions under which the unfolded protein is suspended, the addition of Ni-NTA to the suspension allows for the binding of AIDH in its unfolded state to the nickel via the His$_{10}$ tag. In this case, EDTA added in error to the extraction buffer chelated the nickel rendering the binding of the AIDH to the Ni-NTA insufficient. Thus, the removal of the extraction buffer and its denaturing components gradually promotes refolding of the protein in solution, the addition of the 100mM HEPES pH 7.5, 10% glycerol, 50mM MgCl$_2$ buffer further promotes refolding of the protein. With the nickel chelated via the EDTA, there is insufficient binding of the AIDH to the Ni-NTA hence protein-protein self-interactions could have caused the aggregates observed during the wash buffers. This is in part tested by centrifuging the buffer wash (100mM HEPES pH 7.5, 10% glycerol, 50mM MgCl$_2$) fractions obtained from the Ni-NTA purification attempt (Figure 7.13, Lanes 3-5) and centrifuging out the presumed AIDH protein aggregates and supernatant which should not contain any soluble protein. The 3 washes obtained from the column were centrifuged out at 13,000rpm for 5 minutes, with the pellet being resuspended in water and loaded onto SDS-PAGE for analysis along with the supernatant from each corresponding wash.
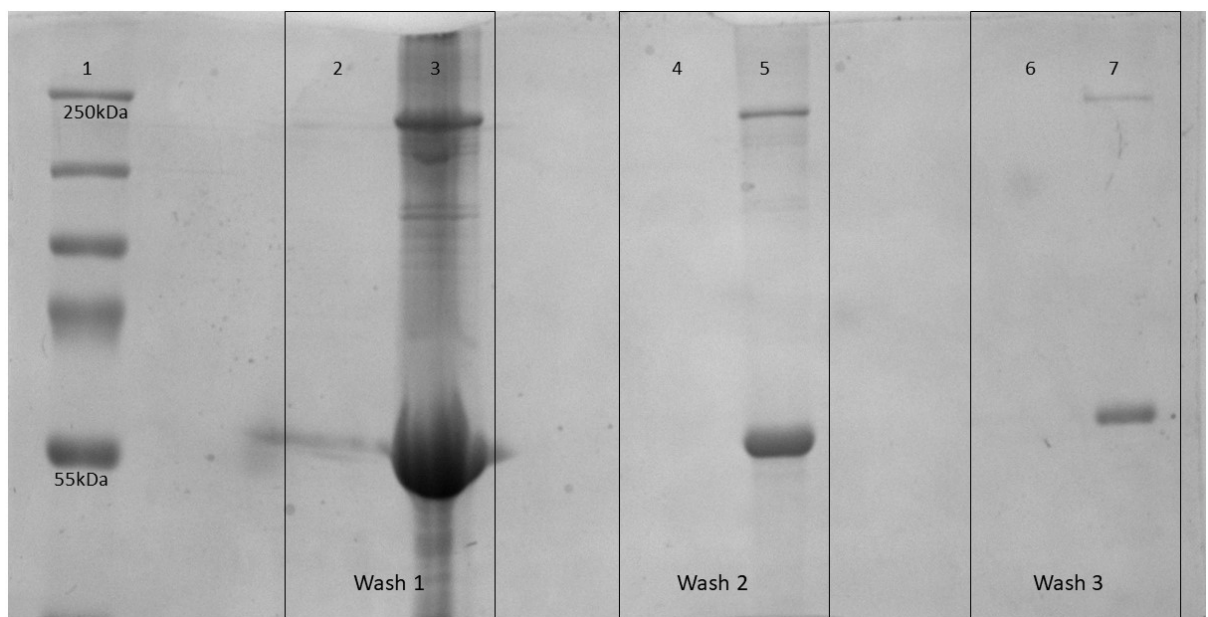
Figure 7.14. SDS-PAGE analysis of supernatants and pellets obtained from the centrifugation of 3 HEPES buffer washes (100mM HEPES pH 7.5, 10% glycerol, 50mM MgCl$_2$) collected during the Ni-NTA purification attempt of AIDH inclusion bodies. Lane 2, 4 and 6 contains the supernatants from the 3 washes and Lane 3, 5 and 7 contain the pellets from the 3 washes.

2 of the most intense bands seen all the pellet samples in lanes 3, 5 and 7 correlate with the size of the AIDH monomer (57kDa) and the AIDH tetramer (228kDa). The volume of sample loaded for each sample is the same (15µl), the difference observed in the intensity of the bands was noted to be due to the concentration of aggregated protein in each wash. Presumably majority of the aggregates were removed during the initial buffer wash. Very little soluble AIDH was present in the supernatant

obtained following the centrifugation of all the pellets indicating that majority of the protein present had aggregated.

Following this, all the buffer washes from the Ni-NTA purification containing the protein aggregates (150ml total) were pooled and centrifuged at 32,000rpm for 1 hour. Following this, the supernatant was discarded and the pellet of AIDH aggregated protein retained (0.64g). This pellet was resuspended and homogenized into 5ml of extraction buffer overnight at 4°C. An attempt was made to dialyse this suspension, therefore DTT was used in the extraction buffer instead of β-mercaptoethanol. Previously dialysis buffer has comprised of 100mM HEPES pH 7.5, 10% glycerol, 50mM MgCl$_2$, however to aid the gradual removal of GdnHCl to avoid protein precipitation, MgCl$_2$ was left out of the buffer. 1M of GdnHCl was also added to the dialysis buffer to aid the gradual removal as well. The dialysis buffer volume was of 300ml with the final composition of 100mM HEPES pH 7.5, 1M GdnHCl and 10% glycerol. Dialysis was then performed for 3 hours at room temperature, however the altered dialysis conditions did not work successfully as white aggregates could be seen in the dialysis tubing (Figure 7.15). The precipitated suspension was centrifuged and the pellet retained. This attempt was terminated at this point and changes were reviewed before attempting extraction and purification of AIDH inclusion bodies again.
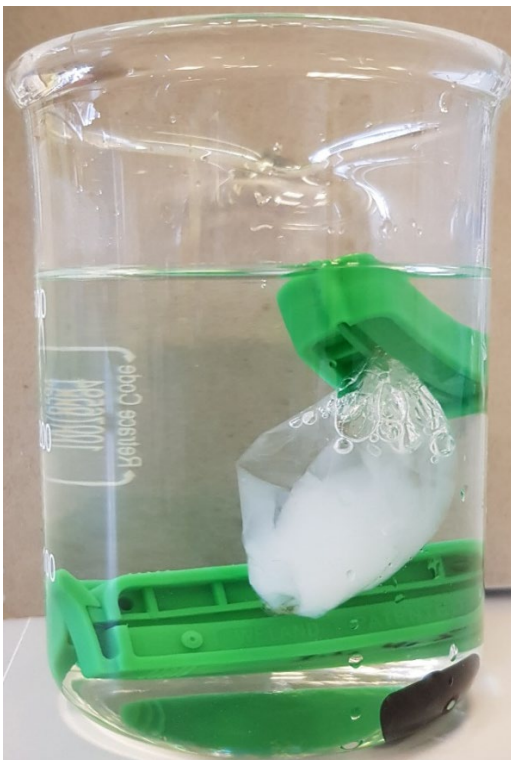
Figure 7.15. Dialysis of 5ml aggregated AIDH homogenized in extraction buffer consisting of HEPES, EDTA, GdnHCl and DTT, dialysed against 300ml of 100mM HEPES pH 7.5, 1M GdnHCl, 10% glycerol buffer at dilution factor of 60. Dialysis attempt was not successful and protein aggregates can be seen in the dialysis tubing.

7.8 Attempt 3 at extraction and purification of soluble AIDH from AIDH inclusion bodies using Ni-NTA via changes in buffer components

The attempt made in section 7.6 had some clear issues which needed to be addressed in order to effectively purify AIDH extracted from inclusion bodies. For this attempt, the following changes were considered to the AIDH exclusion bodies protocol as outlined in section 7.5. During the buffer wash step, as many washes as required were done until the supernatant was no longer cloudy, with the wash buffer composition being as follows:

- 100mM HEPES pH 7.5
- 5mM EDTA
- 5mM DTT
- 10% Glycerol
- 2% Triton X-100
- 2M GdnHCl

The final wash buffer is usually made up without the addition of Triton X-100 and GdnHCl, however for this attempt, EDTA was also excluded from the final wash buffer. This was to ensure that no residual EDTA remained in the pellet to interfere with binding of protein to Ni-NTA downstream. The volume of Ni-NTA was also increased in this attempt to allow for sufficient binding. 100mM HEPES pH 7.5, 10% glycerol, 50mM $MgCl_2$, 500mM imidazole elutions were employed to elute any AIDH bound to Ni-NTA in the attempt outlined in section 7.7 (Figure 7.14). The concentration of $MgCl_2$ included in the elutions in this attempt was also increased to 200mM from 50mM to aid refolding and stability of AIDH.

26g of AIDH cell pellet was obtained following expression of AIDH in 4L of AI media. The cell pellet was resuspended in 130ml of lysis buffer made up as detailed in 7.5. After homogenization, the cell suspension was sonicated as outlined in the methods. The lysed cell suspension was centrifuged and the supernatant was removed from the cell pellet. 20g of cell pellet was obtained following the lysis, sonication and centrifugation steps. This cell pellet was then resuspended in 100ml of wash buffer until completely homogenized before being centrifuged and supernatant removed and pellet retained. This wash step was repeated a total of 3 times with 2 additional washes without any GdnHCl, Triton X-100 and EDTA for the reasons previously discussed in section 7.5 and exclusion of EDTA per reasoning discussed above. Washes 4 and 5 were observed to have colourless and clear supernatant which is indicative of removal of most cellular components, lipids and membrane associate components. A white pellet indicative of successful exclusion bodies isolation was obtained at the end of the wash stages. This pellet was then homogenized into extraction buffer which was added as 1 ml per wet pellet weight of original cells (26g). 30ml of extraction buffer was used with the changes made as discussed at the start of this section.

The components of the original extraction buffer as outlined in section 7.5 are as follows:

- 100mM HEPES pH 7.5
- 5mM EDTA
- 6M GdnHCl
- 5mM DTT

The changes made during this attempt were the exclusion of EDTA to avoid chelation of the nickel during binding with Ni-NTA and the replacement of DTT with β-mercaptoethanol for the reasoning outlined in section 7.5. The inclusion bodies pellet following the wash steps was homogenized with 30ml of the amended extraction buffer and bound with 10ml of Ni-NTA overnight at room temperature. Following this, the suspension was transferred into a polypropylene column and flow through was collected. The Ni-NTA resin was then washed through with 200ml of 100mM HEPES pH 7.5, 10% glycerol, 50mM $MgCl_2$ buffer before eluting off any bound AIDH with 2x 100mM HEPES pH 7.5, 10% glycerol, 200mM $MgCl_2$, 500mM imidazole elutions. As discussed previously during the purification strategies of GDH and DHAD in chapters 4 and 5 respectively, EDTA has been successfully used to improve dialysis efficiency of soluble proteins as protein precipitation was significantly reduced via addition of 100mM final concentration of EDTA to collection tubes during protein elutions when performing Ni-NTA affinity chromatography. The concept behind this strategy was that leached nickel from the column enhances protein-protein self-interactions which were then contributing to protein precipitation during dialysis. For this reasoning, 100mM final concentration of EDTA was added to the collection tubes for the HEPES buffer imidazole elutions. All elutions obtained from the Ni-NTA affinity chromatography were analysed via SDS-PAGE (Figure 7.16).
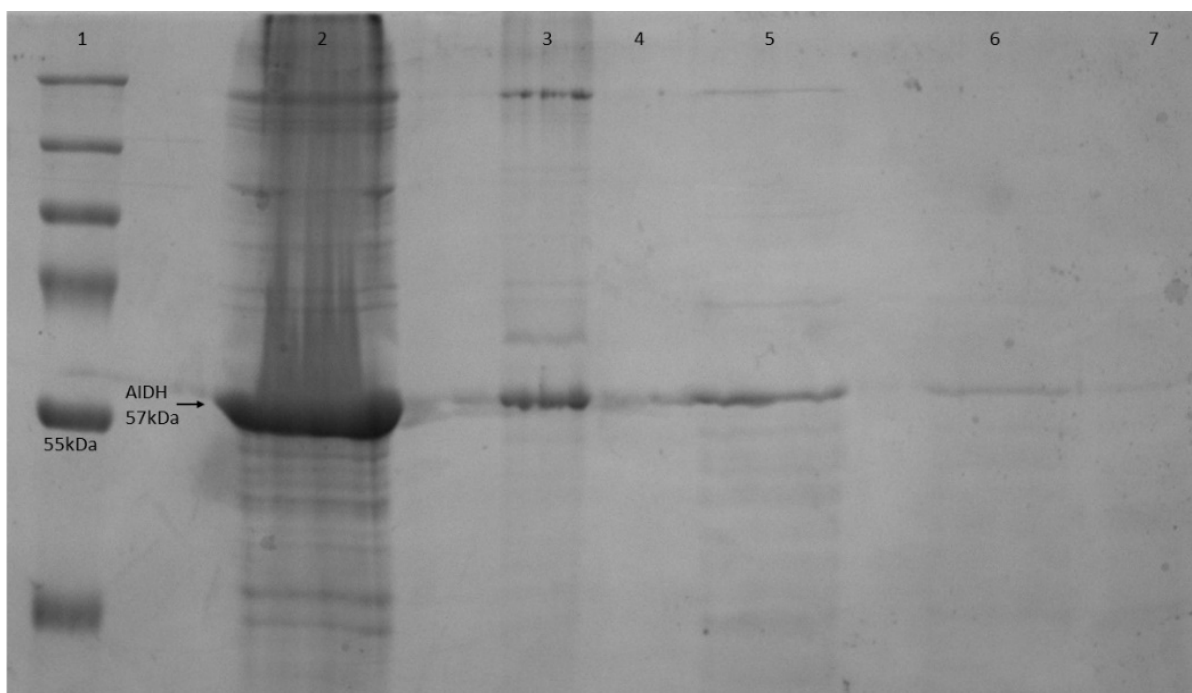
Figure 7.16. SDS-PAGE analysis of Ni-NTA purification attempt of AIDH inclusion bodies following extraction with GdnHCl. Samples in all lanes are from elutions obtained from the column following Ni-NTA affinity chromatography. Lane 2 contains flow through of extraction buffer. Lanes 3 and 4 contain samples from HEPES buffer washes (100mM HEPES pH 7.5, 10% glycerol, 50mM $MgCl_2$). Lanes 5 and 6 contain HEPES buffer (100mM HEPES pH 7.5, 10% glycerol, 200mM $MgCl_2$) imidazole elutions with 500mM imidazole and lane 7 with 1M imidazole respectively.

From Figure 7.16 lane 2, which contains the flow through of the extraction buffer suspension bound with Ni-NTA, it is evident that a lot of the AIDH has been lost in the flow through. This sample was 30ml in volume and this flow through was attempted to be dialysed into 100mM HEPES pH 7.5, 10% glycerol, 50mM $MgCl_2$ buffer to try and salvage the unbound AIDH, however protein sample was seen to be aggregating soon in the dialysis tubing. Lanes 5 and 6 from Figure 7.16 containing the 100mM HEPES pH 7.5, 10% glycerol, 200mM $MgCl_2$, 500mM imidazole elutions show bands corresponding to AIDH, albeit the bands are not high intensity indicating low protein recovery, the elutions were pooled and dialysed to remove the imidazole and EDTA added during collection of elutions.

3 cycles of dialysis were performed:

3- 30ml elution dialysed in 1L of 100mM HEPES pH 7.5, 10% glycerol, 100mM $MgCl_2$ buffer at a dilution factor of 33.

4- 30ml elution dialysed in 1L of 100mM HEPES pH 7.5, 10% glycerol, 100mM $MgCl_2$ buffer at a dilution factor of 33.

5- 30ml elution dialysed in 1L of 100mM HEPES pH 7.5, 10% glycerol, 50mM $MgCl_2$ buffer at a dilution factor of 33.

All 3 cycles of dialysis were successful with no signs of protein aggregation seen in the dialysis tubing, the presence of 100mM EDTA in the 30ml elutions containing the eluted AIDH presumably contributed to this as previously demonstrated with GDH and DHAD. The 3 cycles of dialysis sufficiently diluted EDTA and imidazole present in the fraction to negligible concentrations and the $MgCl_2$ concentration was gradually lowered to 50mM as well. Following dialysis, the sample was concentrated down to a final volume of 4ml with a concentration of 1mg/ml as determined via BCA. However, during the final concentration stages, the sample started to display signs of aggregation so protein stability was an issue that required addressing. It could be possible that 50mM of $MgCl_2$ was too low for the protein stability over time and an increased concentration was required for protein stability. The insufficient binding of the AIDH to the Ni-NTA and its subsequent loss through the flow through is also of concern and binding efficiency was explored in the next attempt.

7.9 Attempt 4 at extraction and purification of soluble AIDH from AIDH inclusion bodies using Ni-NTA via changes in buffer components

Following on from the findings of the previous section, the key issue of loss of unbound protein (AIDH) through the flow through of Ni-NTA affinity chromatography was explored. The changes made to the wash buffer and extraction buffer in section 7.8 were maintained in this attempt as well. An additional change was made to the wash buffer; in the previous section, GdnHCl, Triton X-100, and EDTA were excluded from the final 2 washes to ensure no residual EDTA remained to interfere with binding of protein with Ni-NTA. Additionally, in this attempt, DTT was also removed from the final 2 washes as it is a strong reducing agent and will reduce the nickel ions in the Ni-NTA resin. This was done to test if the Ni-NTA efficiency is being reduced by any trace components involved in the wash or extraction buffers. So, the wash buffer for the final 2 washes consisted only of 100mM HEPES pH 7.5 and 10% glycerol. The volume of Ni-NTA used was also doubled from 10ml used in the last attempt to 20ml in this attempt as there was a lot of unbound protein, so here it was tested to see if increased amount of Ni-NTA solves the issue.

26.8g of AIDH cell pellet was obtained following expression of AIDH in 4L of AI media. The cell pellet was resuspended in 130ml of lysis buffer made up as detailed in 7.5. After homogenization, the cell suspension was sonicated as outlined in the methods. The lysed cell suspension was centrifuged and the supernatant was removed from the cell pellet. 19g of cell pellet was obtained following the lysis, sonication and centrifugation steps. This cell pellet was then resuspended in 100ml of wash buffer until completely homogenized before being centrifuged and supernatant removed and pellet retained. This wash step was repeated a total of 3 times with 2 additional washes without any GdnHCl, Triton X-100, EDTA and DTT for the reasons previously discussed in section 7.5, 7.8 and exclusion of DTT as discussed

above. Washes 4 and 5 were observed to have colourless and clear supernatant which is indicative of removal of most cellular components, lipids and membrane associate components. A white pellet indicative of successful exclusion bodies isolation was obtained at the end of the wash stages. This pellet was then homogenized into extraction buffer which was added as 1 ml per wet pellet weight of original cells (26.8g). 30ml of extraction buffer was used with the changes made as discussed at the start of section 7.8 (replacement of DTT with β-mercaptoethanol for the reasoning outlined in 7.5).

The inclusion bodies pellet following the wash steps was homogenized with 30ml of the amended extraction buffer and bound with 20ml of Ni-NTA overnight at room temperature. Following this, the suspension was transferred into 4 polypropylene columns (for ease of handling) and flow through was collected. Each column containing 5ml of Ni-NTA resin was then washed through with 200ml of 100mM HEPES pH 7.5, 10% glycerol, 100mM $MgCl_2$ buffer before eluting off any bound AIDH with 100mM HEPES pH 7.5, 10% glycerol, 100mM $MgCl_2$, 600mM imidazole elutions. Final concentration of 100mM EDTA was added to the collection tubes as discussed in section 7.8 (it has been demonstrated to decrease the instances of protein aggregation in dialysis tubing). All elutions obtained from the Ni-NTA affinity chromatography were analysed via SDS-PAGE (Figure 7.17).
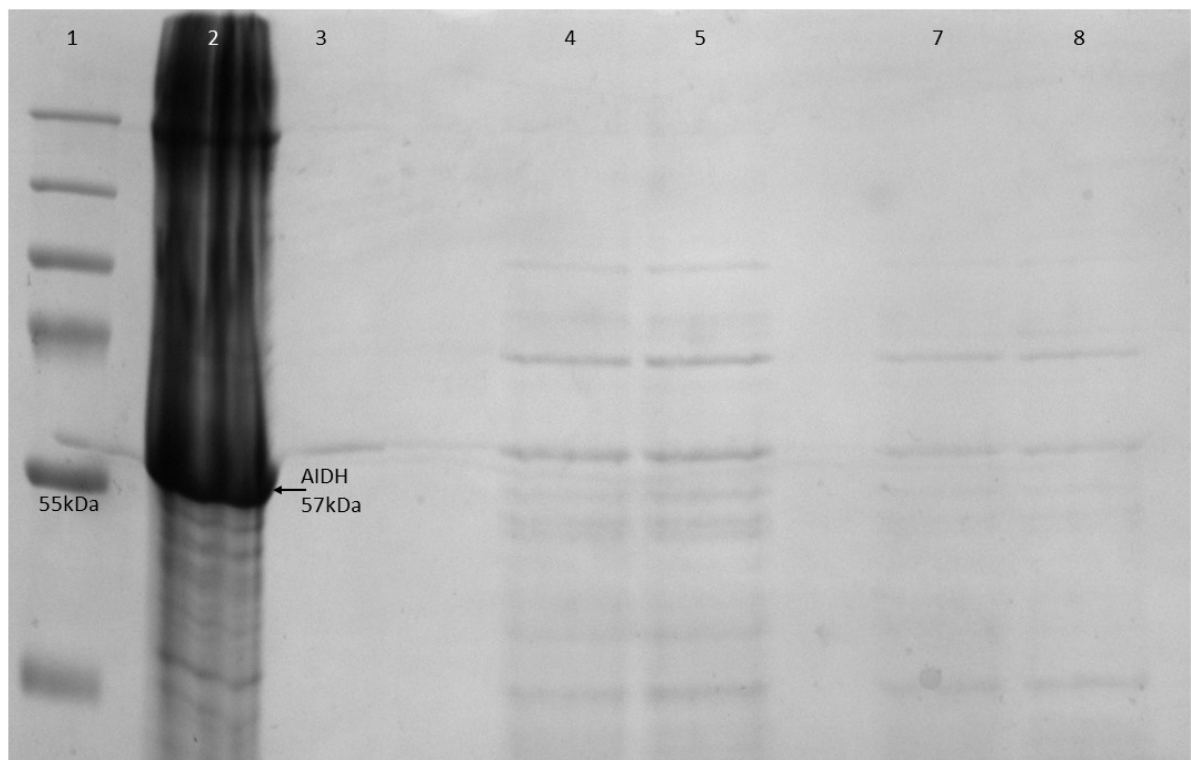
Figure 7.17. SDS-PAGE analysis of Ni-NTA purification attempt of AIDH inclusion bodies following extraction with GdnHCl. Samples in all lanes are from elutions obtained from the column following Ni-NTA affinity chromatography. Lane 2 contains flow through of extraction buffer. Lane 3 contains samples from HEPES buffer wash (100mM HEPES pH 7.5, 10% glycerol, 100mM $MgCl_2$). Lanes 4 and 5 contain HEPES buffer (100mM HEPES pH 7.5, 10% glycerol, 200mM $MgCl_2$) imidazole elutions with 500mM imidazole and lanes 7 and 8 with 1M imidazole respectively.

As seen previously with the attempt in section 7.8 Figure 7.16, Figure 7.17 Lane 2 also contains evidence of unbound AIDH which is subsequently being lost in the flow through. In comparison to Figure 7.16, very little soluble AIDH has been obtained from the imidazole elutions indicating that very little protein has actually bound to the Ni-NTA in the first instance. Due to poor soluble AIDH recovery from the Ni-NTA affinity purification, no fractions were pooled as the amount of protein concentrated would be very small. This attempt had twice the amount of Ni-NTA as the previous attempt hence it was deduced that binding possibly is not the issue, poor expression might be the root cause of the issue leading to poor protein recovery in this instance. The pH of the extraction buffer was checked through the flow through (pH 7.84) as one of the potential causes of insufficient binding of protein to Ni-NTA could be the protonation of histidine which occurs at pH below 6 rendering the His tag non-functional, however as the pH of the extraction buffer was confirmed to be above 6, this was not the cause of the insufficient binding.

The flow through with the unbound AIDH was then thought to be diluted before attempting dialysis again as the fast dilution of the extraction buffer components was thought to be the main factor contributing towards the failure of dialysis. 30ml of flow through with unbound AIDH was obtained from the Ni-NTA affinity chromatography in extraction buffer (100mM HEPES pH 7.5, 6M GdnHCl, 2mM β-mercaptoethanol). This 30ml was diluted into 100mM HEPES pH 7.5, 10% glycerol, 35mM EDTA and 50mM $MgCl_2$ (EDTA added to chelate any leached nickel during Ni-NTA affinity chromatography and $MgCl_2$ added to stabilise and promote refolding during dialysis). During the dilution of the 30ml of flow through into 100ml, the suspension was noticed to immediately turn white, indicating protein precipitation. This lead to the conclusion that the protein is stable when unfolded under denaturing conditions and removal or dilution of denaturing environment and introduction of refolding conditions do not cooperate well, resulting in the protein precipitating. The 100ml suspension was centrifuged the AIDH aggregated protein pellet was retained and pooled together with the aggregated protein pellet from section 7.7.

7.10 Change of denaturant from GdnHCl to urea

The aggregated protein pellets from previous attempts (7.7 and 7.9) were pooled and the denaturant was changed from GdnHCl to urea. No success had been achieved with dialysis of extraction buffer containing GdnHCl in the past attempts so the denaturant was changed to urea and glycerol was also added to the extraction buffer to aid protein stability. The extraction buffer used to resolubilise the precipitated AIDH pellet was as follows:

> 100mM HEPES pH 7.5
> 8M Urea
> 2mM β-mercaptoethanol
> 10% Glycerol

40ml of the extraction buffer was prepared and the precipitated AIDH pellets were resuspended into this buffer until completely homogenized overnight at room temperature. Following this, the suspension was centrifuged to remove any insoluble fractions and obtain a clear suspension, and dialysis was attempted again to gradually dialyse out the urea and β-mercaptoethanol. 2 cycles of dialysis were carried out in 300ml buffer volumes at a dilution factor of 7.5 as outlined below:

1- 40ml precipitated AIDH homogenized in extraction buffer dialysed in 300ml of 100mM HEPES pH 7.5, 10% glycerol, 5M urea buffer at a dilution factor of 7.5.

2- 40ml precipitated AIDH homogenized in extraction buffer dialysed in 300ml of 100mM HEPES pH 7.5, 10% glycerol, 2M urea buffer at a dilution factor of 7.5.

The composition of the dialysis buffer was kept the same with the exception of reducing the concentration of urea from 8M to 5M in the first cycle and then to 2M in the second cycle of dialysis. β-mercaptoethanol was also exempted from both cycles of dialysis buffer. The first cycle of dialysis was carried out at room temperature for 3 hours and displayed no signs of aggregation. Following this, when the dialysis tubing was transferred to the second cycle of dialysis buffer with 2M of urea, 30 minutes into the planned 2 hours dialysis cycle, aggregation was seen inside of the dialysis tubing. Dialysis was terminated at this point, the aggregated protein suspension was centrifuged and the pellet retained at -80°C. Changing the denaturant from GdnHCl to urea did not made a significant difference to the success of dialysis as protein aggregates were still being observed during dialysis. The main issue still to be resolved is the binding of the denatured AIDH to the Ni-NTA.

7.11 Western blots to confirm functionality of His$_{10}$ tag

After subsequent attempts of failure to efficiently bind AIDH in the denatured state to Ni-NTA, the binding issue was investigated via a western blot to determine if the His$_{10}$ tag is actually accessible in the first place. 1mg/ml of soluble AIDH was successfully obtained following Ni-NTA affinity chromatography as outline in section 7.8. Sections 7.9 and 7.10 discuss the attempts to resolubilise aggregates of AIDH into GdnHCl and urea respectively. Samples from all 3 conditions were analysed via SDS-PAGE (Figure 7.18) followed by western blot (Figure 7.19) to determine efficiency of His$_{10}$ tag.
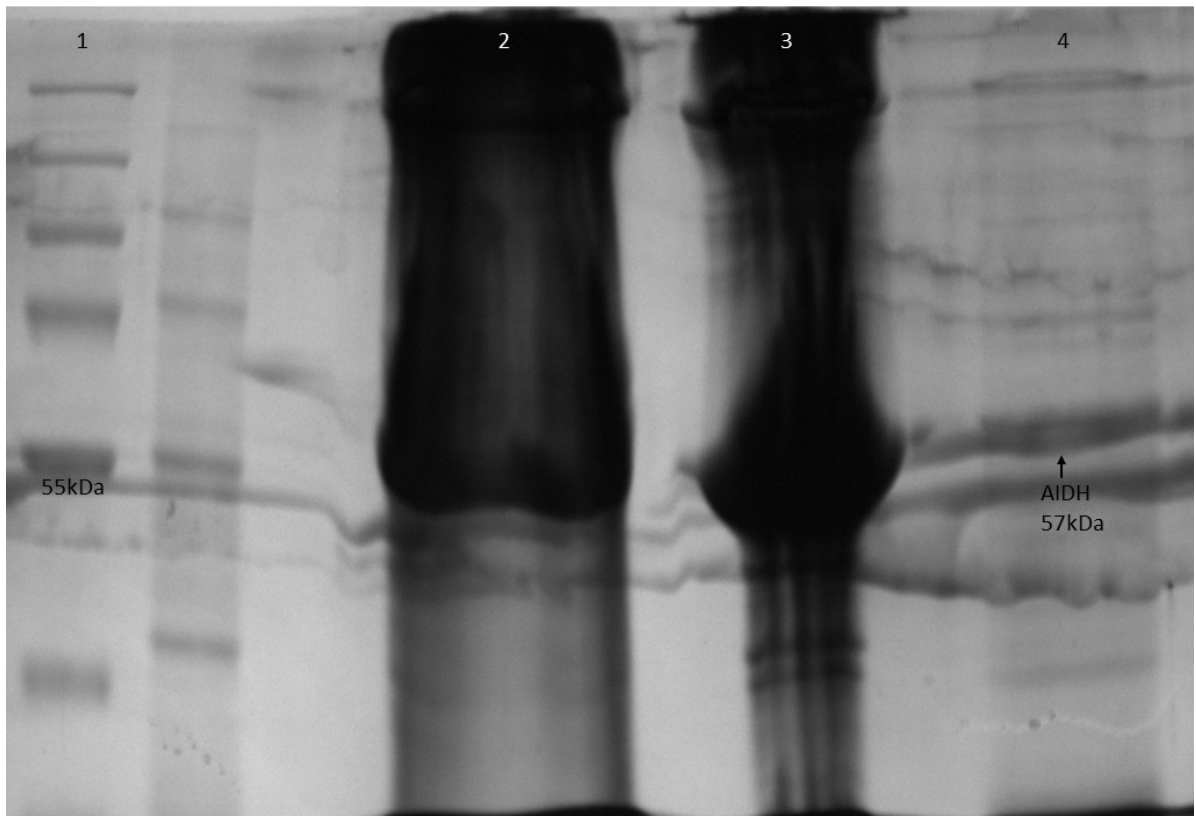
Figure 7.18. SDS-PAGE analysis of AIDH samples obtained from 3 different conditions. Lane 2 contains AIDH aggregates homogenized in GdnHCl, Lane 3 contains AIDH aggregates homogenized in urea and Lane 4 contains soluble AIDH obtained during Ni-NTA affinity chromatography.
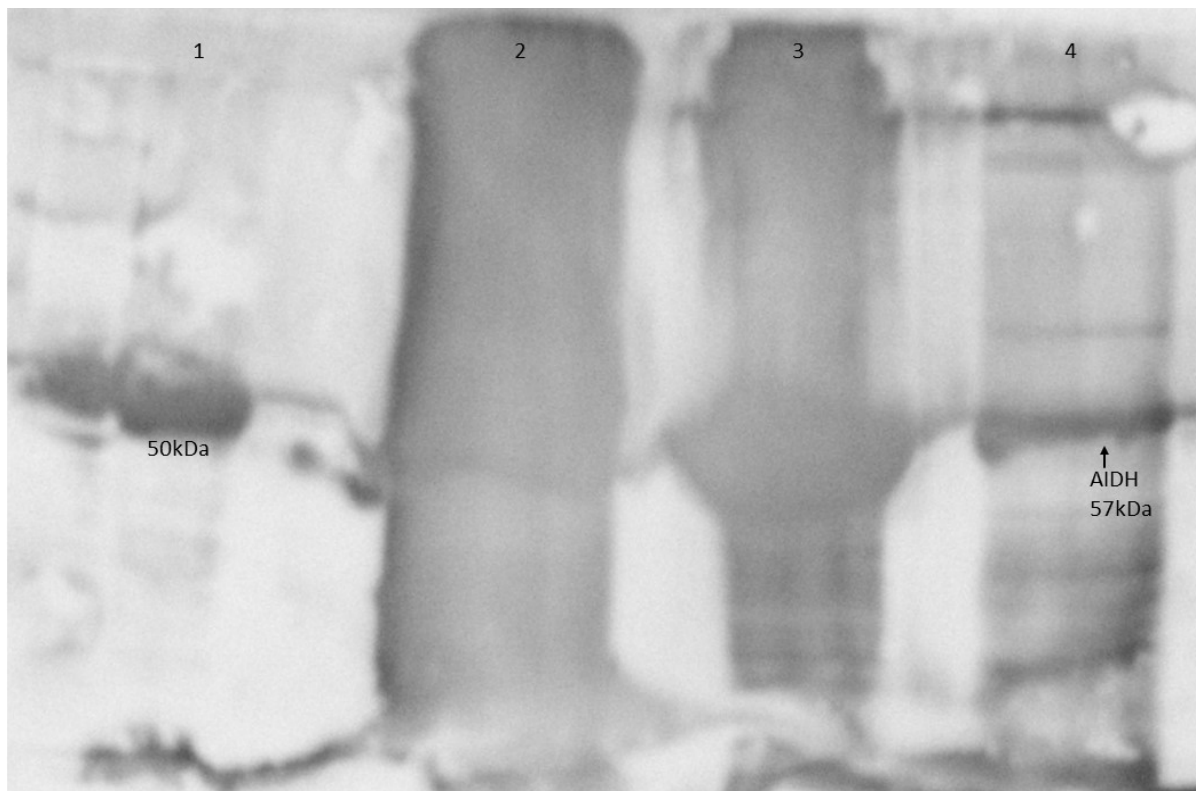
Figure 7.19. Western blot analysis of AIDH samples obtained from 3 different conditions. Lane 2 contains AIDH aggregates homogenized in GdnHCl, Lane 3 contains AIDH aggregates homogenized in urea and Lane 4 contains soluble AIDH obtained during Ni-NTA affinity chromatography.

From the western blot analysis in Figure 7.19, it can be deduced that the His_{10} tag on AIDH is functional as there are clear bands seen in the SDS-PAGE followed by the western blot. The sample of AIDH loaded on both gels (Figure 7.18 and 19, Lanes 2) are from AIDH aggregates homogenized in GdnHCl, it is already known that SDS forms aggregates with GdnHCl so the samples were expected to give a smear as evident from the gels ran (Figure 7.18 and 19). Presence of a distinctive band can be clearly seen in lane 4 of the western blot (Figure 7.19) corresponding to the weight of AIDH (57kDa), and blots are seen at around the 50kDa in both of the samples where ADIH has been resolubilised with denaturants, confirming the presence of AIDH via the His_{10} tag. Having established the functionality of the His_{10} tag, the insufficient binding of the protein to the Ni-NTA could still not be explained and the original protocol was replicated to establish if the modified protocol has retarded the binding process.

7.12 Replicating original attempt of AIDH inclusion bodies extraction and purification

The most successful attempt to date with extraction of inclusion bodies and purification is as outlined in section 7.2.2. In this attempt, it was presumed that inclusion bodies were not extracted efficiently enough as the protocol developed for use in the preparation and extraction of the AIDH inclusion bodies was simplified at the time of attempt. However, this attempt gave the highest yield of AIDH to date and therefore an attempt was made to repeat the exact methodology employed during this attempt to determine if optimizing the extraction and purification protocol of soluble AIDH from AIDH inclusion bodies protocol and outlined and discussed in section 7.5 has reduced efficiency.

Fresh transformation of AIDH vector was carried out into BL21-DE3 cells. Following successful transformation of AIDH vector DNA, protein expression for crude protein fraction preparation was carried out in a 4L final volume of AI media with a final concentration of kanamycin at 50µg/ml. An average OD_{600} of 11.4 was read across the 4 flasks. The cell pellet obtained from the cultures was resuspended, sonicated and heat treated as outlined in the methods sections. All resuspension, sonication, heat treatment and centrifugation steps were carried out in a 100mM HEPES pH 7.5, 10% glycerol buffer unless otherwise stated. As previously discussed in section 7.5, this cell pellet was processed with the main goal of downstream processing of AIDH inclusion bodies, therefore no $MgCl_2$ was added to the buffer used for resuspension, sonication and heat treatment of the cell pellet as presence of salt promotes refolding and the inclusion bodies protocol was to be done under denaturing conditions to unfold and correctly refold the protein. The supernatant obtained from this step was previously used as the soluble fraction which was purified using Ni-NTA affinity chromatography as outlined in section 7.2.1, however since then, the focus has been on the inclusion bodies extraction from the pellet only, and the soluble fraction has not been used to check for presence and purification

of any soluble AIDH expressed as only a low protein yield was obtained previously. This supernatant was retained for analysis.

The cell pellet obtained following the sonication, heat treatment and centrifugation was processed for AIDH inclusion bodies. The cell pellet was resuspended in 50ml of denaturation buffer consisting of 6M GdnHCl, 2mM DTT and 20mM HEPES pH 7.5 as outlined in the materials section and incubated to denature the protein and unfold it completely. The expectation after incubation of the cell pellet with denaturation buffer was to have the AIDH completely unfolded in solution which was followed by centrifugation to get rid of cellular debris. The 50ml suspension with AIDH in the denatured state was incubated with 7.5ml of Ni-NTA and bound overnight at room temperature. This was followed by affinity chromatography which gradually removes the GdnHCl and DTT in the flow through from the column, and the excess HEPES buffer (100mM HEPES pH 7.5, 10% glycerol, 200mM MgCl$_2$) washes remove traces of GdnHCl and DTT from the Ni-NTA resin until their concentrations are negligible. Removing AIDH from GdnHCl solution promotes refolding and the introduction of MgCl$_2$ and glycerol in the buffer further encourages protein refolding and stability. This was followed by imidazole elutions to elute any bound protein from the Ni-NTA. 3 different imidazole concentrations were used to elute any bound protein (Figure 7.20).
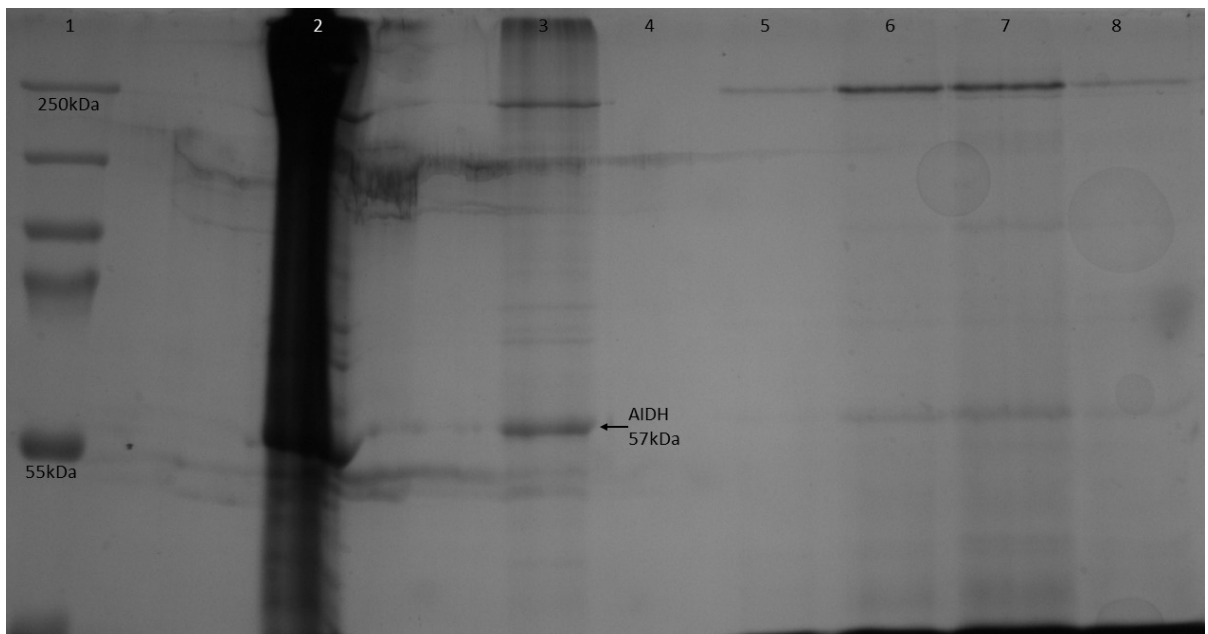
Figure 7.20. SDS-PAGE analysis of Ni-NTA purification attempt of AIDH inclusion bodies following extraction with GdnHCl. Samples in all lanes are from elutions obtained from the column following Ni-NTA affinity chromatography. Lane 2 contains flow through of denaturation buffer. Lanes 3 and 4 contain samples from HEPES buffer washes (100mM HEPES pH 7.5, 10% glycerol, 200mM MgCl$_2$). Lanes 5, 6, 7 and 8 contain HEPES buffer imidazole elutions with 100, 500, 500 and 1000mM imidazole respectively.

The precipitation of the flow through as seen in Lane 2 is expected as it is of the flow through which contains the denaturation buffer consisting of 6M of GdnHCl. A band is still visible at 57kDa indicating

presence of AIDH. In comparison to the attempt outlined in section 7.2.2, little protein has been recovered following binding of AIDH in the denatured state to Ni-NTA and eluting with imidazole (Figure 7.20, Lanes 6 and 7). The supernatant retained following the resuspension, sonication, heat treatment and centrifugation of the cell pellet obtained from AIDH cultures was treated as the soluble fraction. Any soluble AIDH expressed during the expression of AIDH in AI media should be present in this fraction. In the attempt made in section 7.2.1 to purify the soluble fraction of AIDH, some soluble AIDH expressed was purified and SDS-PAGE analysis of the soluble fraction obtained during this attempt was used to estimate the efficiency of expression (Figure 7.21).
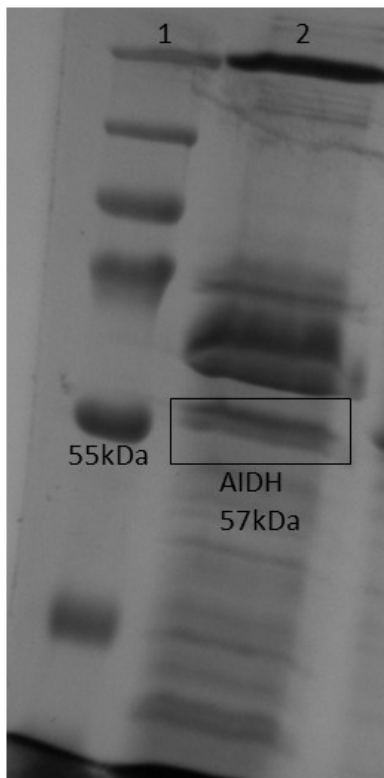
Figure 7.21. SDS-PAGE analysis of soluble fraction of AIDH in 100mM HEPES pH 7.5, 10% glycerol buffer obtained following the resuspension, sonication, heat treatment and centrifugation of the cell pellet obtained from AIDH cultures (Lane 2).

The SDS-PAGE analysis of the soluble fraction of AIDH gives an indication that the expression of AIDH may not have been efficient enough leading to poor protein yield overall. There is very little protein in the soluble fraction in comparison to that seen in Figure 7.2. Considering this, the next step was to explore whether or not the protein expression of AIDH itself is optimal in the first place. The attempts so far have been focused on the binding of AIDH in its denatured state to Ni-NTA. Changes to the protocol were explored to test binding, however increasing the volume of Ni-NTA, changes to wash and extraction buffer components, change of denaturing agent from GdnHCl to urea and optimizing dialysis conditions did not alter the outcome of the inclusion bodies extraction and purification protocol. For these reasons, the expression methodology was explored and the details were examined

to determine if any small variations in protocol could have contributed to the successful attempt of AIDH purification as outlined in section 7.2.2.1 and the failure of all attempts since.

7.13 Examining AIDH expression protocol to determine any contribution to successful protein yield

Upon detailed examination of the methodology used to purify the soluble AIDH and extract and purify the AIDH from inclusion bodies, one difference was identified. The precultures used to inoculate the large scale media for expression and growth of AIDH were grown overnight before diluting the starter cultures to OD_{600} of 0.6 in larger volumes of fresh media. All large scale culture preparation done since the first attempt by utilising modified protocol for extraction and purification protocol of soluble AIDH from AIDH inclusion bodies as outlined in section 7.6, were done with precultures grown for 4 hours and added to the larger volume of media in mid-log phase. Therefore, the question arose of whether inducing expression with cells that are not fully saturated in growth possibly could be limiting the growth of large scale media and the quantity of protein expressed both as soluble AIDH and AIDH in inclusion bodies. The strategy going forward was to explore whether the actual protein expression was an issue and whether growth of precultures to full saturation before inoculation of large scale cultures was the key to obtaining a good yield of both soluble AIDH and AIDH inclusion bodies.

For this attempt, AIDH precultures over grown overnight to lag phase before being diluted down to OD_{600} 0.6 in the 1L large scale volumes. The large scale flasks were grown at room temperature overnight in 4L final volume of AI media with a final concentration of kanamycin at 50µg/ml. An average OD_{600} of 12.17 was read across the 4 flasks. The cell pellet (26.92g) obtained from the cultures was resuspended, sonicated and heat treated as outlined in the methods section. All resuspension, sonication, heat treatment and centrifugation steps were carried out in a 100mM HEPES pH 7.5, 10% glycerol buffer unless otherwise stated. No $MgCl_2$ was added to the buffer used for resuspension, sonication and heat treatment of the cell pellet as presence of salt promotes refolding and the inclusion bodies protocol was to be done under denaturing conditions to unfold and correctly refold the protein.

The cell pellet (19.26g) obtained following the sonication, heat treatment and centrifugation was processed for AIDH inclusion bodies. The cell pellet was resuspended in 50ml of denaturation buffer consisting of 6M GdnHCl, 2mM DTT and 20mM HEPES pH 7.5 as outlined in the materials section and incubated to denature the protein and unfold it completely. The expectation after incubation of the cell pellet with denaturation buffer was to have the AIDH completely unfolded in solution which was followed by centrifugation to get rid of cellular debris. The 50ml suspension with AIDH in the denatured state was incubated with 5ml of Ni-NTA and bound overnight at room temperature. This was followed by affinity chromatography which gradually removes the GdnHCl and DTT in the flow through from the

column, and the excess HEPES buffer (100mM HEPES pH 7.5, 10% glycerol, 200mM MgCl$_2$) washes remove traces of GdnHCl and DTT from the Ni-NTA resin until their concentrations are negligible. This step proved problematic as during the buffer washes, heavy aggregate formation was seen in the column and in the washes as well. The suspension was attempted to be transferred to fresh polypropylene columns but the issue persisted and due to the clogging of multiple polypropylene columns, the experiment was abandoned.

Section and attempt	Protocol summary	Outcomes
7.6 Attempt 1	-Modified protocol (as described in section 7.5) -Refolding via dialysis	-Failure of dialysis
7.7 Attempt 2	-Modified protocol -Refolding via binding with Ni-NTA resin -EDTA added in error to extraction buffer causing leaching of nickel ions -Unbound AIDH in flow through	-AIDH recovered from Ni-NTA purification (low yield) -Failure of dialysis
7.8 Attempt 3	-Modified protocol -Refolding via binding with Ni-NTA resin -No EDTA added to extraction buffer -Unbound AIDH in flow through	-AIDH recovered from Ni-NTA purification (low yield) -Failure of dialysis during buffer exchange
7.9 Attempt 4	-Modified protocol -Refolding via binding with Ni-NTA resin -No EDTA added to final wash buffer -Dilution of unbound protein in flow through	-AIDH recovered from Ni-NTA purification (very low yield) -Failure of dilution leading to protein precipitation
7.10 Attempt 5	-Modified protocol, GdnHCl replaced by Urea	-Failure of dialysis

Table 7.1. Summary of inclusion bodies extraction and purification attempts with modified protocol.

This chapter has outlined the multiple issues faced during expression, purification and quantification for the production of AIDH. Initial positive activity of AIDH has been established with one batch only and multiple batches could not be tested due to failure of purification techniques. The activity assay established for testing AIDH activity has not given conclusive results due to uncertainty regarding false positives being obtained from the assay readings. There are outstanding issues of optimizing expression, extraction of inclusion bodies and their successful purification. Despite attempting multiple protocol changes to address issues regarding binding of denatured AIDH to Ni-NTA, this issue has persisted and unable to be solved, coupled with dialysis failures, isolation of soluble AIDH has proven to be a big challenge (Table 7.1). Multistep optimizations are required to be tackled before obtaining an improved outcome.

8. Engineered malate dehydrogenase for improved malate production

The wildtype malate dehydrogenase (MDH) from the thermotolerant *Thermococcus kodakarensis* catalyses the reductive carboxylation of pyruvate to malate accompanied by bicarbonate independent reduction of pyruvate and produces lactate as a by-product. A triple mutant has been identified by Morimoto et al. with altered cofactor preference of the enzyme NADP(H) to NAD(H), furthermore the reaction specificity significantly shifted towards malate production and less lactate by-product than the wildtype (Morimoto et al. 2013). This triple mutant was utilized in the cascade design as the fifth and final enzyme to catalyse the conversion of pyruvate to malate. This chapter discusses the protein expression, purification and characterization of MDH. The key challenges faced in finding suitable assay protocols for optimization and detecting enzyme activity are also reviewed.

8.1 Transformation of MDH vector DNA into BL21-DE3 competent cells

Synthesised pET30a vectors containing the MDH sequence arrived as a concentrated miniprep of ~4µg of DNA from GenScript. The original vector sample was archived and transformation of vector into DH5α competent cells was done followed by a miniprep to obtain 50µl of quantified vector DNA. MDH DNA was transformed into BL21-DE3 cells and single colonies were used to initiate protein expression. LB agar kanamycin plates with the successful transformation of vector DNA into BL21-DE3 were also used to prepare glycerol stocks for storage at -80°C for future applications.
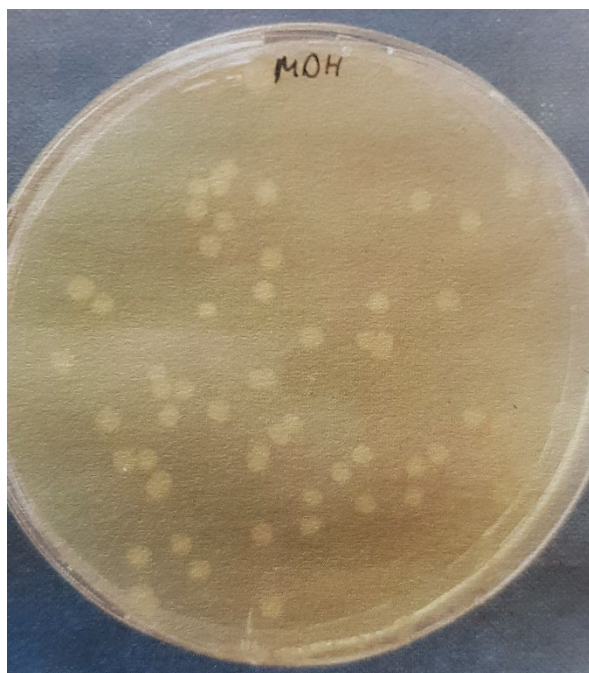
Figure 8.1. Quantified vector DNA obtained following miniprep was transformed into competent BL21-DE3 cells, successful transformation is shown in this figure.

8.2 Small scale MDH protein expression and purification in AI media

Following successful transformation of MDH vector DNA, protein expression and purification was initially carried out in a 2L final volume. Initial MDH expression was carried out in AI media with a final concentration of kanamycin at 50µg/ml. The cell pellets obtained from the cultures were resuspended, sonicated and heat treated as outlined in the methods sections. The crude protein fraction obtained from the prior steps was purified using 5 ml of Ni-NTA resin. All resuspension, sonication, heat treatment and purification steps were carried out in a 100mM HEPES pH 7.5, 200mM $MgCl_2$, 10% glycerol buffer unless otherwise stated.
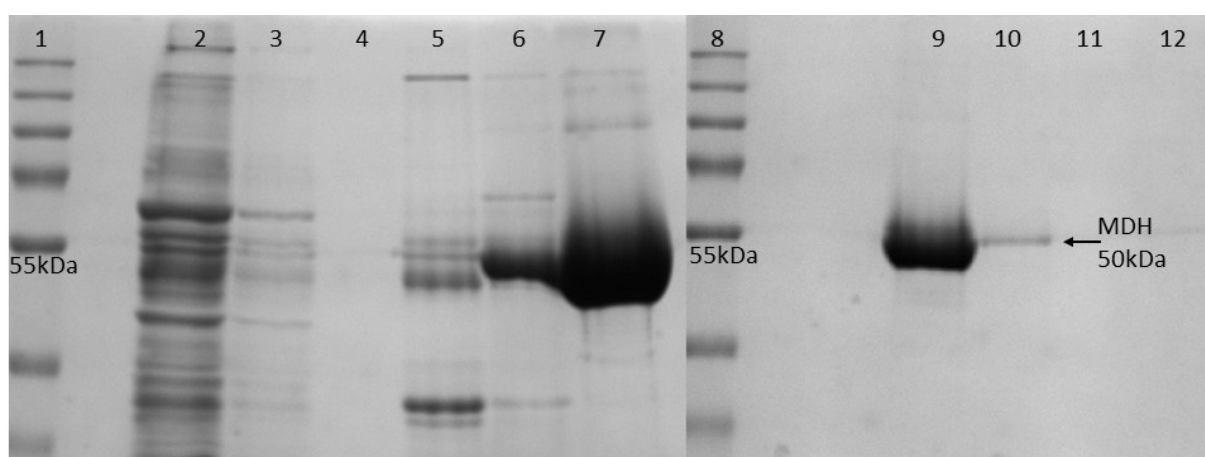
Figure 8.2. SDS-PAGE analysis of MDH expressed in *E. coli* BL21-DE3 and AI media. Lane 2 contains flow through from the column and lanes 3 and 4 contain HEPES buffer washes. Lane 5, 6, and 7 contain HEPES buffer washes with 50, 100 and 200mM imidazole. Lanes 9, 10, 11 and 12 contain HEPES buffer washes with 400, 600, 800 and 1000mM imidazole.

Fractions from lanes 7 and 9 in Figure 8.2 were pooled, imidazole was removed by desalting using a PD-10 desalting column and the final fraction was concentrated. Its protein concentration was determined to be 1.5mg/ml by BCA. Prior to desalting, signs of protein aggregation were seen and the pooled fraction was centrifuged to separate the soluble fraction from the aggregates in an effort to minimise any further aggregation. Large scale expression of MDH was then attempted while addressing this issue.

8.3 Large scale expression of MDH in AI media and purification with the aid of EDTA to minimize aggregation

As previously attempted with proteins earlier in the cascade, EDTA was utilised with MDH large scale expression and purification to reduce protein aggregation. 4L of AI media were inoculated with precultures and a wet weight pellet of 19.72g was obtained. This was processed as per methodology described in chapter 2, and purified using Ni-NTA resin (Figure 8.3).
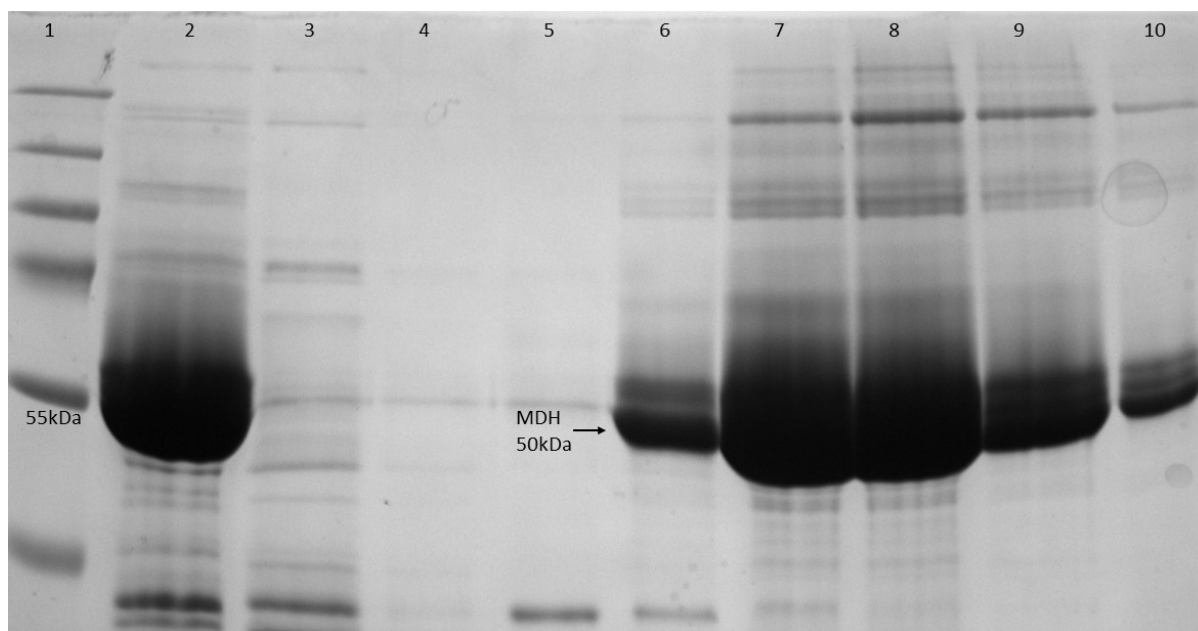
Figure 8.3. SDS-PAGE analysis of MDH expressed in *E. coli* BL21-DE3 and AI media. Lane 2 contains crude protein prior to binding with Ni-NTA. Lane 3 contains flow through from the column and lane 4 contains HEPES buffer wash. Lanes 5, 6, 7, 8, 9 and 10 contain HEPES buffer washes with 50, 100, 200, 400, 600 and 1000mM imidazole respectively.

The 200, 400 and 600mM imidazole elutions were pooled (30ml) with 100mM final concentration of EDTA. Three cycles of dialysis were performed as the pooled fraction size was too large to be processed using PD-10 columns. The repeated dialysis cycles were calculated to have diluted the imidazole and EDTA to a negligible amount (<0.01mM). No aggregation was noticed at any point during the dialysis cycles. On the last cycle of dialysis, the exchange buffer was altered to be 100mM $MgCl_2$ instead of 200mM $MgCl_2$ for final storage of MDH. Following dialysis, the fraction was split and both fractions were concentrated to different volumes and the protein concentration was determined via BCA to be 3.7mg/ml and 8mg/ml.

8.4 Size-exclusion chromatography and protein identification of MDH to determine presence of oligomers

The small scale expression of MDH gave a single band on the SDS-PAGE matching the expected size of the MDH monomer (Figure 8.2, lane 9), however the large scale expression done in Figure 8.3 gave other non-specific bands of which some were suspected to be oligomers. To confirm the presence of oligomers and the positively identify the protein, the 8mg/ml MDH concentrated from section 8.3 was loaded onto the ÄKTA system and as size-exclusion chromatography separates molecules in solution based on their molecular weight, the peaks on a chromatogram are indicative of the different size proteins in the sample. The chromatogram obtained from size-exclusion chromatography of MDH (Figure 8.4) automatically identified 3 peaks and aliquoted them into a collection plate as different fractions.
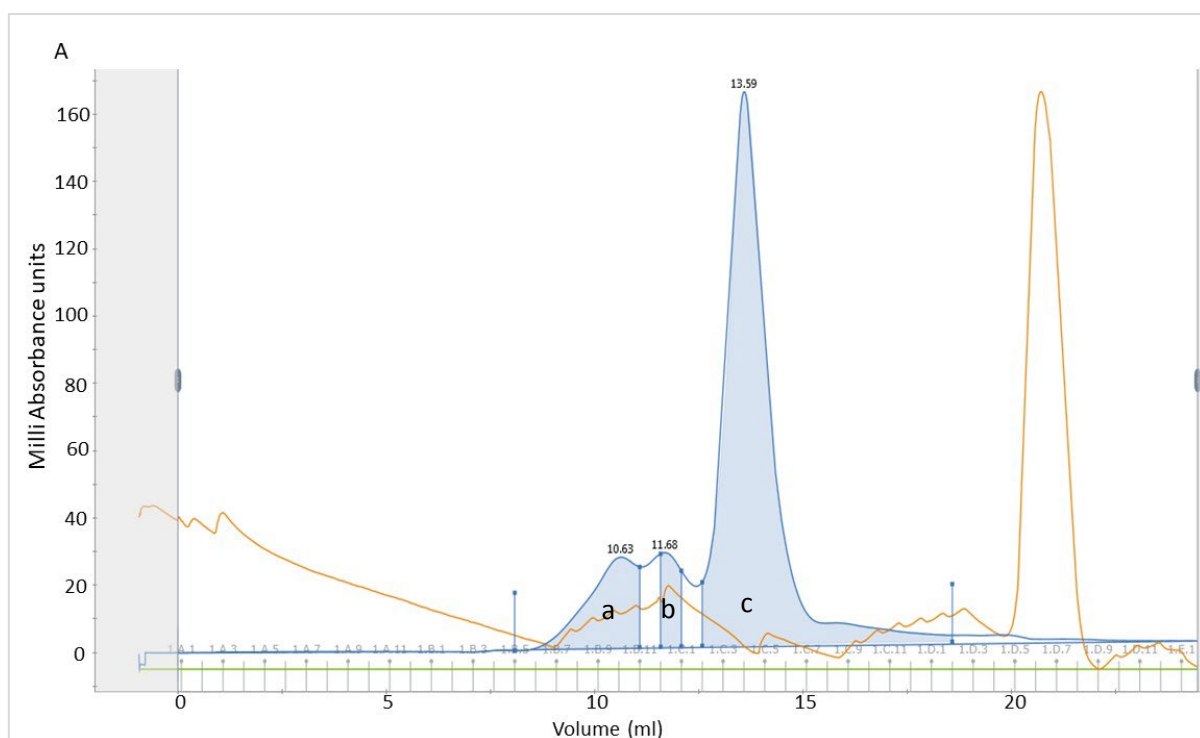
Figure 8.4. Size exclusion chromatography of MDH. Figure 8.4A displays the chromatogram obtained from the software. The blue trace represents the UV absorbance at 280nm and the 3 peaks are indicative of the quantity of protein detected. The brown trace reflects the conductivity monitor which measures conductivity of buffer and samples for online monitoring of the true gradient. The green trace is applied if there is another buffer being used, since this sample was run in one buffer only, the trace has a value of 0. Figure 8.4B lists the retention time of each peak as well as the final volume collected of all fractions.

Multiple samples from each identified peak, a, b and c, were loaded onto a SDS-PAGE gel in order to visualise their composition. The SDS-PAGE analysis of the samples (Figure 8.5) shows the composition is exactly the same in all samples loaded, confirming the presence of oligomers. Despite being identified as different peaks, the only difference among them is the quantity of protein present. A concentrated protein sample has been previously observed to elute off in multiple peaks in size-exclusion chromatography and it would seem that this is the case here. In Figure 8.5, sample in lane 2 is from peak a, sample in lane 3 is from peak b and lastly, sample in lane 4 is from peak c (Figure 8.4a). It is evident from the gel in Figure 8.5 that the same bands are constantly seen in all the samples, differing only in their intensities, which correlates with the different concentrations of protein present in the different fractions. Following the SDS-PAGE, as a further confirmation of oligomers, the MDH bands indicated in Figure 8.5 were excised from the gel and were analysed with mass spectrometry to confirm protein identification.
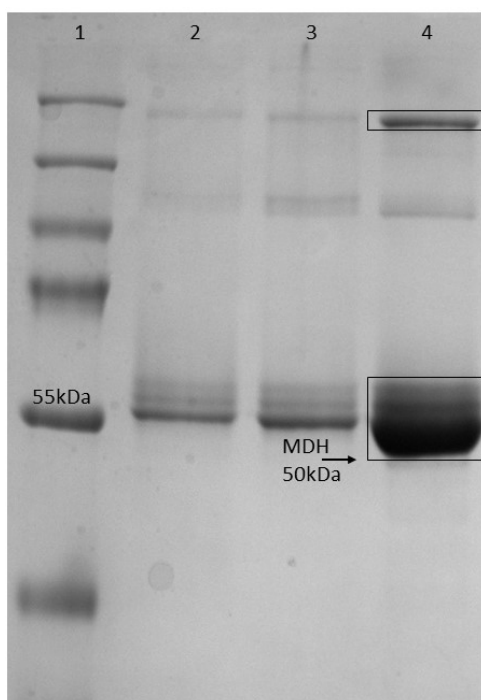
Figure 8.5. SDS-PAGE analysis of MDH following size exclusion chromatography. Lane 2 contains samples from peak A, taken from fraction B9. Lane 3 contains sample from peak B, taken from fraction B12. Lane 4 contains sample from peak C, taken from fraction C5. The bands indicated in the figure were excised for mass spectrometry analysis.

Mass spectrometry analysis of the bands shown in Figure 8.5 positively identified both as being MDH (data in appendix). Using ImageJ scientific image analysis, the confirmed MDH bands were calculated as a percentage of the total protein concentration. Using this method allowed for the actual concentration of MDH to be determined in a sample with other non-specific proteins purified during Ni-NTA purification in future experiments.

8.5 Initial activity analysis of engineered MDH for malate production via IC

Following on from the successful expression purification and positive protein identification of MDH, its activity for conversion of pyruvate to malate was analysed. The reaction conditions for this assay are required to be high in CO_2 and low in O_2. Due to equipment limitations at the time, this was done by equilibrating the container space of a sealed vial with CO_2 before any given activity analysis. All assay conditions were analysed via the IC as well as pyruvate and malate standards (Figure 2.4 and 2.5), and these were used to analyse all activity assays.

After establishing successful standards of pyruvic and malic acid (Figure 2.4 and 2.5), an initial test of MDH activity was done with 30mM pyruvic acid as substrate and using 2 different enzyme concentrations of 0.003mg/ml and 0.024mg/ml MDH. 5mM NADH was added to the reaction as the cofactor. 5% CO_2 was bubbled into each assay condition vials for 5 minutes followed by the addition of pyruvate and incubation of vials at 50°C for 3 hours. After the end of incubation period, assay conditions were analysed via IC. A control condition without any MDH was run alongside assay conditions.

	0.003mg/ml MDH	0.024mg/ml MDH
Malic acid (mM)	2.19	1.40

Table 8.1. IC activity analysis of 2 different MDH concentrations, 0.003 and 0.024mg/ml to monitor malic acid production. Standard deviation for all conditions= <0.045.

Figure 8.6 shows the 2 enzyme concentration assay peaks obtained from the IC.
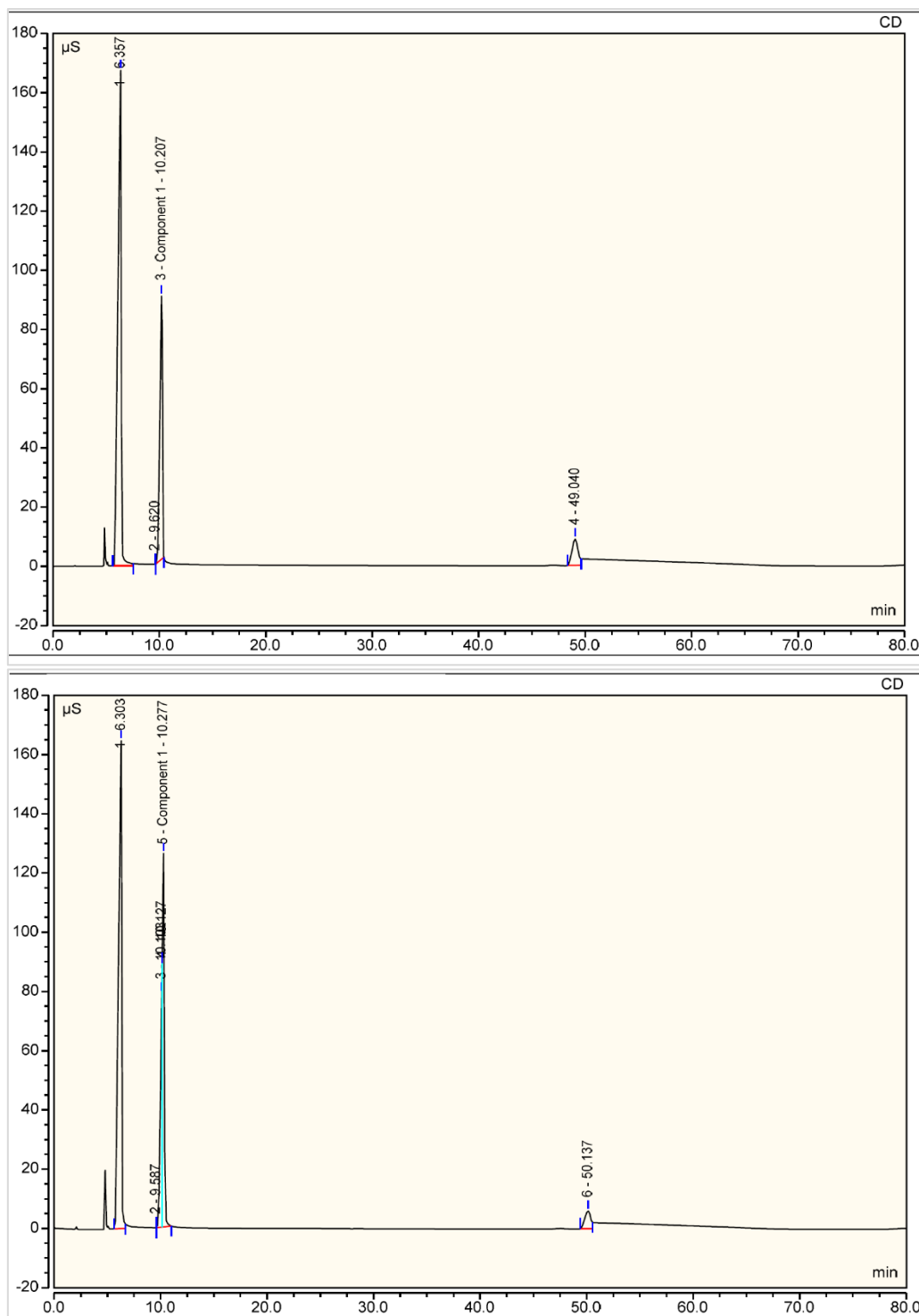
Figure 8.6. IC chromatogram of the peaks obtained from MDH activity assays, top chromatogram is from activity assay with 5mM NADH and 0.003mg/ml MDH and bottom chromatogram is from activity assay with 5mM NADH and 0.024mg/ml MDH. The malic acid peak can be seen at around ~50 minutes.

A control without any MDH was also tested on the IC. From Figure 8.6, there is a significant shift in the baseline from around the 50 minute point, following the malic acid peak. The reaction assay was tested without the MDH as control to rule out the baseline shift being related to malic acid production (Figure 8.7).
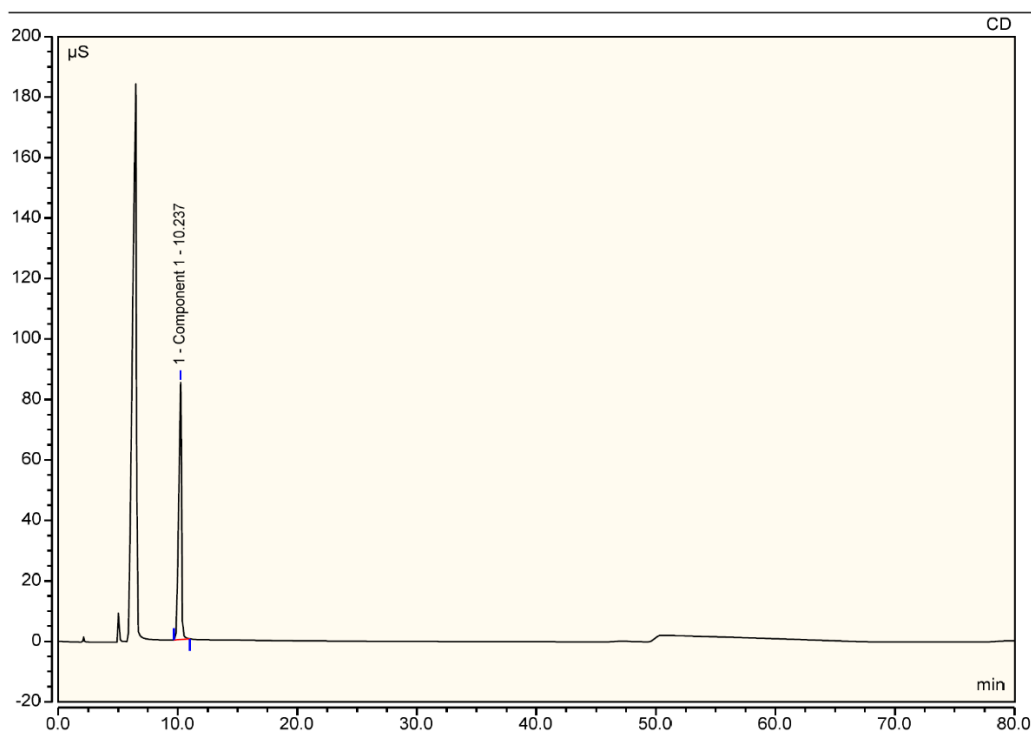
Figure 8.7. Reaction control with 30mM pyruvic acid and 5mM NADH.

From the reaction control in Figure 8.7, it is apparent that the reaction reagents are causing the shift in baseline at around the 50 minute mark. Since the malic acid retention time is also around 50 minutes, the peak was selected and the shift in baseline did not affect the analysis.

8.6 IC activity analysis of MDH assays at 2 different enzyme concentrations by equilibrating assay conditions in 5% CO_2 incubator

Following the IC activity analysis of MDH at 2 different enzyme concentrations by bubbling CO_2 through samples, another method of equilibrating assay conditions with CO_2 was attempted to determine which would be more successful to take forward. From Figure 8.6 and 8.7, it can be seen that malic acid was successfully produced from the 2 enzymatic assays tested. In this section, the assay conditions tested previously in section 8.5 were expanded while the CO_2 equilibration method was changed to incubation of samples in a 5% CO_2 incubator before analysis via IC. All other reaction components were the same as previously stated in section 8.5. Since the 0.024mg/ml assay condition was shown to give lower malic acid production than the 0.003mg/ml assay, the MDH concentration in assay was reduced along with a reduced NADH concentration. 4 assay conditions were set up, 0.003mg/ml MDH with 1mM NADH, 0.003mg/ml MDH with 2mM NADH, 0.006mg/ml MADH with 1mM NADH, 0.006mg/ml MDH with 2mM NADH. Two reaction controls were also set up, one without any NADH and one without any MDH. After the 3 hour incubation period, all samples were analysed via IC. No peaks were seen at the expected retention time of malic acid for any of the reaction conditions. This ruled out equilibrating

samples in the 5% CO_2 incubator and the method of equilibrating samples while bubbling through CO_2 was used for further experimentation.

8.7 IC activity analysis of MDH assays at 4 different enzyme concentrations and 2 NADH concentrations by bubbling CO_2 through samples

Following the unsuccessful attempt of establishing enzyme activity by equilibrating assay conditions in a 5% CO_2 incubator, further attempts moving forwards were only made with bubbling CO_2 conditions. In an attempt to further explore the range of enzyme and cofactor concentrations and activity levels, 8 reaction conditions were tested as outlined in section 8.5. 0.003mg/ml, 0.006mg/ml, 0.012mg/ml and 0.024mg/ml MDH assays were set up with both 5mM and 10mM NADH. All conditions were analysed via IC and the concentration of malic acid was calculated using a standard curve (Figure 2.5). Malic acid production from all 8 assay conditions is shown in Table 8.2.

	5mM NADH				10mM NADH			
	0.003 mg/ml MDH	0.006 mg/ml MDH	0.012 mg/ml MDH	0.024 mg/ml MDH	0.003 mg/ml MDH	0.006 mg/ml MDH	0.012 mg/ml MDH	0.024 mg/ml MDH
Area (μS*min)	4.58	3.48	3.17	2.34	4.96	4.27	3.07	3.47
Malic acid (mM)	1.68	1.28	1.17	0.86	1.82	1.57	1.13	1.28

Table 8.2. IC activity analysis of malic acid production from 4 MDH enzyme concentrations, each MDH concentration was tested with both 5mM and 10mM NADH. Standard deviation for all conditions= <0.2.

The reaction controls gave the same chromatogram profile as that shown in Figure 8.7. Additionally, further reaction controls were run to confirm that the pyruvic and malic acid standard curves obtained were accurate. 30mM of pyruvic acid was run without addition of any MDH assay buffers. The retention time obtained from the chromatogram was 5.72 minutes as expected, the peak area (μS*min) was 65.297 and using the standard curve, the calculated pyruvic acid amount added to sample was 29.74mM. This is only underestimated by 0.26mM and fits within the expected outcome. The chromatogram obtained from this control is shown in Figure 8.8.

Figure 8.8. Reaction control with 30mM pyruvic acid without any assay reagents.

1mM of malic acid was also loaded as another control in 2 different conditions, the first being without any assay reagents like the pyruvic acid control in Figure 8.8, and secondly 1mM of malic acid with all the assay reagents (Figure 8.11 and 8.12).
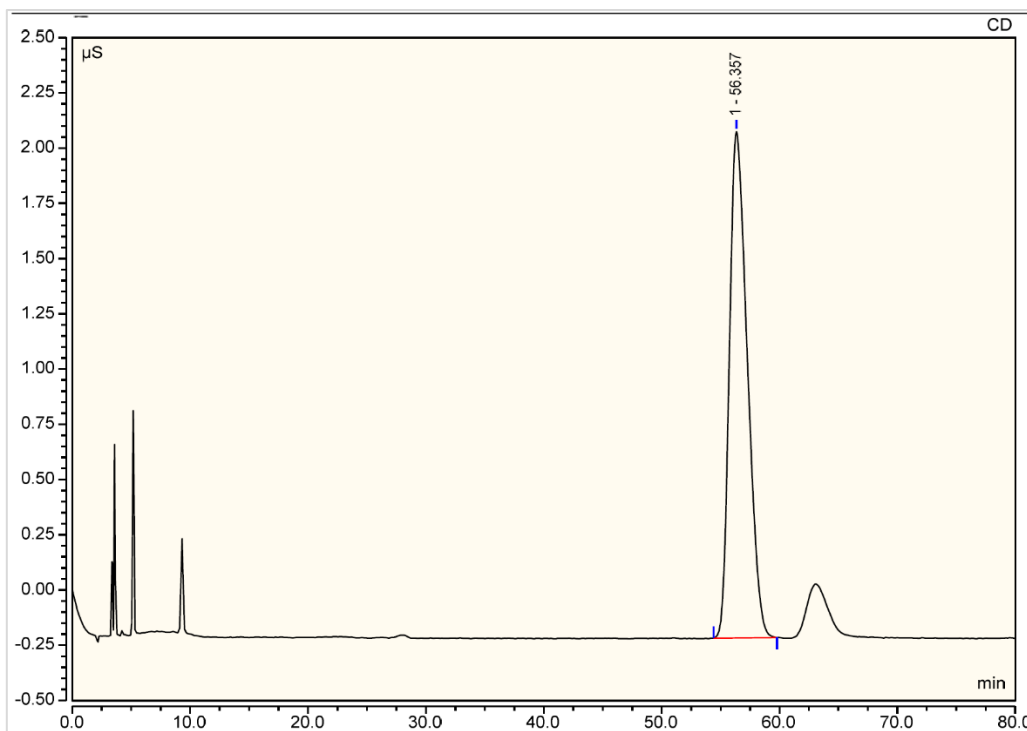
Figure 8.9. Reaction control with 1mM malic acid without any assay reagents.

For the malic acid control without any assay reagents (Figure 8.9), the retention time obtained from the chromatogram was 55.36 minutes, as expected. The peak area (µS*min) was 4.03 and using the standard curve, the calculated malic acid amount added to sample was 1.48mM which is an overestimation by 0.48mM. 1mM of malic acid was also analysed via IC under the addition of MDH assay reagents. For this control of 1mM malic acid with MDH assay reagents (Figure 8.10) the retention time obtained from the chromatogram was 49.62 minutes as expected. The peak area (µS*min) was 4.687 and using the standard curve, the calculated malic acid amount added to sample was 1.72mM which is an overestimation by 0.72mM.
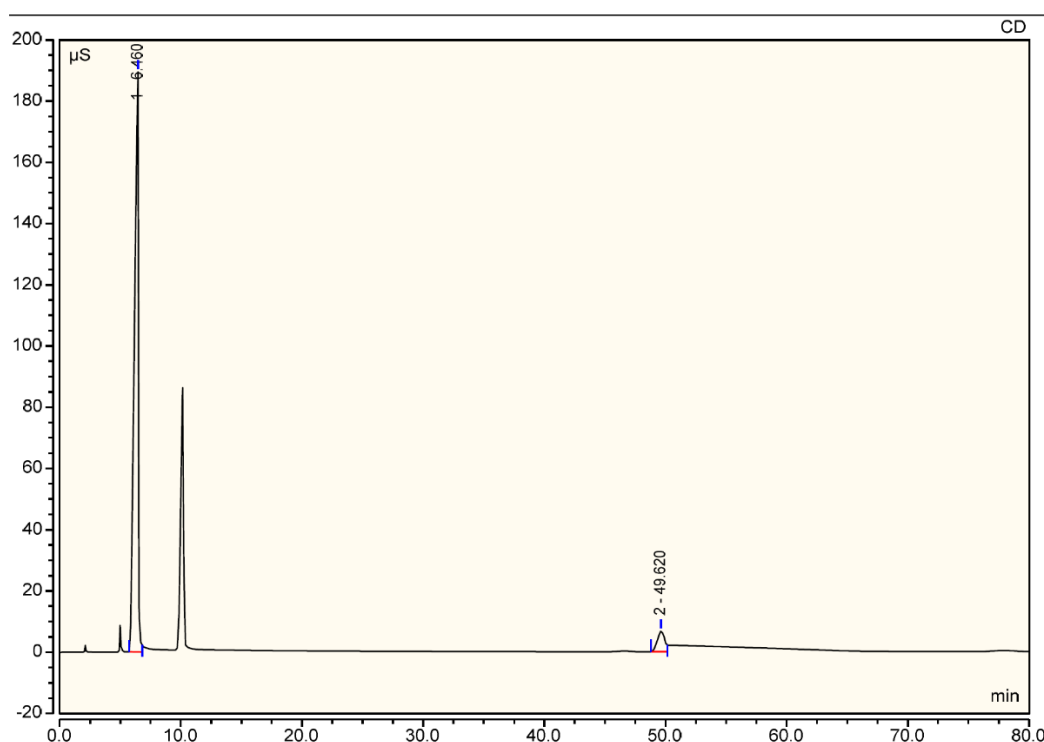
Figure 8.10. Reaction control with 1mM malic acid with assay reagents.

Given that the malic acid is being over estimated in both controls, even more so under assay conditions with assay reagents, a different approach to measuring MDH activity was explored.

8.8 MDH 0.003mg/ml activity analysis with 0.5 and 1mM NADH at 340nm

Equilibrating the headspace of the reaction containers with CO_2 was done as previously established in section 8.7. Reaction conditions were tested with 0.003mg/ml MDH; 0.5 and 1mM NADH (Figure 8.11), with the consumption of NADH, as indicated by decreased 340nm absorbance values, indicative of enzyme activity as the reaction proceeded with the oxidation of NADH to form NAD^+.
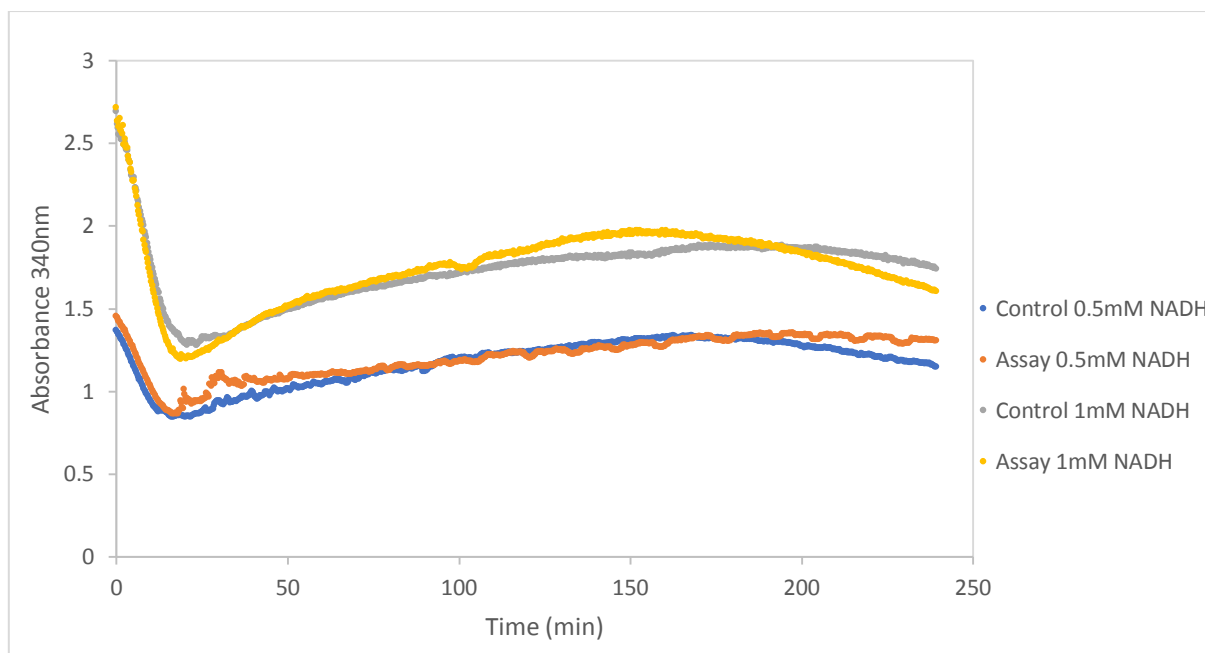
Figure 8.11. Testing 0.003mg/ml MDH activity with 0.5 and 1mM of NADH, both shown with individual controls. Standard deviation for 0.5mM NADH assay and control= <0.06, and standard deviation for 1mM NADH assay and control= <0.17.

This assay was done by equilibrating the headspace of the reaction container with CO_2 for 5 minutes before transferring samples to a 96 well plate for absorbance readings over a 4 hour period. As evident from Figure 8.11, the absorbance values from the assay and their respective controls with MDH follow a similar absorbance pattern, meaning there was no activity displayed by the enzyme. To explore this further, the assay components were investigated.

8.9 Investigating MDH assay components

Following the MDH activity assay with 2 different cofactor concentrations in section 8.8, the assay components in the assay were tested with CO_2 bubbling and without to determine if pushing reaction equilibrium towards carbonate was the cause of the unexpected curve shape. The reaction components are outlined in the materials and methods section and for the purpose of this experiment, they were isolated individually or into certain combinations (Figure 8.12 and 8.13). CO_2 was bubbled into each sample for 5 minutes and then measured for absorbance at 340nm at 50°C whereas the conditions without CO_2 were left to equilibrate at room temperature for 5 minutes before being measured for absorbance at 340nm at 50°C.
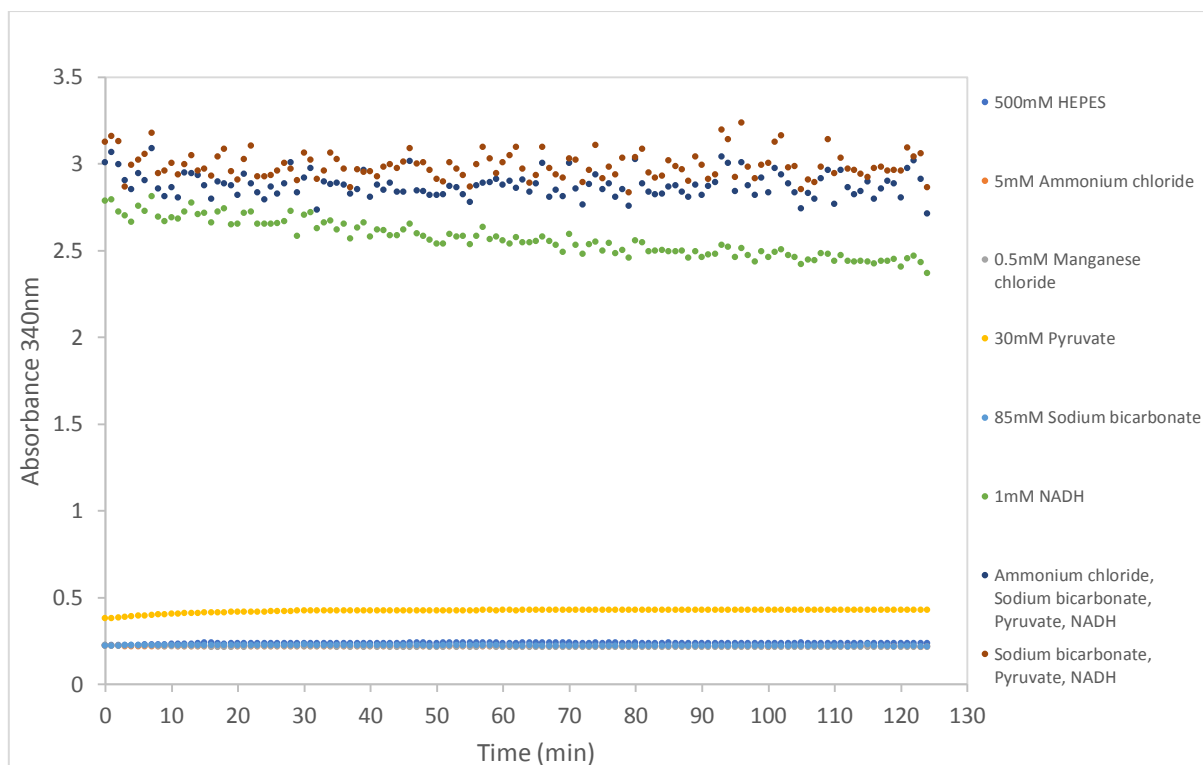
Figure 8.12. Analysis of assay components without bubbling through CO_2. Standard deviations for all 8 conditions are as follows: 500mM HEPES <0.1; 5mM Ammonium chloride <0.08; 0.5mM Manganese chloride <0.033; 30mM Pyruvate <0.055; 85mM Sodium bicarbonate <0.006; 1mM NADH <0.12; Ammonium chloride, Sodium bicarbonate, Pyruvate, NADH <0.096; and Sodium bicarbonate, Pyruvate, NADH <0.097.
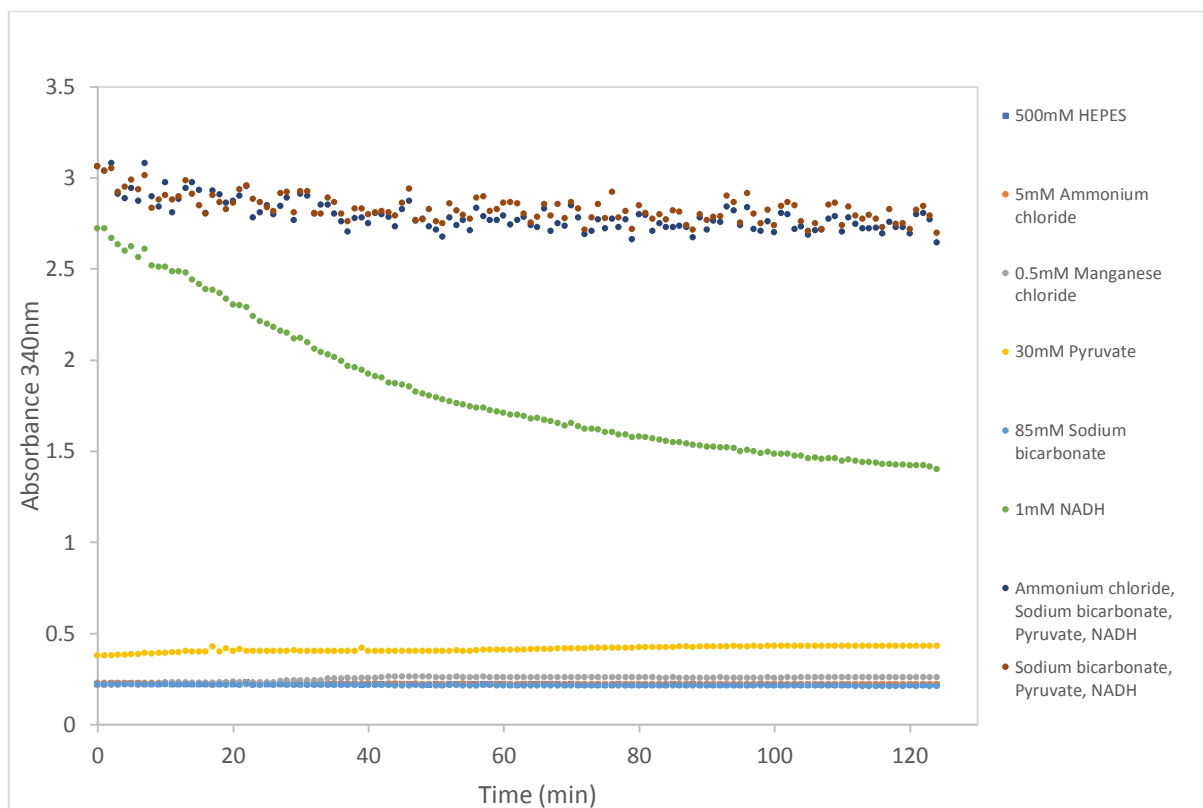
Figure 8.13. Analysis of assay components with bubbling through CO_2. Standard deviations for all 8 conditions are as follows: 500mM HEPES <0.174; 5mM Ammonium chloride <0.028; 0.5mM Manganese chloride <0.041; 30mM Pyruvate <0.069; 85mM Sodium bicarbonate <0.023; 1mM NADH <0.146; Ammonium chloride, Sodium bicarbonate, Pyruvate, NADH <0.308; and Sodium bicarbonate, Pyruvate, NADH <0.232.

Comparing the two conditions, degradation of NADH occurred much faster in the condition where equilibrium was shifted towards carbonate, the remainder of the assay reagents displayed similar absorbance profiles. Conditions of ammonium chloride, sodium bicarbonate, pyruvate, NADH and sodium bicarbonate, pyruvate, NADH displayed a higher decrease in absorbance under the carbonate rich condition in comparison to that without. This could be due to the presence of NADH and its increased degradation in the carbonate rich condition as all other components in the two conditions mentioned display a somewhat linear absorbance individually.

8.10 Sixteen hour MDH activity test

Having tested MDH activity via absorbance at 340nm as in section 8.8, a key change was made before attempting another activity test. In the experiment done in section 8.8, CO_2 was bubbled through the assay reagents including the substrate, pyruvate, for 5 minutes before starting absorbance readings, therefore initial changes in absorbance were missed. This was addressed by equilibrating the headspace of reaction container with all assay reagents except pyruvate and adding it immediately prior to starting absorbance readings. This allowed for the initial absorbance readings to be recorded (Figure 8.14).
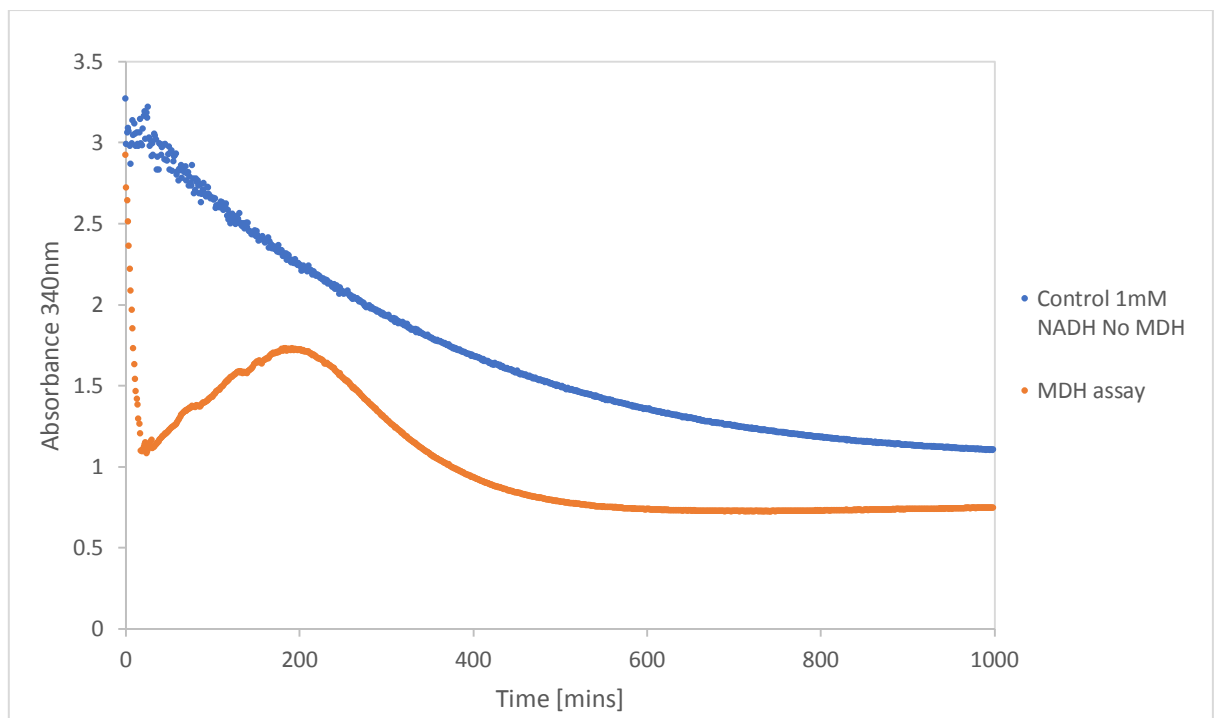
Figure 8.14. 16 hour activity analysis of 0.003mg/ml MDH with 1mM NADH. Standard deviation for control condition= < 0.22, and standard deviation for assay condition= <0.25.

The following work was done in collaboration with Dr Pinar Karagoz.

8.11 Utilization of atmospheric control unit to measure activity of MDH

All MDH enzymatic assays analysed as outlined in sections prior to this point were done using the technique of bubbling through CO_2 before measuring any potential activity. However, it was apparent that a tight monitoring of atmospheric conditions is essential to be able to determine the activity parameters of MDH with certainty. An atmospheric control unit was sourced with the capability to fully and independently regulate both O_2 and CO_2 levels within the microplate reader chamber. This provided the opportunity for analysis of real time reaction parameters via absorbance at 340nm.

8.12 Effect of atmospheric conditions on the activity of purified MDH enzyme

To determine the effects of various atmospheric conditions on the activity of MDH followed by subsequent optimization, the activity of MDH was tested under different O_2 and CO_2 ratios. Box-Behnken design and Response Surface Methodology were applied to find optimum conditions followed by application of mathematical software, MATLAB 2019a, to develop a model. The three variables and their tested values are outlined in Table 8.3.

	-	0	+
O_2, (x_1)	2.5	5	7.5
CO_2, (x_2)	5	10	15
Temperature, (x_3)	45	55	65

Table 8.3. Atmospheric conditions independent variables and their values. O_2 and CO_2 are in % and temperature is in °C.

15 independent experiments were performed, whereby the effect of the experimental variables on the initial rate of MDH was calculated. The initial rate was calculated via the decrease in the NADH concentration at the beginning of the reaction. The experimental conditions are outlined in Table 8.4.

Experiment number	O_2 (x_1)	CO_2 (x_2)	Temperature (x_3)
1	-	-	0
2	+	-	0
3	-	+	0
4	+	+	0
5	-	0	-
6	+	0	-
7	-	0	+
8	+	0	+
9	0	-	-
10	0	+	-
11	0	-	+
12	0	+	+
13	0	0	0
14	0	0	0
15	0	0	0

Table 8.4. Box-Behnken design for 3 factors with 3 centre points. O_2 and CO_2 are in % and temperature is in °C.

The full data set from all 15 conditions with experimentally obtained values are shown in Table 8.5. The highest initial rate, 0.103 mM/min, was detected at 65°C, with atmospheric conditions set as 7.5% O_2 and 10% CO_2 (Table 8.5, Experiment number 8). The highest initial rate value as calculated by the model was 0.102 mM/min with temperature, O_2 and CO_2 values accepted as 65°C, 5.625% and 12.5%, respectively. The experimentally obtained value and the value calculated by the model are in very close range of each other and this indicates the success of the model.

Experiment number	O_2 (%)	CO_2 (%)	Temperature (°C)	Initial rate (mM/min)
1	2.5	5	55	0.068
2	7.5	5	55	0.061
3	2.5	15	55	0.067
4	7.5	15	55	0.086
5	2.5	10	45	0.030
6	7.5	10	45	0.059
7	2.5	10	65	0.098
8	7.5	10	65	0.103
9	5	5	45	0.052
10	5	15	45	0.054
11	5	5	65	0.076
12	5	15	65	0.092
13	5	10	55	0.078
14	5	10	55	0.092
15	5	10	55	0.088

Table 8.5. Experimental conditions and initial rates of MDH as experimentally obtained following the experimental conditions as outlined in Table 8.4.

The accuracy of the model was experimentally tested at the model calculated optimum conditions. Atmospheric control unit was set to 5.6% O_2 and 12.5% CO_2 which is the closest matching values achievable to the calculated optimum atmosphere conditions via the model (5.625% O_2 and 12.5% CO_2) and the activity of MDH was tested at 65°C. Due to technically related issues with the equipment required for this experiment, this experiment was carried out after a lag of 2 weeks. During this time, MDH enzyme stock was stored at 4°C. Possible activity loss due to enzyme degradation was anticipated and this was experimentally confirmed by repeating some of the experiments listed in Table 8.5. Experiment number 7, 13, 14 and 15 were repeated to detect possible activity loss caused by enzyme storage. As can be seen from Table 8.6, the observed initial rate at optimum conditions was 0.092mM/min which is 9.6% lower than the calculated maximum initial rate. However, similar to this result, when the experimental conditions (Experiment number 7, 13, 14 and 15) were repeated with MDH stock that had been stored at 4°C for 2 weeks, the initial rate of the MDH was approximately 10%

lower than the previous results. Thereby, the 9.6% difference was theorised to be caused by the long storage of the MDH at 4°C. This data further goes to display the accuracy of the model.

	O_2 (%)	CO_2 (%)	Temp (°C)	Initial rate (mM/min)
Optimum conditions as calculated by model	5.6	12.5	65	0.09
Experiment number 7	2.5	10	65	0.08
Experiment number 13, 14 and 15	5	10	55	0.08

Table 8.6. Initial rate of MDH experimentally calculated under optimum conditions by the model and the repeated experiments from Table 8.5 with MDH stock from 2 weeks at 4°C.

The results obtained from the model are shown in Figure 8.15. Figure 8.15A shows the effect of the temperature and CO_2 concentration on initial NADH consumption rate of MDH, initial velocity (V_i), at constant oxygen levels (5%). Increasing temperature from 45°C to 65°C increased the V_i by 2-fold. However, increasing the CO_2 level from 5% to 10% caused approximately 20% increase in V_i. The effect of CO_2 on the V_i was less significant when CO_2 level was between 10% to 15%. This might be because of the maximum solubility of CO_2 in water. After it reaches its maximum solubility, adding excessive amount of CO_2 does not change the amount of soluble CO_2.

Figure 8.15B shows the effect of the reaction temperatures and the O_2 levels on the V_i. Similarly to Figure 8.15A, temperature change affected the V_i most significantly. The effect of O_2 was more visible at low temperatures. At 45°C, increasing the O_2 level from 2.5% to 5% increased the V_i from 0.4 to 0.56 mM/min. The similar change in the O_2 levels did not show a visible effect on the reaction rate at 65°C. Solubility of oxygen is strongly dependant on temperature and it decreases at high temperatures. It was theorized that at 65°C the amount of soluble oxygen was not significantly affected by the addition of excessive oxygen, since it was already at the equilibrium.

Figure 8.15C shows the effect of the atmospheric conditions on the initial reaction rate at 55 °C. Similar to previous results, higher reaction rates were achieved when the O_2 and CO_2 concentrations were higher than 5% and 10%, respectively.
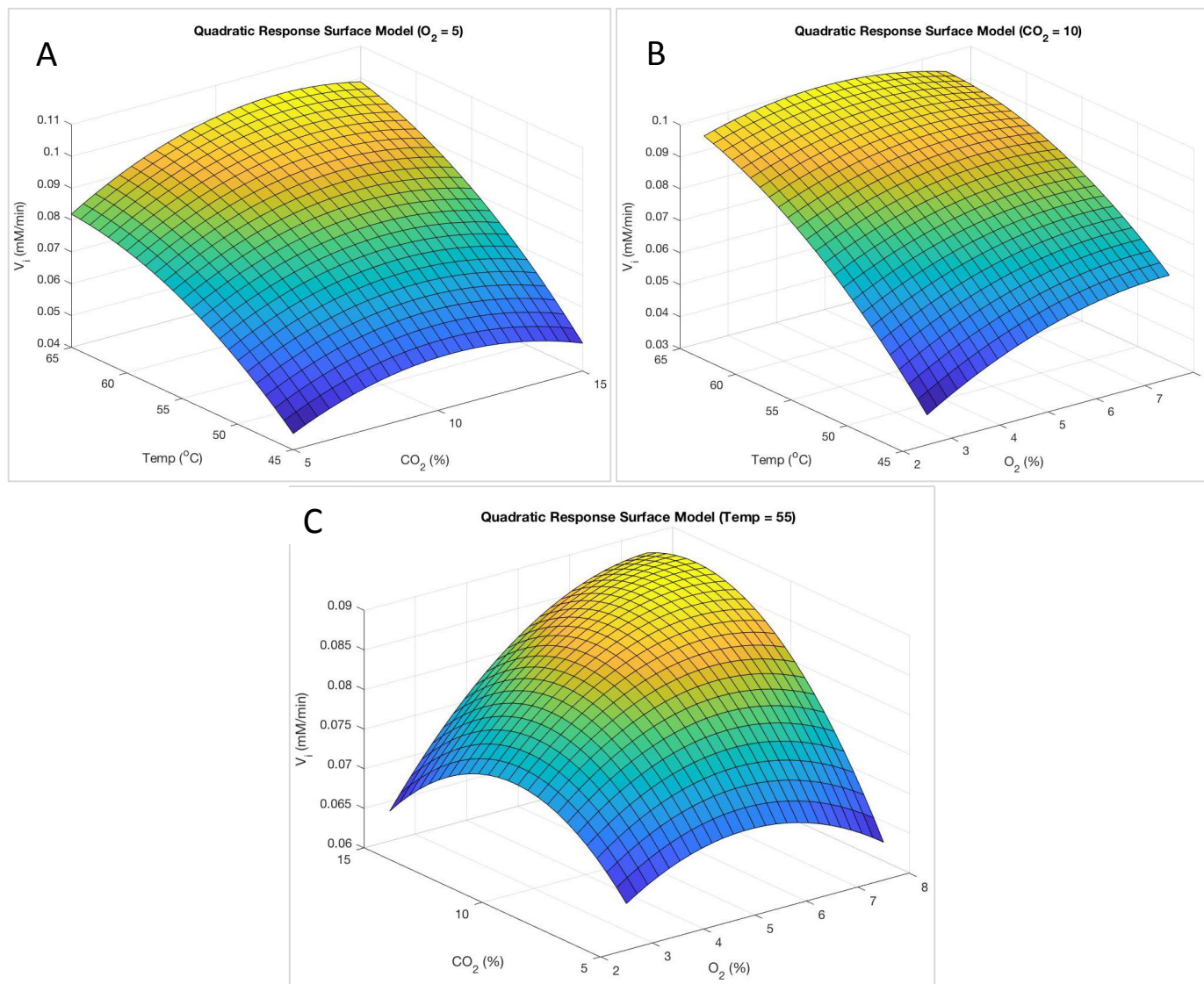
Figure 8.15. Effect of atmospheric conditions and the reaction temperature on the initial rate of MDH.

8.13 Establishing enzyme kinetics of MDH

Following the establishment of optimum atmospheric and temperature conditions for reaction conditions, enzyme kinetics were determined at 55°C under 5% O_2 and 15% CO_2 at 340nm. MDH reaction mix was as previously described in the methods section, with MDH being used at 0.3mg/ml final concentration. The substrate (pyruvate) concentration was tested in the range of 0-75mM. Figure 8.16A shows the initial activity of the MDH at different substrate concentrations. Figure 8.16B shows the Lineweaver-Burk plot for the kinetic calculations. Based on the equation of the linear function, K_m and V_{max} were calculated as 5.33mM and 0.041 mM/min, respectively.
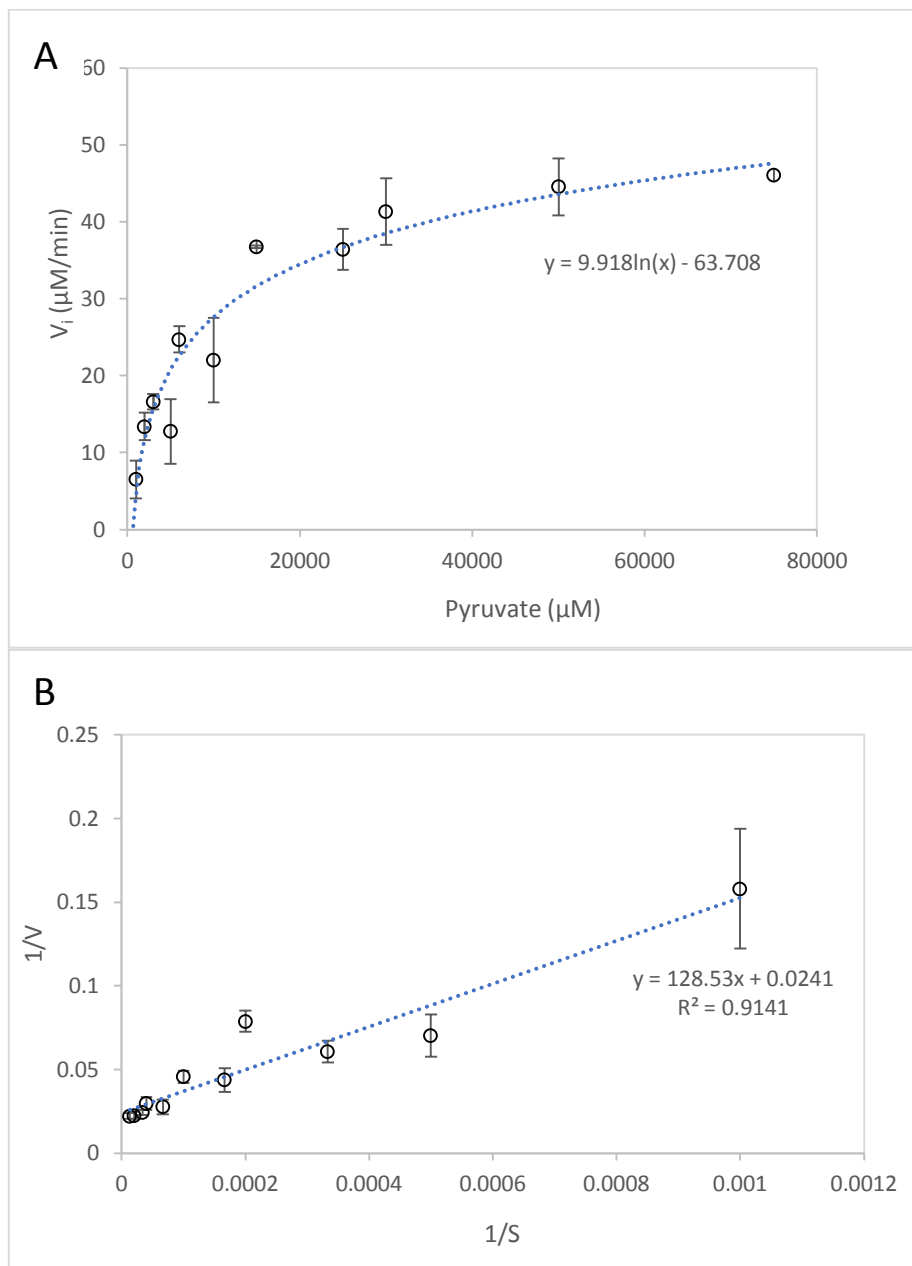
Figure 8.16. Initial activity of the MDH at different pyruvate concentrations (A), Lineweaver-Burk plot for the kinetic analysis of MDH at different substrate levels (B).

8.14 Coupling MDH with GDH for cofactor recycling

The first enzyme (GDH) of the cascade design utilizes NAD^+ as cofactor forming NADH along with the product gluconate. GDH presents itself to be an optimal pairing partner with MDH for testing cofactor recycling as MDH utilizes NADH, thereby sets up a well-balanced cofactor recycling opportunity.

8.14.1 Effect of buffer components of GDH on the activity of MDH

The assay reagents utilized in GDH and MDH vary with some being added at different concentrations whilst others only being utilized in one assay and not required for the other. MDH has higher assay condition requirements with additional assay reagents required in comparison to GDH, as well as the additional atmospheric condition requirements (Table 8.7). Thereby the effect of GDH assay components was tested on the relative activity of MDH.

GDH standard assay conditions	MDH standard assay conditions
No atmospheric control required	15% CO_2 and 5% O_2
100 mM HEPES pH 7.5	500mM HEPES pH 7.5,
2.5% glycerol	5mM NH_4Cl
30mM $MgCl_2$	0.5mM $MnCl_2$
100mM glucose	30mM pyruvate
5mM NAD+	85mM $NaHCO_3$
	1mM NADH

Table 8.7. Standard assay conditions for GDH and MDH.

All experiments were done with 15% CO_2 and 5% O_2. Initial pyruvate concentration was adjusted to 30mM. To detect the effect of the reaction components of GDH on the activity of the MDH, only one component of the GDH assay buffer was added to the MDH reaction mixture at one time. The final concentration of each chemical was the same as their concentration in the GDH assay buffer. Every component in the MDH reaction mixture (NH_4Cl, $MnCl_2$, $NaHCO_3$, Pyruvate, NADH) was kept constant.

The most significant effect was seen when the HEPES concentration of the reaction mixture reduced from 500mM to 100 mM, which is the concentration of the GDH buffer (Figure 8.17). As a result of reduced HEPES concentration, the activity of MDH reduced by 20%. Addition of glycerol, glucose and $MgCl_2$ into MDH reaction mixture did not affect the activity of the MDH significantly. However, to successfully couple MDH and GDH in the same environment, a similar study was to be done for the activity of GDH enzyme under the reaction conditions of MDH.
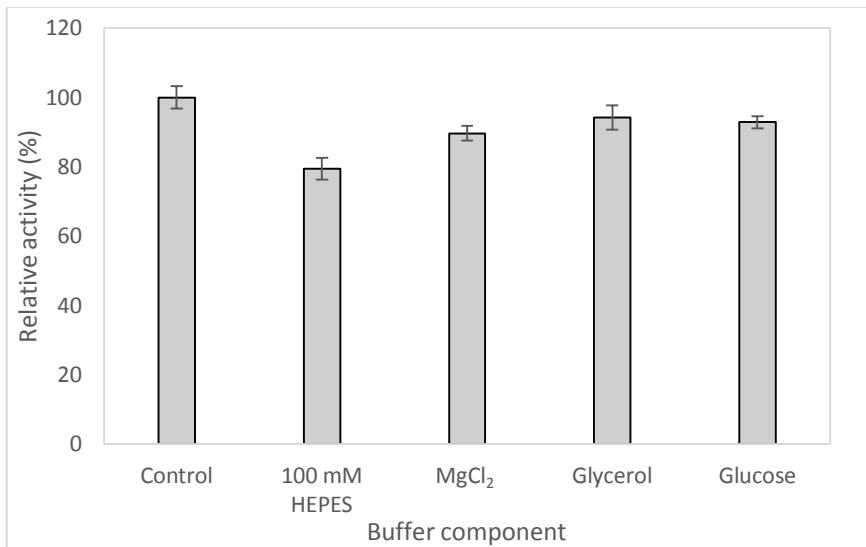
Figure 8.17. Effect of GDH assay components on the activity of MDH.

8.14.2 Effect of atmospheric conditions required by MDH on the activity of GDH

The activity of GDH was tested at 55°C under 15% CO_2 and 5% O_2 atmospheric conditions in a standard GDH reaction mix. The activity of the GDH under these conditions was compared with the activity of GDH under its standard aerobic (without atmospheric control) assay conditions. As outlined in Figure 8.18, activity of GDH was determined not to be affected by the atmospheric conditions required by MDH.
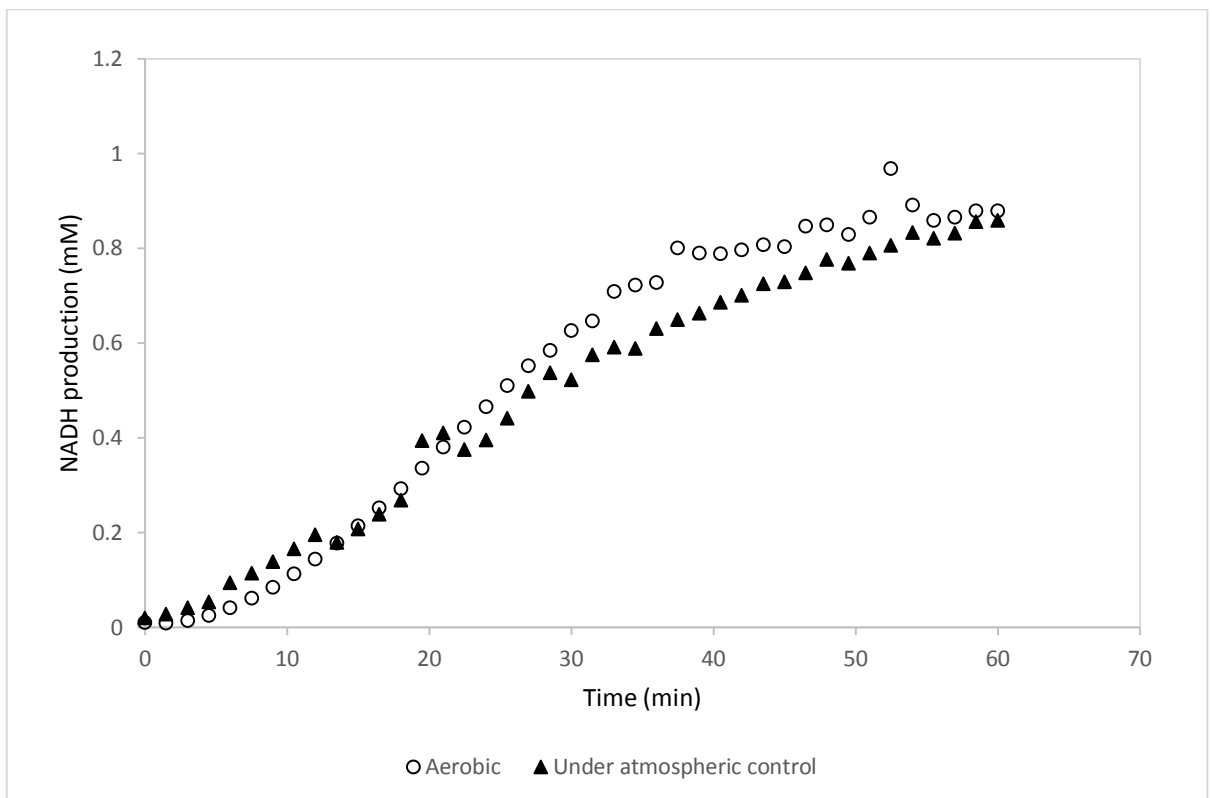
Figure 8.18. Activity of GDH under aerobic and 15% CO2 and 5% O2 atmospheric condition (results are the average of 3 different readings, standard deviation for all conditions = <0.07).

8.14.3 Effect of MDH assay buffer components on the activity of GDH

As MDH requires a variety of assay components, any effect of MDH buffer components on the activity of GDH was tested under 15% CO_2 and 5% O_2 atmospheric condition. Initial glucose concentration was 100mM. Similarly to the MDH experiment in section 8.14.1, only one component of the MDH buffer was added to the GDH reaction mixture at any one time, and all components of the GDH reaction mixture ($MgCl_2$, glycerol, glucose, NAD^+) were kept constant in their standard reaction concentrations. Figure 8.19 shows the effect of each buffer component on the activity of GDH. As evident from Figure 8.19, pyruvate has a significant effect on the activity of GDH. Presence of 30mM final pyruvate concentration in the buffer decreased the activity of GDH about 96.7%. Increasing final concentration of HEPES from 100 mM to 500 mM, decreased the activity of GDH about 15.5%. When $MnCl_2$ and $NaHCO_3$ were added into the buffer, the activity of the GDH was slightly increased about 6.9 and 8.2%, respectively.
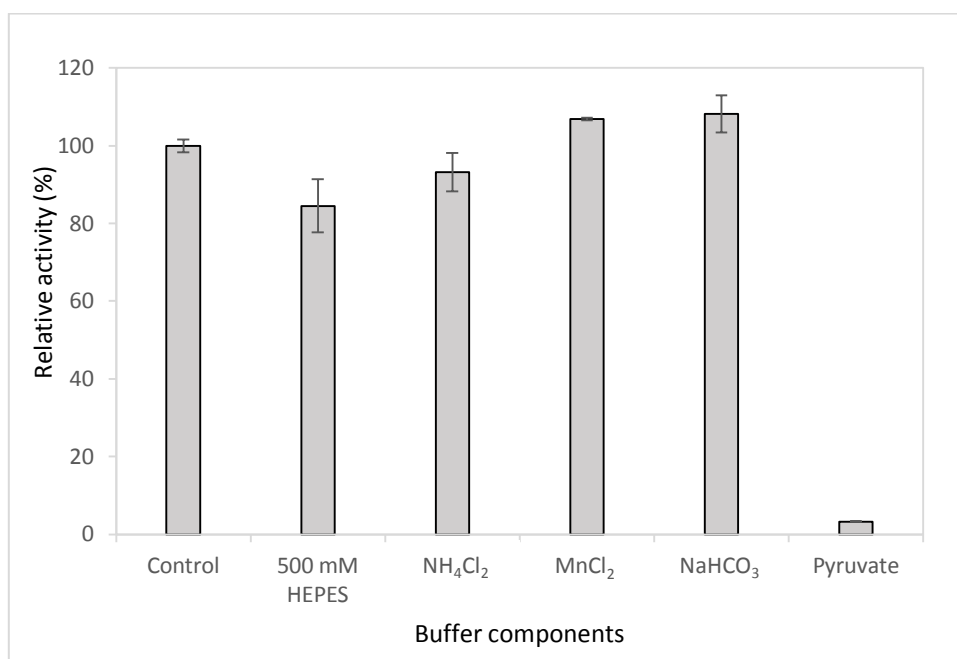
Figure 8.19. Effect of MDH assay components on the activity of GDH.

As pyruvate displayed a significant negative effect on the activity of GDH (Figure 8.19), this was explored further. To investigate the effect of the pyruvate concentration on the activity of GDH, different concentrations of pyruvate were tested by addition into the standard GDH reaction mixture and the NADH formation was detected for 2.5 hours. Based on the accumulated NADH concentration at the end of 2.5 hour reaction period, the relative activity of GDH was calculated as shown in Figure 8.20. As can be seen from Figure 8.20, pyruvate concentrations above 10mM, have significant effect on the activity of GDH and reducing the activity of GDH more than 50%. Figure 8.21 shows the effect of different inhibitor concentrations on the activity of the GDH during the first hour of the experiment.
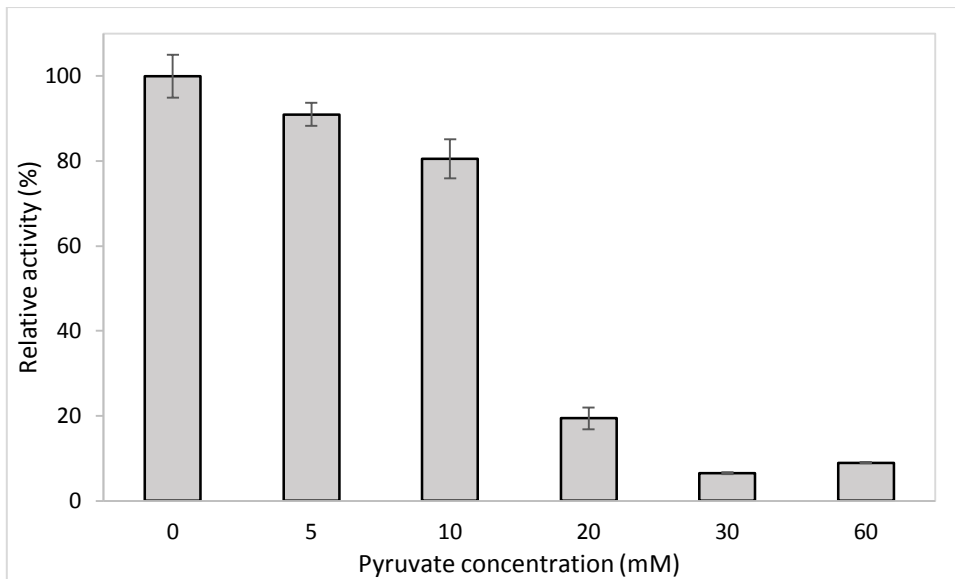
Figure 8.20. Effect of pyruvate concentration on activity of GDH.
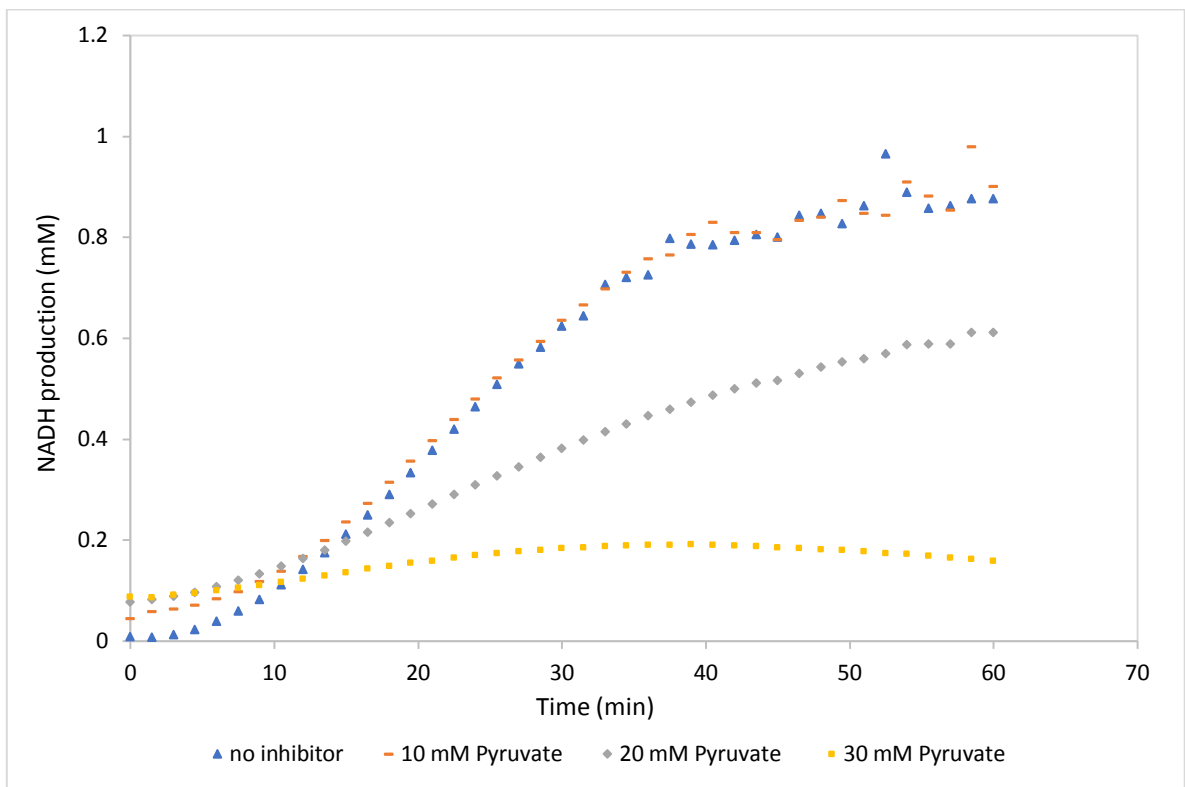
Figure 8.21. Effect of pyruvate concentration on the NADH production profile of GDH using 100mM glucose as substrate (results are the average of 3 different readings, standard deviation for all conditions = <0.03).

8.14.4 Exploring pyruvate inhibition

To understand the cause of the pyruvate inhibition, activity of GDH was monitored at different substrate levels, between 2.5-100mM, in the presence of inhibitor (pyruvate). Due to the amount of GDH required for this set of experiments, a new batch of GDH was purified and this new batch was used to analyse the effect of the inhibitor on the V_i of GDH, results are outlined in Figure 8.22 and

Table 8.8. The V_{max} value of the GDH from this batch was calculated to be 1.5U/mg which is lower than the previous batch (5.911U/mg). Table 8.8 shows the change of the kinetics values of the GDH (new batch) at different inhibitor concentrations. Even though the V_i is not significantly changed by the increase of the inhibitor, the Km value was significantly increased by the increase in pyruvate concentrations. This suggests that the inhibitor, pyruvate, is affecting the binding of the enzyme to substrate which was concluded to be competitive inhibition.
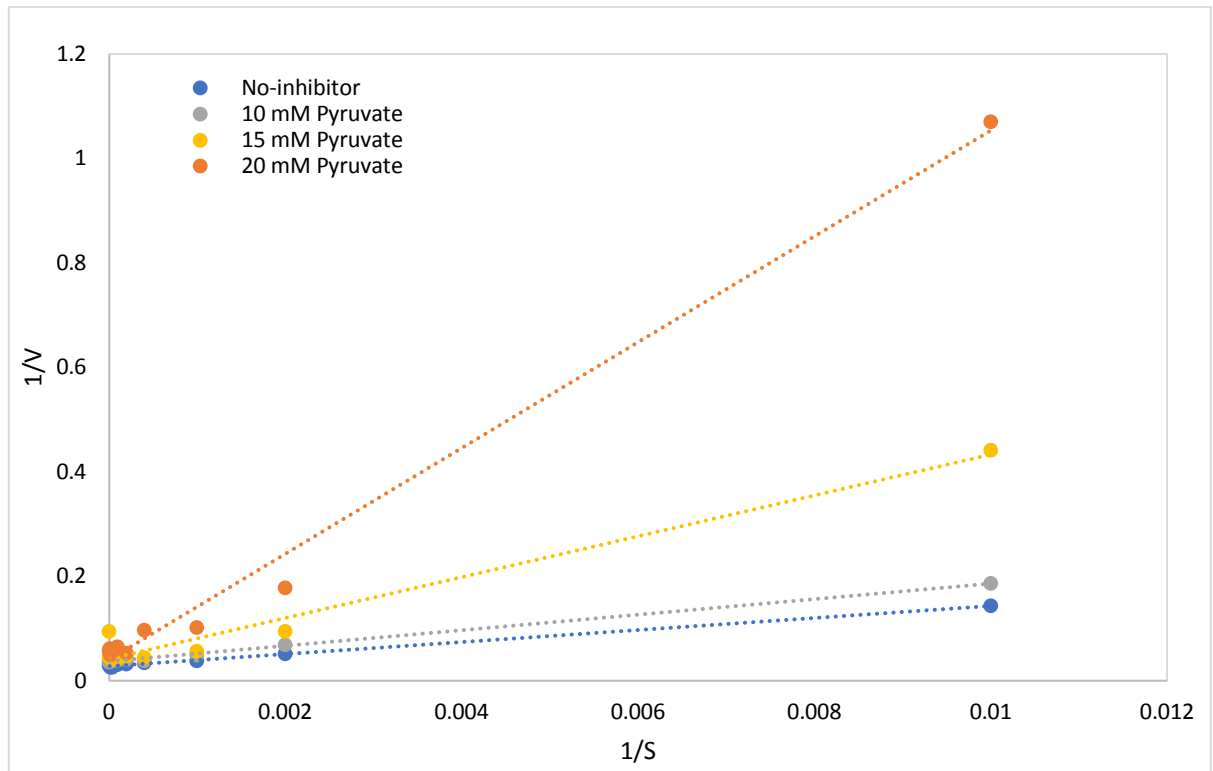
Figure 8.22. Lineweaver-Burk plot for the kinetic analysis of MDH at different substrate and pyruvate levels.

Kinetic parameters	Pyruvate concentration (mM)			
	0	10	15	20
Km (mM)	0.42	0.41	0.95	2.55
Vmax (mM/min)	0.04	0.03	0.02	0.03

Table 8.8. Change in kinetic parameters of MDH in the presence of different pyruvate concentrations.

8.14.5 Coupling MDH and GDH for cofactor recycling enzyme system

Despite the inhibitory effect of pyruvate on the activity of GDH, purified MDH and GDH enzymes were placed in the same assay condition to investigate their simultaneous activities and co-factor recycling capabilities. The final pyruvate and glucose concentrations in the reaction mixture were adjusted to 30mM, (30mM pyruvate and 30mM glucose). The final concentration of HEPES was 500mM and the

reaction mixture contained the same amount of other reagents as specified in their standard reaction mixtures. Two different scenarios were used to detect the success of the process. In the first scenario, the rapid reduction of pyruvate concentration was aimed for. In this case, NADH would be utilized as a co-factor and MDH would catalyse its conversion to NAD^+ while simultaneously converting pyruvate to malate. The reaction was tested at 55°C, under atmospheric conditions described previously, by the addition of NADH.

In the second scenario, the same reaction mixture and condition was used but the reaction was started by the addition of NAD^+ to the reaction mixture. Change in the NADH concentration was observed during 2 hours via plate reader. The final NADH concentrations were compared with an enzyme-free reaction control containing same amount of initial NADH concentration with the first scenario (Table 8.9). Despite the presence of pyruvate, GDH enzyme still displayed activity (Scenario 2). Furthermore, the NADH consumption in the first scenario shows the activity of MDH. However, these results are not sufficient to discuss the success of the co-factor recycling, since they are only showing the activity of only one side of reaction. Hence, the amount of produced malate and gluconate must be detected. Samples taken from the reaction mixtures were deproteinized, diluted 10-fold and analysed via IC. Due to high dilution factor, malate peaks were under the detection limit. However, gluconic acid production was detected in both cases. Hence, we can conclude that co-factor recycling was successfully done through both scenarios.

	Scenario 1: Presence of both enzyme (GDH and MDH), NADH as a co-factor	Scenario 2: Presence of both enzyme (GDH and MDH), NAD^+ as a co-factor	Control: No enzyme, Contains same amount of NADH with Scenario 1
Final NADH concentration, mM	1.21 ±0.06	1.31 ±0.01	1.74 ±0.04
Gluconic acid concentration, mM	8.81	10.45	0

Table 8.9. Coupling GDH and MDH for co-factor recycling.

This chapter has discussed the production of recombinant MDH from *T. kodakarensis* and its successful purification and characterization. Atmospheric condition requirements for MDH have also been optimized and successful analysis methods were also determined. The cofactor recycling was also explored via coupling MDH with GDH, and demonstrated to be successful. Coupled enzyme reactions display great potential and we have demonstrated the utilization of engineered MDH and GDH for the successful co-production of malate and gluconate.

9. Discussion

9.1 Enzymatic cascade design for the conversion of glucose to malate

The overall aim of the project described in this thesis was to enzymatically convert glucose to malate as shown in Chapter 3, Figure 3.1. A summary of experimental work carried out with each protein is shown in Table 9.1.

Enzyme	Experimental summary
Glucose dehydrogenase (GDH)	-Transformation, expression, protein purification -Positive enzymatic activity -Immobilization onto novel supports -Thermal stability, storage stability and reusability determined -Enzyme kinetics determined
Dihydroxy-acid dehydratase (DHAD)	-Transformation, expression and purification -Positive enzymatic activity (crude only) -Storage stability determined -Enzyme kinetics determined
2-Keto-3-deoxygluconate aldolase (KDGA)	-Transformation, expression, protein purification -Positive enzyme activity (reverse) -Enzyme kinetics determined
Glyceraldehyde dehydrogenase (AIDH)	-Transformation, expression -Partially successful protein purification -Analysis of several protein refolding strategies
Malate dehydrogenase (MDH)	-Transformation, expression, protein purification -Positive enzymatic activity -Atmospheric conditions optimized for assay -Coupling of GDH with MDH

Table 9.1. Summary of experimental achievements with each protein in the cascade.

The cascade constructed for the production of malate from glucose was achieved via utilization of 4 thermophilic enzymes from the non-phosphorylative Entner-Doudoroff pathway (Ahmed et al. 2005). In this system design, a single mole of glucose is converted into 2 moles pyruvate with the concomitant reduction of two NAD^+, followed by the use of an engineered enzyme with altered cofactor preference (Morimoto et al. 2013) to utilize the NADH formed and catalyse the conversion of pyruvate to malate maintaining redox neutrality (Guterl et al. 2012). Phosphorylation/dephosphorylation steps have been eliminated from the cascade design by employing an archaeal dihydroxy-acid dehydratase which has been reported to display substrate promiscuity and catalyse conversion of gluconate to 2-keto-3-deoxygluconate along with the conversion of glycerate to pyruvate (Kim and Lee 2006), with the latter step improving reaction efficiency as it redirects the transformation of unwanted glycerate into the key substrate, pyruvate. The cascade was designed to be redox balanced and utilizing enzymes from the Entner-Doudoroff pathway provided a feasible solution for enzyme stability and ease of purification. In a novel approach, an engineered malate dehydrogenase was utilized to convert glucose to malate in just 5 enzymes.

The enzymes in the cascade design were chosen keeping in mind the challenges associated with cell-free cascade systems. Enzyme stability is a key challenge hindering large scale implementation of *in vitro* synthetic biosystems for biomanufacturing, and 3 strategies can be scrutinized to meet this challenge: immobilization, thermostable enzymes and enzyme engineering (Zhang 2015). In the design of the cascade discussed here, the criteria required for efficient design were met; firstly, recombinant glucose dehydrogenase (GDH) from *S. solfataricus* was successfully purified and immobilized onto different supports. GDH immobilized onto a novel, hierarchically-structured macroporous-mesoporous silica support showed great potential for gluconic acid production and excellent reusability. Secondly, thermostable enzymes were selected in the cascade design as they can withstand higher solvent concentrations and tolerate higher process conditions (Cowan 1997, Iyer and Ananthanarayan 2008) leading to higher rates of reaction, substrate diffusion, lower viscosities, improved phase separation and decreased bacterial contamination (Guterl et al. 2012). Enzyme purification costs can also be reduced by employing thermostable enzymes as these are stable at higher temperatures, and heat treatment at higher temperatures can deactivate endogenous mesophilic host proteins and following centrifugation, thermostable soluble proteins can be found in the supernatant (Zhang 2015). Lastly, the use of engineered malate dehydrogenase allowed for the redox neutrality of the cascade to be in place as the wildtype enzyme has a different cofactor preference (Morimoto et al. 2013). Overall, objective 1 as outlined for the project was completed.

9.2 Production, purification, characterization and immobilization of GDH

GDH from *Sulfolobus solfataricus* was successfully purified and immobilized as outlined in Chapter 4. Effective enzyme immobilization is known to be critically-dependent on the choice of support material (dos Santos et al. 2015) and the purity of the enzyme being immobilized: the presence of other, contaminating proteins in an enzyme preparation reduces both enzyme loading and the apparent biocatalytic performance of the enzyme. The high purity of the GDH preparation (99.83%) achieved as outlined in Chapter 4, is therefore a substantial benefit to further studies (Figure 4.3). For applications outside of immobilization, crude preparations of recombinant thermophilic proteins such as GDH, offer multiple advantages. Costly purification protocols can be avoided involving resins or columns, which while manageable on the lab scale and for analytical purposes, scale up on an industrial scale may not be desirable due to costs involved and have difficulties to compete economically with petroleum derived equivalents (Guterl et al. 2012). Thermophilic proteins offer an advantage in comparison to mesophiles due to increased stability at higher temperatures. This allowed for the 5 thermophilic proteins characterized in this thesis to use heat treatment as a primary purification step. Following cell lysis, lysates can be heated to temperatures in the range of 60-80°C for 30-60 minutes, resulting in the denaturation and precipitation of most endogenous *E.coli* proteins followed by centrifugation to

remove host cellular debris. This method can be used to achieve a rapid and simple partial purification of thermostable proteins free of contaminating activities (Patchett et al. 1986, Xu et al. 2015).

In earlier attempts of Ni-NTA affinity chromatography of GDH, multiple large preparations of GDH were lost to protein aggregation during the dialysis stages. This is a wide issue faced by many researchers when using proteins for *in vitro* studies or as therapeutic agents. There are a large number of protein stabilizers available, however determining the most appropriate one is a time consuming task (Bondos and Bicknell, 2003). Large scale preparation of purified GDH posed an issue when attempting to remove the imidazole used to elute the protein from the affinity column. As the protein sample volumes were large, buffer exchanging the elutions into imidazole-free buffer using spin columns was an inefficiently laborious and time-consuming process. Dialysis was the best option, however, despite multiple attempts at variation of dialysis protocol to optimize dialysis ratios, step-wise reduction in buffer components (namely imidazole), the aggregation issue persisted. To overcome this issue, addition of EDTA to the protein sample was explored as a solution. The elution of bound protein with imidazole also leads to leached nickel ions from the column and into the collection tubing. During Ni-NTA affinity chromatography, both imidazole the His_{10} tag chelate the nickel, and the removal of just imidazole during dialysis could have resulted in the sample being insoluble. The addition of 100mM EDTA aided successful dialysis as it was assuming to be chelating the nickel ions and thereby prevents protein-protein self-interactions and a successful dialysis cycle (section 4.4). Protein aggregation was not observed in any dialysis samples onwards after the addition of EDTA. EDTA was thereby successfully removed along with the imidazole in subsequent dialysis cycles as well. Maximum GDH activity has previously been established at Mg^{2+}, Mn^{2+} or Ca^{2+} concentrations of 20mM, however the presence of 50mM EDTA in the standard reaction mixture reduces the enzyme activity to about 5%; which is restored upon the excess addition of Mg^{2+} (Giardina et al. 1986). 200mM of $MgCl_2$ was used for the initial cycle of dialysis to provide the excess of Mg^{2+} required to restore activity of GDH following addition of EDTA to elutions. The concentration of Mg^{2+} in subsequent cycles of dialysis was reduced to 100mM and finally 50mM for storage and assay conditions. Despite 20mM Mg^{2+} identified as providing maximum activity, for storage stability 50mM of Mg^{2+} was adapted as being the standard.

Due to the presence of hydroxyl groups that facilitate enzyme binding, silica-based materials are efficient and attractive supports for enzyme immobilization (Zdarta et al. 2018) and were therefore the subject of immobilization as outlined in Chapter 4. The surface area and pore diameter of an immobilization support determines its loading capacity and the size of protein that can be immobilized (Mohamad et al. 2015). Small pore sizes may limit diffusion and increase the risk of pore blockage. Furthermore, immobilization can only be achieved on the external surface of a support if the pore size is too small (Mohamad et al. 2015) desorption is also more likely to occur as the operating temperature

is increased (Li et al. 2010). It has therefore been suggested that the pore diameter should be at least 4-5 fold larger than the equivalent dimension of the enzyme to be immobilized, but not so large such that it affects the mechanical properties of the support material (dos Santos et al. 2015). In this study, the immobilization efficiency of GDH was significantly higher on the novel MM-SBA-15 silica support materials with macro-meso structured hierarchical pores than on commercially-available silica supports. As a result of its smaller pore diameter, and consistent with the observations above, more immobilized enzyme was visible on the surface of MM-SBA-15-200 than MM-SBA-15-300 (Figure 4.6).

The activity of an enzyme under different physicochemical conditions is a function of its stability (Poorakbar et al. 2018). Immobilization often increases enzyme thermostability (Kumar et al. 2017, Mission et al. 2015). The chemistry of a support material, including the nature of its functional groups and the length of the matrix-enzyme spacer all affect thermostability (Zdarta et al. 2018). The thermostability of immobilized GDH on commercial supports and the novel hierarchically-structured MM-SBA-15 was explored (section 4.10). Thermal shocks were carried out on immobilized and free-state GDH at 55, 65, and 80°C overnight; no significant activity loss was detected at 55 and 65°C. However, when the temperature was increased to 80°C, all immobilized and free-state GDH lost activity (Figure 4.7). To understand the robustness of immobilized GDH on different supports, heat shocks at 80°C were carried out for shorter periods. Compared to free-state GDH, the thermostability of GDH immobilized on ECR8309F was significantly improved. The activity of immobilized GDH on other commercial supports had similar activities to free-state GDH. Unexpectedly, GDH immobilized on MM-SBA-15 showed reduced thermostability. This may be caused by the thermal conductance properties of silica. Similar observations have been reported in previous studies using silica-based support materials at very high temperatures (Masuda et al. 2013).

Free-state enzymes are difficult to recover and re-use (Li et al. 2018), while immobilization of enzymes allows their cost-effective re-use in repeated batch or continuously-running processes (Yu et al. 2017). As outlined in section 4.11, immobilized GDH was used 10 times. At the end of the 5th cycle, GDH immobilized on commercial supports had lost more than 65% of its initial activity. However, GDH immobilized on MM-SBA-15-300 and MM-SBA-15-200 had lost 41% and 51% of their initial activities, respectively (Figure 4.8). In previous studies, GDH immobilized on nanoSiO$_2$ and SBA-15 retained 50% and 43% of its initial activity, respectively (Zdarta et al. 2018), while glucose-6-phosphate dehydrogenase (G6PD) immobilized on silanized silicon retained 38% of its initial activity after 6 cycles (Aissaoui et al. 2013). Improved storage stability of immobilized enzymes is another advantage over the corresponding free-state preparations (Kunjukunju et al. 2018). The activity of GDH immobilized on commercial supports was significantly reduced over time compared with GDH immobilized on MM-SBA-15.

Despite the reduced thermostability of GDH on MM-SBA-15 supports at 80°C (Figure 4.7), the data demonstrated substantial enzyme activity at normal working temperatures, long term enzyme re-usability and improved storability. To further improve the activity of GDH immobilized on MM-SBA-15, the effects of temperature and pH on the activity of free and immobilized GDH were tested (section 4.14). It was noted that immobilization on MM-SBA-15 did not shift the optimum working temperature of GDH. The activity of the free-state enzyme was slightly decreased when the temperature increased from 50°C to 60 °C, while the activity of the immobilized enzyme was not affected (Figure 4.10a). The optimum pH of an immobilized enzyme depends upon the particular enzyme and the chemistry of the support (Sahin and Ozmen 2016). In this study, the activity of GDH was tested over a range of pH. At pH greater than 7.5, the activity of immobilized GDH on MM-SBA-15 supports was significantly higher than free-state GDH (Figure 4.10b). Usefully, at high pH, above the pKa of gluconic acid, gluconic acid can be separated from the reaction mixture by simple separation methods, such as membrane filtration (Zdarta et al. 2018).

Specific area determines the loading capacity of a support and the ratio of enzyme to support material is a crucial immobilization parameter for achieving high efficiency and high reaction rates (Patel et al. 2014). Immobilizing high concentrations of enzyme is preferable from an economical point of view (dos Santos et al. 2015), but increasing enzyme concentrations on the support material can also increase the cost of the process (Fernandez-Lopez et al. 2017). Furthermore, excessive loading may have an effect on enzyme leakage, pore blockage and mass transfer between liquid and solid (Sahin and Ozmen 2016). Hence, working at a reasonable enzyme/support ratio is important in developing catalytic bioprocesses. Different enzyme/support ratios were tested and immobilization efficiencies and GDH activity were quantified (Table 4.9). At enzyme loading ratios between 1/1 and 10/1 (mg/g), almost all of the GDH was immobilized onto the MM-SBA-15 supports. However, enzyme activity was reduced at decreased enzyme loading ratios, which might be a result of diffusional constraints. The highest GDH/support ratio tested in this study was 25/1 (mg/g) where more than 80% of the enzyme was successfully immobilized on MM-SBA-15-200. Under the same conditions, 98% of the enzyme was immobilized on MM-SBA-15-300, probably due to its higher surface area and pore diameter.

The kinetic parameters of free-state GDH and GDH immobilized on MM-SBA-15 supports showed that immobilization leads to drop in the V_{max}. This expected result might be caused by mass transfer limitations (Patel et al. 2014). As a result of enzyme attachment, some of the active sites of GDH could be blocked, which would reduce the reaction rate and V_{max} (Zdarta et al. 2018). Similar observations have been made when GDH from *Bacillus megaterium* was immobilized on DEAE-Sephadex (Baron et al. 1997). Diffusional limitations caused by immobilization also lead to an increase in Km values for GDH immobilized on MM-SBA-15 supports. As shown in Figure 4.6, while GDH was mainly immobilized

on the surface of MM-SBA200, GDH was predominantly immobilized inside of the pores of MM-SBA-15-300. Similarly, after immobilization of commercial GDH onto silica supports, depending of the pore structure of the supports, a reduction in V_{max} of up to 1.87-fold, and an increase in Km of up to 1.78-fold were reported (Zdarta et al. 2018).

Increasing generation rates and quantities of food waste are a global concern (Dahiya et al. 2018). Bread waste contains high amounts of carbohydrate that can be used as a potential feedstock in bioprocesses for the generation of various biobased products, replacing those from fossil resources with their associated economic and environmental concerns (Mirabella et al. 2014). As outlined in section 4.15, bread waste was converted to gluconic acid, a potential platform chemical, by using free-state and immobilized GDH. Immobilized GDH was reused 10 times in reaction mixtures containing BWH (bread waste hydrolysate) as a substrate (Figure 4.11). After the 7th cycle, the activity of GDH immobilized on MM-SBA-15 was above 50% of its initial activity. The gluconic acid yield from GDH immobilized on MM-SBA-15-300 was higher than that on MM-SBA-15-200, in each cycle. Further investigations such as the effect of substrate levels and BWH/enzyme loading ratios on the gluconic acid production yield are needed. To develop a more effective and economic bioprocess, GDH could be coupled with an additional enzyme for co-factor recycling. In a previous study, commercial GDH was successfully co-immobilized with xylose dehydrogenase (XDH) on a silica surface for co-factor recycling (Zdarta et al. 2018). Co-enzyme re-cycling as a part of multi-enzyme cascades could be an attractive route for green chemical production from waste.

9.3 Production, purification and characterization of DHAD

Following the oxidation of glucose to gluconate by GDH, gluconate is further dehydrated via dihydroxy-acid dehydratase (DHAD) to 2-keto-3-deoxygluconate (Kim and Lee 2006, Lamble et al. 2004). DHAD utilised for the purpose of studies carried out in this thesis was sourced from the hyperthermophilic archaea, *S. solfataricus*. Biochemical studies suggest that the metabolic conversion of glucose in hyperthermophilic archaea occurs via the non-phosphorylative branch of the Entner-Doudoroff pathway (Ahmed et al. 2005). DHAD has previously been identified as a key enzyme in the non-phosphorylative branch of the Entner-Doudoroff pathway. Its expression and purification was successfully established following heat treatment of crude lysates followed by Ni-NTA affinity chromatography in the earlier attempts. Large scale protein production was aided by dialysis carried out following the addition of EDTA to the eluted protein fractions as previously done with GDH (Figure 5.9).

Previous studies performed with DHAD from multiple hyperthermophilic sources have utilised separation and quantification techniques such HPLC and LC-MS for enzymatic analysis of DHAD

(Carsten et al. 2015, Guterl et al. 2012, Matsubara et al. 2004). DHAD activity was analysed using HPIC for the purpose of activity analysis, however a few challenges were encountered. The retention times for the substrate and product of the reaction were close in values (typically around 3.5 minutes for gluconic acid and 3.8 minutes for 2-keto-3-deoxygluconate respectively). The enzymatic activity was analysed under standard reaction conditions and combinations, such as high/low enzyme concentration and high/low substrate concentrations. As concentrations of the substrate were increased in the assay, the area of the peak also widened leading to a less sharp peak with a wider base on the chromatogram. If little product was obtained during the assay, then the gluconic acid peak overshadowed the peak corresponding to 2-keto-3-deoxygluconate leading to the start of the peak not being visible clearly and therefore the concentrations of 2-keto-3-deoxyglucunate being inaccurately calculated. This issue was somewhat resolved by limiting the concentrations of gluconic acid used in assay conditions to those forming sharp distinguishable peaks under the same dilution factors. Overlaying control chromatograms were also used to identify the 2-keto-3-deoxygluconate peaks in assay conditions where product yields were low. Positive DHAD activity was established with freshly-purified DHAD (Ni-NTA affinity chromatography) samples that had not undergone long term storage either at 4 or -80°C (Table 5.1), where 10mM gluconic acid was used as substrate with 0.1mg of DHAD and on average, 4.14mM of 2-keto-3-deoxygluconate was obtained following incubation for 20 hours at 60°C. After solving the issue of protein aggregation by employing EDTA before dialysis of large-scale preparations of DHAD (Figure 5.9), further DHAD samples that had not undergone long term storage at either 4 or -80°C were tested for activity using 50mM gluconic acid as substrate (Table 5.3). Due to technical issues with the range of values in the standard curve for 2-keto-3-deoxygluconic acid, the analysis from these assay conditions was only done by assaying the consumption of gluconic acid. Positive confirmation of DHAD activity was established through these experiments by deducting the gluconic acid concentrations from the assay condition from those of the control condition. Higher DHAD concentration containing assays were shown to be consuming more gluconic acid, thereby presumably producing more 2-keto-3-deoxygluconic acid.

To confidently identify the consumption of gluconic acid under assay condition, gluconic acid assay kits were employed. This method provided the sensitivity required that could not be achieved with the IC analysis. Section 5.8.1 discussed how a suitable dilution factor was determined to be around 200 as it fit within the range of the gluconic acid standards run alongside each assay. Since the detection limit for the gluconate present inside a sample had to be <2μM, the samples had to be diluted x200 to fit within the range of the standard curve. With a high dilution factor, a considerable error factor was also introduced considering sizeable pipetting errors that come with handling very low volumes of liquid. Fresh gluconate standards were run alongside each assay, however the same pipetting errors applied

and the low R^2 values obtained during a few experiments are testament to this. Despite the assay's shortcomings, repeated checks were performed when carrying out the assay at each stage and it was the best method to confirm DHAD activity at low levels. 0.01mg/ml of DHAD was tested for activity with 20mM of gluconic acid via the gluconate assay kit (Table 5.5) . The 450nm absorbance values for the control condition and the 0.01mg/ml DHAD 120 minute assay condition were 0.406 and 0.405 respectively. As the values only varied by 0.001, an apparent lack of activity was attributed to possible batch degradation because the set of experiments carried out in section 5.8 were performed with snap frozen DHAD stored at -80°C, and it was evident that DHAD cannot be frozen and retain high activity.

DHAD from *S. solfataricus* displays substrate promiscuity and is furthermore able to convert glycerate to pyruvate in a reaction which does not occur in natural metabolic pathways (Carsten et al. 2015, Guterl et al. 2012, Kim and Lee 2006). DHAD catalyses the conversion of gluconate to 2-keto-3-deoxygluconate, the latter then undergoes a reversible aldol cleavage catalysed by 2-keto-3-deoxygluconate aldolase (KDGA) to give pyruvate and glyceraldehyde. Glyceraldehyde is an unwanted intermediate in the cascade design which can be converted to glycerate via glyceraldehyde dehydrogenase. The glycerate can be then utilised by DHAD and converted into pyruvate reducing unwanted intermediates in the overall cascade design. The previous set of experiments outlined in the last paragraph discussed the apparent lack of activity displayed by thawed DHAD stored at -80°C when assayed for activity with gluconic acid as substrate for formation of 2-keto-3-deoxygluconate. Following inconclusive data about activity displayed by DHAD, its substrate promiscuity was exploited to confirm or deny activity. As DHAD also facilitates the conversion of glyceric acid to pyruvic acid, accumulation of pyruvate was monitored (section 5.9). Multiple batches of DHAD were tested to ensure the results obtained in section 5.8.2 were not due to a single batch anomaly. 2 batches of DHAD were tested, DHAD batch 1, which was snap frozen and stored at -80°C, DHAD from the same batch hereby referred to as batch 1a, which was stored at 4°C and DHAD batch 2 snap frozen and stored at -80°C. 2 concentrations of DHAD were tested, 0.01mg/ml and 0.1mg/ml with 20mM glyceric acid as substrate at a reaction time of 1 hour. DHAD batch 1 and 1a were from the same original batch with the notable difference being their final storage conditions after protein purification and concentration. The highest pyruvate concentration was detected in 0.1mg/ml of DHAD from batch 1 (snap frozen and stored at -80°C for 5 months) which gave 9.55ng/μl of pyruvate. The same batch of DHAD stored at 4°C for 5 months (DHAD batch 1a) assayed under identical assay conditions with 0.1mg/ml DHAD produced 2.04ng/μl of pyruvate (Table 5.6, shown below).

	DHAD batch 1		DHAD batch 1a		DHAD batch 2		Control no DHAD
DHAD mg/ml	0.01	0.1	0.01	0.1	0.01	0.1	N/A
Absorbance 570nm	0.06	0.6	0.01	0.13	0.01	0.09	0.00
Pyruvate ng/µl	0.93	9.55	0.21	2.04	0.13	1.46	0.05

Table 5.6. Analysis of pyruvate production using pyruvic acid assay kit from 2 different batches of DHAD and storage conditions. Standard deviation for all conditions= <0.02.

This results in a 78% loss in relative activity of DHAD with the storage at 4°C in comparison to snap freezing and storage at -80°C. Similar observations were made by Carsten et al. 2015, who recommend that storage at -80°C is best only if DHAD cannot be prepared fresh and used immediately, as activity degradation was noted with prolonged storage at -80°C as well. This would explain the low pyruvate production seen in the assays performed with this batch (1.46ng/µl pyruvate), as the DHAD stored at -80°C in batch 2 was an even older sample and prolonged storage over time could have led to diminished activity.

Using the gluconate and pyruvate detection kits confirmed the DHAD displaying activity, albeit poor levels of activity but enzyme functionality was established. Following on from this, the reasons for poor activity and ways to improve it were explored. Carsten et al. 2015 reported the purification of His-tagged DHAD decreased the total enzyme activity to 43% of the crude extract and even further to 17% when stored at -80°C for one day. Ni-NTA purification is reported to severely diminish enzyme activity, imidazole elutions reported no measurable activity, leading to a complete elimination of DHAD activity towards gluconate. Buffer exchange of protein into another buffer would then be required to restore any % of initial activity. Nickel has been reported to strongly inhibit DHAD and reduce residual activity to 3% so diminished enzyme activity within the imidazole fraction could be due to the Ni-NTA purification associated with the entire protocol (Carsten et al. 2015, Kim and Lee 2006). Nickel ion leakage during Ni-NTA affinity chromatography and the higher concentrations of imidazole present in samples during purifications can be presumed to be the main contributor to diminished activity of His-tag purified protein fractions.

Carsten et al utilised a wildtype variant of DHAD without His-tag and employed heat treatment at 80°C as the only purification method. This methodology was adapted and crude DHAD lysate was purified using heat treatment only followed by centrifugation to remove host protein precipitates. Crude lysate was quantified using ImageJ scientific image analysis, the DHAD monomer and confirmed oligomers were calculated as a total % of the total sample giving % of DHAD in the crude lysate. This was an efficient method at isolating % protein present in the crude as image J was used to select entire lanes of samples run on SDS-PAGE and there was no subjective selection error associated with the analysis. Carsten et al reported the 2 methods of purification (Ni-NTA and heat treatment) and reported their

specific activities, which were 0.13 and 0.54U/mg for Ni-NTA and heat treated DHAD respectively. This leads to the conclusion that as the number of purification steps is increased, the activity levels decrease, as supported by Flint and Allen who describes an increased leakage of [Fe-S] cluster when more purification steps are performed (Flint and Allen 1996). Originally studied with DHAD isolated from spinach, a [2Fe-2S] cluster was suggested to be directly involved in catalysis as the reduction of the [2Fe-2S] cluster led to decreased enzyme activity by 6 fold (Flint and Emptage 1988), furthermore, DHAD has also been purified from *Escherichia coli* which contains a [4Fe-4S] cluster (Flint et al. 1993). Flint et al found an amino acid pattern that is unique for [2Fe-2S] cluster containing DHAD enzymes and based on the homology of the sequence, the same pattern was found within the *S. solfataricus* DHAD, leading to the assumption that the latter also contains a [2Fe-2S] cluster. Similarly to the results seen with DHAD when assayed for activity with gluconate and pyruvate (section 5.7-5.10), Carsten et al also reported low levels of DHAD activity. As the [2Fe-2S] has previously been suggested to have a direct catalytic role within DHAD purified from spinach, extending the same principle to DHAD from *S. solfataricus* utilised in this thesis, the problem of low activity levels could be due to an ineffective [2Fe-2S] cluster supply during the expression of DHAD in *E. coli*. This however is most likely not the case as DHAD activity yield was attempted to be enhanced by the addition of additional $FeSO_4$ (1-20mg/L) to the expression medium to ensure excess ions are available to supplement DHAD active sites with [Fe-S] clusters (Carsten et al. 2015). Excess ions availability in expression media did not affect overall expression or specific activity of DHAD expressed in in *E. coli*. From this it was concluded that there are either sufficient ferrous ions to load the catalytic sites of DHAD with an [Fe-S] cluster or the cluster assembly in *E. coli* works at its maximum efficiency and DHAD catalytic sites cannot be loaded with more functional [Fe-S] clusters.

A reducing agent has been previously employed as an activation method to increase activity of other DHAD via possible [Fe-S] cluster repair, activation and/or stabilization following enzyme purification. The mechanism behind this activation is unknown but it is assumed that a reducing agent such as β-mercaptoethanol is able to alter the [Fe-S] cluster's oxidative state culminating in the active form of the cluster followed by removal of the reducing agent (Gottschalk and Bender 1982, Carsten et al. 2015). Carsten et al studied apparent activation of [Fe-S] cluster with β-mercaptoethanol with *S. solfataricus* DHAD and reported an increased DHAD activity towards gluconate. This was only done with native DHAD without a His-tag, and Ni-NTA purified DHAD was not subjected to an activation protocol in the cited literature. The activation protocol was tested with Ni-NTA purified DHAD as outlined in section 5.11. Gluconic acid assay kits were utilised to monitor the depletion of gluconic acid in activated and non-activated DHAD assay conditions (control). Under the circumstances that the activation protocol indeed increased the DHAD activity towards gluconate, lower corresponding

450nm absorbance values would be recorded for the condition displaying the highest DHAD activity. The control for this assay were not sufficiently in range of the gluconate standards, however the absorbance values for the activated DHAD non-activated DHAD 0.1mg/ml assay conditions gave absorbance 450nm values of 0.438 and 0.456 leading to the conclusion that activation of DHAD using β-mercaptoethanol has no significant effect on improving activity within fractions of Ni-NTA purified DHAD. Nickel and imidazole could be irreversibly diminishing activity of Ni-NTA purified DHAD leading to the activation protocol being ineffective.

Following unsuccessful experiments to establish higher levels of activity from the purified DHAD even after using an activation protocol, an approach was devised to use crude DHAD in an attempt to establish activity instead. As previously mentioned, Ni-NTA purification diminishes the activity of DHAD thereby cited literature protocols utilised heat treatment of crude DHAD as a method of purification. The activation protocol was repeated with crude heat treatment purified DHAD to establish if a DHAD sample not having undergone Ni-NTA purification is more susceptible to activation to give improved enzyme activity. The gluconic acid consumption in the activated crude DHAD and non-activated crude DHAD 0.1mg/ml were 8.506 and 7.804mM respectively (Table 5.9). In comparison, the most successful activation condition tested by Carsten et al reported an 2.5 fold increase in enzyme activity following activation with β-mercaptoethanol. To confirm the analysis obtained by gluconic acid assay, the samples were analysed via IC as well and the actual concentration of 2-keto-3-deoxygluconate was calculated from a standard curve. IC analysis confirmed the findings of the gluconic acid assay kit, whereby 6.772mM and 6.545mM of 2-keto-3-deoxyglcuonate was obtained from the activated crude DHAD and the non-activated crude DHAD respectively. With both analysis methods showing no significant difference between the activated and non-activated enzyme activity, this contradicts to what is reported in the literature. Due to differences in expression and possible media preferences (Auto-induction media), [Fe-S] clusters in our samples did not require or respond to repair/activation/stabilization. The batch to batch variation in crude DHAD preparations could also have led to improperly folded DHAD proteins causing the activation process to have a more significant effect on enzyme activity in some batches compared to others.

As previously established, Ni-NTA-purified DHAD displays poor enzyme activity and the activation protocol with β-mercaptoethanol had no significant effect on the improvement of enzyme activity. It was also shown than activation protocol did not significantly affect crude DHAD activity either. Thereby, crude DHAD without any activation protocol was used to establish DHAD activity with any subsequent assays and kinetics analysis. Crude DHAD was used to analyse enzyme activity as outlined in section 5.13. 2 and 20mM of gluconic acid were tested with various DHAD concentrations at 3 time points, all end reactions were deproteinized and analysed for gluconic acid depletion with gluconic

acid assay kit. The data for both substrate conditions indicated positive DHAD activity, 2mM of gluconic acid was all consumed when analysed at 30 minutes at all DHAD concentrations tested (1, 2.5 and 5mg/ml). 20mM gluconic acid condition showed increased gluconic consumption with the higher DHAD concentration consuming more gluconic acid with increasing time. The gluconic acid assay kit application became difficult to utilise with higher concentrations of gluconic acid under assay conditions, given the high error factors involved with dilution of samples. In the gluconate detection kit, gluconate is utilized by gluconokinase to form gluconate-6-phosphate and ADP, producing a coupled enzyme reaction that generates a colorimetric signal at 450 nm, proportional to the amount of gluconate present and the assay is sensitive to less than 2 μM of gluconate. As it is a coupled enzyme reaction, assay components could potentially be contributing to absorbance readings, also it does not give a direct measure of the amount of 2-keto-3-deoxygluconate produced during the reaction. Using the IC mitigates these issues and allows for direct visualization of product formed and its subsequent quantification. Although both methods of activity analysis for DHAD have their own advantages and disadvantages, ultimately, IC analysis is a better option as it offers analysis of a wider range of gluconic acid concentrations and direct detection and quantification of 2-keto-3-deoxygluconate.

Kim and Lee have reported DHAD activity towards its natural substrate to be 47U/mg (Kim and Lee 2006), and this is very high compared to other DHAD's. A possible reason for this could be in the detection method employed by Kim and Lee, whereby a semicarbazide based method was employed where the dehydration reaction is quantified by measuring the absorption of semicarbazone with a ketoacid at 250nm. The issue is that at this wavelength, crude cell extract components such as DNA and proteins show high absorption, therefore there is a high likelihood of quantifying false positives leading to a high specific activity determination (Carsten et al. 2015). K_m values in the range of 2.42mM (determined at 80°C) and 7.8mM (determined at 50°C) by DHAD have been reported towards D-gluconate by Kim and Lee and Carsten et al, respectively. Kim and Lee have reported the highest K_m to be at 80°C which falls in the optimal range for the native organism, *S. solfataricus.* The DHAD employed by Kim and Lee underwent Ni-NTA affinity chromatography followed by size exclusion chromatography. As Ni-NTA purification was later reported to lower enzyme activity, this could potentially be increasing the K_m value due to lowered substrate affinity caused by catalytic site inefficiency. Without the activation protocol, Carsten et al reported specific activity of 0.13U/mg for Ni-NTA purified DHAD, increasing to 0.54U/mg for heat treatment purified DHAD. The enzyme preparation used by Carsten et al was desalted into reaction buffer using an ÄKTA system, presumably the impurities present in that sample were reduced in comparison to the crude enzyme preparation achieved in the preparation done for this study.

9.4 Production, purification and characterization of KDGA

Archaea exhibit a complex carbohydrate metabolism in which glucose is utilized through several branches of the Entner-Doudoroff pathway and KDGA is a unique enzyme in the pathway. In the common part of the branches Entner-Doudoroff pathway, glucose is first oxidized to gluconate by GDH followed by the dehydration of gluconate to 2-keto-3-deoxygluconate by DHAD. In the non-phosphorylative branch of the Entner-Doudoroff pathway, 2-keto-3-deoxygluconate is then reversibly cleaved by KDGA into pyruvate and glyceraldehyde (Kouril et al. 2012). KDGAs from thermophilic sources showcase high thermostability and activity on non-phosphorylated substrates which makes them high potential candidates for biocatalysts in the industrial applications (Schurink et al. 2014). GDH, DHAD and KDGA utilised as the first 3 enzyme in the cascade featured in this thesis have been modelled on the non-phosphorylative branch of the Entner-Doudoroff pathway. This pathway has been reported for the hyperthermophilic archaea *S. solfataricus, Sulfolobus acidocaldarius* and *Thermoproteus tenax* amongst others (Ahmed et al. 2005, Selig et al. 1997). The GDH and DHAD utilized in the cascade are from *S. solfataricus*, however KDGA has been sourced from *S. acidocaldarius.* A minimized reaction cascade as reported by Guterl et al. 2012, utilized the enzymes derived from hyperthermophilic archaea from a modified non-phosphorylative Entner-Doudoroff pathway, whereby GDH and DHAD were sourced from *S. solfataricus* and KDGA from *S. acidocaldarius*. Noting that both of these organisms are hyperthermophilic and from the *Sulfolobus* family, the reasoning for this change was not commented upon by Guterl et al. As the cascade reported by Guterl et al was a huge step forward in the development of minimized cascades, the same experimental strategy as Guterl et al was adapted for the cascade design outlined in this thesis.

Glyceraldehyde-3-phosphate has been reported to be the best reacting substrate for *S. solfataricus* KDGA, with the non-phosphorylated analogue of glyceraldehyde-3-phosphate having a 38% reaction as that of phosphorylated analogue (Ahmed et al. 2005). BLAST analysis with the KDGA of *S. solfataricus* showed high homology with KDGA from *S. acidocaldarius*, on the basis of which KDGA from *S. acidocaldarius* was expected to have similar activity with pyruvate and glyceraldehyde as KDGA from *S. solfataricus* (Wolterink-van Loo et al. 2007). Wolterink-van Loo et al. 2007 tested 2 KDGAs from the *Sulfolobus* family (*S. solfataricus* and *S. tokodaii*) and compared their characteristics to the KDGA from *S. solfataricus*. Activity of KDGAs was assayed in the synthesis direction of 2-keto-3-deoxygluconate, utilizing pyruvate and glyceraldehyde and it was reported that the 2 tested KDGAs had activity in the same range as that of *S. solfataricus*. Biochemical data comparisons between the three KDGAs from the *Sulfolobus* family highlighted the differences between them. KDGA from *S. acidocaldarius* displays higher specific activity towards both reaction substrates (pyruvate 26.3U/mg and glyceraldehyde 33.1U/mg) when compared to KDGAs from *S. solfataricus* (pyruvate 15.7U/mg and

glyceraldehyde 17.1U/mg) and *S. tokodaii* (pyruvate 17.8U/mg and glyceraldehyde 20.3U/mg) (Buchanan et al. 1999, Wolterink-van Loo et al. 2007). This could potential be reasoning for utilization of KDGA from *S. solfataricus* as the KDGA of choice for integration into the cascade by Guterl et al. 2012. However, all biochemical data gathered on the activity of KDGA from various organisms of the *Sulfolobus* family is in the synthesis direction of 2-keto-3-deoxygluconate.

At the time of writing, Guterl et al are alone to have reported KDGA activity analysis followed in the cleavage direction using 2-keto-3-deoxygluconate as substrate, however this only seems to have been achievable with the addition of pyruvate decarboxylase to the activity assay which catalyses the conversion of pyruvate to acetaldehyde. As pyruvate is one of the two products obtained from the cleavage of 2-keto-3-deoxygluconate, its removal from the reaction equilibrium should theoretically be pushing the reaction forward towards the cleavage direction. From the KDGA activity experiment performed in section 6.6, there was no secondary enzyme or removal method to facilitate the removal of either pyruvate or glyceraldehyde formed from the cleavage reaction, thereby the reaction equilibrium seems to have stayed at its preferred equilibrium with the control and assay conditions showing no significant differences in concentrations when analysed via IC (Figure 6.5). This activity assay was not run at optimal reaction conditions, due to reasons discussed in section 6.5, commercial 2-keto-3-deoxygluconate was not utilized for activity analysis of KDGA as it is not commercially favourable due to limited quantities available for purchase. 2-Keto-3-deoxygluconate was instead synthesised in the lab with the utilization of DHAD which catalyses the conversion of gluconate to 2-keto-3-deoxygluconate. However, due to protein degradation issues resulting from storage of the batch of DHAD utilized in the large scale reaction to produce 2-keto-3-deoxygluconate, the resulting reaction mixture consisted of a 50/50 split of the substrate, gluconic acid and product, 2-keto-3-deoxygluconate. The presence of gluconic acid in the reaction mix could potentially have inhibitory effects on the cleavage of 2-keto-3-deoxygluconate, however this has not been reported in related literature of minimized cascades which have utilized similar enzymes.

Characterization of KDGA activity analysis has been reported to be done with 20mM glyceraldehyde and 50mM pyruvate (Buchanan et al. 1999, Wolterink-van Loo et al. 2007) and as the theoretical reaction ratios are 1:1, the effect of altered substrate ratios were explored on the final product yield and also to understand the rationale behind using said ratios for activity analysis. The standard substrate concentrations modelled on the KDGA activity assays run in previous literature were modified to be 10mM glyceraldehyde and 20mM pyruvate as tested in section 6.8.2. Substrate ratios of 10mM glyceraldehyde and 20mM pyruvate were used as assay control and a further 2 substrate ratios were tested; 20mM glyceraldehyde + 20mM pyruvate (1:1 substrate ratio) and 20mM glyceraldehyde + 10mM pyruvate (reverse ratio of the standard assay condition). Analysis of the

product formed (2-keto-3-deoxygluconate) showed that the product yield is in similar concentrations to the conditions where the substrate concentration ratio is 1:2 (10mM:20mM) with respect to either pyruvate or glyceraldehyde. Either one or the other is not required to be in excess and is not capable of giving a higher final yield of product (Table 6.5). Assay condition with 10mM glyceraldehyde + 20mM pyruvate gave a final yield of 8.34mM of 2-keto-3-deoxygluconate whereas assay condition with 20mM glyceraldehyde + 10mM pyruvate gave a final yield of 7.9mM of 2-keto-3-deoxygluconate. The experimental condition where the concentration of both glyceraldehyde and pyruvate was the same (20mM glyceraldehyde + 20mM pyruvate) gave a final yield of 13.1mM under the same assay conditions as previously mentioned. Given the theoretical yield maximum has not doubled as calculated when compared to the previous conditions, increasing the substrate concentrations ratios to be equal was determined to be waste of resources and therefore was not adapted for any further assays performed.

KDGA from thermophilic sources is a unique enzyme with the potential of large industry applications. Its unique metabolic properties and substrate promiscuity make it ideal for applications in catalysis of phosphorylated and non-phosphorylated chemicals. Paired with its wildtype preceding enzymes GDH and DHAD from the Entner-Doudoroff pathway, KDGA forms the industrially valuable platform chemical pyruvate which can be paired with further downstream artificial enzyme cascades to obtain higher value chemicals.

9.5 Improving yields of refolded AIDH from inclusion bodies

GDH, DHAD and KDGA are enzymes derived from the naturally occurring non-phosphorylating branch of the Entner-Doudoroff pathway functioning in multiple thermophilic archaea (Ahmed et al. 2005). The next enzyme to follow in the non-phosphorylating branch of the pathway is glyceraldehyde dehydrogenase (AIDH) (Ahmed et al. 2005, Ettema et al. 2007, Reher and Schönheit 2006) . KDGA cleaves 2-keto-3-deoxygluconate into pyruvate and glyceraldehyde, and while pyruvate is a key intermediate in the cascade design outlined in this thesis, the second product of cleavage, glyceraldehyde, is not. Guterl et al proposed a solution to this by utilizing the natural fourth enzyme to redirect the glyceraldehyde towards pyruvate formation. This was achieved by the addition of a thermophilic AIDH from *Thermoplasma acidophilum*, which facilitates the conversion of glyceraldehyde to glycerate, the latter is then redirected towards pyruvate formation courtesy of the substrate promiscuity displayed by DHAD. The removal of glyceraldehyde from the reaction equilibrium of DHAD also pushes reaction equilibrium forward in the direction of pyruvate formation. Previous literature has established protein characterization and biochemical properties of AIDH from multiple hyperthermophilic sources including *Picrophilus torridus, S. solfataricus* and *T. acidophilum.*

The analysis from these has shown inconsistencies between findings relating to the same protein. AIDHs purified from *P. torridus, T. acidophilum* and *S. solfataricus* have all been reported to display negligible activity with NAD$^+$ (Ettema et al. 2007, Reher and Schönheit 2006). The design of the cascade outlined in this thesis is dependent on the usage of NAD$^+$ as cofactor as the other enzymes in the cascade were designed to be NAD$^+$/NADH dependent, thereby the AIDH to be utilized in the cascade was required to accept NAD$^+$/NADH as a cofactor. On the contrary, it has been reported that the AIDH from *T. acidophilum* to accept NAD$^+$ as a cofactor under technically relevant conditions whereby the cofactor concentration is <1mM (Steffler and Sieber 2013), this supports the utilization of AIDH in the current cascade design for the production of malic acid where NAD$^+$/NADH are the only utilized cofactors. Albeit, all three AIDHs from *P. torridus, T. acidophilum* and *S. solfataricus* are reported to show strong substrate specificity for glyceraldehyde (Ettema et al. 2007, Reher and Schönheit 2006, Steffler and Sieber 2013) which makes them attractive for utilization in minimized cascades in case there are other aldehydes intermediates, which must not be the target for oxidation by AIDH.

Previously, expression and purification of AIDH from *T. acidophilum* has been reported as standard. Recombinant *T. acidophilum* was obtained as a His-tagged protein after expression in LB broth using IPTG. Crude AIDH lysate was purified via Ni-NTA affinity chromatography and the protein was eluted via an imidazole gradient however no yield information was provided (Reher and Schönheit 2006). On an attempt to replicate Ni-NTA purified AIDH, we were also able to recover some soluble protein (Figure 7.2), which was further positively identified as the protein of interest via mass spectrometry analysis. However, before any positive confirmation of activity could be attempted, the protein fraction aggregated following imidazole removal during the protein concentration process. Contrary to soluble protein recovery of the other proteins featured in the cascade design, the amount of AIDH soluble protein recovered was low. The efficiency of AIDH soluble protein recovery could not be compared to that reported by Reher and Schönheit (2006) as no yield information was provided. Our findings are consistent with those reported by Steffler and Sieber, who also reported very small amounts of AIDH in the soluble form. Based on our observations and experimental data, band intensities around the size of AIDH were low in comparison to supported by the report of Steffler and Sieber, we concluded that the majority of the protein produced was formed as inclusion bodies. A protocol was developed for the refolding of AIDH found in the inclusion bodies whereby guanidine hydrochloride (GdnHCl) and dithiothreitol (DTT) were utilized in a simplified denaturation buffer methodology (section 7.2.2.1). The cell pellet obtained following the sonication, heat treatment and centrifugation during the soluble fraction preparation was processed downstream for AIDH inclusion bodies so both of the soluble and insoluble purifications were carried out on the same batch of culture. The simplified denaturation buffer consisting only of GdnHCl and DTT was used to unfold the protein

and 2 methods of refolding the protein were explored. Firstly, while in its denatured state, AIDH was bound to Ni-NTA resin, followed by standard column affinity chromatography, and secondly the denatured AIDH solution was dialysed against buffer. With the first strategy, the gradual removal of denaturation buffer during the washing of the Ni-NTA resin and reintroduction of standard buffer conditions during washes and imidazole elutions promotes refolding of the protein to its native structure, while the salt promotes proteins stability. This was successfully achieved as demonstrated by SDS-PAGE analysis of Ni-NTA purification attempt of AIDH inclusion bodies following extraction with GdnHCl (Figure 7.3). The recovery of some soluble AIDH mentioned earlier and insoluble AIDH were both analysed via SDS-PAGE and the suspected oligomers were all positively confirmed to be AIDH from *T. acidophilum* via mass spectrometry analysis.

Refolding insoluble AIDH on the affinity column proved to be a more successful strategy in comparison to utilizing dialysis for the same purpose. Heavy aggregation was observed in the first cycle of dialysis (Figure 7.4) carried out to remove the GdnHCl and DTT from the protein solution, again with the understanding the removal of the denaturation components would promote refolding of the extracted protein to its native state. Following the heavy aggregation seen in the dialysis tubing, the aggregated suspension was centrifuged to isolate aggregates from solution. A subsequent SDS-PAGE analysis of the supernatant displayed a significant band matching the size of AIDH (Figure 7.5), indicating very low quantities of soluble protein salvaged. However, in comparison to the method of refolding denatured AIDH with Ni-NTA affinity chromatography, the dialysis method is prone to containing a lot of non-specific host proteins. Given the dialysis protocol could be optimized and protein aggregation during refolding of denatured AIDH could be prevented, the non-specific proteins would still require removal via Ni-NTA affinity chromatography. This concludes the dialysis step to be moot as binding denatured AIDH to Ni-NTA facilitates the refolding of AIDH and the removal of non-specific protein in one single step.

The failure of dialysis has multiple contributing factors and a combination of these have presumably contributed to the multiple failures observed. The presence of cysteines in protein sequence has been reported to contribute towards aggregation of proteins (Ramkumar et al. 2018) and require the additions of reductants such as DTT to compensate. The denaturation buffer containing AIDH in its denatured state was supplemented with DTT and thereby this theoretically should have mitigated any aggregation due to cysteine residues. Depending on the concentration of the protein present in the sample, high salt is another requirement for the protein to remain in solution. 200mM of $MgCl_2$ was added to the dialysis buffer and this was not sufficient as heavy aggregation was seen in the dialysis tubing. Possibly higher concentrations of $MgCl_2$ could be experimentally tested to determine if aggregation levels can be reduced. The temperature of dialysis conditions can also contribute towards

protein aggregation (Yamaguchi and Miyazaki 2014) as some proteins, during refolding, can aggregate if the dialysis buffer is exchanged too quickly. Low temperatures can be utilized to slow down the dialysis process and prevent aggregation. This was testing by repeating the dialysis process at different temperatures (room temperature and 4°C), however it failed to prevent aggregation and visually there was no difference in the amount of aggregates observed in both conditions. Some success was achieved with step wise dialysis but only with protein fractions with low concentrations. Given that we had previously successfully displayed recovery of insoluble AIDH via binding to Ni-NTA and elution with imidazole, removal of denaturing buffer via dialysis and attempted refolding of AIDH was not trouble-shot any further.

Further attempts at refolding denatured AIDH extracted from inclusion bodies was optimized for yield purposes. Inclusion bodies contain very little host protein and are a potential pure source of the desired recombinant protein (Ramon et al. 2014). However the inclusion bodies need to extracted from the cell lysates as they are heavily contaminated with host cellular components, which can be removed by selectively extracting with detergents and low concentrations of chaotropic agents. Following the proper extraction of inclusion bodies from cell lysates results in a significant purification of the recombinant protein (Palmer and Wingfield 2004). The recombinant protein in the inclusion bodies can thereby be solubilised and refolded into native structure proteins and optimistically be biologically active. We adapted these strategies into our resolubilisation protocol and achieved the typical white inclusion bodies pellet indicative of a pure inclusion bodies pellet free of any host cellular components (Figure 7.12). The biggest issue faced during the modified attempts to increase recovery yield of AIDH was the AIDH not binding sufficiently to the Ni-NTA. Through consistent attempts, a high intensity band was observed at the expected size of AIDH in SDS-PAGE analysis while unsuccessfully attempting to bind and later elute protein via imidazole. During these failed attempts of binding AIDH to Ni-NTA, dialysis was explored again as an option. AIDH aggregates from unsuccessful dialysis attempts were attempted to be dialysed into urea to evaluate if the change in chaotropic agents makes dialysis more likely to succeed. Step-wise dialysis was explored where the concentration of urea was reduced to 5M from the original 8M which this was a successful cycle with no aggregation seen in the dialysis tubing. The second cycle of dialysis whereby the concentration of urea was reduced to 2M from 5M was not successful and protein aggregates were observed in the dialysis tubing.

The unsuccessful binding of AIDH in its denatured state to Ni-NTA was a persistent issue as a lot of AIDH recovered from the inclusion bodies was being lost in the flow through during Ni-NTA affinity chromatography leading to very low yields in terms of soluble protein recovery. Primary factors suspected of decreasing binding efficiency were tested to rule them out, different batches of Ni-NTA resin were used to ensure the resin was fully charged for successful binding; resin amount, binding

times and binding temperatures were explored and after concluding there was no significant difference made to the binding efficiency, further troubleshooting was attempted. A main reason for His-tagged fusion proteins not binding to metal affinity chromatography resin is the inaccessibility of the tag as it could potentially be buried inside the protein's three-dimensional confirmation in its native folded state. The inaccessibility of the tag can be experimentally determined via binding the protein in the presence of denaturants such as GdnHCl or urea (Clark 1998) and if the binding is successful, then it indicates that the protein folding is to blame. As we were trying to bind our protein to Ni-NTA resin under denaturing conditions already, a western blot was performed to analyse the efficiency of the His-tag which confirmed the presence of a functional His-tag (Figure 7.19). Standard protocols and general lab practices are known to utilize the addition of a small amount of imidazole to the binding buffer in order to inhibit binding of non-specific proteins, however an excess amount can inhibit binding as the imidazole could potentially outcompete the tag for metal binding. This was also ruled out as a potential cause of unsuccessful binding of denatured AIDH to Ni-NTA as no imidazole was added to the binding buffers in any attempts. The AIDH protein construct was also designed to contain a serine-glycine linker to separate the tag from the protein, which thereby essentially exposes the tag and prevents it being buried (Chen et al. 2013). The ability of the His-tag to bind coordinate with the Ni-NTA was also explored as a probable cause for impaired binding, as at low buffer pH, protonation of the histidine side chains can impair the binding of histidine to nickel (Bornhorst and Falke 2000). This was examined and the pH of the buffer was monitored to ensure it stayed within buffering range. Imidazole can also lower the pH of a buffer, therefore a buffered stock of imidazole was used as well, ruling it out as the probable cause for unsuccessful binding of AIDH in its denatured state to Ni-NTA. Following several attempts of optimizing the washing, extraction and purification of AIDH from inclusion bodies, the overall soluble protein recovery yield was not significantly improved, the issues with unsuccessful binding of AIDH in the denatured state and aggregation of any recovered AIDH remained unsolved.

It was hypothesised that the success of soluble AIDH recovery in the original attempt (section 7.2.2.1) could potentially be due to the simplified nature of the extraction and purification of inclusion bodies. The extraction of the inclusion bodies in the initial attempt was not accompanied by extensive washing of the pellet with detergent, reducing agent, chelating agent and denaturant, thereby the eventual inclusion bodies pellet exposed to high denaturing conditions did not exclusively consist of pure inclusion bodies, but also contained host cellular components. The presence of these components cold have potentially prevented protein-protein self-interactions and reduced the chance of aggregation. Impartial extraction of AIDH from the inclusion bodies could have led to lower concentrations of AIDH binding to Ni-NTA. Moreover, Ni-NTA affinity chromatography is high capacity but low specificity, so,

often using nickel to purify His-tagged proteins leads to the co-purification of contaminants (Porath 1992). The inclusion bodies protocols were modified and optimized based on multiple recommendations in literature and was trouble shot to identify and rectify the potential issues casing the problem. However, no significant advances were achieved. Further experimental work with modified purification strategies could provide a potential solution to the issue at hand. There are a variety of affinity tags available for protein purification purposes and individually they can vary significantly in purity, yield and cost (Lichty et al. 2005), a change in tag could offer more success in the purification and subsequent soluble protein recovery.

The initial attempt made at refolding unfolded AIDH on the Ni-NTA affinity column was successful and AIDH recovered from inclusion bodies was successfully buffer exchanged to remove imidazole, GdnHCl and DTT to negligible amounts. 1.27mg/ml of AIDH was obtained in 100mM HEPES pH 7.5, 10% glycerol, 200mM $MgCl_2$ buffer. The enzymatic assay for confirmation of positive enzymatic activity highlighted an issue with the control condition. Without the presence of AIDH, an increase in the absorbance values at 340nm was absorbed over time which indicates the formation of NADH. Further experimentation with the control reagents and isolation suggested the breakdown of the substrate aldehyde to carboxylic acid providing the required electrons for the formation of the carboxylic acid. Activity measurements via analysis at 340nm was not an efficient method to follow the reaction as it is an indirect measurement by following the concomitant reduction of NAD^+ to NADH. Due to unavailability of IC analysis at the time of the experiment this could not be done. Ideally this reaction would be efficiently analysed via IC, whereby the product formation can be monitored and quantified by subsequent peak selection. However, there was a substantial difference in absorbance values between the assay and control conditions which was taken as confirmation of functional activity. AIDH offers a valuable addition to the overall design of the cascade as it facilitates the conversion of an unwanted intermediate towards a central valuable intermediate. Possible change of tag and/or expression vector could be explored further to either optimize soluble expression of AIDH or to improve purification of AIDH from inclusion bodies.

9.6 Production, purification and characterization of MDH, coupled with GDH

Wildtype NADP(H)-dependent malate dehydrogenase (MDH_{wt}) from the thermophilic archaeon *Thermococcus kodakarensis*, catalyses the HCO_3^- independent reductive carboxylation of pyruvate to malate with lactate as a by-product, presenting itself suitable for application as the final enzyme in our cascade design. A suitable enzyme for application in the cascade design was presented in the form of engineered MDH from *T. kodakarensis* whereby a triple mutant was identified via directed evolution (Morimoto et al. 2013). Directed evolution was carried out with the MDH in reference to alter its

cofactor preference from NADP(H) to NAD(H). A triple mutant was thereby identified which exhibited the desired properties; it exhibited a 6-fold higher k_{cat}/k_m with NAD^+ than the wildtype and in addition to the change in cofactor preference, it was also serendipitously reported that the reaction specificity of the mutant was significantly shifted towards malate production and it also gave less by-product in comparison to the wildtype. Using the triple mutant MDH (hereby referred to as MDH) to catalyse pyruvate carboxylation with NADH, 1.2 times higher malate concentrations were achieved than the wildtype MDH with NADPH (Morimoto et al. 2013). This MDH was therefore the ideal candidate to catalyse the conversion of pyruvate to malate as due to the altered cofactor preference from NADPH to NADH, the cofactor recycling is possible within the closed reaction environment.

Activity analysis of MDH via equilibrating reaction components with CO_2 prior to addition of substrate was not a well-designed experiment, the dissolved CO_2 was only equilibrated at the start of the reactions, followed by incubation of the sealed reaction vials at the reaction temperature. This method of activity analysis did not provide an efficient method for this as the reaction vials were not leak-proof and without constant regulation of CO_2 levels, eventually the carbonate levels in the assay mixture would reach equilibrium. Furthermore, the solubility of CO_2 in water decreases with increases in temperature (Carroll et al. 1992, Crovetto 1991, Prini and Crovetto 1989), thereby the decrease in carbonate levels dissolved in liquid is accelerated. Given that the experimental parameters could not be controlled, the series of MDH activity analysis experiments performed in section 8.5-8.10, were not taken under consideration, given the nature of the flawed experimental designs.

The atmospheric control unit provided an excellent solution to the problems faced in experimental design prior to its use. There are 3 independent variables affecting reaction parameters of MDH, % of O_2, % of CO_2 and temperature. The earlier experiments (section 8.5-8.10) were performed in 5ml glass vials with seal caps. Given the container used, the suitable incubation methods for reaction duration included either a water bath or an incubator, both of which vary in their incubation efficiencies due to one offering an option to shake the containers while the other not having that option. As discussed in the last paragraph, the issues with CO_2 level control occur in both incubatory conditions. As the atmospheric control unit is designed to be utilized with the plate reader, which itself is fitted with temperature control in the chamber with ability to incubate up to 65°C, all variables of the assay could be controlled and monitored. Real time absorbance readings also allowed for the reaction progression to be monitored and the indirect product formation to be followed. All reaction variables could then be objectively controlled and their monitoring was done under high levels of confidence, the reaction parameters were optimized to identify the optimum reaction conditions. The optimization was done via Box-Behnken design (Table 8.4) and response methodology (Figure 8.15), Box-Behnken is good design for response surface methodology as it permits the estimation of the quadric model

parameters, sequential design building, detection of the lack of lack of fit of the model and finally, the use of blocks (Bezerra et al. 2008, Ferreira et al. 2007). The application of Box-Behnken designs for optimization of analytical methods has wide applications and has been utilized for optimizations for industrial to pharmaceutical applications (Campone et al. 2018, Diaz-Dinamarca et al. 2018, GilPavas et al. 2018).

Biocatalysis contributes to global goals of sustainable chemical processing however its practical application can be limited due to dependence on cofactors, which can be expensive (Wang et al. 2017). Many enzymatic redox reactions require the use of one or more cofactors that are utilized during the reaction (Bornscheuer et al. 2012) and their supply is not economically favourable, thereby an effective system of cofactor regeneration is required of practical large-scale application of enzymatic reactions (Wang et al. 2017). GDH along with formate dehydrogenase (FDH) are the two most widely used enzymes for cofactor recycling in industrial/commercial processes, with GDH from the *Bacillus* species showing the highest activity and stability, leading to its wide applications in industry (Hollmann et al. 2011). Consequently, the pairing of MDH with GDH to test cofactor recycling was anticipated to be an efficient system and utilizing GDH as the cofactor recycling system mimicked commercial processes whereby this class of enzymes are the optimal choice for the purpose of cofactor recycling. Although there are other methods of cofactor NAD(P)H regeneration, for example, chemical regeneration, homogeneous catalytic regeneration and electrochemical regeneration; cofactor regeneration using enzymes is the only method industrially employed despite it also having setbacks. Water soluble by-products formed require costly downstream processing and can cause deactivation of enzymes, enzyme instability and can involve complex product separation and purification (Wang et al. 2017). Use of thermophilic enzymes has the potential to alleviate some of these setbacks, notably those relating to enzyme instability and costly enzyme production/purification as thermophilic proteins offer the advantage of single step heat purification as we have demonstrated.

For a successful coupled reaction system, any potential effects of the reaction reagents of GDH (acting as the regeneration enzyme) on the activity of MDH (the production enzyme) were tested. The highest reduction in MDH enzymatic activity was caused by the decrease in HEPES buffer concentration from the standard 500Mm HEPES in MDH assays to 100Mm HEPES in GDH assays, where the activity of MDH was reduced by 20% (Figure 8.17). Higher stabilization capacity is offered by higher concentrated buffer system, but majority of enzymes accept only moderate ionic strength, ranging commonly between 50-200Mm. This is not the case for thermophilic enzymes which prefer higher buffer concentration up to 1M (Vieille and Zeikus 2001), the decrease in activity can be attributed to the reduction in buffer strength, which along with any added components can reduce obligatory enzyme activity (Bisswanger 2014). Aside from HEPES, the addition of other GDH assay components such as

MgCl$_2$, glycerol and GDH substrate glucose, did not reduce MDH activity by any more than 10% (Figure 8.17). MDH activity assay are required to be carried out under 15% CO$_2$ and 5% O$_2$ atmospheric conditions, therefore GDH activity was assayed under atmospheric conditions required by MDH and activity levels of GHD were measured by the concomitant production of NADH from the oxidation of glucose to gluconate. After 60 minutes, there was no significant difference between the amount of NADH produced by GDH assayed under aerobic conditions and GDH assayed under atmospheric control (Figure 8.18). From these findings, it was concluded that GDH is a suitable cofactor recycling partner and its reaction components do not drastically inhibit the activity of MDH and GDH is capable of its role under altered atmospheric conditions as per the requirements of MDH.

For a fully feasible cofactor recycling coupling, the assay components of MDH were also tested on the activity of the GDH under atmospheric conditions. This experiment demonstrated the drastic effect of pyruvate on the activity of GDH where it was almost completely diminished at only retained 3.3% of its relative activity (Figure 8.19). This loss of activity was determined to be due to competitive inhibition of GDH by pyruvate as concentrations of +10mM pyruvate reduce GDH activity by ~60% and a 2-fold increase in pyruvate concentration increased the k$_m$ value 6-fold (Table 8.8). 30mM of pyruvate and 30mM of glucose were then employed as compromised concentrations to mitigate the issue of GDH inhibition by pyruvate. Considering all the optimizations and substrate inhibition issues, cofactor recycling was successfully displayed when using NAD$^+$ or NADH as cofactor in the presence of both GDH and MDH (Table 8.9). Further optimization regarding the separation of the products can be explored further in an attempt at potentially commercializing this process. As outlined earlier, there are numerous pitfalls of enzymatic cofactor regeneration system including costs associated with enzymes (Wang et al. 2017). However, in large scale industrial operations, enzymatic cofactor regeneration is still preferred as it offers high activity and mild operating conditions (Presecki et al. 2007). Immobilization of the coupled enzymes provides a possible solution to the issues linked with enzyme cost, recyclability and stability (Kumar et al. 2017, Mission et al. 2015), thereby immobilized enzymes are utilized in industry for catalyst recycling (Sheldon and van Pelt 2013) and offer advantages of both economy and sustainability.

9.7 Overall conclusions

This thesis has described a cofactor balanced, cell-free, 5 enzyme biosystem for the sustainable production of malic acid from glucose. All 4 objectives of this project have been fulfilled whereby: (i) an enzymatic cascade was designed to convert glucose to malic acid, (ii) With the exception of AIDH which was obtained in low yields, GDH, DHAD, KDGA and MDH were successfully produced and

purified, (iii) the successfully produced enzymes were characterized and finally, (iv) enzyme immobilization was investigated in detailed with GDH and a novel support.

GDH immobilized onto a novel, hierarchically-structured macroporous-mesoporous silica support showed great potential for gluconic acid production from glucose as well as bread waste hydrolysate. Hierarchically porous MM-SBA-15 showed better immobilization efficiency than commercial supports. Moreover, GDH immobilized onto these materials showed excellent reusability. The use of GDH immobilized onto hierarchically-structured supports has the potential to be incorporated into next generation bio-refineries and waste valorization studies. GDH and MDH were also successfully coupled together and demonstrated cofactor recycling, showing potential for applications into a feasible cell-free biosystem.

10. References

Abe S, Akira F, Ken-Ichiro T. 1962. Method of producing L-malic acid by fermentation. US patent 3,063,910.

Ahmed H, Ettema TJG, Tjaden B, Geerling ACM, van der Oost J, Siebers B. 2005. The semi-phosphorylative Entner-Doudoroff pathway in hyperthermophilic archaea: a re-evaluation. Biochemical Journal 390:529-540.

Ahmed IN, Chang R, Tsai WB. 2017. Poly(acrylic acid) nanogel as a substrate for cellulase immobilization for hydrolysis of cellulose. Colloids and Surfaces B-Biointerfaces 152:339-343.

Aissaoui N, Landoulsi J, Bergaoui L, Boujday S, Lambert JF. 2013. Catalytic activity and thermostability of enzymes immobilized on silanized surface: Influence of the crosslinking agent," Enzyme and Microbial Technology 52:(6-7)336-343.

Akacha NB, Gargouri M. 2015. Microbial and enzymatic technologies used for the production of natural aroma Compounds: Synthesis, recovery modeling, and bioprocesses. Food and Bioproducts Processing, 94:675-709.

Alkhudhiri A. 2011. Membrane distillation: A comprehensive review. Desalination 287.

Badgujar KC, Sasaki T, Bhanage BM. 2015. Synthesis of lipase nano-bioconjugates as an efficient biocatalyst: Characterization and activitye stability studies with potential biocatalytic applications. Royal Society of Chemistry Advances. 5(68):55238-55251.

Baron M, Fontana J, Guimaraes M, Woodward J. 1997. Stabilization and reutilization of Bacillus megaterium glucose dehydrogenase by immobilization. Applied Biochemistry and Biotechnology 63:257-268.

Bastian S, Liu X, Meyerowitz JT, Snow CD, Chen MMY, Arnold FH. 2011. Engineered ketol-acid reductoisomerase and alcohol dehydrogenase enable anaerobic 2-methylpropan-1-ol production at theoretical yield in Escherichia coli. Metabolic Engineering 13:345-352.

Battat E, Peleg Y, Bercovitz A, Rokem JS, Goldberg I. 1991. OPTIMIZATION OF L-MALIC ACID PRODUCTION BY ASPERGILLUS-FLAVUS IN A STIRRED FERMENTER. Biotechnology and Bioengineering 37:1108-1116.

Betancor L, Hidalgo A, Fernandez-Lorente G, Mateo C, Fernandez-Lafuente R, Guisan JM. 2003. Preparation of a stable biocatalyst of bovine liver catalase using immobilization and postimmobilization techniques. Biotechnology Progress 19:763-767.

Bezerra MA, Santelli RE, Oliveira EP, Villar LS, Escaleira LA. 2008. Response surface methodology (RSM) as a tool for optimization in analytical chemistry. Talanta 76:965-977.

Bisswanger H. 2014. Enzyme assays. Perspectives in Science 1:41-55.

Bondos SE, Bicknell A. 2003. Detection and prevention of protein aggregation before, during, and after purification. Analytical Biochemistry 316:223-231.

Bornhorst JA, Falke JJ. 2000. Purification of proteins using polyhistidine affinity tags. Applications of Chimeric Genes and Hybrid Proteins, Pt A 326:245-254.

Bornscheuer UT, Huisman GW, Kazlauskas RJ, Lutz S, Moore JC, Robins K. 2012. Engineering the third wave of biocatalysis. Nature 485:185-194.

Bortone N, Fidaleo M, Moresi M. 2014. Internal and external mass transfer limitations on the activity of immobilised acid urease derivatives differing in enzyme loading. Biochemical Engineering Journal 82:22-33.

Bozell JJ, Petersen GR. 2010. Technology development for the production of biobased products from biorefinery carbohydrates-the US Department of Energy's "Top 10" revisited. Green Chemistry 12:539-554.

Buchanan CL, Connaris H, Danson MJ, Reeve CD, Hough DW. 1999. An extremely thermostable aldolase from Sulfolobus solfataricus with specificity for non-phosphorylated substrates. Biochemical Journal 343:563-570.

Campbell E, Wheeldon IR, Banta S. 2010. Broadening the Cofactor Specificity of a Thermostable Alcohol Dehydrogenase Using Rational Protein Design Introduces Novel Kinetic Transient Behavior. Biotechnology and Bioengineering 107:763-774.

Campone L, Celano R, Piccinelli AL, Pagano I, Carabetta S, Di Sanzo R, Russo M, Ibanez E, Cifuentes A, Rastrelli L. 2018. Response surface methodology to optimize supercritical carbon dioxide/co-solvent extraction of brown onion skin by-product as source of nutraceutical compounds. Food Chemistry 269:495-502.

Carroll JJ, Slupsky JD, Mather AE. 1991. THE SOLUBILITY OF CARBON-DIOXIDE IN WATER AT LOW-PRESSURE. Journal of Physical and Chemical Reference Data 20:1201-1209.

Carsten JM, Schmidt A, Sieber V. 2015. Characterization of recombinantly expressed dihydroxy-acid dehydratase from Sulfobus solfataricus - A key enzyme for the conversion of carbohydrates into chemicals. Journal of Biotechnology 211:31-41.

Chemoxy. Custom Processing. (2018) [ONLINE] Available at: http://www.chemoxy.com/custom-processing-services/. [Accessed 26 September 2018].

Chemoxy. Performance Products. (2018) [ONLINE] Available at: http://chemoxy.com/products-and-applications/. [Accessed 27 September 2018]

Chemoxy. Solvent Recovery. (2018). [ONLINE] Available at: http://chemoxy.com/solvent-recovery/. [Accessed 27 September 2018].

Chen XY, Zaro JL, Shen WC. 2013. Fusion protein linkers: Property, design and functionality. Advanced Drug Delivery Reviews 65:1357-1369.

Chenault HK, Simon ES, Whitesides GM. 1988. Cofactor Regeneration for Enzyme-Catalysed Synthesis. Biotechnology Genet. Eng. Rev. 6:221–70.

Clark EDB. 1998. Refolding of recombinant proteins. Current Opinion in Biotechnology 9:157-163.

Conway T. 1992. The Entner-Doudoroff pathway: history, physiology and molecular biology. FEMS microbiology reviews 9:1-27.

Cowan DA. 1997. Thermophilic proteins: Stability and function in aqueous and organic solvents. Comparative Biochemistry and Physiology a-Molecular & Integrative Physiology 118:429-438.

Crovetto R. 1991. EVALUATION OF SOLUBILITY DATA OF THE SYSTEM CO2-H2O FROM 273-K TO THE CRITICAL-POINT OF WATER. Journal of Physical and Chemical Reference Data 20:575-589.

Dahiya S, Kumar A, Sravan J, Chatterjee S, Sarkar O, Mohan S. 2018. Food waste biorefinery: Sustainable strategy for circular bioeconomy. Bioresource Technology 248:2-12.

Dakin H. 1924. The formation of l-malic acid as a product of alcoholic fermentation by yeast. http://www.jbc.org/.

Deng WP, Wang Y, Yan N. 2016. Production of organic acids from biomass resources. Current Opinion in Green and Sustainable Chemistry 2:54-58.

Diaz-Dinamarca DA, Jerias JI, Soto DA, Soto JA, Diaz NV, Leyton YY, Villegas RA, Kalergis AM, Vasquez AE. 2018. The Optimisation of the Expression of Recombinant Surface Immunogenic Protein of Group B Streptococcus in Escherichia coli by Response Surface Methodology Improves Humoral Immunity. Molecular Biotechnology 60:215-225.

dos Santos JCS, Barbosa O, Ortiz C, Berenguer-Murcia A, Rodrigues RC, Fernandez-Lafuente R. 2015. Importance of the Support Properties for Immobilization or Purification of Enzymes. Chemcatchem 7:2413-2432.

Dudley QM, Karim AS, Jewett MC. 2015. Cell-free metabolic engineering: Biomanufacturing beyond the cell. Biotechnology Journal 10:69-82.

Erickson B, Nelson JE, Winters P. 2012. Perspective on opportunities in industrial biotechnology in renewable chemicals. Biotechnology Journal 7:176-185.

Ettema TJG, Ahmed H, Geerling ACM, van der Oost J, Siebers B. 2008. The non-phosphorylating glyceraldehyde-3-phosphate dehydrogenase (GAPN) of Sulfolobus solfataricus: a key-enzyme of the semi-phosphorylative branch of the Entner-Doudoroff pathway. Extremophiles 12:75-88.

Fernandez-Lopez L, Pedrero S, Lopez-Carrobles N, Gorines B, Virgen-Ortiz J, Fernandez-Lafuente R. 2017. Effect of protein load on stability of immobilized enzymes. Enzyme and Microbial Technology 98:18-25.

Ferraz LIR, Possebom G, Alvez EV, Cansian RL. 2015. Application of home-made lipase in the production of geranyl propionate by esterification of geraniol and propionic acid in solvent-free system. Biocatalysis and Agricultural Biotechnology, 4(1):44-48.

Ferreira SLC, et al. 2007. Box-Behnken design: An alternative for the optimization of analytical methods. Analytica Chimica Acta 597:179-186.

Flikweert MT, de Swaaf M, van Dijken JP, Pronk JT. 1999. Growth requirements of pyruvate-decarboxylase-negative Saccharomyces cerevisiae. Fems Microbiology Letters 174:73-79.

Flint DH, Allen RM. 1996. Iron-sulfur proteins with nonredox functions. Chemical Reviews 96:2315-2334.

Flint DH, Emptage MH. 1988. DIHYDROXY ACID DEHYDRATASE FROM SPINACH CONTAINS A 2FE-2S CLUSTER. Journal of Biological Chemistry 263:3558-3564.

Flint DH, Emptage MH, Finnegan MG, Fu WG, Johnson MK. 1993. THE ROLE AND PROPERTIES OF THE IRON-SULFUR CLUSTER IN ESCHERICHIA-COLI DIHYDROXY-ACID DEHYDRATASE. Journal of Biological Chemistry 268:14732-14742.

France SP, Hepworth LJ, Turner NJ, Flitsch SL. 2017. Constructing Biocatalytic Cascades: In Vitro and in Vivo Approaches to de Novo Multi-Enzyme Pathways. Acs Catalysis 7:710-724.

Gao C, Li Z, Zhang L, Wang C, Li K, Ma C, Xu P. 2015. An artificial enzymatic reaction cascade for a cell-free bio-system based on glycerol. Green Chemistry 17:804-807.

Ghiaci M, Aghaei H, Soleimanian S, Sedaghat ME. 2009. Enzyme immobilization Part 1. Modified bentonite as a new and efficient support for immobilization of Candida rugoso lipase. Applied Clay Science 43:289-295.

Giardina P, Debiasi MG, Derosa M, Gambacorta A, Buonocore V. 1986. GLUCOSE-DEHYDROGENASE FROM THE THERMOACIDOPHILIC ARCHAEBACTERIUM SULFOLOBUS-SOLFATARICUS. Biochemical Journal 239:517-522.

GilPavas E, Dobrosz-Gomez I, Gomez-Garcia MA. 2018. Optimization of sequential chemical coagulation - electro-oxidation process for the treatment of an industrial textile wastewater. Journal of Water Process Engineering 22:73-79.

Gottschalk G, Bender R. 1982. D-GLUCONATE DEHYDRATASE FROM CLOSTRIDIUM-PASTEURIANUM. Methods in Enzymology 90:283-287.

Grimaldi J, Collins CH, Belfort G. 2016. Towards cell-free isobutanol production: Development of a novel immobilized enzyme system. Biotechnology Progress 32:66-73.

Guterl J-K, et al. 2012. Cell-Free Metabolic Engineering: Production of Chemicals by Minimized Reaction Cascades. Chemsuschem 5:2165-2172.

Guterl J-K, Sieber V. 2013. Biosynthesis "debugged": Novel bioproduction strategies. Engineering in Life Sciences 13:4-18.

Guzik U, Hupert-Kocurek K, Wojcieszynska D. 2014. Immobilization as a Strategy for Improving Enzyme Properties-Application to Oxidoreductases. Molecules 19:8995-9018.

Harmsen G. 2007. Reactive distillation: The front-runner of industrial process intensification A full review of commercial applications, research, scale-up design and operation. Chemical Engineering And Processing 46.

Hartmann M, Kostrov X. 2013. Immobilization of enzymes on porous silicas - benefits and challenges. Chemical Society Reviews 42:6277-6289.

Hirata M, Ishikawa K, Naruto S. 1987. Japan. Pat. 62,096,453.

Hohmann S. 1991. CHARACTERIZATION OF PDC6, A 3RD STRUCTURAL GENE FOR PYRUVATE DECARBOXYLASE IN SACCHAROMYCES-CEREVISIAE. Journal of Bacteriology 173:7963-7969.

Hollmann F, Arends I, Holtmann D. 2011. Enzymatic reductions for the chemist. Green Chemistry 13:2285-2314.

Homaei AA, Sariri R, Vianello F, Stevanato R. 2013. Enzyme immobilization: an update. J Chem Biol 6:185-205.

Honda T, Miyazaki M, Nakamura H, Maeda H. 2005. Immobilization of enzymes on a microchannel surface through cross-linking polymerization. Chemical Communications:5062-5064.

Hudson S, Cooney J, Magner E. 2008. Proteins in Mesoporous Silicates. Angewandte Chemie-International Edition 47:8582-8594.

Iyer PV, Ananthanarayan L. 2008. Enzyme stability and stabilization - Aqueous and non-aqueous environment. Process Biochemistry 43:1019-1032.

Jandt U, You C, Zhang YHP, Zeng AP. 2013. Compartmentalization and Metabolic Channeling for Multienzymatic Biosynthesis: Practical Strategies and Modeling Approaches. Pages 41-65 in Zeng AP, ed. Fundamentals and Application of New Bioproduction Systems, vol. 137.

Jang YS, Kim B, Shin JH, Choi YJ, Choi S, Song CW, Lee J, Park HG, Lee SY. 2012. Bio-based production of C2-C6 platform chemicals. Biotechnology and Bioengineering 109:2437-2459.

Jantama K, Haupt MJ, Svoronos SA, Zhang X, Moore JC, Shanmugam KT, Ingram LO. 2008. Combining metabolic engineering and metabolic evolution to develop nonrecombinant strains of Escherichia coli C that produce succinate and malate. Biotechnology and Bioengineering 99:1140-1153.

Jesionowski T, Krysztafkiewicz A. 2002. Preparation of, the hydrophilic/hydrophobic silica particles. Colloids and Surfaces a-Physicochemical and Engineering Aspects 207 (art. Pii s0927-7757(02)00137-1):49-58.

Jesionowski T, Zdarta J, Krajewska B. 2014. Enzyme immobilization by adsorption: a review. Adsorption-Journal of the International Adsorption Society 20:801-821.

Jewett MC, Swartz JR. 2004. Mimicking the Escherichia coli cytoplasmic environment activates long-lived and efficient cell-free protein synthesis. Biotechnology and Bioengineering 86:19-26.

Kardinahl S, Schmidt CL, Hansen T, Anemuller S, Petersen A, Schafer G. 1999. The strict molybdate-dependence of glucose-degradation by the thermoacidophile Sulfolobus acidocaldarius reveals the first crenarchaeotic molybdenum containing enzyme - an aldehyde oxidoreductase. European Journal of Biochemistry 260:540-548.

Khan NR, Rathod VK. 2015. Enzyme catalyzed synthesis of cosmetic esters and its intensification: A review. Process Biochemistry 50(11):1793-1806.

Kim S, Lee SB. 2006. Catalytic promiscuity in dihydroxy-acid dehydratase from the thermoacidophilic archaeon Sulfolobus solfataricus. J Biochem 139:591-596.

Kirk RA, Othmer DF. 2000. Kirk-Othmer Encyclopedia of Chemical Technology. 4th ed. New York: Wiley

Kiss A. 2013. Azeotropic Distillation.

Knuf C, Nookaew I, Brown SH, McCulloch M, Berry A, Nielsen J. 2013. Investigation of Malic Acid Production in Aspergillus oryzae under Nitrogen Starvation Conditions. Applied and Environmental Microbiology 79:6050-6058.

Kouril T, Wieloch P, Reimann J, Wagner M, Zaparty M, Albers SV, Schomburg D, Ruoff P, Siebers B. 2013. Unraveling the function of the two EntnerDoudoroff branches in the thermoacidophilic Crenarchaeon Sulfolobussolfataricus P2. Febs Journal 280:1126-1138.

Kumar P, Ryan B, Henehan G. 2017. B-Glucosidase from Streptomyces griseus: Nanoparticle immobilization and application to alkyl glucoside synthesis. Protein Expression and Purification 132:164-170.

Kunjukunju S, Roy A, Shekhar S, Kumta P. 2018 Cross-linked enzyme aggregates of alginate lyase: A systematic engineered approach to controlled degradation of alginate hydrogel. International Journal of Biological Macromolecules 115:176-184.

Kwok R. 2010. FIVE HARD TRUTHS FOR SYNTHETIC BIOLOGY. Nature 463:288-290.

Lamble HJ, Theodossis A, Milburn CC, Taylor GL, Bull SD, Hough DW, Danson MJ. 2005. Promiscuity in the part-phosphorylative Entner-Doudoroff pathway of the archaeon Sulfolobus solfataricus. Febs Letters 579:6865-6869.

Le Chatelier's Principle. 2018. [ONLINE] Available at:
https://www.chemguide.co.uk/physical/equilibria/lechatelier.html [Accessed 12 October 2018]

Li Y, Gao F, Wei W, Qu JB, Ma GH, Zhou WQ. 2010. Pore size of macroporous polystyrene microspheres affects lipase immobilization," Journal of Molecular Catalysis B: Enzymatic, vol. doi:10.1016/j.molcatb.2010.05.007, 2010.

Li H, Xiao WH, Xie PP, Zheng LY. 2018. Co-immobilization of enoate reductase with a cofactor-recycling partner enzyme. Enzyme and Microbial Technology 109:66-73.

Li Z, Zhang MM, Jiang TT, Sheng BB, Ma CQ, Xu P, Gao C. 2017. Enzymatic Cascades for Efficient Biotransformation of Racemic Lactate Derived from Corn Steep Water. Acs Sustainable Chemistry & Engineering 5:3456-3464.

Lichty JJ, Malecki JL, Agnew HD, Michelson-Horowitz DJ, Tan S. 2005. Comparison of affinity tags for protein purification. Protein Expression and Purification 41:98-105.

Magliery TJ, Lavinder JJ, Sullivan BJ. 2011. Protein stability by number: high-throughput and statistical approaches to one of protein science's most difficult problems. Current Opinion in Chemical Biology 15:443-451.

Masuda Y, Kugimiya SI, Murai K, Hayashi A, Kato K. 2013. Enhancement of activity and stability of the formaldehyde dehydrogenase by immobilizing onto phenyl-functionalized mesoporous silica. Colloids and Surfaces B: Biointerfaces 101:26-33.

Matsubara K, Kohling R, Schonenberger B, Kouril T, Esser D, Brasen C, Siebers B, Wohlgemuth R. 2014. One-step synthesis of 2-keto-3-deoxy-D-gluconate by biocatalytic dehydration of D-gluconate. Journal of Biotechnology 191:69-77.

Matsuda F, Ishii J, Kondo T, Ida K, Tezuka H, Kondo A. 2013. Increased isobutanol production in Saccharomyces cerevisiae by eliminating competing pathways and resolving cofactor imbalance. Microbial Cell Factories 12 (art. 119).

Matuszek K, Chrobok A, Latos P, Markiton M, Szymanska K, Jarzebski A, Swadzba-Kwasny M. 2016. Silica-supported chlorometallate(III) ionic liquids as recyclable catalysts for Diels-Alder reaction under solventless conditions. Catalysis Science & Technology 6:8129-8137.

Milburn CC, Lamble HJ, Theodossis A, Bull SD, Hough DW, Danson MJ, Taylor GL. 2006. The structural basis of substrate promiscuity in glucose dehydrogenase from the hyperthermophilic archaeon Sulfolobus solfataricus. Journal of Biological Chemistry 281:14796-14804.

Miltenberger K. 2000. In Ullmann's Encyclopedia of Industrial Chemistry; Wiley-VCH: Weinheim, 2000. 18:481.

Mirabella N, Castellani V, Sala S. 2014. Current options for the valorization of food manufacturing waste: a review. Journal of Cleaner Production 65:28-41.

Misson M, Zhang H, Jin B. 2015. Nanobiocatalyst advancements and bioprocessing applications. The Royal Society Publishing: Interface 12:20140891.

Mohamad NR, Marzuki NHC, Buang NA, Huyop F, Wahab RA. 2015. An overview of technologies for immobilization of enzymes and surface analysis techniques for immobilized enzymes. Biotechnology & Biotechnological Equipment 29:205-220.

Morimoto Y, Honda K, Ye XT, Okano K, Ohtake H. 2014. Directed evolution of thermotolerant malic enzyme for improved malate production. Journal of Bioscience and Bioengineering 117:147-152.

Ninh PH, Honda K, Sakai T, Okano K, Ohtake H. 2015. Assembly and Multiple Gene Expression of Thermophilic Enzymes in Escherichia Coli for In Vitro Metabolic Engineering. Biotechnology and Bioengineering 112:189-196.

Nisha S, Arun Karthick S, Gobi N. 2012. A Review on Methods, Applications and Properties of Immobilized Enzyme. Chemical Science Review and Letters 1:3:148-155.

Nowak C, Pick A, Lommes P, Sieber V. 2017. Enzymatic Reduction of Nicotinamide Biomimetic Cofactors Using an Engineered Glucose Dehydrogenase: Providing a Regeneration System for Artificial Cofactors. Acs Catalysis 7:5202-5208.

Ohno Y, Nakamori T, Zheng H, Suye S-i. 2008. Reverse reaction of malic enzyme for HCO3- fixation into pyruvic acid to synthesize L-malic acid with enzymatic coenzyme regeneration. Bioscience Biotechnology and Biochemistry 72:1278-1282.

Palmer I, Wingfield PT. 2004. Preparation and extraction of insoluble (inclusion-body) proteins from Escherichia coli. Curr Protoc Protein Sci Chapter 6:Unit 6 3.

Patchett ML, Neal TL, Schofield LR, Strange RC, Daniel RM, Morgan HW. 1989. HEAT-TREATMENT PURIFICATION OF THERMOSTABLE CELLULASE AND HEMICELLULASE ENZYMES EXPRESSED IN ESCHERICHIA-COLI. Enzyme and Microbial Technology 11:113-115.

Patel S, Kalia V, Choi H, Haw JR, Kim IWLJ. 2014. Immobilization of laccase on SiO_2 nanocarriers improves its stability and reusability. Journal of Micrbiology and Biotechnology 24(5):639-647.

Payne GA, Nierman WC, Wortman JR, Pritchard BL, Brown D, Dean RA, Bhatnagar D, Cleveland TE, Machida M, Yu J. 2006. Whole genome comparison of Aspergillus flavus and A-oryzae. Medical Mycology 44:S9-S11.

Peleg Y, Stieglitz B, Goldberg I. 1988. MALIC-ACID ACCUMULATION BY ASPERGILLUS-FLAVUS .1. BIOCHEMICAL ASPECTS OF ACID BIOSYNTHESIS. Applied Microbiology and Biotechnology 28:69-75.

Petroll K, Kopp D, Care A, Bergquist PL, Sunna A. 2019. Tools and strategies for constructing cell-free enzyme pathways. Biotechnol Adv 37:91-108.

Pines O, Shemesh S, Battat E, Goldberg I. 1997. Overexpression of cytosolic malate dehydrogenase (MDH2) causes overproduction of specific organic acids in Saccharomyces cerevisiae. Applied Microbiology and Biotechnology 48:248-255.

Podrebarac G, Ng F, Rempel G. 1997. More uses for catalytic distillation. Chemtech, 5:37-45.

Porath J. 1992. IMMOBILIZED METAL-ION AFFINITY-CHROMATOGRAPHY. Protein Expression and Purification 3:263-281.

Poorakbar E, Shaee A, Saboury A, Rad B, Khoshevisan K, Ma'mani L, Derakhshankhah H, Ganjali M, Hosseini M. 2018. Synthesis of magnetic gold mesoporous silica nanoparticles core shell forcellulase enzyme immobilization: Improvement of enzymatic activity andthermal stability. Process Biochemistry 71:92-100.

Postma E, Verduyn C, Scheffers WA, Vandijken JP. 1989. ENZYMIC ANALYSIS OF THE CRABTREE EFFECT IN GLUCOSE-LIMITED CHEMOSTAT CULTURES OF SACCHAROMYCES-CEREVISIAE. Applied and Environmental Microbiology 55:468-477.

Presecki AV, Zelic B, Vasic-Racki D. 2007. Comparison of the L-malic acid production by isolated fumarase and fumarase in permeabilized baker's yeast cells. Enzyme and Microbial Technology 41:605-612.

Prini RF, Crovetto R. 1989. EVALUATION OF DATA ON SOLUBILITY OF SIMPLE APOLAR GASES IN LIGHT AND HEAVY-WATER AT HIGH-TEMPERATURE. Journal of Physical and Chemical Reference Data 18:1231-1243.

Ramkumar S, Fan XJ, Wang BL, Yang SC, Monnier VM. 2018. Reactive cysteine residues in the oxidative dimerization and Cu2+ induced aggregation of human gamma D-crystallin: Implications for age-related cataract. Biochimica Et Biophysica Acta-Molecular Basis of Disease 1864:3595-3604.

Ramon A, Senorale-Pose M, Marin M. 2014. Inclusion bodies: not that bad. Front Microbiol 5:56.

Rausch KD, Belyea RL. 2006. The future of coproducts from corn processing. Applied Biochemistry and Biotechnology 128:47-86.

Reher M, Schonheit P. 2006. Glyceraldehyde dehydrogenases from the thermoacidophilic euryarchaeota Picrophilus torridus and Thermoplasma acidophilum, key enzymes of the non-phosphorylative Entner-Doudoroff pathway, constitute a novel enzyme family within the aldehyde dehydrogenase superfamily. FEBS Lett 580:1198-1204.

Rollin JA, Tam TK, Zhang YHP. 2013. New biotechnology paradigm: cell-free biosystems for biomanufacturing. Green Chemistry 15:1708-1719.

Sahin S, Ozmen I. 2016. Determination of optimum conditions for glucose-6-phosphatedehydrogenase immobilization on chitosan-coated magnetic nanoparticles and its characterization. Journal of Molecular Catalysis B: Enzymatic 133:S25-S33.

Sakuth M, Reusch, D., Janowsky, R. 2012. Reactive Distillation. Ullmann's Encyclopedia of Industrial Chemistry 31:264-275.

Schrittwieser JH, Velikogne S, Hall M, Kroutil W. 2018. Artificial Biocatalytic Linear Cascades for Preparation of Organic Molecules. Chemical Reviews 118:270-348.

Schurink M, Wolterink-van Loo S, van der Oost J, Sonke T, Franssen MCR. 2014. Substrate Specificity and Stereoselectivity of Two Sulfolobus 2-Keto-3-deoxygluconate Aldolases towards Azido- Substituted Aldehydes. Chemcatchem 6:1073-1081.

Selig M, Xavier KB, Santos H, Schonheit P. 1997. Comparative analysis of Embden-Meyerhof and Entner-Doudoroff glycolytic pathways in hyperthermophilic archaea and the bacterium Thermotoga. Arch. Microbiol. 167:217–232

Sellek GA, Chaudhuri JB. 1999. Biocatalysis in organic media using enzymes from extremophiles. Enzyme and Microbial Technology 25:471-482.

Sengupta D, Pike RW. 2012. Chemicals from Biomass; Integrating Bioprocesses into Chemical Production Complexes for Sustainable Development; CRC Press: Boca Raton, FL.

Sheldon RA. 2007. Cross-linked enzyme aggregates (CLEA (R) s): stable and recyclable biocatalysts. Biochemical Society Transactions 35:1583-1587.

Sheldon RA, van Pelt S. 2013. Enzyme immobilisation in biocatalysis: why, what and how. Chemical Society Reviews 42:6223-6235.

Siebers B, Schonheit P. 2005. Unusual pathways and enzymes of central carbohydrate metabolism in Archaea. Current Opinion in Microbiology 8:695-705.

Singh A, Upadhyay V, Upadhyay AK, Singh SM, Panda AK. 2015. Protein recovery from inclusion bodies of Escherichia coli using mild solubilization process. Microbial Cell Factories 14 (art. 41).

Singhvi M, Gokhale D. 2013. Biomass to biodegradable polymer (PLA). Rsc Advances 3:13558-13568.

Sperl JM, Sieber V. 2018. Multienzyme Cascade Reactions-Status and Recent Advances. Acs Catalysis 8:2385-2396.

Steffler F, Guterl JK, Sieber V. 2013. Improvement of thermostable aldehyde dehydrogenase by directed evolution for application in Synthetic Cascade Biomanufacturing. Enzyme and Microbial Technology 53:307-314.

Straathof AJJ. 2014. Transformation of Biomass into Commodity Chemicals Using Enzymes or Cells. Chemical Reviews 114:1871-1908.

Swartz JR. 2012. Transforming Biochemical Engineering with Cell-Free Biology. Aiche Journal 58:5-13.

---. 2018. Expanding biological applications using cell-free metabolic engineering: An overview. Metab Eng 50:156-172.

Taing O, Taing K. 2007. Production of malic and succinic acids by sugar-tolerant yeast Zygosaccharomyces rouxii. European Food Research and Technology 224:343-347.

Takata I, Tosa T. 1993. In Industrial Application of Immobilized Biocatalysts; Tanaka, A., Tosa, T., Kobayashi, T., Eds.; Marcel Dekker: New York, 1993, p 53.

Takors R. 2012. Scale-up of microbial processes: Impacts, tools and open questions. Journal of Biotechnology 160:3-9.

Theodossis A, Milburn CC, Heyer NI, Lamble HJ, Hough DW, Danson MJ, Taylor G. 2005. Preliminary crystallographic studies of glucose dehydrogenase from the promiscuous Entner-Doudoroff pathway in the hyperthermophilic archaeon Sulfolobus solfataricus. Acta Crystallographica Section F-Structural Biology and Crystallization Communications 61:112-115.

Tomke PD, Rathod VK. 2015. Ultrasound assisted lipase catalyzed synthesis of cinnamyl acetate via transesterification reaction in a solvent free medium. Ultrasonics Sonochemistry, 27:241-246.

Trimble HM, Richardson EL. 1932. Journal of the American Chemical Society 62:3721.

van Maris AJA, Geertman JMA, Vermeulen A, Groothuizen MK, Winkler AA, Piper MDW, van Dijken JP, Pronk JT. 2004. Directed evolution of pyruvate decarboxylase-negative Saccharomyces cerevisiae, yielding a C-2-independent, glucose-tolerant, and pyruvate-hyperproducing yeast. Applied and Environmental Microbiology 70:159-166.

Viana QM, Viana MB, Vasconcelos EAF, Santaella ST, Leitao RC. 2014. Fermentative H-2 production from residual glycerol: a review. Biotechnology Letters 36:1381-1390.

Vieille C, Zeikus GJ. 2001. Hyperthermophilic enzymes: Sources, uses, and molecular mechanisms for thermostability. Microbiology and Molecular Biology Reviews 65:1-+.

Wang XD, Saba T, Yiu HHP, Howe RF, Anderson JA, Shi JF. 2017. Cofactor NAD(P)H Regeneration Inspired by Heterogeneous Pathways. Chem 2:621-654.

Welch P, Scopes RK. 1985. STUDIES ON CELL-FREE METABOLISM - ETHANOL-PRODUCTION BY A YEAST GLYCOLYTIC SYSTEM RECONSTITUTED FROM PURIFIED ENZYMES. Journal of Biotechnology 2:257-273.

Wolterink-van Loo S, van Eerde A, Siemerink MA, Akerboom J, Dijkstra BW, van der Oost J. 2007. Biochemical and structural exploration of the catalytic capacity of Sulfolobus KDG aldolases. Biochem J 403:421-430.

Xie LP, Wei XL, Zhou XG, Meng DD, Zhou RM, Zhang Y, Xu SX, You C. 2018. Conversion of D-glucose to L-lactate via pyruvate by an optimized cell-free enzymatic biosystem containing minimized reactions. Synthetic and Systems Biotechnology 3:204-210.

Xu J, Luo H, Lopez C, Xiao J, Chang YH. 2015. Novel immobilization process of a thermophilic catalase: efficient purification by heat treatment and subsequent immobilization at high temperature. Bioprocess and Biosystems Engineering 38:1983-1991.

Yamaguchi H, Miyazaki M. 2014. Refolding techniques for recovering biologically active recombinant proteins from inclusion bodies. Biomolecules 4:235-251.

Yaoi T, Miyazaki K, Oshima T, Komukai Y, Go M. 1996. Conversion of the coenzyme specificity of isocitrate dehydrogenase by module replacement. Journal of Biochemistry 119:1014-1018.

Ye XH, Wang YR, Hopkins RC, Adams MWW, Evans BR, Mielenz JR, Zhang YHP. 2009. Spontaneous High-Yield Production of Hydrogen from Cellulosic Materials and Water Catalyzed by Enzyme Cocktails. Chemsuschem 2:149-152.

Ye XT, Honda K, Morimoto Y, Okano K, Ohtake H. 2013. Direct conversion of glucose to malate by synthetic metabolic engineering. Journal of Biotechnology 164:34-40.

Yu MG, Liu DQ, Sun LL, Li J, Chen Q, Pan LJ, Shang JC, Zhang SR, Li W. 2017. Facile fabrication of 3D porous hybrid sphere by co-immobilization of multi-enzyme directly from cell lysates as an efficient and recyclable biocatalyst for asymmetric reduction with coenzyme regeneration in situ. International Journal of Biological Macromolecules 103:424-434.

Zdarta J, Meyer AS, Jesionowski T, Pinelo M. 2018. A General Overview of Support Materials for Enzyme Immobilization: Characteristics, Properties, Practical Utility. Catalysts 8 (art. 92).

Zdarta J, Pinelo M, Jesionowski, Meyer T. 2018. Upgrading of Biomass Monosaccharides by Immobilized Glucose Dehydrogenase and Xylose Dehydrogenase. ChemCatChem 10:1-11.

Zeikus JG, Jain MK, Elankovan P. 1999. Biotechnology of succinic acid production and markets for derived industrial products. Applied Microbiology and Biotechnology 51:545-552.

Zelle RM, de Hulster E, van Winden WA, de Waard P, Dijkema C, Winkler AA, Geertman J-MA, van Dijken JP, Pronk JT, van Maris AJA. 2008. Malic acid production by Saccharomyces cerevisiae: Engineering of pyruvate carboxylation, oxaloacetate reduction, and malate export. Applied and Environmental Microbiology 74:2766-2777.

Zhang X, Wang X, Shanmugam KT, Ingram LO. 2011a. L-Malate Production by Metabolically Engineered Escherichia coli. Applied and Environmental Microbiology 77:427-434.

Zhang YHP. 2010. Renewable carbohydrates are a potential high-density hydrogen carrier. International Journal of Hydrogen Energy 35:10334-10342.

---. 2011. Simpler Is Better: High-Yield and Potential Low-Cost Biofuels Production through Cell-Free Synthetic Pathway Biotransformation (SyPaB). Acs Catalysis 1:998-1009.

---. 2015. Production of biofuels and biochemicals by in vitro synthetic biosystems: Opportunities and challenges. Biotechnology Advances 33:1467-1483.

Zhang YHP, Evans BR, Mielenz JR, Hopkins RC, Adams MWW. 2007. High-Yield Hydrogen Production from Starch and Water by a Synthetic Enzymatic Pathway. Plos One 2 (art. e456).

Zhang YHP, Myung S, You C, Zhu ZG, Rollin JA. 2011b. Toward low-cost biomanufacturing through in vitro synthetic biology: bottom-up design. Journal of Materials Chemistry 21:18877-18886.

Zheng H, Ohno Y, Nakamori T, Suye S-i. 2009. Production of L-malic acid with fixation of HCO3- by malic enzyme-catalyzed reaction based on regeneration of coenzyme on electrode modified by layer-by-layer self-assembly method. Journal of Bioscience and Bioengineering 107:16-20.

Zucca P, Sanjust E. 2014. Inorganic Materials as Supports for Covalent Enzyme Immobilization: Methods and Mechanisms. Molecules 19:14139-14194.

Appendix

11. Chemoxy placement report

Being supported by a BBSRC iCASE studentship which is co-sponsored by Chemoxy, as part of my studentship, I was to spend some time of my PhD at Chemoxy.

The aim of this placement was to become familiar with industrial processes, their setup, planning and execution on a larger scale in comparison to academic research. Since Chemoxy mainly serves as a contract manufacturer, the projects coming into the research and development department vary in their nature, duration, and analysis techniques etc. Customers could have requested a certain amount of a chemical and R&D would then carry out the reaction on a smaller scale, identify and optimize any productivity issues before the reaction can be approved for production on a plant scale. Chemoxy also have their own line of performance products which are also developed and optimized for large scale production by the R&D department. Occasionally there is developmental analysis carried out on established products to serve either as further optimization or when the product faces external analysis. During this placement, 2 custom products were produced via esterification followed by distillation on a small scale to optimize production conditions and carry out yield analysis for production on plant scale. These two products are n-butyl propionate and di-n-propyl malate. Both of these esters are chemically valuable to industry due to their varied uses as platform chemicals and subsequent applications into a range of industries. A Chemoxy performance product was also separated into its 3 main components for new blending analysis in another project (data not shown as it is a straight forward distillation to separate components and then blend them in different ratios for external testing).

11.1 Introduction

Chemoxy is a large independent contract manufactures based at two sites in the UK, with the Middlesbrough site carrying out distillations since 1868 and the Billingham site added in 1994. The company has 3 main activities, custom processing solutions, solvent recovery and performance products. They manufacture a range of environmentally friendly solvents which are used in the latest generation of paints and cleaning products. They serve a diverse range of industries to include specialty chemicals, petrochemicals, oil and gas, fuel and lube additives, household and personal care, flavour and fragrance, agricultural chemicals and surface coatings (Chemoxy 2018).

11.1.1 Custom Processing

Chemoxy's core activity is custom processing which allows them to combine their versatile reactors with the distillation capabilities. Efficiency can further be improved by adding increased value to by-

product or recycle streams via the solvent recovery service. The approach towards custom processing consists of initial feasibility studies to include environmental and health and safety and also equipment evaluation. This is followed by computerised process simulation and cost estimate. A suitable process can then be developed by the R&D lab which includes sample analysis methods and anticipated yields. This is then experimentally tested using the R&D pilot equipment, which serves as an indication of actual yields and any contamination issues. The product is then developed to the specification required, followed by quality control. A product sample can then be submitted to customer for approval or it can be processed on a large scale, using plant equipment. Any required plant modification are accounted for, final costing is done and then as before, sample can be submitted to customer for approval (Chemoxy Custom Processing 2018).

Technologies and Processes	Routine chemistries carried out	Other capabilities chemistries available	Typical raw materials handled
Adsorption	Esterification	Acetal formation	Acetic acid/Anhydride
Batch reactions	Etherification	Acetylation	Acrylonitrile
Batch-to-continuous	Epoxidation	Aldol condensation	Epichlorohydrin
Catalyst regeneration	Methylation/Methyl capping	Alkylation	Ethyl chloride
Distillation	Quaternization	Amination	Hydrogen peroxide
Reactive distillation	Transesterification	Borationn	Methyl chloride
Extractions		Dehydration	Phenol
Filtration		Diels-Alder	Toluene diisocyanate
Fixed-bed reaction		Epoxidation	
Molecular sieve treatment		Hydrolysis	
Solvent recovery		Isomerization	
		Oligomerization	
		Oxidation	
		Phase transfer catalysis	
		Polymerization	

Table 11.1. Custom processing options available to customers by Chemoxy (Chemoxy Custom Processing 2018).

11.1.2 Solvent recovery

Chemoxy offer a wide range of solvent recovery solutions, they have expertise in the recovery and recycling of a wide range of streams and by-products from across multiple manufacturing sectors. Solvent recovery can be defined as the process of extracting useful products from waste/by-product solvents generated during the manufacture of a desired product. If extracted, these chemicals can be recycled back into processes, reducing the need to generate new solvents, while also reducing waste and extracting potentially hazardous substances. Solvent recovery can be achieved using a few methods, which include fractionation, azeotropic distillation and extractive distillation (Chemoxy Solvent Recovery 2018).
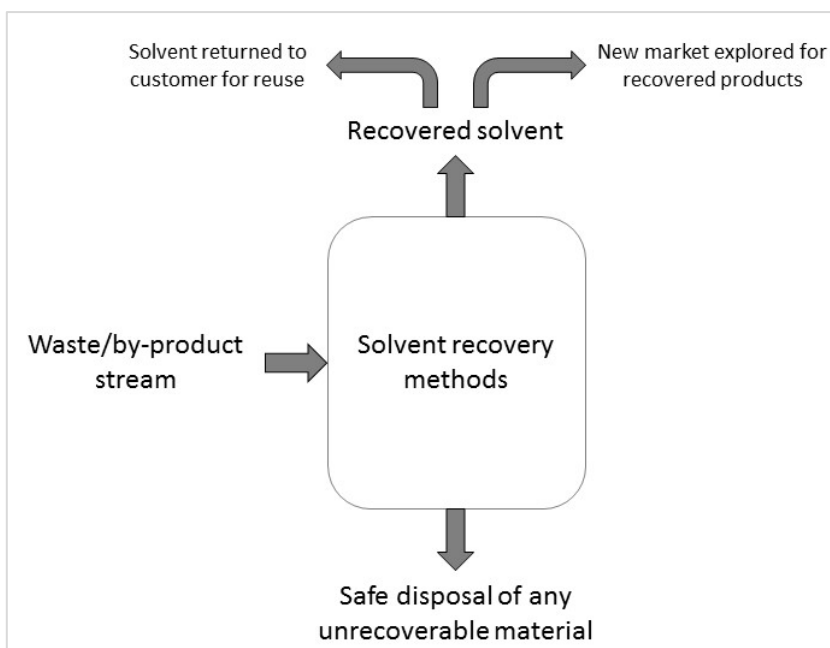
Figure 11.1. Solvent recovery process summary showing potential outcomes as employed by Chemoxy (Chemoxy Solvent Recovery 2018).

There are multiples types of solvents that can be recovered on site by Chemoxy. These include:

- Alcohols
- Hydrocarbons
- Aromatic solvents
- Halogenated solvents
- Ketones
- Esters
- Organic acids
- Amines

11.1.3 Performance products

Chemoxy also has a line of their own performance products which feature low toxicity, environmentally-friendly solvents. These have a variety of applications in adhesives, architectural coatings, automotive coatings, cleaners, coatings, coil coatings, compact discs, fragrance and flavouring, home care, inks, leather and soil stabilisation and oilfield chemicals.

11.1.4 Distillation

One of the most routinely done processes in the department is distillations. Distillation is the main process used to separate liquid mixtures and it is based on the differences in the boiling points or relative volatility of the components. The mixture of liquids can be heated which forces the different components of different boiling points into the gaseous state. The vapour can then be channelled into a condenser. There are various types of distillations used on the basis of the properties of the reactants/products. These include but are not limited to: fractional distillation, steam distillation,

vacuum distillation, air-sensitive vacuum distillation, short path distillation, zone distillation, azeotropic distillation, membrane distillation and reactive distillation (Kiss 2013).

11.1.4.1 Reactive distillation

Reactive distillation is a technique in which the catalytic chemical reaction and distillation (fractionation of products and reactants) occurs simultaneously in a single apparatus. This technique can be classified as a process intensification technology and in the literature this integrated technique can be referred to as catalytic distillation or reaction with distillation. Catalytic distillation can be defined as a process in which a heterogeneous catalyst is localised at a particular position in a distillation column. Reactive distillation is an umbrella term for catalytic distillation as under reactive distillations, the catalyst being homogenous or heterogeneous is not distinguished (Sakuth 2012). The focus of this report is catalytic distillation because it is the main established method at Chemoxy. Catalytic distillations offer a major advantage in the way of eliminating equilibrium limitations of conversion by continuous removal of product from the reaction mix. Le Chatelier's principle states that if a dynamic equilibrium is disturbed by changing conditions, the position of the equilibrium will shift to counteract said change. The application of Le Chatelier's principle here drives the reaction forward by increasing the concentration of reactants on one side and decreasing the product concentration of the other side owing to its continuous removal.

Alongside increased conversion, the following benefits arise from the use of catalytic distillations (Podrebarac et al. 1997):

- Low capital investment as 2 process steps are combined and carried out in the same equipment.
- Catalytic distillation with exothermic reactions offer their own subset of advantages, the reaction heat can be used to vaporise the surrounding liquid which offers simple and reliable temperature control and also the integration of reaction heat in the distillation process reduces boiler duty by saving energy.
- Product selectivity improved due to removal of desired component as the probability of consecutive reactions is lowered.

As with any process, there are certain drawbacks to the catalytic distillations technologies:

- Catalytic distillations can only be employed in circumstances where the temperature window of the vapour-liquid equilibrium is equivalent to the reaction temperature. This can be altered by changing the column operating pressure.
- The thermal stability of the catalyst can limit the upper operating temperature.

- Wet catalyst pellets are required, hence the reaction is entirely limited to being performed in the liquid phase only.

- Since a catalytic distillation column is packed, it can be very expensive to change the catalyst and hence the requirement for the catalyst to have a long lifetime is critical.

- Catalytic distillation technologies can be mathematically difficult to model which can complicate the scale up from the research lab to full plant production.

Industrial application of reactive distillations has rapidly developed in the last 25 years. In 2007, there were more than 150 industrial scale reactive distillations operated worldwide at capacities varying from 100 to 3000 kilo tonnes per year (Harmsen 2007). Since their development, reactive distillations have been favoured by industry and there are key business interests behind it being the case. Variable cost, capital expenditure and reduced energy requirement all favour use of reactive distillations as the above mentioned factors are reduced by 20% or more in comparison to the set-up of a reactor and then distillation. There are also environmental factors to consider such as lower emissions and also social factors, such as improvements on health and safety (Harmsen 2007).

11.1.4.2 Membrane distillation

Membrane distillation refers to a thermally driven separation process in which only vapour molecules transfer through a microporous hydrophobic membrane. The driving principle behind this distillation technique is that the hydrophobic membrane temperature difference induces a vapour pressure difference. This process is of great interest to industry as it has multiple applications across fields such as desalination, wastewater treatment and in the food industry. Membrane distillation applications in desalination are of obvious interest as they contribute towards tackling the global issue of increased supply and demand of fresh water. As mentioned earlier, this separation process is driven by the vapour pressure difference existing between the porous hydrophobic membrane surfaces. Use of membrane distillation has many advantages, the operating temperatures are not high compared to those seen in conventional processes. Membrane distillation systems also have the feasibility to be combined with other separation processes to create an integrated separation system such as ultrafiltration. Further enhancing the appeal is the ability of membrane distillation to utilise alternative energy resources such as solar energy. The main competitive application of membrane distillation is desalination of sea water and it also has effective applications for removing organic and heavy metals from waste water. A further example of application is using membrane distillation to treat radioactive waste where the product is considered safe to be discharged into the environment after treatment (Alkhudhiri 2011).

11.1.5 Esterification

One of the routine techniques done in the R&D department at Chemoxy is esterification. Esters are a functional group commonly found in organic chemistry. It is characterized by a carbon bound to three other atoms of which a single bond is to a carbon, a double bond to an oxygen and a single bond to another oxygen. The single oxygen is bound to another carbon (RCOOR'). Esters are most commonly derived by reacting together carboxylic acids with alcohols in most cases under acid catalysis which also forms water as a by-product.

$$K= [Ester] [water] / [acid] [alcohol]$$

Their names are derived from the parent alcohol and acid based on the name of the acid followed by the suffix '-oate'. For example, an ester derived from butanol and propionic acid is butyl propionate.

With respect to bulk productions, ethylene terephthalate manufacture is the most important ester producing process. It's produced either by direct esterification of the terephthalic acid and ethylene glycol or by the transesterification of dimethyl terephthalate with ethylene glycol, the former being produced by direct esterification of terephthalic acid and methanol (Chem Eng News 1991). Other esters of bulk production interest are vinyl acetate, methyl methacrylate and dioctyl phthalate. The acetates of common alcohols are readily available commercially and are used in diverse industries such as coatings, flavouring components and additives in perfumes (Kirk and Othmer 2000).

As mentioned previously, esters are most commonly derived by reacting together carboxylic acids with alcohols in most cases under acid catalysis which also forms water as a by-product. In many cases this equilibrium is affected by the proportion of reactants, the temperature and any salt presence may also affect it (Trimble and Richardson 1932). As there is an equilibrium present, usually esterification reactions do not go to completion. To achieve conversions close to 100%, the equilibrium has be shifted in favour of product formation and this can be done by either removing the formed ester or water via a variety of distillation methods providing that the reaction is equilibrium limited and not rate limited. There are other methods of removing the distillation products such as reactive extraction and reverse osmosis (Hirata et al. 1987). The ease at which the esters formed can be removed from the reaction mix via distillation depends on their volatility. High volatility esters have a lower boiling point than those of corresponding alcohols, therefore can be easily separated from reaction mix using distillation. Medium volatility esters are capable of removing the water formed by distillation and low volatility esters can be extracted by the removal of water as a binary azeotrope mixture with the alcohol. It is to be noted here than an azeotrope, also known as a constant boiling point mixture, is a mixture of two or more liquids whose proportions cannot be altered or changed by simple distillation

as it has the same proportions of constituents as the reaction mixture. Binary azeotropes may form between the alcohol and water, the alcohol and ester, and the ester and water. Ternary azeotropes are also possible with the alcohol, ester and water and these generally have the lowest boiling points. Azeotropes can exist as homogeneous, where the liquids are miscible and form a solution, or as heterogeneous where the liquids are immiscible and form two liquid phases. An entrainer in the form of a water-insoluble solvent might also be necessary to increase the amount of distilled water in case of immiscible azeotropes (Kirk and Othmer 2000).

The process of esterification is carried out by refluxing the reaction mixture until the majority of the carboxylic acid has reacted with the alcohol and the water has been separated off. Either the water or ester can be removed via distillation depending on the properties mentioned above. There is no universally applicable process for a given esterification, in order to obtain maximum yield, it has be optimized based on multiple factors dependent on reaction components.

11.1.5.1 Enzymatic esterification

Multiple sectors of industry have increased their interest in esters owing to their flavour properties. Flavour esters are versatile and serve as important ingredients in food, beverages, cosmetics, pharmaceuticals, chemicals and personal care products (Akacha and Gargouri 2015). Flavour esters contain an aromatic ring are known as aromatic esters. These are widely naturally occurring and can be extracted via natural routes directly from plants or synthetically made in the lab. However, natural extraction is not fit for industrial applications as source is dependent on season and climatic factors (Badgujar et al. 2015). Chemical production of aromatic esters also has several disadvantages such as use of hazardous chemicals, toxic solvents, high temperatures and pressure, high costs, excessive consumption of energy, by product removal and possible corrosion of equipment. Moreover, the final products cannot be legally labelled as natural and may contain trace toxic impurities which may result in it being unsuitable for human consumption, and therefore the process can be industrially disadvantageous (Khan and Rathod 2015).

A combination of the factors above makes a biotechnological (microbial and enzymatic) approach to the production of esters very appealing. It is a useful sustainable approach with several offered advantages such as high specificity, high yields in mild reaction conditions, reduced by-product formation, biocatalyst recycling and overall reduced production costs (Ferraz et al. 2015). Additionally, esters produced biotechnologically are identified as natural thereby attracting certain industries and satisfying consumer interests (Tomke and Rathod 2015). Furthermore, Chemoxy and Proteus are two companies under management by Novacap, with Proteus's main interest being biocatalysis and

industrial biotechnology. Under their shared parent company, Chemoxy and Proteus are looking to develop partnerships to set up large scale biobased productions of commodities.

11.2 Methods and Materials

11.2.1 Materials

All materials were provided by Chemoxy including propionic acid, n-butanol, pTSA, malic acid, n-propanol, XSA (65%), toluene and gas chromatography column DB 1701 30m x 0.32mm (film thickness 0.25µm).

11.2.2 Methods

11.2.2.1 Esterification

Starting materials were placed into a 3-necked round bottomed flask (3L) along with metal coupons identical to the internal lining of the industrial plant where the eventual large scale production would occur. This allows to check for any out of normal range corrosion directly stemming from the reaction procedure. The contents of the round bottomed flask were then placed into the base mantle, heat applied and brought to boil gently. The reactants in the base react together to form product and water as a by-product. The reaction can be driven to completion by removing the water from the reaction mixture. The system is closed off with a condenser so the boil up in the column condenses at the top and drains back into the base ensuring any unreacted materials are constantly being fed back into the reaction mixture (Figure 11.2). The Dean & Stark (D&S) (removable glassware fitted onto column, used to collect water) was drained periodically until the reaction is deemed to have been completed.

Figure 11.2. Distillation column in its typical setup, heat is applied to the 3 necked flask via the mantle it is placed in (2a). 2 temperature probes set up, one typically measuring the base temperature and the other measuring the temperature at the top of the column. For the first pass of the reaction, which involves an esterification, the overheads are fitted with a D&S (2b, circled) to collect water from the esterification reaction. (Overheads here refer to the glass equipment fitted on top the column which differs depending on the type of reaction being carried out e.g. D&S.)

11.2.2.2 Distillation

After the esterification has been terminated, the flask and its contents were placed onto the base mantle and heat applied again. The distillation protocol uses the same column as shown in Figure 11.2, however the overheads were changed as shown in Figure 11.3. The condenser was fit with a reflux head which allows for the reflux ratio to be adjusted either to total, meaning all condensed components are drained straight back down the column into the base, or the reflux controller can be opened to allow a certain ratio of components to go into the collection flask. A Perkin triangle was also added onto the system. By the use of taps, this specialised piece of equipment allows for the isolation and collection of fractions under vacuum distillation without disturbing the vacuum being applied to the main distillation column.
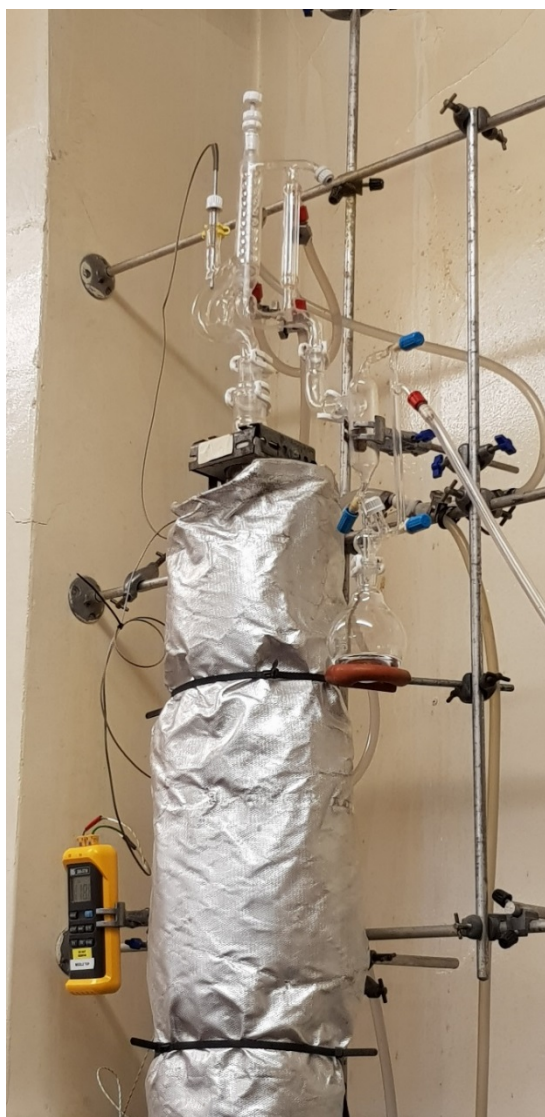
Figure 11.3. Standard distillation setup with a reflux condenser, Perkin triangle and collection flask for collecting fractions. The column is the same for carrying out all reactions with just the overheads being altered depending on the type of reaction.

11.2.2.3 Gas Chromatography (GC)

All fractions distilled off the column and some base samples were put through the GC to isolate components and determine their % in the fraction. Individual methods were set up for the 2 esterification products as follows. n-Butyl propionate samples were analysed using hydrogen at a pressure of 5.0 psig. The injector and detector temperature was set to 240°C and 260°C respectively. A standard sample size of 0.1µl was loaded into the GC for all fractions analysed. The programme temperature increased from 60°C (isolated for 2 mins) to 240°C (isolated for 6 mins) at an increase of 15°C/min. The total run time for one sample was 20 minutes.

Di-n-propyl malate samples were analysed using hydrogen at a pressure of 5.0 psig. The injector and detector temperature was 260°C. A standard sample size of 0.1µl was loaded into the GC for all

fractions analysed. The run temperature ranged from 50°C to 260°C at an increase of 15°C/min with a final isolated hold of 19.5 minutes at 260°C. The total run time for one sample was 30 minutes.

11.2.2.4 Acid number

Reaction mixtures are also analysed throughout to check progress of product formation via acid number. As one of the reactants in both esterifications is an acid, a low acid number is a good indication of reaction completion. Acid numbers are also tightly monitored to ensure customer specifications are met for the final product. An automated titration system was used to determine all acid numbers, this is the mass of potassium hydroxide (KOH) in milligrams that is required to neutralise one gram of chemical substance. This acid number could then be converted into % acid present in sample and further distillation steps could be determined dependent of whether or not the % acid present in sample is within acceptable range.

11.3. Results and Discussion

The overall objective for the placement was to synthesise 2 industrially important products as mentioned earlier, n-butyl propionate and di-n-propyl malate. The experimental approach for was an esterification followed by a distillation, the details of which are in the previous section.

11.3.1 Synthesis of n-Butyl Propionate

n-Butyl propionate is a water-white (approaching water in colourlessness and clarity) liquid with an apple-like odour, its main industrial application lies in making perfumes, flavourings. Previously, similar esters had been successfully produced in the R&D lab before production on a large scale therefore no major issues were expected during manufacture. n-Butyl propionate is produced by various industries and depending on the final application, there is a product specification which the product has to adhere to. The following specification is from Eastman which is a specialist chemical manufacturer. The final product reported here is produced and analysed keeping in mind the following specification. Chemoxy did not have a product specification for this product, hence a specification available in the public domain by Eastman was used as a guide (Table 11.2).

Property	Limits
n-Butyl propionate %	99.5 minimum
n-Butanol %	0.5 maximum
Water %	0.05 maximum
Acid as Propionic %	0.01 maximum
Visual colour, pcs	10 maximum
Appearance	Clear and free of suspended matter

Table 11.2. Product specification for n-butyl propionate.

A standard protocol was used with 2 part reactions, the first being esterification and the second being distillation of pure product. The esterification reaction is as follows:

Propionic acid + n-butanol (in excess) → n-butyl propionate + water
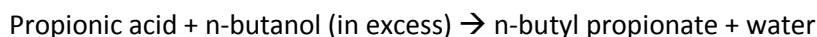
Prior to charging the reactants to the flask and commencing the reaction, the azeotropes in the reaction mix needed to be identified. As mentioned in the introduction, this information is needed to determine if an entrainer needs to be added to the reaction mix. Azeotrope data was obtained from databases online and there were 2 azeotropes identified, the details of which are listed below.

Compound	Boiling point/°C	Azeotrope b.p./°C	Composition in azeotrope/wt%	Upper layer/wt%	Lower layer/wt%
n-Butanol	117.7	93	55.5	79.9	7.7
Water	100		44.5	20.1	92.3

Compound	Boiling point/°C	Azeotrope b.p./°C	Composition in azeotrope/wt%	Upper layer/wt%	Lower layer/wt%
Propionic acid	141.6	99.9	17.7	Miscible	
Water	100		82.3		

Table 11.3. 2 azeotropes identified in the reaction mixture, one consisting of n-butanol and water and second of propionic acid and water. The boiling points of both azeotropes are relatively close with the former being 93° C and the latter being 99.9° C.

11.3.1.1 Preparation of crude n-Butyl Propionate

n-Butanol (1208g), propionic acid (1051.6g), pTSA (4.531g) and 1.6g of corrosion inhibitors were charged into a 3L three necked flask and placed under a 30 theoretical plate column fitted with a D&S. Heat was applied and the mixture was heated to total reflux. Water formed in the reaction was removed as a lower layer from the D&S. The reaction was continued and the overheads appearance and temperature were monitored. Once the system appeared dry at the top of the column, the reaction was continued for a further 2 hours and then heat was turned off. Upon cooling, the base was analysed for acidity. At this point sodium carbonate (powder, 3g, in excess) was added to neutralise the acidity present. The neutralisation was effective at neutralising the pTSA strong acid but not the propionic weaker acid.

Time	Base T (°C)	Top T (°C)	D&S lower layer	Action/Observations
13-09-18 12:04				Heat turned on 6
13:20	104			Boiling in base
13:32	102.3	92.9		Refluxing
15:24	110.1	93	D&S LL 97g	
16:24	132.8	93	D&S LL 88g	
17:04	143.1	93		Heat off Cloudy light yellow in base
14-09-18 08:36				Heat turned on 6
11:10	144.2	113.7		Overheads appear dry
11:50	144.9	112.9		
12:30	145.1	111.6		
13:00	145.1	111.2		Heat off
17-09-18 14:11			D&S LL 79.2g D&S UL 44.55g	Base sample taken Acidity 0.055% as propionic acid

Table 11.4. Timeline of esterification reaction.

As mentioned previously, there are 2 azeotrope identified (Table 11.4) which is of butanol and water (bp of 93° C) and propionic acid and water (bp of 99° C). As the reaction proceeded, water was formed as the by-product as well as the desired ester as it is a condensation reaction. This water formed an azeotrope with the reactant n-butanol which had been added in excess to drive the reaction forward. This water and n-butanol azeotrope boiled up through the column before any other component. The water also formed an azeotrope with the propionic acid but this had a higher boiling point than that of the butanol-water azeotrope so it moved up the column after the butanol-water azeotrope. The experimental strategy employed here was to drain the D&S less often as the butanol-water azeotrope is non miscible so it split into an upper layer of butanol and lower layer of water. By keeping the D&S full, the butanol in the upper layer was drained back into the base containing the catalyst, thus forcing the reaction forward. There were advantages to this as the excess butanol was kept feeding back into base, moreover the butanol-water azeotrope also occupied the space in the middle and top of the column which stopped the propionic acid-water azeotrope from being pulled into the D&S. This was an added advantage as the propionic acid and water azeotrope is miscible so it would have required additional processing to strip any carried over propionic acid and feed it back into the base rather than easy separation via upper and lower layers.

The boiling points of all the individual reaction components are much higher, butanol boils at 117.7°C, propionic acid at 141.6°C and the product of butyl propionate, boils at 146°C and by-product of water boils at 100°C. Given the molar ratio of reaction is 1 mole of reactants give 1 mole of product then using Mass = moles x Mr, the amount of water expected if reaction has gone to completion was calculated. Another good indication for the reaction to have gone to completion was the base

temperature reaching around the boiling point of the ester (146°C). The temperature at the top of the column was higher than both of the azeotropes which concluded that majority of the azeotropes have been pulled out of the system. There were no 2 phase liquid droplets seen in the overheads, as these are indicative of water in the system, the system was declared as being dry and all in 1 phase. At this stage, the reaction mix was left to react for another 2 hours.

After the base had cooled down, a base sample was removed to determine its acid number. There was a strong acid catalyst in the base but all the propionic acid was expected to have been consumed during the esterification. The acid number showed that this was not the case as there was still 0.055% acidity left as propionic acid (Table 11.4). This posed a slight problem as this propionic acid was now to be removed during the distillation before the pure product can be distilled off. This acid number was done with the main purpose of checking how much neutralising agent was needed to neutralise it before the distillation to get off pure product. After determining the acid number, the amount of carbonate required to neutralise it was calculated and added and the distillation was carried out.

11.3.1.2 Distillation of crude n-butyl propionate

The distillation was carried out in a 3L three necked flask under a 30 theoretical plate column fitted with a reflux controller as the overheads. The reflux controller was set to total reflux as the system was brought to boil. At this point, it was allowed to reflux in the overheads for around 30 minutes. The first part of the distillation focused on the removal of the excess n-butanol and any unreacted propionic acid. The butanol was removed without much issue at a reflux ratio of 7:1, however the acid number tests showed the propionic acid was being removed from the reaction at a very slow rate due to the close boiling points. Removing the unreacted propionic acid was slightly more difficult, this was carried out at a reflux ratio of 10:1. When the distillate was in specification the reflux ratio was adjusted to 1:1 and high purity n-butyl propionate was collected down to a small heel.

Time	Base T (°C)	Top T (°C)	Reflux ratio	Fraction/Mass (g)	Action/Observation
18-09-18 8:55			Total		Heat turned on 5
10:38	141.6	21.1	Total		Boiling in base
11:24	143.2	22.0	Total		Column heat on 3
12:00	144.7	100.3	Total		Heat 6 column heat 5 Refluxing
12:15			7:1		
12:38	145.2	115.2	5:1		
13.00	146	117.2	3:1		
14:34	147.8	132.3	10:1	F1 109.83g	0.14% Propionic acid
15:52	147.9	133.7	10:1	F2 20.85g	0.49% Propionic acid
16:54	148	138.3	10:1	F3 19.10g	0.26% Propionic acid
17:19	148		Total		Heat off

Time	Base T (°C)	Top T (°C)	Reflux ratio	Fraction/Mass (g)	Action/Observation
19-09-18 8:30			Total		Heat turned on 6 column heat 5
9:40	147.6	23	Total		Boiling in base
10:30	147.8	49.9	Total		Refluxing
11.00	147.8	96	10:1		
11.17	147.9	138.7	10:1	F4 14.06g	0.2% Propionic acid
11:45	147.8	142	10:1		
12:05	147.8	143.5	10:1	F5 16.09g	0.14% Propionic acid
12:28	147.8	144.2	Total		
13:04	147.8	143.9	10:1		
13:40	147.9	144.5	10:1	F6 17.01g	0.27% Propionic acid
14:48	147.9	144.2	10:1	F7 16.86g	0.047% Propionic acid
15:48	147.9	144.3	10:1	F8 14.89g	0.037% Propionic acid
16.42	148	144.5	10:1	F9 13.94g	0.033% Propionic acid
16:45	148	144.5	Total		Heat off
20-09-18 8:48				Base sample 19.02g	0.0077% Propionic acid
8:55			Total		Heat turned on 6 column heat 5
10:07	148.2	22.3	Total		Boiling in base
10:45	148.3	115	Total		Refluxing
11.00	148.4	140	10:1		
11:40	148.4	144.4	10:1	F10 13.63g	0.037% Propionic acid
12:44	148.3	145.3	10:1	F11 18.93g	0.023% Propionic acid
12:53	148.2	145.4	1:1		
13:09	148.3	145.8	1:1	F12 74.41g	0.011% Propionic acid
14:12	148.3	146	1:1	F13 188.62g	0.0087% Propionic acid
14:42	148.3	146.1	1:1	F14 105.83g	0.0054% Propionic acid
15:50	148.3	145.8	1:1	F15 252.38g	0.0054% Propionic acid
16:40	148.4	146.3	1:1	F16 237.93g	0.005% Propionic acid
17:10	148.4	146.2	1:1	F17 160.65g	0.006% Propionic acid
17:18	148.3	145.9	Total		Heat off
21-09-18 8:20			Total		Heat turned on 6 column 5
9:02	148	17	Total		Boiling in base
9:44	148	79.5	Total		Refluxing
10:10	148.1	140.4	3:1		
10:27	148.1	143.3	1:1	F18 14.64g	0.0245% Propionic acid
11:35	147.7	145.2	1:1	F19 225.45g	0.005% Propionic acid
12:30	147	145.3	1:1	F20 229.89g	0.004% Propionic acid

Table 11.5. Timeline of distillation reaction, pass 2 to obtain pure product of n-butyl propionate. The reflux ratio is kept high and smaller fractions are collected to monitor the acidity. Once the acidity is low enough, the reflux ratio is adjusted and bigger volumes can start to be collected.

11.3.1.3 GC analysis of distilled fractions

All fractions obtained from the distillation were put through the GC for analysis. All the samples were checked for acidity to monitor the propionic acid levels, butanol and n-butyl propionate were monitored via GC.

Fraction	Mass (g)	% n-butanol	% n-butyl propionate	% GC lights	% GC heavies
1	109.83	90.29	7.1	92	n/d
2	20.85	12.16	85.79	14.21	n/d
3	19.10	1.5	97.1	2.84	n/d
4	14.06	0.46	98.4	1.56	n/d
5	16.09	0.06	99.4	0.59	n/d
6	17.01	0.037	99.5	0.46	n/d
7	16.86	0.02	99.7	0.3	n/d
8	14.89	0.018	99.79	0.21	n/d
9	13.94	0.016	99.83	0.16	n/d
10	13.63	0.00997	99.7		
11	18.93	0.0178	99.91		
12	74.41	<0.01	99.73		
13	188.62	<0.01	99.98	0.02	n/d
14	105.83	<0.01	99.99	0.006	n/d
15	252.38	<0.01	99.99	0.003	n/d
16	237.93	<0.01	99.98	0.002	0.02
17	160.65	<0.01	99.98	0.0027	0.02
18	14.64	0.0469	99.9		
19	225.45	<0.01	99.99	n/d	0.004
20	229.89	<0.01	99.94	0.0034	0.061

Table 11.6. Each fraction from the distillation of crude n-butyl propionate was analysed via GC. GC lights refer to any components coming off before the main product of interest, in this case n-butyl propionate (this also includes any unreacted reactant such as butanol in this case). GC heavies refer to any components coming off after the product of interest.

After the product was on specification in all the analysis (acidity, %purity), the final fractions were collected in larger amounts and analysed to confirm all samples were still on specification. After confirmation of this, the fractions which fall under the specification were pooled together and a composite sample was made and analysed for acidity and purity by GC as well checking the colour and water content as well.

11.3.1.4 Composite sample

A sample was made by combining fractions 7-17, 19 and 20 (1553.42g). The analysis was as follows:

Test	Specification	Result
Water %	0.0500 Maximum	0.01
Acid as propionic %	0.0100 Maximum	0.005
n-Butanol %	0.50 Maximum	<0.01
n-Butyl Propionate %	99.50 Minimum	99.97
Visual colour, pcs	10 Maximum	3
Appearance	Clear and Free of Suspended Matter	Pass

Table 11.7. Analysis of n-butyl propionate in comparison to specification.

The final product fell well within the specification range, the composite could now be sent off to potential customers for analysis and then be scaled up as required on the plant.

11.3.2 Synthesis of Di-n-propyl malate

Previously, the following esters had already been made by the R&D department at Chemoxy:

- Di-isopropyl malate
- Di-isobutyl malate
- Di-n-butyl malate

The latter proved rather difficult to synthesise due to product breakdown and the need for a second pass of the distilled product. It was decided that a previously unattempted malate ester could be attempted, di-n-propyl malate (DnPM), the reaction for which is as follows.

Malic acid + n-propanol (in excess) → Di-n-propyl malate + water

It is to be noted here that toluene was added into the reaction with malic acid and n-propanol as the entrainer to separate out the water into layers in the D&S as the azeotropes are immiscible.

As with the n-butyl propionate, before all the reactants are charged to the flask and the reaction is started, the azeotropes in the reaction mix needed to be identified. This information was found in databases online and is detailed below.

Compound	Boiling point/°C	Azeotrope b.p./°C
n-Propanol	97	80
Toluene	110.6	
Water	100	

Compound	Boiling point/°C	Azeotrope b.p./°C
Toluene	110.6	85
Water	100	

Compound	Boiling point/°C	Azeotrope b.p./°C
n-Propanol	97	88.1
Water	100	

Compound	Boiling point/°C	Azeotrope b.p./°C
n-Propanol	97	92.6
Toluene	110.6	

Table 11.8. 4 azeotropes were identified from the reaction mix. There was no information on the existence of an azeotrope between malic acid and di-propyl malate.

The azeotropes were identified as listed in Table 11.8, however not all azeotropes are available in databases. Information could not be sourced about the presence of an azeotrope between the reactant, malic acid and the product formed, di-n-propyl malate. This does not necessarily mean that it does not exist, it just has not been reported at that given time. Only if experimental analysis has shown that an azeotrope doesn't form, it can be reported as 'non azeotrope'.

11.3.2.1 Preparation of crude di-n-propyl malate

n-Propanol (1271.8g), malic acid (975.90g), toluene (185.160g) and XSA (8.185g) as the catalyst were charged into a 3L three necked flask and placed under a 30 theoretical plate column fitted with a D&S. Since the malic acid was added as a powder, heat was applied and the mixture was gently heated to avoid any bumping and to allow the reagents to form a homogenous solution. Until all the reactant in powder form had dissolved into solution, gentle heating in the base was essential as too much heat could cause heat spots in the base of the flask which on occasion could have shot up the length of the column and potentially damage equipment. When all of the solids had been dissolved/partially reacted, the heat source was increased and the water formed in the reaction was removed by the D&S. The reaction was to be continued until the acid no. in the base was <2mgKOH/g. Actual acid number at termination of reaction, base sample 3 (BS3), (Table 11.9) was 2.22mgKOH/g. The reaction was deemed complete once no more water was collecting in the D&S. A total of 605.71g (D&S and base samples) was removed from the system. At this point, neutralising agent (25% molar excess) was added to neutralise the acidity in the base and the mixture was ready to be distilled to obtain pure di-n-propyl malate.

Time	Base T (°C)	Top T (°C)	D&S lower layer	Action/Observations
_23-10_ 9:30				Heat on 2
14:54	125	21.2		Heat 3
15:10	141.4	21.1		Malic acid in solution
15:30				Heat 5 column 3
15:45	98.5	80.8		Boiling, Refluxing
16:25	99.7	80.9		D&S full, cloudy with no distinct layers
16:40	99.8	80.9		D&S not drained, heat off, straw yellow base
_24-10_ 8:50			BS1 29.07g	Heat 4 column 3
9:25	41.5	20.5	D&S1 22.52g	
11:00				Boiling in base, small solids of Malic acid
11:20	98	80.9		Refluxing
13:10	106.5	80.9	D&S2 59.28g	
13:52	109.8	81	D&S3 50.57g	
14:30	114.3	84.7		Dry overheads
15:30	117.4	80.9	D&S4 91.34g	Droplets seen in O/H
16:07	120.7	91.4	D&S5 50.36g	Dry overheads again, Layers seen in D&S
16:30	122.8	87.8		D&S layers cloudy Heat off, D&S not drained
_25-10_ 9:00			BS2 24.25g D&S6 23.22g D&S7 90.09g	2 layers in the D&S, drained
14:50				Heat on 5 column 3
16:00	121.6	79.8		Boiling in base
16:18	127.8	83.4		Refluxing
17:05	132	94.4	D&S8 34.26g	
18:35	132.7	70.6		Heat off
_26-10_ 9:00			BS3 7.34g D&S9 2.34g D&S10 109.82g	

Table 11.9. Timeline of esterification reaction.

11.3.2.2 Distillation of crude di-n-propyl malate (Pass 1)

After adding neutralising agent into the base to neutralise all acidic species, the flask was placed under a 30 theoretical plate column fitted with a reflux controller and a Perkin triangle as the overheads. The first part of the distillation was to strip off the excess n-propanol and toluene. This was done at atmospheric pressure while gradually pulling in the vacuum to a final pressure of 50 mm Hg at a reflux ratio of 10:1. The distillation was done under vacuum as the boiling point of the product is too high to safely carry out distillation at atmospheric pressure. By doing the reaction under vacuum, the boiling points of the reaction components were decreased, thereby achievable under standard lab conditions. When the majority of n-propanol/toluene had been removed, the vacuum was pulled in further to a final pressure of 10 mm Hg to try and strip off any by-products formed, at a reflux ratio of 10:1 (Table 11.10). However, product breakdown was suspected as indicated by the presence of fumarate and

other lighter boilers in the GC analysis of fractions (Table 11.9). The reflux ratio was changed to 1:3 followed by 1:1 and product was collected for redistillation.

Time	Base T (°C)	Top T (°C)	Reflux ratio	Fraction (g)	Pressure (mm Hg)	Action/observation
29-10 12:15			Total		Atm	Heat on 4
14:45	128.2	73.6	Total		660	Refluxing
15:05	128.5	73.4	10:1		660	
16:12	131.3	84.3	10:1	F1 26.55g	660	Heat off
30-10 8:50			Total		660	Heat 4 column 2
10:30	125.3	21.0	Total		660	Boiling in base
10:36	131	72.1	Total		660	Refluxing
11:15	133.4	81.9	10:1		660	
12:30	138.2	86	10:1	F2 26.39g	660	
13:50	146.3	86.5	10:1	F3 32.36g	660	Heat off
14:20	101.5	58	Total		200	Heat 4 column 2
14:55	104.2	59.9	1:1		200	
16:15	151.8	55.5	1:1	F4 132.09g	200	Heat off
31-10 8:55			Total		200	Heat 4 column 3
10:10	124.3	33	Total		200	Boiling
10:30	158.8	49.3	1:1		50	
12:50	176.2	27.1	Total	F5 36.87g	50	Heat off
13:30					18	Heat on
14:10	156.1	20.1	Total		18	
15:50	157.5	23.2	Total		8	Heat 6.5 column 6
16:05	165.3	100	Total		8	Refluxing
16:22	170.3	127.5	1:2		8	
16:38	171.6	127.2	1:1	F6 20.13	8	Solids in collection flask, Heat off
1-11 8:45			Total	BS4 9:35g		
9:00			Total		10	Heat 6.5 column 6
9:45	135.5	19.8	Total		10	Boiling in base
10:25	165.7	119.4	Total		10	Refluxing
10:40	168.2	120.6	10:1		10	
11:35	172	121.5	10:1	F7 16.02g	10	
12:15	172.5	121.5	10:1	F8 16.7g	10	
13:45	171.1	129	10:1	F9 32.32g	10	
14:55	179.1	143.7	10:1	F10 15.49g	10	
15:10	176.9	145.1	5:1		10	
15:30	176.3	144.9	5:1	F11 22.19g	10	
16:20	176.1	145.2	5:1	F12 30.91g	10	Heat off
2-11 8:20			Total	BS5 8.88g	10	Heat 7 column 6
9:20	137.7	20.2	Total		10	Boiling in base
10:20	170.2	126.3	Total		10	Refluxing
10:30	172.3	132.5	5:1		8	
10:50	173.9	139.1	5:1	F13 13.48g	10	
11:45	175.2	145.7	5:1	F14 23.46g	10	
12:25	176.2	146.5	Total	F15 27.4g	Atm	Product breakdown, decided to flash over
5-11 12:50			Total		12	Heat 7, column 6
13.30	125.7	20.2	Total		10	Boiling in base
14:10	169.8	124.6	Total		10	Refluxing
14:30	172.9	145.7	1:3		10	

Time	Base T (°C)	Top T (°C)	Reflux ratio	Fraction (g)	Pressure (mm Hg)	Action/observation
15:36	184.6	147.6	1:1	F15A 247.14g	10	
16:30	198.7	148.6	1:1	F15B 264.50g	10	
16:50	211	147.7	1:1	F15C 99.69g	10	Heat off

Table 11.10. DnPM distillation pass 1, the first part of the distillation was to strip off the excess n-propanol and toluene. This was done at atmospheric pressure while gradually pulling in the vacuum to a final pressure of 50 mm Hg at a reflux ratio of 10:1. After the removal of n-propanol/toluene, the vacuum was pulled in further to a final pressure of 10 mm Hg to try and strip off any by-products formed, at a reflux ratio of 10:1.

Fraction	Mass/g	% n-Propanol	% Toluene	% Di-n-propyl fumarate	% Di-n-propyl malate	% GC others
1	26.55	36.45	63.28			0.27
2	26.39	37.51	61.31			1.18
3	32.36	41.89	57.94			0.17
4	132.09	98.95	0.7			0.35
5	36.87	99.15	0.06			0.79
6	20.13	0.51	0.006	98.71		0.774
7	16.02	0.85		98.41		0.74
8	16.7	0.91		98.65		0.44
9	32.32	0.99		96.15	2.35	0.51
10	15.49	1.9		33.65	63.30	1.15
11	22.19	1.97		8.66	88.71	0.66
12	30.19	1.97		5.74	91.84	0.45
13	13.48	1.93		19.36	77.17	1.54
14	23.46	2.24		10.62	86.17	0.97
15	27.4	1.86		7.16	90.54	0.44
15ABC	611.33	1.34		3.69	94.14	0.83

Table 11.11. GC analysis of all fractions collected during pass 1, the reaction was terminated and the reflux ratio was adjusted at 1:1 to collect large fractions of semi-pure DnPM so that it could be redistilled again. Fraction 6 onwards, unwanted by product was collected as the majority of the fraction and fraction 10 onwards was when majority of the product was collected, however % of GC others started to increase from fraction 10 onwards and therefore the reaction was terminated.

The product di-n-propyl malate can react with itself to form a dimer which can produce propanol again, it can also further dehydrate to form di-n-propyl fumarate which was the majority breakdown product as seen in fraction 6-9 (Table 11.11). Di-n-propyl malate can also cyclise to form maleic anhydride and it was discussed that if pass 1 of distillation had been continued, the next set of product breakdown would have included maleic anhydride which contributes to the increased acidity in the fraction collected. The acid numbers were therefore analysed for pass 1 fractions 12-14 and it showed the acid number increasing (data not shown) which was an indication of accelerated product breakdown, thereby the decision was made to flash over as much of the remaining product in the base and redistill it in distillation pass 2. The base temperature was cut off at 210°C and no more product was collected after the base had reached that temperature, this was for safety and product breakdown reasons. There was still a substantial amount of residues left in the base and these are suspected to be the

dimers and trimers formed during reaction. Before starting pass 2 of distillation to hopefully recover pure DnPM, a composite was made from fractions collected in pass 1.

A composite was made by pooling together fractions 11-15 from the first pass; this was analysed by GC before starting the second pass.

Fraction	Mass/g	% n-Propanol	% Toluene	% Di-n-propyl fumarate	% Di-n-propyl malate	% GC others
Composite	688.78	1.34	n/d	4.37	93.69	0.6

Table 11.12. GC analysis of composite di-n-propyl malate.

This composite had an acid number of 6.99 mgKOH/g and 0.17% water. 688.78g of the composite was charged to a 1.5L three necked flask and second pass of distillation carried out.

11.3.2.3 DnPM Distillation pass 2

Time	Base T (°C)	Top T (°C)	Reflux ratio	Fraction (g)	Pressure (mm Hg)	Action/observation
6-11 11:35			Total		8	Heat 5 column 3
12:50	137	23	Total		8	Boiling in base
13:30	146.7	70.8	Total		8	Refluxing
14.00	152.8	98.8	10:1		8	Solids forming in condenser*
14:15	153.3	107.7	10:1		8	System settled, collecting
14:20	153.4	108.6	5:1		8	
16:30	158.9	133.5	5:1	F16 68.15g	8	Base straw yellow, Heat off
7-11 9:00			Total		10	Heat 7 column 6
9:55	142.9	21	Total		8	Boiling in base
11:00	154	132	5:1		8	Refluxing
11:50	164.5	134.4	5:1	F17 21.25g	8	
12:05	160.5	134.7	5:1	F18 12.82g	8	
12:45	165.7	134.7	5:1	F19 28.37g	8	
13:05	166	135.3	1:2		8	
14:05	161.9	135.5	1:2	F20 233.41g	8	
15:05	194.1	135.1	1:2	F21 227.45g	8	Small heel, base heat off, still collecting
15:40	81.8	26.6	1:2	F22 27.59g	8	Vac off, heat off

Table 11.13. Distillation pass 2 carried out as detailed above. *****Solids formed suspected to be Maleic anhydride.

During the second pass, as fraction 16 was being collected at a reflux ratio of 5:1, solids were observed to being formed in the condenser (Figure 11.4).
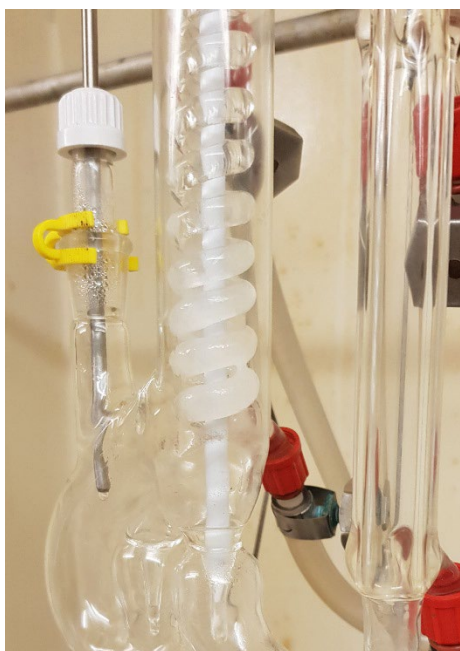
Figure 11.4. Solids were observed being formed around the condenser, a heat gun was used to melt them and drain back into the base.

The solids formed around the condenser were suspected of being maleic anhydride which was another breakdown product of the reaction. To confirm this, a sample was taken from fraction 16 and as well as doing the GC analysis as with all the other fractions, a GC-MS run was also done. This positively identified the sample to contain maleic anhydride. The distillation was continued with the expectation that majority of the maleic anhydride formed had been removed in fraction 16. Fractions were collected as standard and run through the GC for product % purity analysis (Table 11.14).

Fraction	Mass/g	% n-Propanol	% Di-n-propyl fumarate	% Di-n-propyl malate	% GC others
16	68.15	0.088	43.12	52.4	4.392
17	21.25	0.23	0.55	98.63	0.59
18	12.82	0.2	0.22	99.29	0.29
19	28.37	0.2	0.07	99.52	0.21
20	233.41	0.07	0.02	99.89	0.02
21	227.45	0.06	0.02	99.78	0.14
22	27.59	0.05	0.05	99.77	0.13

Table 11.14. GC analysis of all fraction collected during distillation pass 2. The highest % purity obtained for DnPM was in fraction 20 where 99.89% of the fraction collected was the product of interest.

All the fractions collected during pass 2 were also analysed for acid number and water content as maleic anhydride contributes to acidity in the fractions, therefore acid numbers are a good indication of product degradation in the samples (Table 11.15).

Fraction	Mass/g	Acid number mgKOH/g	% Water
16	68.15	71.89	0.03
17	21.25	7.62	0.04
18	12.82	4.01	0.05
19	28.37	2.96	0.05
20	233.41	1.12	0.02
21	227.45	2.07	0.02
22	27.59	1.62	0.03

Table 11.15. Fraction collected during pass 2 analysed for acid number and water content to monitor levels of product breakdown.

A composite sample was made by combining fractions 17-22 (530.42g) for which the final analysis is as follows.

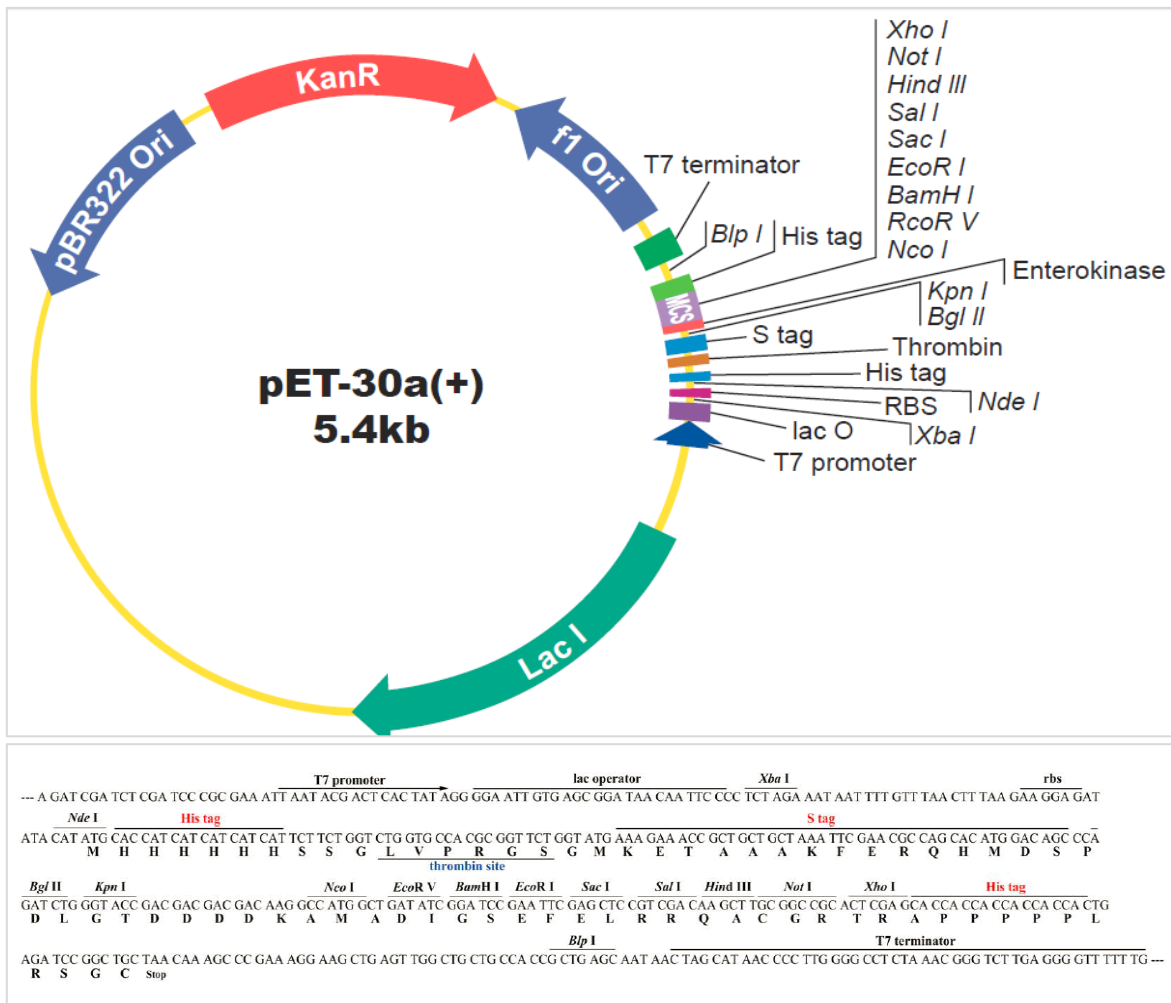| Test	Result
Water %	0.02
Acid number mgKOH/g	2.11
n-Propanol %	0.1
Di-n-propyl fumarate %	0.04
Di-n-propyl malate %	99.71
Others %	0.15
Colour, Hazen	2

Table 11.16. Final analysis of di-n-propyl malate.

The acid number is not ideal and is higher than desired but as with previously made similar esters, product breakdown is a big issue with malate esters.

Malic acid is an expensive feedstock to start with and its addition to reactions in its solid form leads to a much long processing time. On a lab scale it is manageable but on a plant scale it can pose serious handling complications. In addition to this, product breakdown of malic esters means that specialised processes would have to be developed to make the ester more stable. Chemoxy mainly would use the malic esters as coalescing agents, however, the current feedstocks used to make their range of coalescing agents are much cheaper and stable than malic acid, and therefore there is no incentive to produce malic esters. If the feedstock (malic acid) could be obtained cheaply, then there may be an incentive there which is where biobased production strategies can be explored to give a sustainable solution.

Acknowledgments

12.1 pET30a Vector as supplied by GenScript

T7 promoter / lac operator / Xba I / rbs
--- A GAT CGA TCT CGA TCC CGC GAA ATT AAT ACG ACT CAC TAT AGG GGA ATT GTG AGC GGA TAA CAA TTC CCC TCT AGA AAT AAT TTT GTT TAA CTT TAA GAA GGA GAT

Nde I / His tag / S tag
ATA CAT ATG CAC CAT CAT CAT CAT CAT TCT TCT GGT CTG GTG CCA CGC GGT TCT GGT ATG AAA GAA ACC GCT GCT GCT AAA TTC GAA CGC CAG CAC ATG GAC AGC CCA
M H H H H H H S S G L V P R G S G M K E T A A A K F E R Q H M D S P
thrombin site

Bgl II / Kpn I / Nco I / EcoR V / BamH I / EcoR I / Sac I / Sal I / Hind III / Not I / Xho I / His tag
GAT CTG GGT ACC GAC GAC GAC GAC AAG GCC ATG GCT GAT ATC GGA TCC GAA TTC GAG CTC CGT CGA CAA GCT TGC GGC CGC ACT CGA GCA CCA CCA CCA CCA CCA CTG
D L G T D D D D K A M A D I G S E F L R R Q A C G R T A P P P P P L

Blp I / T7 terminator
AGA TCC GGC TGC TAA CAA AGC CC GAA AGG AAG CTG AGT TGG CTG CTG CCA CCG CTG AGC AAT AAC TAG CAT AAC CCC TTG GGG CCT CTA AAC GGG TCT TGA GGG GTT TTT TG ---
R S G C Stop

12.2 GDH optimized sequence for expression in *E. coli* (Optimized Sequence Length:1158, GC%:53.82), with the 5' *Nde*I and 3' *Bam*HI sites highlighted in blue.

CATATG
CACCACCACCACCATCATCACCACCACCATGGTAGCGGCAGCGGTAGCAAGGCGATCATTGTGAAACCGCCGAAC
GCGGGTGTGCAGGTTAAAGACGTTGATGAAAAGAAACTGGACAGCTACGGCAAGATCAAAATTCGTACCATTTAT
AACGGCATCTGCGGTACCGATCGTGAAATTGTGAACGGCAAGCTGACCCTGAGCACCCTGCCGAAGGGCAAAGAC
TTCCTGGTTCTGGGTCACGAGGCGATCGGCGTGGTTGAGGAAAGCTACCACGGTTTTAGCCAAGGCGATCTGGTG
ATGCCGGTTAACCGTCGTGGCTGCGGTATTTGCCGTAACTGCCTGGTGGGTCGTCCGGACTTCTGCGAGACCGGC
GAATTTGGCGAGGCGGGCATCCACAAAATGGATGGCTTCATGCGTGAATGGTGGTACGACGATCCGAAGTATCTG
GTGAAGATTCCGAAAAGCATCGAGGACATCGGTATTCTGGCGCAGCCGCTGGCGGATATCGAAAAGAGCATTGAG
GAAATCCTGGAAGTGCAAAAACGTGTGCCGGTTTGGACCTGCGACGATGGCACCCTGAACTGCCGTAAAGTTCTG
GTGGTGGGCACCGGTCCGATTGGTGTTCTGTTCACCCTGCTGTTTCGTACCTACGGCCTGGAAGTTTGGATGGCG
AACCGTCGTGAGCCGACCGAGGTGGAACAGACCGTTATCGAGGAAACCAAAACCAACTACTATAACAGCAGCAAC
GGTTATGACAAGCTGAAAGATAGCGTGGGCAAGTTCGACGTTATCATTGATGCGACCGGTGCGGATGTGAACATT
CTGGGCAACGTTATTCCGCTGCTGGGTCGTAACGGTGTGCTGGGTCTGTTCGGCTTTAGCACCAGCGGTAGCGTT
CCGCTGGACTACAAGACCCTGCAGGAGATCGTGCACACCAACAAAACCATCATTGGTCTGGTTAACGGCCAAAAG
CCGCACTTTCAGCAAGCGGTGGTTCACCTGGCGAGCTGGAAAACCCTGTATCCGAAGGCGGCGAAAATGCTGATT
ACCAAGACCGTGAGCATCAACGACGAGAAGGAACTGCTGAAAGTTCTGCGTGAGAAGGAACACGGTGAAATCAAA
ATTCGTATCCTGTGGGAGTAA
GGATCC

12.3 DHAD optimized sequence for expression in *E. coli* (Optimized Sequence Length: 1734, GC%:58.76), with the 5' *Nde*I and 3' *Bam*HI sites highlighted in blue.

CATATG
CACCACCACCACCATCATCACCATCATCATGGTAGCGGCAGCGGTAGCCCGGCGAAGCTGAACAGCCCGAGCCGT
TACCACGGTATCTATAACGCGCCGCACCGTGCGTTCCTGCGTAGCGTGGGTCTGACCGACGAGGAAATCGGCAAA
CCGCTGGTTGCGATTGCGACCGCGTGGAGCGAAGCGGGTCCGTGCAACTTTCACACCCTGGCGCTGGCGCGTGTG
GCGAAGGAAGGTACCAAAGAGGCGGGCCTGAGCCCGCTGGCGTTTCCGACCATGGTGGTTAACGATAACATCGGC
ATGGGTAGCGAGGGTATGCGTTACAGCCTGGTGAGCCGTGACCTGATTGCGGATATGGTTGAGGCGCAGTTCAAC
GCGCACGCGTTTGACGGCCTGGTGGGTATCGGTGGCTGCGATAAGACCACCCCGGGTATTCTGATGGCGATGGCG
CGTCTGAACGTTCCGAGCATCTACATTATGGTGGCAGCGCGGAGCCGGGTTACTTCATGGGCAAACGTCTGACC
ATCGAAGACGTTCACGAGGCGATTGGTGCGTACCTGGCGAAGCGTATCACCGAAAACGAGCTGTATGAAATTGAG
AAACGTGCGCATCCGACCCTGGGTACCTGCAGCGGCCTGTTTACCGCGAACACCATGGGCAGCATGAGCGAAGCG
CTGGGTATGGCGCTGCCGGGCAGCGCGAGCCCGACCGCGACCAGCAGCCGTCGTGTGATGTACGTTAAGGAAACC
GGTAAAGCGCTGGGCAGCCTGATCGAAAACGGTATTAAGAGCCGTGAGATCCTGACCTTCGAAGCGTTTGAGAAC
GCGATTACCACCCTGATGGCGATGGGTGGCAGCACCAACGCGGTGCTGCACCTGCTGGCGATCGCGTATGAAGCG
GGTGTTAAACTGACCCTGGACGATTTCAACCGTATCAGCAAGCGTACCCCGTACATTGCGAGCATGAAACCGGGT
GGCGACTATGTGATGGCGGACCTGGATGAAGTGGGTGGCGTTCCGGTGGTTCTGAAGAAACTGCTGGACGCGGGT
CTGCTGCACGGCGATGTGCTGACCGTTACCGGCAAGACCATGAAACAGAACCTGGAGCAATACAAGTATCCGAAC
GTGCCGCACAGCCACATCGTGCGTGATGTTAAGAACCCGATTAAACCGCGTGGTGGCATCGTTATTCTGAAAGGT
AGCCTGGCGCCGGAGGGTGCGGTGATCAAGGTTGCGGCGACCAACGTGGTTAAATTCGAAGGCAAGGCGAAAGTG
TACAACAGCGAGGACGATGCGTTTAAGGGTGTGCAGAGCGGCGAGGTTAGCGAAGGCGAGGTGGTTATCATTCGT
TATGAAGGTCCGAAGGGTGCGCCGGGTATGCCGGAGATGCTGCGTGTTACCGCGGCGATTATGGGCGCGGGTCTG
AACAACGTGGCGCTGGTTACCGATGGTCGTTTTAGCGGTGCGACCCGTGGTCCGATGGTTGGTCATGTTGCGCCG
GAAGCGATGGTGGGTGGCCCGATCGCGATTGTTGAGGACGGTGATACCATCGTGATTGACGTTGAAAGCGAGCGT
CTGGATCTGAAGCTGAGCGAGGAAGAGATCAAGAACCGTCTGAAACGTTGGAGCCCGCCGAGCCCGCGTTACAAG
AGCGGTCTGCTGGCGAAATATGCGAGCCTGGTGAGCCAAGCGAGCATGGGTGCGGTTACCCGTCCGGCGTAA
GGATCC

12.4 KDGA optimized sequence for expression in *E. coli* (Optimized Sequence Length: 924, GC%:53.27), with the 5' *Nde*I and 3' *Bam*HI sites highlighted in blue.

CATATG
CACCACCACCACCATCATCACCACCACCATGGTAGCGGCAGCGGTAGCGAGATCATTAGCCCGATCATTACCCCG
TTCGACAAGCAGGGTAAAGTGAACGTTGATGCGCTGAAGACCCACGCGAAAAACCTGCTGGAGAAGGGCATCGAC
GCGATTTGCGTGAACGGTACCACCGGCCTGGGTCCGGCGCTGAGCAAGGACGAAAAACGTCAGAACCTGAACGCG
CTGTATGATGTGACCCACAAGCTGATCTTCCAAGTTGGCAGCCTGAACCTGAACGACGTGATGGAGCTGGTTAAA
TTTAGCAACGAAATGGATATTCTGGGTGTGAGCAGCCACAGCCCGTACTATTTCCCGCGTCTGCCGGAGAAGTTT
CTGGCGAAATACTATGAGGAAATCGCGCGTATTAGCAGCCACAGCCTGTACATCTATAACTATCCGGCGGCGACC
GGTTATGACATCCCGCCGAGCATTCTGAAAAGCCTGCCGGTTAAGGGTATTAAAGACACCAACCAGGATCTGGCG
CACAGCCTGGAATATAAGCTGAACCTGCCGGGCGTGAAAGTTTACAACGGTAGCAACACCCTGATCTACTATAGC
CTGCTGAGCCTGGACGGCGTGGTTGCGAGCTTCACCAACTTTATCCCGGAAGTGATTGTTAAGCAGCGTGATCTG
ATTAAGCAAGGTAAACTGGACGATGCGCTGCGTCTGCAGGAACTGATCAACCGTCTGGCGGATATTCTGCGTAAA
TATGGCAGCATCAGCGCGATTTACGTGCTGGTTAACGAGTTCCAAGGCATGACGTGGGTTACCCGCGTCCGCCG
ATCTTTCCGCTGACCGATGAGGAAGCGCTGAGCCTGAAGCGTGAGATCGAACCGCTGAAGCGTAAAATTCAAGAA
CTGGTTCACTAA
GGATCC

12.5 AIDH optimized sequence for expression in *E. coli* (Optimized Sequence Length:1539, GC%:54.69) with the 5' *Nde*I and 3' *Bam*HI sites highlighted in blue.

CATATG

CACCATCATCACCATCATCACCACCACCACGGAAGTGGGTCAGGAAGCGACACCAAACTGTATATCGACGGC
CAATGGGTTAATAGCAGCAGCGGTAAAACCGTGGACAAGTACAGCCCGGTGACCGGTCAGGTTATCGGCCGTTTT
GAGGCGGCGACCCGTGACGATGTGGATCGTGCGATTGATGCGGCGGAGGATGCGTTCTGGGCGTGGAACGATCTG
GGCAGCGTTGAACGTAGCAAAATCATTTATCGTGCGAAAGAGCTGATCGAAAAGAACCGTGCGGAGCTGGAAAAC
ATCATTATGGAGGAAAACGGCAAGCCGGTTAAAGAGGCGAAGGAAGAGGTGGACGGCGTTATCGATCAGATTCAA
TACTATGCGGAATGGGCGCGTAAGCTGAACGGTGAGGTGGTTGAAGGCACCAGCAGCCACCGTAAAATCTTTCAA
TACAAGGTGCCGTATGGTATTGTGGTTGCGCTGACCCCGTGGAACTTCCCGGCGGGTATGGTTGCGCGTAAACTG
GCGCCGGCGCTGCTGACCGGTAACACCGTGGTTCTGAAACCGAGCAGCGACACCCCGGGCAGCGCGGAGTGGATC
GTGCGTAAATTTGTGGAAGCGGGTGTGCCGAAGGGCGTTCTGAACTTCATTACCGGTCGTGGCAGCGAGATCGGT
GATTACATTGTGGAACACAAGAAAGTTAACCTGATTACCATGACCGGTAGCACCGCGACCGGTCAGCGTATCATG
CAAAAAGCGAGCGCGAACATGGCGAAGCTGATTCTGGAGCTGGGTGGCAAAGCGCCGTTTATGGTGTGGAAGGAC
GCGGATATGGACAACGCGCTGAAAACCCTGCTGTGGGCGAAGTATTGGAACGCGGGTCAGAGCTGCATTGCGGCG
GAGCGTCTGTACGTGCACGAAGATATTTATGACACCTTCATGAGCCGTTTTGTTGAACTGAGCCGTAAACTGGCG
CTGGGTGACCCGAAGAACGCGGATATGGGTCCGCTGATCAACAAAGGCGCGCTGCAGGCGACCAGCGAGATTGTT
GAGGAAGCGAAAGAAAGCGGCGCGAAGATCCTGTTTGGTGGCAGCCAACCGAGCCTGAGCGGTCCGTACCGTAAC
GGCTATTTCTTTCTGCCGACCATCATTGGTAACGCGGACCAGAAGAGCAAAATCTTCCAAGAGGAAATTTTTGCG
CCGGTGATCGGCGCGCGTAAGATTAGCAGCGTTGAGGAAATGTACGACCTGGCGAACGATAGCAAATACGGTCTG
GCGAGCTACCTGTTCACCAAGGACCCGAACATCATTTTTGAGGCGAGCGAACGTATCCGTTTCGGCGAGCTGTAC
GTTAACATGCCGGGTCCGGAAGCGAGCCAGGGTTATCACACCGGCTTTCGTATGACCGGTCAAGCGGGCGAGGGC
AGCAAATACGGCATCAGCGAATATCTGAAGCTGAAAAACATTTACGTGGATTATAGCGGCAAACCGCTGCATATC
AATACCGTGCGTGACGACCTGTTTCAGTAA

GGATCC

12.6 MDH optimized sequence for expression in *E.coli* (Optimized Sequence Length:1335, GC%:57.29), with the 5' *Nde*I and 3' *Bam*HI sites highlighted in blue.

CATATG

CACCATCACCATCATCATCACCATCATCACGGTAGCGGTAGCGGTAGCAATCCGCTGGAGTTTCATCGCGACAAT
TTTCCGGGTAATGGCAAGATCGAGGTTATTCCGAAAGTGCCGGTTAACCGTGAAACCCTGAGCCTGGCGTATACC
CCGGGTGTGGCGGAGCCGAGCAAGGCGATTGCGAACGGTGCGGACCCGGATGAATATACCGTGATTCCGAACACC
GTTGCGGTGGTTACCGATGGTAGCGCGATCCTGGGTCTGGGTGATATTGGTCCGGTGGCGGGCATGCCGGTTATG
GAGGGCAAGGCGGTTCTGTTCAAAGCGCTGGCGGGCGTGGATGCGTTTCCGATCCTGATTAACACCAAGGACGTT
GATGAGATCGTGCGTACCGTTGAACTGATTAGCCCGGGCTTCGGTGGCATCAACCTGGAAGACATTAGCGCGCCG
CGTTGCTTTGAGATCGAGGAACGTCTGCGTGAACGTCTGGATATTCCGGTGTTCCACGACGATCAACATGGTACC
GCGGTGGTTACCCTGGCGGGCCTGATCAACGCGCTGAAACTGGTTGGTAAGAAATTTAGCGAGATCAAAGTGGCG
ATTAGCGGTGCGGGTGCGGCGGGTATTGCGATTGCGAAGATCCTGCACAGCGTGGGCGTTAAAGAAATTGTGACC
GTTGACCGTAAGGGTATCATTCACGAGGGTGGCGAAGATCTGAACCCGTACCGTCGTGAGGTGGCGGAATATAAC
GTTCACGGTATCGAGGGTGGCCTGAAAGAGGCGATGGAGGGTGCGGACGTGTTCATCGGCGTTAGCGCGGGTGGC
ATTGTGACCCCGGATATGGTTCGTGCGATGGCGGACGATGCGATTGTTTTTGCGATGGCGAACCCGATCCCGGAA
ATTATGCCGGAGGAAGCGAAACGTGCGGGTGCGCGTATTGTGGCGACCGGCCGTAGCGATTTCCCGAACCAAGTG
AACAACGTTCTGGGTTTCCCGGGCATCTTTCGTGGCGCGCTGGACGTTAAAGCGGAGGATATTACCCCGAGCATG
AAACTGGCGGCGGCGGAAGCGATTGCGAGCGTGGTTAGCGACGATGAGCTGGGTGAAGACTACATCATTCCGAGC
CCGCTGCACCCGGATGTGTTCCCGAAAGAGGCGCGTGCGGTGGCGGAAGTGGCGATGAAGGAAGGTGTGGCGGGC
CGTAAAGTTAGCGGCGAGTGGGTGGAGGAACACACCCGTCGTCTGCGTGAATTTTATAGCGCGTTTATTGAGCCG
CTGAATGAGAAGCGTAAGACCTTTAGCGGTCGTGGTAGCAGCCCGTAA

GGATCC

249

12.7 Mass spectrometry protein identification of GDH, DHAD, KDGA, AIDH and MDH

MATRIX SCIENCE MASCOT Search Results

Protein View: gi|499225564

UDP-glucose 6-dehydrogenase [Sulfolobus solfataricus]

Database:	NCBInr
Score:	953
Monoisotopic mass (M_r):	45151
Calculated pI:	8.52
Taxonomy:	Saccharolobus solfataricus

MATRIX SCIENCE MASCOT Search Results

Protein View: WP_009990927.1

MULTISPECIES: dihydroxy-acid dehydratase [Sulfolobus]

Database:	NCBIprot
Score:	147
Monoisotopic mass (M_r):	59555
Calculated pI:	6.86
Taxonomy:	Sulfolobus

MATRIX SCIENCE MASCOT Search Results

Protein View: WP_015385819.1

2-keto-3-deoxygluconate/2-keto-3-deoxy-6-phospho gluconate aldolase [Sulfolobus acidocaldarius]

Database:	NCBIprot
Score:	678
Monoisotopic mass (M_r):	32508
Calculated pI:	6.61
Taxonomy:	Sulfolobus acidocaldarius

MATRIX SCIENCE MASCOT Search Results

Protein View: gi|499203681

aldehyde dehydrogenase [Thermoplasma acidophilum]

Database:	NCBInr
Score:	96
Monoisotopic mass (M_r):	54805
Calculated pI:	5.80
Taxonomy:	Thermoplasma acidophilum

MATRIX SCIENCE MASCOT Search Results

Protein View: WP_011250913.1

NADP-dependent malic enzyme [Thermococcus kodakarensis]

Database:	NCBIprot
Score:	725
Monoisotopic mass (M_r):	45410
Calculated pI:	5.01
Taxonomy:	Thermococcus kodakarensis